

# **Target Identification and Validation of novel Lipid Storage Inhibitors**

Inaugural-Dissertation

zur Erlangung des Doktorgrades  
der Mathematisch-Naturwissenschaftlichen Fakultät  
der Heinrich-Heine-Universität Düsseldorf

vorgelegt von

**Kirsten Tschapalda**

aus Oelde

Düsseldorf, Dezember 2014



Aus dem Institut für Mathematische Modellierung biologischer Systeme  
der Heinrich-Heine-Universität Düsseldorf.



Gedruckt mit der Genehmigung der  
Mathematisch-Naturwissenschaftlichen Fakultät der  
Heinrich-Heine-Universität Düsseldorf

**Referent:** Dr. Mathias Beller

**Korreferent:** Prof. Dr. Markus Kollmann

**Tag der mündlichen Prüfung:** *02.02.2015*



Die vorliegende Arbeit entstand im Zeitraum von März 2011 bis Dezember 2014 unter Anleitung von Dr. Mathias Beller an der Heinrich- Heine Universität Düsseldorf. Die Arbeit wurde in Kollaboration mit Prof. Dr. Herbert Waldmann an dem Max- Planck- Institut für molekulare Physiologie in Dortmund angefertigt.





Keiner kommt von einer Reise so zurück wie er weggefahren ist.

Graham Greene



# TABLE OF CONTENTS

Abbreviations  
Summary  
Zusammenfassung

## CHAPTER 1: GENERAL INTRODUCTION

<b>The need for novel Lipid Storage Modulators.....</b>	<b>1</b>
1.1 Obesity- A consequence of Lipid Overstorage.....	2
1.2 Current Approaches in Obesity Treatment .....	4
1.2.1 Targeting Obesity via Peripheral Pathways.....	4
1.1.2 Targeting Obesity via Hypothalamic Neuroendocrine Pathways.....	5
1.1.3 Supplemental Therapy .....	6

## CHAPTER 2: THEORETICAL BACKGROUND

<b>Lipid Droplets- The Lipid Storage Organelles .....</b>	<b>9</b>
2.1 The Life Cycle of Lipid Droplets .....	10
2.2 Lipid Droplets dependent Disease Pathologies.....	13
2.2.1 Lipid Droplets in Atherosclerosis.....	13
2.2.2 Lipid Droplets and Pathogens .....	13
2.2.3 Lipid Droplets and Steatosis .....	14

## CHAPTER 3: HISTORY AND PURPOSE OF THE PROJECT

<b>Characterization of newly Discovered Inhibitors of Lipid Droplet Formation .....</b>	<b>15</b>
3.1 Part 1: Characterization of three Novel LD Modulators.....	15
3.1.1 History in the Identification of Chemotype 1-3.....	16
3.1.2 Multidimensional Approach in Target Identification .....	17
3.2 Part 2: Adaption of Lipid Droplet Screens .....	18

## CHAPTER 4: RESULTS AND DISCUSSION- PART 1

<b>4.1 Functional Characterization of novel Lipid Droplet Storage Inhibitors .....</b>	<b>19</b>
4.1.1 Chemical Probes.....	21
4.1.2 Confirmation of Biological Activity.....	21
4.1.3 Physiological Examination of the Phenotype.....	27
4.1.4 Three Chemotypes- One Phenotype .....	31
4.1.5 Metabolic Changes upon Small Molecule Treatment in Cells.....	33
4.1.6 Pathways involved in Lipid Storage Modulation .....	44
4.1.7 Atherosclerosis Models.....	466
4.1.8 Summary .....	48
<b>4.2 Chemical Proteomic Approach for Target Identification .....</b>	<b>49</b>
4.2.1 Chemical Probe Optimization (1 <sup>st</sup> generation).....	50
4.2.2 Modification of the Affinity Tag (2 <sup>nd</sup> Generation) .....	51
4.2.3 Optimized Sample Preparation (3 <sup>rd</sup> Generation) .....	53
4.2.4 Optimization by Metabolic Labeling (4 <sup>th</sup> Generation).....	55
4.2.5 Altered experimental Setups in Chemical Proteomics.....	55
4.2.6 Predicted Targets for Chemotype 1 .....	58
4.2.7 Predicted Targets for Chemotype 2 .....	58
4.2.8 Summary .....	59

<b>4.3 Target Validation for Chemotype 1</b> .....	<b>60</b>
4.3.1 High Priority Targets.....	61
4.3.2 Low Priority Targets .....	71
4.3.3 Summary .....	77
<b>4.4 Target Validation for Chemotype 2</b> .....	<b>79</b>
4.4.1 DGAT1 Validation by different Approaches .....	80
4.4.2 Remaining Questions regarding DGAT1 specificity .....	88
4.4.3 Outlook.....	90
<b>4.5 Target Identification for Chemotype 3</b> .....	<b>92</b>
<b>CHAPTER 5: RESULTS AND DISCUSSION- PART 2</b> .....	<b>93</b>
<b>5.1 Adaption of LD based Screens</b> .....	<b>93</b>
5.1 HCS Lipid Droplet Screen in AML12 cells.....	94
5.2 HCS LD Assay for Modulators in Foam Cell LD storage .....	100
5.3 Summary .....	104
<b>CHAPTER 6: MATERIAL</b> .....	<b>106</b>
6.1 Laboratory Equipment .....	106
6.2 Consumables .....	107
6.3 Chemicals .....	108
6.4 Fluorophores .....	109
6.5 Buffer & Solutions .....	110
6.5.1 Buffers in Molecular Biology .....	110
6.5.2 Buffers in Cell Biology .....	110
6.5.3 Buffers and Solutions in Protein Biochemistry.....	111
6.5.4 Buffers and Solutions in Proteomics .....	112
6.5.5 Buffers and Solutions in Enzyme Assays .....	113
6.6 Media .....	113
6.6.1 Mammalian Cell Culture Medium .....	113
6.6.3 Insect Cell Culture Medium.....	114
6.6.4 Bacterial Culture Medium .....	114
6.6.5 Drosophila Fly Food.....	114
6.7 Organisms .....	115
6.7.1 Mammalian Cell Lines .....	115
6.7.2 Insect Cell Lines .....	115
6.7.3 Bacterial Strains .....	115
6.7.4 Drosophila Fly Strains.....	116
6.8 Enzymes .....	116
6.9 Proteins .....	116
6.10 Antibodies .....	117
6.10.1 Primary Antibodies.....	117
6.10.2 Secondary Antibodies .....	117
6.11 Kits & Standards.....	118
6.11.1 Commercial Kits .....	118
6.11.2 Protein and DNA Standards .....	118
6.12 Oligonucleotides .....	119
6.12.1 Sequencing.....	119
6.12.2 RNA Interference.....	119
6.12.3 Quantitative PCR .....	119
6.13 Plasmids .....	120
6.14 Software.....	120

<b>CHAPTER 7: METHODS</b> .....	<b>121</b>
<b>7.1 Methods in molecular Biology</b> .....	<b>121</b>
7.1.1 Cultivation of Bacteria .....	121
7.1.2 Storage of Bacteria .....	121
7.1.3 Heat Shock Transformation of Bacteria .....	121
7.1.4 Plasmid DNA Isolation from Bacteria .....	121
7.1.5 Determination of DNA and RNA Concentration .....	122
7.1.6 pDNA and dsRNA Verification via Agarose Gel Electrophoresis .....	122
7.1.7 Plasmid Verification by Sequencing .....	122
<b>7.2 Methods in Cell Biology</b> .....	<b>123</b>
7.2.1 Mammalian Cell Culture .....	123
7.2.2 Insect Cell Culture .....	125
7.2.3 Generation of Cell Lysates .....	125
7.2.4 Transfection of Mammalian and Insect Cells .....	126
7.2.5 Adipocyte Differentiation .....	126
7.2.6 Generating an AML12- SILAC Cell Line .....	127
7.2.7 Cell Treatment with Biological Active Small Molecules .....	128
7.2.8 (Immune-) Fluorescence Staining of Cells .....	128
7.3.1 Purification and Isolation of Proteins .....	130
7.3.2 Protein Concentration Determination .....	130
7.3.3 Concentration of Proteins Solutions .....	130
7.3.4 SDS- Polyacrylamide Gel Electrophoresis (SDS-PAGE) .....	130
7.3.5 Protein Visualization in PAGE .....	131
7.3.6 Electrophoretic Transfer of Proteins (Blotting) .....	132
7.3.7 Immunodetection of immobilized Proteins .....	132
<b>7.4 Methods in Chemical Proteomics for Target ID</b> .....	<b>133</b>
7.4.1 Affinity Chromatography based Binding Partner Identification (Pull- down) .....	133
7.4.2 Sample Preparation for MS/MS analysis .....	135
7.4.3 Peptide Identification via Nano-LC-MS/MS .....	137
7.4.4 MS and MS/MS Data Evaluation and Statistical Analysis .....	138
<b>7.5 Methods in Transcriptomics</b> .....	<b>139</b>
7.5.1 Isolation of total RNA .....	139
7.5.2 cDNA Preparation .....	140
7.5.3 Quantitative Real-Time PCR (qPCR) .....	140
7.5.4 DsRNA Synthesis for RNAi knock down in <i>Drosophila</i> Cell Culture Cells .....	141
7.5.5 Transcriptome Analysis by Next-Generation-Sequencing .....	142
<b>7.6 Methods to Study Physical Binding</b> .....	<b>142</b>
7.6.1 MicroScale Thermophoresis (MST) .....	142
7.6.2 Proximity ligation Assay (PLA) .....	142
<b>7.7 Methods in Lipid Analysis</b> .....	<b>143</b>
7.7.1 Lipid Droplet Assay .....	143
7.7.2 Determination of Triglyceride Content .....	144
7.7.3 Lipid Uptake Assay .....	145
7.7.4 Cholesterol Storage Assay .....	146
7.7.5 Lipid Extraction .....	146
7.7.6 Thin- layer Chromatography (TLC) .....	146
7.7.7 High Pressure Liquid Chromatography (HPLC) .....	147
<b>7.8 Methods for validation of Enzyme and Pathway Activity</b> .....	<b>147</b>
7.8.1 Cell Viability Assay .....	147
7.8.2 Deoxycytidine Kinase Assay (DCK) .....	147
7.8.3 Diacylglycerol-O-Acyltransferase Assay (DGAT) .....	148
7.8.4 Soluble Epoxide Hydrolase Assay (EPHX2) .....	148
7.8.5 HTS Hedgehog driven Osteogenesis Screen .....	150

7.8.6 11 $\beta$ -Hydroxysteroid Dehydrogenase Assay (HSD) .....	151
7.8.7 Isocitrate Dehydrogenase Activity Assay (IDH) .....	151
7.8.8 Invitrogen™ Kinase Profiling.....	152
7.8.9 Pyruvate Kinase Assay.....	152
7.8.10 <i>WNT</i> reporter gene Assay .....	152
7.8.11 Mitochondrial Depolarization Assay .....	153
<b>7.9 Methods in Microscopy .....</b>	<b>154</b>
7.9.1 Manual fluorescence Microscopy .....	154
7.9.2 Automated fluorescence Microscopy .....	154
7.9.3 Confocal Microscopy.....	154
<b>7.10 Methods using <i>Drosophila</i> as a Modell Organism .....</b>	<b>155</b>
7.10.1 Keeping <i>Drosophila</i> Stocks .....	155
7.10.2 Treating <i>Drosophila</i> Flies with Bioactive Small Molecules.....	155
<b>CHAPTER 8: REFERENCES.....</b>	<b>156</b>
<b>CHAPTER 9: SUPPLEMENTAL DATA.....</b>	<b>171</b>
9.1 Small Molecules .....	171
9.2 Mechanism of Action .....	176
9.3 Chemical Proteomics.....	186
9.4 Target Identification for Chemotype 1.....	204
9.5 Target Identification for Chemotype 2.....	205
9.7 COMAS Screen .....	208
9.8 Background Information on Assays and Methods .....	209
<b>CHAPTER 10: APPENDIX .....</b>	<b>213</b>
10.1 Acknowledgements.....	213
10.2 Index of Figures.....	215
10.3 Collaboration Partners .....	218
10.4 Curriculum Vitae .....	219
10.6 Eidesstattliche Erklärung.....	220

## ABBREVIATIONS

°C	degree celsius; $T(^{\circ}\text{C}) = T(\text{K}) + 273,16 \text{ K}$
A	ampère
ABHD5	$\alpha/\beta$ hydrolase domain-containing protein 5
ACAT	acetyl CoA- Acetyltransferase
AdipoQ	Adiponectin
ADME	absorption, distribution, metabolism, and excretion
AGPAT	acylglycerol-phosphate acyltransferase
Amp	ampicillin
APS	ammonium persulfate
ATCC	American Type Culture Collection
ATGL	adipose triglyceride lipase
BODIPY®	4,4-difluoro-4-bora-3a,4a-diaza-S-indacene
BSA	bovine serum albumine
CAM	chloramphenicol
CE	cholesterylester
CEBP $\alpha$	CCAAT/ enhancer binding protein alpha
CFG	cyan fluorecent protein
CGI-58	comparative gene identification 58
CoA	coenzyme A
Ct value	cycle threshold
cv	Column volumes
Da	dalton
DAG	diacylglycerol
DAPI	4',6-diamidino-2-phenylindole
DCK	deoxycytidine kinase
DGAT	Diaclyglycol-O-acyltransferase
DMSO	dimetylsulfoxid
DNP	2,4-Dinitrophenol
DRSC	<i>Drosophila</i> RNAi Screening Center
dsRNA	double stranded ribonucleic acid
DTE	dithioerythritol
DTT	dithiothreitol
<i>E.coli</i>	<i>Escherichia coli</i>
EC <sub>50</sub>	half maximal effective concentration
EDTA	ethylenediaminetetraacetic acid
EET	epoxyeicosatrienoic acids
eLD	expanding lipid droplet
EM	electron microscopy
EPHX2	soluble epoxide hydrolase
ER	endoplasmic reticulum
FA-CoA	fatty acid coenzyme A
FBS	fetal bovine serum
FC	free cholesterol
FBS	fetal bovine serum
FDA	Food and Drug Administration
FDR	false discovery rate
FFA	free fatty acid
FP	fluorescence polarization
FRET	fluorescence Resonance Energy Transfe
FWD	forward (Primer)
G0S2	G0/G1 switch protein
GA	18 $\beta$ -Glycyrrhetic acid

gDNA	genomic deoxyribonucleic acid
GFP	green fluorescent protein
GI	gastrointestinal tract
GO	gene ontology
GPAT	glycerol-phosphate acyltransferase
GPCR	G protein-coupled receptor
h	hour
HAD	haloacid dehalogenase-like hydrolases
HBSS	hank's balanced salt solution
HCD-2	hydroxyacyl-CoA dehydrogenase 2
HCS	high content screen
HCV	hepatitis C virus
His	histidin
HSL	hormone sensitive lipase
HTS	high throughput screening
IC <sub>50</sub>	half maximal inhibitory concentration
ID	identification
ldh3	isocitrate dehydrogenase
IPTG	isoprpyl-β-D-thiogalactosid
IR	insulin resistance
JNK	c-Jun N-terminal kinases
Kan	kanamycin
L	cell Lysate (used in the legend of immunodetections)
LD	lipid droplet
LFQ	label free quantification
LTQ	linear trap quadrupole
M	molar
M	molecular marker (used in the legend of immunodetections)
m/z	mass to charge ratio
MAPK	mitogen activated protein kinase
MGAT	acyl CoA:monoacylglycerol acyltransferase
min	minute
MST	microscale zhermophoresis
n.D.	not detected
n.S.	not significant
NAFLD	non-alcoholic fatty liver disease
NHS	N-Hydroxysuccinimid
NIDDK	National Institute of Diabetes and Digestive and Kidney Diseases
NIH	National Institutes of Health
NP-40	tergitol-type nonyl phenoxyethoxyethanol.
NT5DC1	nuclotidease domain-containing protein 1
OA	oleic acid
OD <sub>600</sub>	optical density at λ=600 nm
OE	oleoyl-etsrone
PAI-1	plasminogen activator inhibitor type 1
PBS	phosphate buffered saline
PC	hospatidylcholine
PCR	polymerase chain reaction
pDNA	plasmid deoxyribonucleic acid
pH	logarithm of H <sub>3</sub> O <sup>+</sup> Ions in mol/l
PLA	proximity ligation assay
PMA	phorbol 12-myristate 13-acetate
PPARγ	peroxisome proliferator activator receptor gamma
PTM	post translational modification



Pkm	pyruvate kinase
qHTS	quantitative high throughput screening
qPCR	quantitative polymerase chain reaction
QTL	quantitative Trait Locus
REV	reverse (Primer)
RF	retardation factor
rpm	revolts per minute
RT	room Temperature
RTCA	real time cell analysis
RT-PCR	reverse transcription polymerase chain reaction
s	second
S1 level	biological safety level 1
SAR	structure activity relationship
SDS	sodium dodecyl sulfate
sEH	soluble epoxide hydrolase
sHh	sonic hedgehog
slc	glucose uptake transporter (GLUT) gene family
sLD	small lipid droplet
Spr	sepiapterin reductase
ss RNA	single stranded ribonucleic acid
TAG	triacylglyceride, Triacylglycerol
Taq	<i>Thermus aquaticus</i>
TBS	tris buffered saline
TEMED	tetramethylethylenediamine
TGF	transformation growth factor
TMRE	tetramethylrhodamine, ethyl ester
TNF- $\alpha$	tumor necrosis factor $\alpha$
TR-FRET	time resolved fluorescence resonance energy transfer
TRIS	tris(hydroxymethyl)aminomethane)
U	untreated cells (used in the legend of immunodetections)
UCP1	uncoupling protein 1
V	volt
v/v	volume per volume
w/v	weight per volume
Wnt	Wingless + Int 1 genes
YFP	yellow fluorescent protein



# SUMMARY

The storage of lipids as a reservoir for energy and biosynthetic building blocks is an important feature of organisms. The processes involved in storage and remobilization need to be tightly controlled as imbalances have severe organismic consequences and correlate with the prevalence of a variety of human diseases such as obesity, diabetes or atherosclerosis. Three novel small molecule inhibitors that interfere with cellular lipid storage processes by yet unknown mechanisms are in focus of this thesis. The three distinct chemotypes, currently named Chemotypes 1-3, provoke low storage amounts of cellular lipid droplets (LD) in oleic acid rich environments without impairing cytotoxicity. This lack of toxicity combined with excellent activities in the nanomolar range turns these small molecules into valuable tools in lipid research. Worldwide obesity rates and the associated health threats motivate the interest in a better understanding of the underlying metabolic networks which requires the availability of an extended chemical toolbox for directed lipid storage modulation.

These novel lipid storage modulators were originally identified in a quantitative high throughput screen (qHTS) of the *NIH small molecule repository library* following a classical forward chemical genetic design. This leaves the major question concerning the mechanism of action and the targeted cellular interaction partners unanswered. In this thesis, I tried to shed some light into this cellular *black box* by narrowing down affected pathways with the aim to identify and characterize the direct molecular target(s).

Early functional characterization of the investigated small molecules, revealed that the three Chemotypes show a translational activity in a broad set of mammalian cell lines despite of their original identification in a *Drosophila* cell based screen. This on the one hand highlights the suitability of *Drosophila* as an attractive model system for small molecule discovery campaigns with relevance to mammalian systems. On the other hand, it allowed early *in vivo* studies in (mutant) flies, which was advantageous in the later validation process.

The primary employed chemical proteomic strategy for the identification of the molecular target was based on a chemical affinity purification: The respective chemotype was applied as an affinity reagent to bulk protein mixtures. Subsequent mass spectrometric identification of co-purified protein binding partners and quantitative SILAC evaluation, led to the identification of four high priority protein targets for Chemotype 1. Unfortunately, none of those target candidates has so far been securely validated nor devalidated by subsequent functional assays ranging from RNAi based knock down to direct enzymatic tests. Nevertheless, experimental and literature derived functional

indications currently point toward a potential inhibition of the nucleotidase NT5DC1 or the soluble epoxide hydrolase (EPHX2) by Chemotype 1. This direction will be continued in future studies.

Widespread characterization of potentially involved physiological pathways to define the mechanism of action, led to the hypothesis that the diacylglycerol-O-acyltransferase isoforms (DGAT1/ DGAT2) are feasible target candidates for Chemotype 2. Functional inhibition of the DGAT1 catalyzed esterification of acyl-CoA fatty acids to available diacylglycerols subsequently confirmed this hypothesis. The inhibition of the enzymatic activity of DGAT1 by Chemotype 2 was further established in *in vivo* epistasis experiments with the fly homolog *midway*. These experimental findings were demonstrated by the interaction of recombinantly expressed, His-tagged DGAT1 and Chemotype 2 in cell based proximity labeling studies (PLA). Thus, a structurally novel DGAT1 inhibitor is presented as a likely direct target of Chemotype 2.

Besides the molecular characterization of the NIH instigated screening hits, two similar lipid droplet based high content screens were implemented in the COMAS screening facility of the Max-Planck Gesellschaft (MPG). Phenotypic, cell based hepatocyte and foam cell lipid droplet storage assays can now be performed on a routine basis. These assays will lead to future discoveries of novel lipid droplet modulators from a natural scaffold inspired compound collection.

The new set of lipid droplet storage modulators, will help to gain further information on the complex and not yet fully understood network involved in the regulation of lipid metabolism. Chemotypes 1 and 2 are expected to find broad application as new research tools and might even help to gather further knowledge, which will support future approaches in medical applications.

# ZUSAMMENFASSUNG

Die zelluläre und organismische Speicherung von Lipiden stellt ein effizientes Energiereservoir dar und liefert zudem Bausteine für die Synthese von verschiedenen Biomolekülen. Die involvierten Prozesse in der Lipidspeicherung und Remobilisierung sind engmaschig kontrolliert und bereits kleinste Ungleichgewichte können ernsthafte gesundheitliche Konsequenzen zur Folge haben. Eine erhöhte Lipidspeicherung korreliert zum Beispiel mit dem Risiko der Entwicklung von verschiedenen humanen Krankheiten, wie Adipositas, Diabetes oder Arteriosklerose. Im Fokus dieser Doktorarbeit stehen drei neu identifizierte niedermolekulare Verbindungen, die in der Lage sind die Lipidspeicherung durch aktuell noch unbekannte Mechanismen zu beeinflussen. Diese drei chemisch grundverschiedenen Substanzklassen, hier der Einfachheit halber *Chemotype 1-3* genannt, bewirken in Zellen die Abwesenheit von zellulären Lipidspeichern, obwohl die Zellen hohen Konzentrationen von Ölsäure ausgesetzt sind. Zeitgleich wird die Vitalität der Zellen nicht beeinträchtigt. Die neuen Inhibitoren sind hochpotent (nanomolare EC<sub>50</sub> Werte) und verursachen keinerlei Zytotoxizität. Diese Eigenschaften machen diese neuen niedermolekularen Verbindungen zu wertvollen Werkzeugen in der Erforschung der Lipidspeicherung. Dieser Forschungszweig ist unter anderem durch die weltweit stetig steigende Übergewichtsprävalenz und den daraus resultierenden gesundheitlichen Risiken motiviert. Es besteht ein großes Interesse an einem besseren Verständnis der zugrundeliegenden Fettspeichervorgängen und Kontrollmechanismen, sowie an neuen Methoden die erlauben, die involvierten metabolischen Prozesse gezielt zu beeinflussen.

Die hier untersuchten neuen Lipidspeicherinhibitoren wurden ursprünglich in einem quantitativen Hochdurchsatz Screen der NIH Substanzbibliothek (Bethesda, USA) in einem klassischen vorwärtsgerichteten chemisch- genetischen Versuchsaufbau identifiziert. Dieses Vorgehen ließ die Hauptfrage des Wirkmechanismus, sowie die Benennung der zellulären Zielproteine unbeantwortet. In der vorliegenden Doktorarbeit habe ich versucht etwas Licht in diese zelluläre *Black Box* zu bringen, indem ich potenziell beteiligte Stoffwechselwege identifiziert und potenzielle Zielproteine benannt habe.

In ersten funktionalen Experimenten wurde deutlich, dass die drei untersuchten *Chemotypes* eine translationale Aktivität in verschiedenen Säugerzelllinien besitzen, obwohl die niedermolekularen Verbindungen ursprünglich in *Drosophila* Zellen entdeckt und optimiert wurden. Diese Beobachtung verdeutlicht zum einen die Stärken von *Drosophila* als Modellsystem zur Identifizierung von bioaktiven Substanzen mit späterer Relevanz für Säugersysteme. Zum anderen erlaubte dieses System bereits erste *in vivo* Experimente zu einem frühen experimentellem Zeitpunkt. Diese waren für die spätere Zielprotein-Devalidierung von Vorteil.

Für die Identifizierung des direkten, molekularen Zielproteins der verschiedenen *Chemotypes*, wurde ein proteombasierter Versuchsansatz gewählt. Dieser basiert auf einer affinitätsbasierten

Anreicherung des Zielproteins. Hierzu wurde der zu untersuchende *Chemotyp* als Affinitätssonde in Gegenwart von Zelllysaten verwendet. Die über die Interaktion mit der niedermolekularen Verbindung angereicherten Proteine wurden per Massenspektrometrie identifiziert und anhand der SILAC Methode quantifiziert (SILAC für Englisch *stable isotope labeling of amino acids in cell culture*). Für Chemotyp 1 konnten mit diesem Ansatz vier potenzielle Zielproteine identifiziert werden. Gegenwärtig konnte jedoch keines dieser Zielproteine mit Sicherheit validiert oder devalidiert werden. Zur Validierung wurden verschiedene funktionale Experimente wie RNA Interferenz oder Tests für die jeweilige Enzymaktivität herangezogen. Gegenwärtig sind die Nucleotidase NT5DC1 und die lösliche Epoxidhydrolase (EPHX2) zwei interessante Zielprotein-Kandidaten für Chemotyp 1. Die genauen zugrundeliegenden Mechanismen einer potentiellen Beteiligung an dem beobachteten lipidtröpfchenreduzierten Phänotyp müssen jedoch noch geklärt werden.

Die umfassende funktionale Analyse von möglicherweise betroffenen Stoffwechselwegen hat zu der Annahme geführt, dass die Diacylglycerol-O-Acyltransferasen (DGAT1/ DGAT2) mögliche Zielproteine von Chemotyp 2 sein könnten. Die Isoenzyme katalysieren den finalen Schritt der Triacylglyceridsynthese. Experimentell konnte eine funktionale Inhibierung der DGAT1 Enzymaktivität durch Chemotyp 2 gezeigt werden. Eine zusätzliche Bestätigung eines DGAT1 basierten Phänotyps wurde durch *in vivo* Epistasie-Experimente in Deletionsmutanten des DGAT1 Fliegenhomologs *Midway* erbracht. Schlussendlich konnte die direkte Interaktion von Chemotyp 2 und rekombinantem His-getagtem DGAT1 auf molekularer Ebene in einem zellulären, bildbasierten Experiment nachgewiesen werden, das auf enger räumlicher Nähe der Interaktionspartner beruht (*Proximity Ligation Assay*; PLA). Die Kombination dieser Ergebnisse legt nahe, dass Chemotyp 2 eine neue Strukturklasse von DGAT1 Inhibitoren darstellt.

Neben der molekularen Charakterisierung der ursprünglich am NIH identifizierten niedermolekularen Verbindungen wurden noch zwei weitere fetttröpfchenbasierte Screens im COMAS, der Screening- Abteilung der Max-Planck Gesellschaft (MPG), etabliert. Es ist nun routinemäßig möglich die stetig wachsende naturstofforientierte Substanzbibliothek des COMAS in sowohl Hepatozyten- wie auch Schaumzell- Bildbasierten- Assays auf neue Fettspeichermodulatoren zu testen.

Der neue Satz an Modulatoren der Lipidspeicherung wird zukünftig helfen weiterführende Informationen des komplexen und nicht vollständig entschlüsselten metabolischen Netzwerks der Lipidspeicherung zu gewinnen. Die Chemotypen 1 und 2 werden erwartungsweise zukünftig vielfältige Anwendung in der Beantwortung wissenschaftlicher Fragestellungen finden, und vielleicht sogar dazu beitragen neue Ansätze für medizinische Anwendungen zu liefern.

## CHAPTER 1: GENERAL INTRODUCTION

# THE NEED FOR NOVEL LIPID STORAGE MODULATORS

Fine-tuned lipid storage processes are utterly important in living organisms ranging from bacteria, to plants, over non-vertebrates to humans. Lipids are stored in specialized organelles and the involved storage and remobilization processes are tightly regulated in not yet fully understood pathways (see summary in Chapter 2). If the system loses its balance, severe consequences can be observed on multiple layers: most famous is probably obesity as a form of (severe) lipid overstorage. The overstorage correlates with increased risks for a multitude of diseases commonly summarized as the metabolic syndrome (Prasad and Ramesh, 2014; Guebre-Egziabher et al, 2013). Obesity even correlates with the likelihood to develop certain kinds of cancer (Lee et al, 2014) and favors the formation of atherosclerotic plaques (Yoo & Choi, 2014; Rohla & Weiss, 2013). However, the opposite phenotype as seen in lipodystrophy, which is characterized by the lack of stored lipids, also results in health-diminishing conditions (Freitas & Carvalho, 2013).

Aside of disease pathologies defined by lipid over- and understorage, lipid storage processes essentially impact various other pathways. The hepatitis C virus and Rotavirus, for example, rely on the presence of lipids for viral reproduction (Cheung et al, 2010; Herker & Ott, 2011). Modulation of the accumulated lipids is a promising treatment strategy (Ploss & Dubuisson, 2012). Lipid storage in plants on the other hand is targeted in raw oil production, as higher lipid yields within plants and algae relate to a decrease in the required arable land (Andrianov et al, 2010).

Pharmacological and industrial interest in new chemical modulators of lipid storage presents a broad research area, with many questions to solve. New lipid storage modulators will help to increase the understanding of the complex and not yet totally understood interactions in lipid metabolism and storage processes. In this first introductory chapter obesity and its current therapeutic treatment approaches are summarized, in order to highlight that a better understanding of the mechanisms of action is required as well as new specific modulators.

### 1.1 OBESITY- A CONSEQUENCE OF LIPID OVERSTORAGE

Obesity is the most famous form of lipid overstorage. Health concerns, media propagations and self-esteem issues force our body fat content constantly into focus, pointing out a multilayered misbalance in energy expenditure and energy consumption arising from (significant) life style changes in the last century. This pandemic like spreading of obesity (Vickers, 2014) is partly enabled by the overavailability of food to which our metabolism (and mind) are not adapted. Since 2013, obesity is now officially classified as a disease by the *American Medical Association (AMA)* in order to draw global attention towards the associated risks and to request medical approaches in new obesity treatment and prevention strategies (Breymaier, 2013).

Looking at fat storage from an evolutionary point of view, it has commonly been advantageous to store excess lipids as soon as a surplus of nutrition was available (Speakman, 2013). Lipids are the long term storage molecule of choice, since they present the densest energy load possible. The energy reservoir holds an evolutionary advantage to lean individuals in times of food shortage. Furthermore, the lipid stores present a pool of biosynthetic building blocks for membranes and hormones, which are necessary for the solubilization of hydrophobic vitamins (A, D, E, K; Gonnet et al, 2010), to keep the body temperature constant by either insulation or heat production (Marshall, 1961; Diaz et al, 2014) and additionally mechanically protect important organs (Cassisa, 2013). Especially in western life styles, involuntarily caloric restriction is not widespread anymore. Instead sugar and/or fat loaded food is easily available. At the same time, the (need of) energy expenditure was drastically decreased for broad parts of the population. The sedentary life style is rarely able to compensate the increased energy consumption. Under these conditions the long earned evolutionary security system gets imbalanced which results in weight gain over time (Speakman, 2013). This is especially true in such a fine tuned and efficient system as the metabolism: for example only 25 excessive calories a day, which equals an apple every three days, can rise the body weight by 50 kg after 40 years (Nestle, 2007).

Severe forms of lipid overstorage causes ectopic lipid accumulation in nearly all kinds of cells and therewith triggers the risk for a multitude of diseases. Obesity significantly increases the risk in morbidity and mortality relative to lean individuals and can be correlated to insulin resistance, type 2 diabetes, non-alcoholic fatty liver disease, atherosclerosis, ischemic heart disease, strokes, degenerative disorders such as dementia, many instances of cancers, hormonal imbalances or infertility and an overall pro-inflammatory state. These symptoms can be summarized in the metabolic syndrome (reviewed in Lopez-Jimenez, 2009; Guebre-Egziabher et al, 2013).



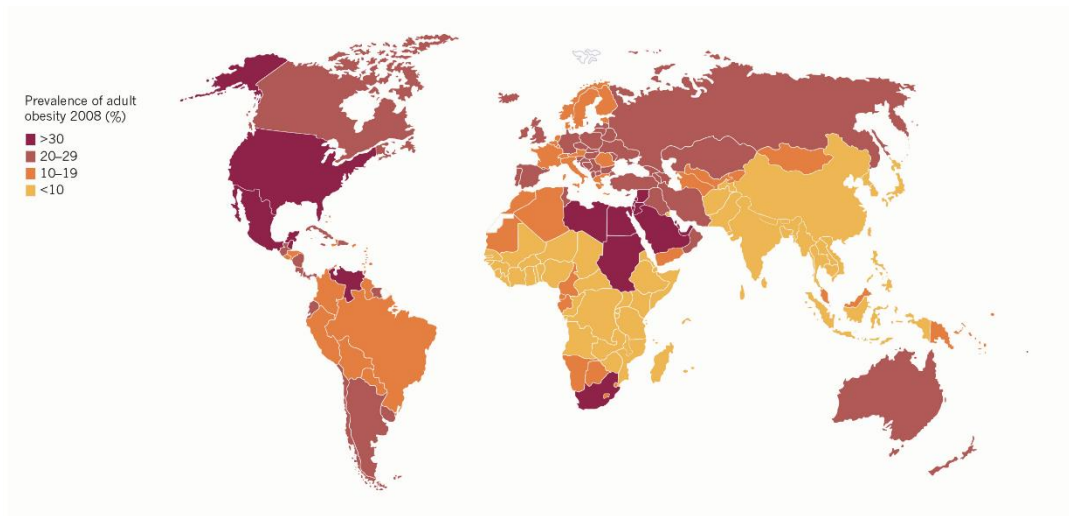


**FIGURE 1: Worldwide prevalence of obesity** has nearly doubled from 6.4% in 1980 to 12.0% in 2008. Half of this rise occurred from 2000 to 2008. The grade of lipid storage can be classified by the body mass index (BMI in  $\text{kg}/\text{m}^2$ ) which can range from underweight (BMI  $<18.5$ ) to (severely) obesity (BME  $> 30$ ). (Figure modified from Scully, 2014; original study by Stevens et al, 2012)

Obesity and its consequences are approaching epidemic proportions in the US and many other industrialized countries as summarized in Figure 1. Nowadays, the prevalence of obesity exceeds 30% of the US population with an even increasing tendency. From 1980 on the prevalence of obesity has increased two-fold in adults and about threefold in children and adolescents (Lakshman et al, 2012). It is estimated that 2.8 million deaths each year are obesity related (Scully, 2014). This implies even higher numbers of patients suffering from the consequences of obesity and thus generates high health care costs which range between \$147 and \$210 billion per year in the US (Finkelstein et al, 2009) and count for nearly 10 percent of all annual medical spending. If the current trend in obesity prevalence continues, the total healthcare costs attributable to obesity could reach from \$861 billion to \$957 billion by 2030 (Mahgerefteh et al, 2013). These costs will severely impact worldwide economics.

New therapy methods, such as a broader awareness of (healthy) food consumption, a change of lifestyle especially motivated for an increased energy expenditure, a reduction of stress and at last measure options for medical treatment, are thus required.

## 1.2 CURRENT APPROACHES IN OBESITY TREATMENT

Lifestyle modification is the first and mainstay treatment for obesity (Mahgerefteh et al, 2013). However, when the medical compliance is not given or possible, such as in severe obesity reaching immobility or in cases of paraplegia, as well as underlying genetic predispositions, the pharmacological treatment might help to intervene with further weight gain or to enhance weight loss on a molecular level. At the same time, pharmacological modulation of the tightly controlled metabolic network is commonly associated with a wide range of severe side-effects (Colon-Gonzalez et al, 2013; Kim et al, 2014). Thus, most of the drugs do not reach approval by *the US Food and Drug Administration* (FDA) and the *European Medicines Agency* (EMA) or were withdrawn after years on the market.

Currently, three drugs keep FDA approval for the treatment of obesity: Orlistat (Xenical), PHEN/TPM (ER Qsymia; VIVUS) and Lorcaserin HCl (Belviq; Arena Pharmaceuticals). Different modes of action and the accorded risks of some anorexic agents are summarized in the following subchapter and in Figure 2.

### 1.2.1 Targeting Obesity via Peripheral Pathways

The “easiest way” to shift the lipid metabolism towards energy expenditure is to directly block lipid uptake. The lack of dietary fat is compensated by remobilizing existing lipid stores. The FDA approved drug Orlistat<sup>1</sup> (Xenical) is the saturated derivate of the naturally occurring lipstatin which inhibits gastric lipases (see Figure 2). The block of dietary lipid uptake within the gastrointestinal tract leads to a caloric imbalance induced body weight reduction (Sjostrom et al, 1998). Orlistat treatment has to be accompanied with low-fat diet, since gastrointestinal imbalances expressed in oily stools and fecal urgencies are triggered (Sjostrom et al, 1998; Davidson et al, 1999).

In the past, protonophores were used to increase the energy expenditure and heat production by uncoupling of the mitochondrial membrane by bypassing the ATP synthase. 2,4-Dinitrophenol (DNP) was a famous ingredient in the 1930s, but was ultimately banned from human use due to lethal overdoses, increasing numbers of cataracts, extensive hyperthermia and other severe side effects (Colman, 2007). Nevertheless, the mechanism of actions still remains under investigation as a potential principle for pharmacological interventions (Harper et al, 2001).

---

<sup>1</sup> Cobese (Ranbaxy Laboratories Ltd), Nipocut (Neelkanth Healthcare), O Trim (Grace Drugs Pharmaceuticals), Obelit (Intas Pharmaceuticals Ltd.), Obree (Bioplasmalmmunological Research), Obitol (Carsyon), Olisat (Biocon), Orlica (Azuca), Orlimac (Macleods Pharmaceuticals), Oritroy (Troikaa Pharmaceuticals), Reeshape (Meyer Organics), Troyslim (Troikaa Pharmaceuticals), Vyfat (Intas Oharmaceuticals), Zerofat (Mankind Pharmaceuticals)

### 1.1.2 Targeting Obesity via Hypothalamic Neuroendocrine Pathways

Another approach to suppress weight gain is by interference with the sympathomimetic system. Current pharmacotherapies base on intentional adjuvment of the hormonal circuits either from the gut (stomach, small intestine, and pancreas) or the adipose tissue via the hypothalamus. The hypothalamus regulates the satiety and emits both hunger and stress signals at the same time, thus affecting energy uptake and expenditure. As a trade-off these drugs are often psychoactive and known anti-depressants, which was associated with a number of physical and psychological side effects (Cabrerizo Garcia et al, 2013; Manning et al, 2014). This resulted in a number of drug approvals and subsequent withdrawals over the recent years.

Amphetamine- related drugs such as Phentermine-HCl<sup>2</sup> (Adipex-P, see Figure 2) cause a non-selective norepinephrine release in the hypothalamus, which stimulates stress signals and thereby decreases the sensation of hunger. At the same time, the release of adrenaline and epinephrine is stimulated, which increases the reduction of existing lipids by  $\beta$ -oxidation (Kaplan, 2010). Generic variants of Phentermine are still on the market, while the original drug was withdrawn by the FDA in 1998 due to various side-effects including tachycardia, nervousness and diarrhea (FDA Release, 1997).

Another CNS- dependent target is the serotonin pathway, which regulates appetite and mood. Sibrutamine<sup>3</sup> (Knoll Pharmaceuticals, Abbott Laboratories, see Figure 2) is a serotonin-norepinephrine reuptake inhibitor that increases satiety (Araújo & Martel, 2012). An alternative way to increase the serotonin level is the disruption of vesicular neurotransmitter storage as targeted by Fenfluramine<sup>4</sup> (Adifax, see Figure 2) (Kaplan, 2010). Reduced side effects were observed when the affinity towards the 5-HT<sub>2C</sub> serotonin receptors was increased as approached in the new drug Lorcaserin-HCl<sup>5</sup> (Belviq; Arena Pharmaceuticals), which was approved in 2012 (Mahgerefteh et al, 2013). Soon after marketing, however, safety concerns were announced by the *European Committee on Human Medicinal Products* (CHMP) regarding the potential risk of tumors and psychiatric disorders connected with long-term use of Lorcaserin (EMA, 2013; Manning et al, 2014).

Other promising targets for the pharmacotherapy are confined to the endocannabinoid system. Inverse agonists for the cannabinoid receptor CB<sub>3</sub>, such as Rimonabant<sup>6</sup> (Acomplia, see Figure 2) have anorectic properties by reducing the appetite and therewith effectively cause weight-loss (Pi-

---

<sup>2</sup> Adiphen, Anoxine-AM, Ionamin, Duromine, Metermine, Mirapront, Obephen, Obermine, Obestin-30, Phentermaxx, Phentrol, Phenterex, Phentromin, Pro-Fast SA, Razin, Redusa, RANbesy, Phentermine Tenker, Obenix, Oby-Trim, Teramine, Zantryl, Sinpet, Supremin, Suprenza, Umine Wiltmine

<sup>3</sup> Meridia, Reductil, Butramin

<sup>4</sup> Adifax, Ponderax, Pondimin

<sup>5</sup> Belviq, Lorqess

<sup>6</sup> Acomplia, Rimoslim, Riobant, Slimona, Zimulti

Sunyer et al, 2006; Fong & Heymsfield, 2009). Rimonabant was originally developed as a smoking cessation drug (Cahill & Ussher, 2007), but strong addictive behavior, mood changes, depression and suicidal thoughts finally resulted in the withdrawal of the drug (FDA Release, 2007).

In addition to single drug prescriptions, several combinatorial therapies are available or under development. Combinatorial therapies have the advantage that the individual drug concentration can be lowered, which results in less severe adverse side effects (Lee et al, 2007). At the same time, the potency can be often increased by synergistic or complementing mechanisms of action. Once in a while, combination concoctions reach FDA approval. Flu-Phen (Pondimin), for example, consists of Fenfluramine and Phentermine. Despite its good activity, it was soon voluntarily removed from the market due to cardiovascular side effects (FDA, 2007). A newly accepted (2012) drug mixture is PHEN/TPM (Qsymia; VIVUS), which combines Phentermine and the antiepileptic drug Topiramate. It combines the sympathomimetic stimulation of phentermine and an enhanced GABA (gamma aminobutyric acid) activity by Topiramate, which influences voltage dependent ion channels. So far, this approach shows good progress in clinical studies (Fidler et al, 2011), even if both therapeutics separately show individually severe side effects (Nathan et al, 2011).

Since the application of most investigated anti-obesity drugs is hampered by severe side effects, a growing trend in off-label use of approved drugs can be observed. Famous examples are the diabetes drugs Pramlintide (Symlin<sup>®</sup>, AstraZeneca) or Liraglutide (Victoza<sup>®</sup>; NovoNordisk). It was found that the pancreatic peptide analogues do not only regulate the blood glucose levels as intended in diabetes treatment, but also slow the gastric emptying and additionally promote satiety via hypothalamic receptors (Dunican et al, 2010). Liraglutide reduces food intake by increased satiety signals in the brain. It showed good first results in clinical studies (Astrup et al, 2012; Novo Nordisk-Company Announcement, 2013), but both FDA and EMA are currently investigating safety concerns in connection with a possible increased risk for pancreatic cancer (Egan et al, 2014).

### 1.1.3 Supplemental Therapy

In cases where genetic causes are responsible for the lipid storage disorder, replacement of the defect or absent enzyme is a suitable therapy approach. One positive example to treat not obesity, but the opposite disorder lipodystrophy (i.e. the lack of fat tissue either due to deficiency or destruction of adipose cells) presents Metreleptin, which got FDA approval in 2014. Absence of fat tissue correlates with decreased leptin levels, signaling the body to rise caloric intake resulting in

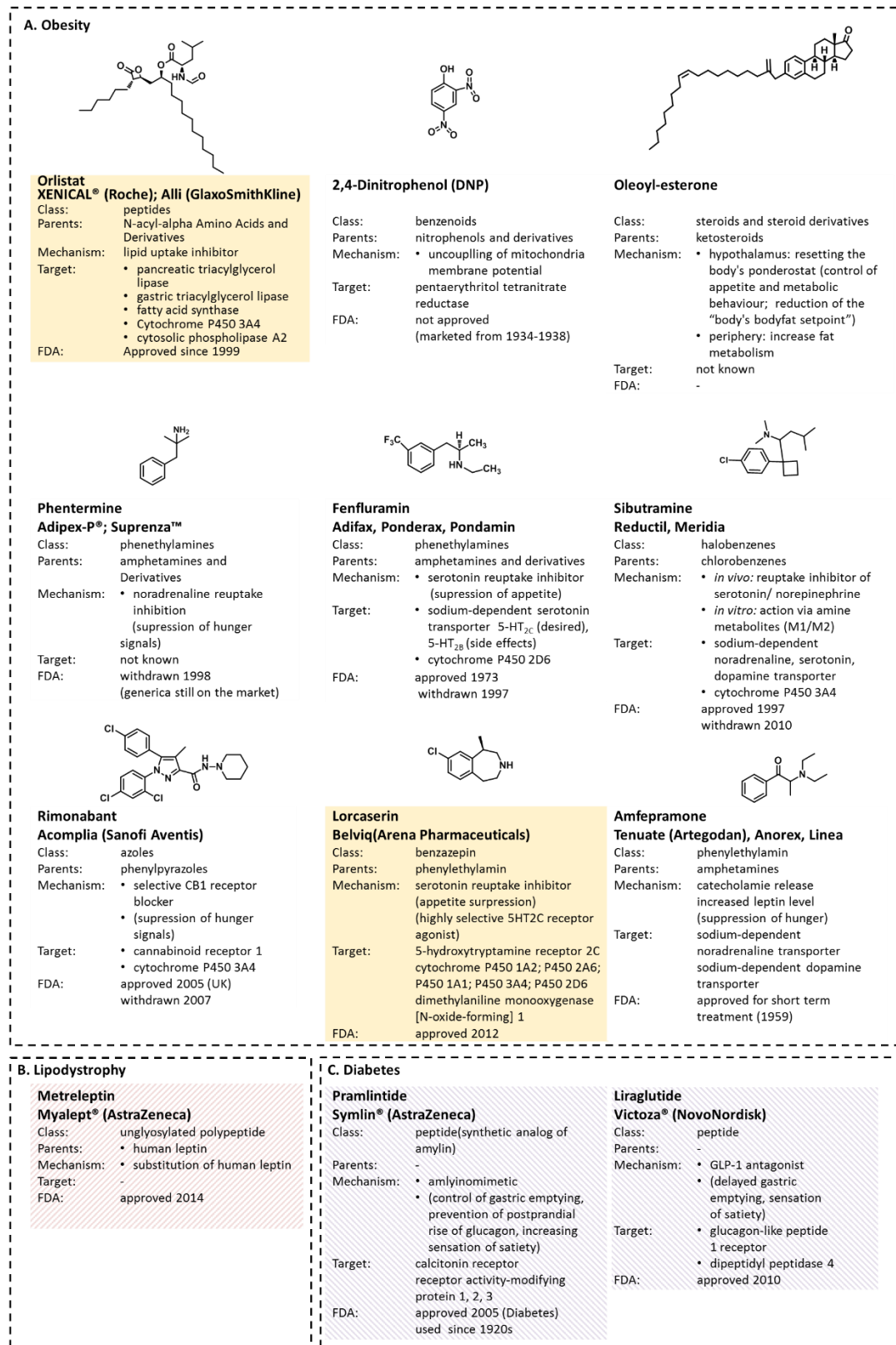


**FIGURE 2: Summary of selected anti-obesity drugs approved or withdrawn from the market. AI** Small molecules for the treatment of obesity. **BI** A newly approved pharmacological peptide for the treatment of lipodystrophy. **CI** Off-label used anti-diabetes drugs that reduce body weight. Yellow boxes indicate FDA approval. (Data source: DrugBank, www.drugbank.ca/; and FDA, www.fda.gov/Drugs/default.htm).

severe metabolic disturbances (Oral et al, 2002). The drug is an analogue of the human hormone leptin and can restore the normal body function by regaining leptin signals. This improves insulin sensitivity, hypertriglyceridemia and hyperglycemia (Chou & Perry, 2013).

Following a similar molecular process, oleoyl-estrone (OE) was considered as a potential anti-obesity drug in the last decade. OE is a fatty acid ester of an estrogenic hormone produced in the ovaries and adipose tissue. In non-obese individuals OE levels correlate with body fat storage amounts, while the level drops in obese patients. It was suggested that OE supplementation rises the plasma OE level to normal, which signals the body the presence of excess of bodyfat levels which allows the body to recognize the lipid stores as an energy source again. First studies implicated successful fat loss after short treatment times. Even after the medication was stopped, animals maintained their body weight (Remesar et al, 2012; Sanchis et al, 1996). However, late clinical studies could not confirm these findings and were stopped in 2007 since no statistical significance over the placebo control group was documented (Manhattan Pharmaceuticals, 2007).

## **CHAPTER 1:**

The summary of the current approaches in obesity treatment emphasizes the need for new therapeutic strategies and the discovery of novel, highly specific molecules which lack prominent side effects. High hopes are allied to the identification of novel cellular (protein) targets, which on one hand would allow a better understanding of lipid storage pathways and might on the other hand lead a way to new approaches in direct or supplemental therapy. Cellular targets have the advantage that side effect-prone hypothalamic or neuroendocrine pathways are likely excluded from the mechanism of action. In order to identify such novel targets, three small molecules which were indentified in a previous cell based lipid storage screen were characterized in this thesis. To follow the chosen experimental approaches, a better and more detailed understanding of lipid metabolism and its underlying storage organelles is required. A current overview of the literature of lipid droplets which are the main intracellular storage organelles is summarized in the following Chapter 2.

## CHAPTER 2: THEORETICAL BACKGROUND

## LIPID DROPLETS- THE LIPID STORAGE ORGANELLES

The storage of lipids as a reservoir for energy and biosynthetic building blocks is an important feature of all organisms (Murphy, 2001). In multicellular organisms, storage lipids are enriched in specialized tissues such as the mammalian adipose tissue. However, if cells are stressed with excess amounts of free fatty acids (FFAs), presumably all cell types can store lipids in form of lipid droplets (LD) (Rasouli et al, 2007).

LDs have a very simple, highly conserved and unique structure (see Figure 3.A). They are composed of a hydrophobic core of neutral lipids, which are predominantly sterol esters (SE) and triacylglycerol (TAG), surrounded by a phospholipid monolayer. Lipid droplet specific proteins are anchored or embedded in the phospholipid monolayer and allow active interaction of LDs in cellular metabolism. LD surface proteins, for example, execute many of the reactions involved in lipid storage (LD expansion) or mobilization (LD shrinkage) (Wilfling et al, 2014).

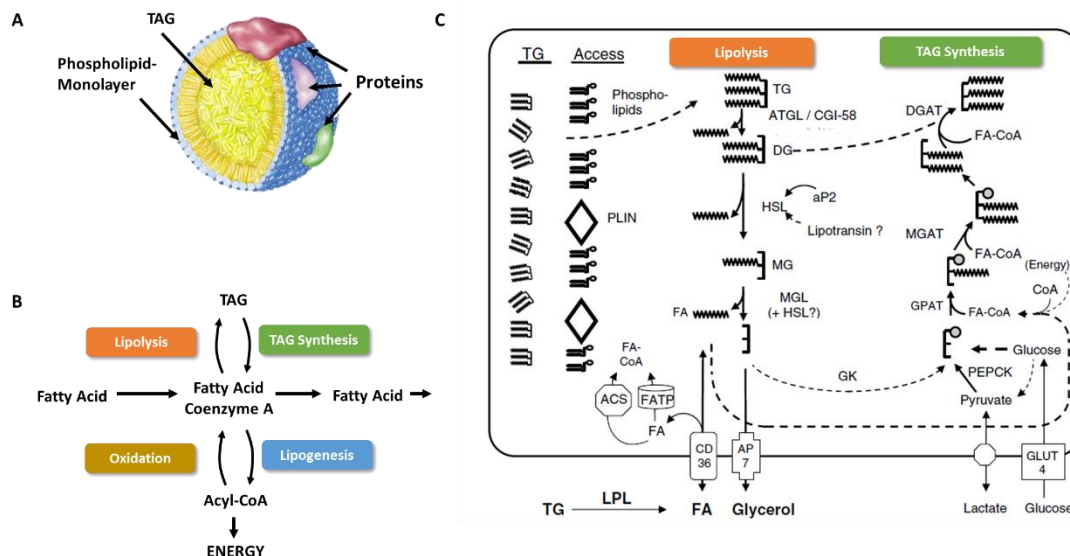


**FIGURE 3: Lipid droplets in closer detail** **AI** Schematic structure of a lipid droplet. Cellular lipid stores have a simple but unique structure. Hydrophobic neutral lipids (yellow) build the core of a lipid droplet, which is surrounded by a phospholipid monolayer (blue) incorporating various specific proteins (red, violet, green). **BI** Lipid droplet formation strongly depends on the level of TAG synthesis and TAG lipolysis. The key metabolites in this step are coenzyme A activated fatty acids. **CI** Detailed summary of the coordination of TAG lipolysis and TAG synthesis. (Images were adapted from AI Mathias Beller, 2005; Images B& CI Wang et al, 2008).

While LDs of diverse organisms such as bacteria and humans share this simple blueprint, the various needs of different cell types result in differences in LD size and cellular distribution. In adipocytes, which are specialized for lipid storage, unilocular LDs occupy the majority of the cell volume and reach up to a diameter of 100  $\mu\text{m}$  (Krahmer et al, 2011). LDs in non-adipocytes are significantly smaller and remain around 1  $\mu\text{m}$  in diameter and rarely exceed 10  $\mu\text{m}$  under non-pathological conditions (Suzuki et al, 2011).

Based on their simple structure, LDs were ignored for a long time as static, spontaneous accumulations of hydrophobic lipids within cells (Farese & Walther, 2009). This view changed and nowadays the LD formation (Andersson et al, 2006), the oriented movement (Zehmer et al, 2009; Gross et al, 2003) and the regulated degradation (Smirnova et al, 2006; Grahn et al, 2014) are known to be tightly controlled. Yet, the underlying LD formation and degradation process is not yet fully understood. The close interaction of lipid biogenesis and lipolysis is schematically summarized in Figure 3.B-C. The LD lifecycle, however, gained even more complexity as it was proposed that LDs operate not only as lipid storage organelles, but also serve as a short and long term storage for proteins (Cermelli et al, 2006). During protein biosynthesis or degradation the LDs serve as a platform to prevent proteins from aggregation and support controlled protein degradation (Fujimoto & Ohsaki, 2006). LDs additionally interact with other cellular organelles such as peroxisomes and mitochondria (Wang et al, 2011) or are important for viral replication (Ogawa et al, 2009). Altogether, these recent findings put LDs at the nexus of cellular signaling, cellular and organismic lipid storage regulation. As a consequence LDs are now acknowledged as true organelles (Martin & Parton, 2006; Beller et al, 2010).

## 2.1 THE LIFE CYCLE OF LIPID DROPLETS

The generation of LDs strongly depends on the nutritional load of the cell's surroundings. Proteins directly located at the LD surface execute many of the reactions in lipid storage or mobilization by mediating TAG synthesis and hydrolysis. As a consequence the LD expands or shrinks, respectively (Wilfling et al, 2014). However, the exact underlying processes have not been revealed yet (Wilfling et al, 2013). Strong indications point towards LD biogenesis at the endoplasmic reticulum (ER), as many TAG biosynthetic enzymes were found in the ER (Buhman et al, 2001) and a close proximity between LDs and the ER is observed in electron micrographs (Kuerschner et al, 2008; Rodgers et al, 2012; Robenek et al, 2006). It was additionally hypothesized that LDs remain in contact with the ER once they are formed and thereby allow proteins that associate with both compartments to move between LD and ER (Jacquier et al, 2011; Beller et al, 2010; Thiam et al, 2013).



Most of the different existent models for LD generation have in common that they propose LD formation from the ER to the cytosol. Specialized cells, such as enterocytes and hepatocytes are additionally capable to form lipoproteins within the ER lumen, which are intended for secretion and partition of dietary fats throughout the body (Yen et al, 2008). Most models start with an initial lens-shaped accumulation of TAGs (or sterol esters) within the ER bilayer. At some point, the growing structure is predicted to bud off the ER, forming a lipid droplet (Thiam et al, 2013). The alternative “eggcup” model postulates that the LDs are formed in concave depressions of the ER (Robenek et al, 2006). Another biophysical view proposes a wetting and de-wetting process, known from studying emulsions, as the fundamental process in LD genesis, driven by the force of an optimal surface tension in LDs (Thiam et al, 2013).

Once formed, cytosolic LDs can increase their volume either by localized lipid synthesis (Kuerschner et al, 2008) or by fusion of LDs (Bostrom et al, 2007). Cell type-dependent LDs are able to grow dramatically (e.g., up to 9-fold increased adipocyte LD volume within hours in case of a nutritional surplus (Krahmer et al, 2011).

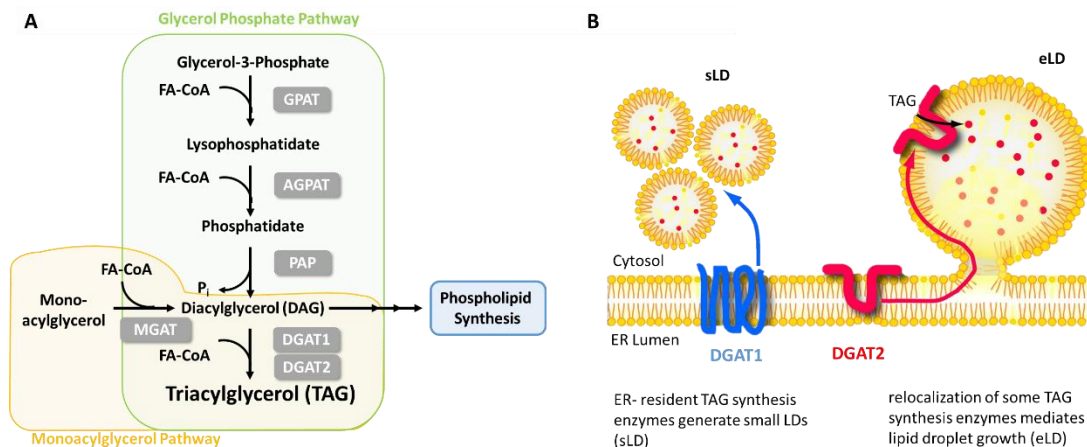


**FIGURE 4: TAG synthesis leads to the generation of LDs** **A** TAGs are synthesized by two distinct biochemical pathways which share the DGAT enzymes in the final synthesis step. (GPAT: glycerol-phosphate acyltransferase; AGPAT: acylglycerol-phosphate acyltransferase; PAP: phosphatidic acid phosphohydrolase; MGAT: acyl CoA:monoacylglycerol acyltransferase; DGAT: diacylglycerol-O-acyltransferase; FA-CoA: fatty acid coenzyme A.) **B** Protein distribution to LD subsets lead either to small LDs (sLD) or expanding LDs (eLD). The two LD types are presumably a result of TAG synthesis and the different localization of the involved enzymes. (Images were adapted from AI Yen et al, 2008 and BI Wilfling et al, 2013, which was modified according to information from Thiam et al, 2013)

The enzymes involved in the lipogenic reaction cascade (see Figure 4.A) are widely conserved. *De novo* synthesis of TAG mostly follows the Kennedy Pathway (Glycerol phosphate Pathway; Kennedy 1957), which is present in most cells. The monoacylglycerol pathway in contrast is only found in specific cell types such as enterocytes, hepatocytes and adipocytes and focuses on the re-esterification of fatty-acid coenzyme A (FA-CoAs) to previously hydrolyzed TAG. (Xia et al, 1993). Both pathways strongly depend on the presence of activated forms of FA-CoA, which is synthesized by various intracellular acyl-CoA synthetases. Both pathways share the final catalytic step is carried out by the two diacylglycerol-O-acyltransferase isoforms (DGAT1/ DGAT2). It was postulated that the DGAT1 remains ER bound and is essential for the generation of new small LDs, while DGAT2 is found in the ER as well as attached to expanding LDs and thus is mainly involved in the local TAG synthesis (Thiam et al, 2013). The isoenzymes are well-studied targets for pharmacological intervention in lipid storage modulation, as they catalyze the proposed rate-limiting step in TAG biosynthesis (Birch et al, 2010; Matsuda & Tomoda, 2010). Early DGAT1 inhibitors were patented in 2003 by a Japan Tobacco/Tulark collaboration (Fox et al, 2003). Structurally similar DGAT1 inhibitors were often derived from this tool compound T863, as for example PF-04630220 (Pfizer; Dow et al, 2011) or AZD7687 (AstraZeneca; Barlind et al, 2012). A selection of literature described DGAT1 inhibitors is summarized in Supplemental Figure 11 (p.206).

The formation and degradation of LDs is in a constant turnover, which allows a flexible response to the nutritional situation on a cellular level. In times of starvation, excess lipids are mobilized by stimulated lipolysis in order to generate energy. As a result the individual LD shrinks and the overall LD number decreases. Stimulated lipolysis is best studied in mammalian adipocytes as reviewed in Lass et al (2011). TAGs are sequentially hydrolyzed by the adipose triglyceride lipase (ATGL), the hormone sensitive lipase (HSL) and monoacylglycerol lipase as summarized in Figure 3.C. In a hormone regulated process, mostly dependent on catecholamine signaling via  $\beta$ -adrenergic receptors, protein kinase A (PKA) is activated and coordinates various cellular processes (Djouder et al, 2010). The conversion of TAG to DAG by ATGL is fine-tuned by either activation via CGI-58 ( $\alpha/\beta$  hydrolase domain-containing protein 5 (ABHD5); Yamaguchi, 2010) or inhibition by the G0S2 (G0/G1 Switch Protein 2; Heckmann et al, 2013). The liberated FAs can either be re-esterified to TAG, can be used in energy production via  $\beta$ -oxidation, can act as second messengers (especially DAGs; Yang & Kazanietz, 2003) or can be converted into building blocks for membranes.

As LDs are surrounded by a unique phospholipid monolayer, the membrane component is another important feature in the life of LDs, as the membrane has to be able to adapt flexibly during LD formation and shrinkage (Brasaemle, 2011). On the one hand, the membrane composition is defined by the percentage of incorporated lipid classes and has an influence on the LD physiology itself. On the other hand, the membrane tension as a result of LD size as well as the kind and the quantity of incorporated proteins has a regulatory function. It was hypothesized that shrinking LDs suffer from protein crowding and with an increased surface tension the proteins are more likely to fall off, presumably dependent on their binding motives (Thiam et al, 2013; Wilfling et al, 2014). This presents new aspects in biophysical based modulation of LDs.

## 2.2 LIPID DROPLETS DEPENDENT DISEASE PATHOLOGIES

### 2.2.1 Lipid Droplets in Atherosclerosis

The high morbidity risk of obesity primarily results from hypertension and cardiovascular diseases and is often caused by atherosclerosis (Yoo & Choi, 2014; Rohla & Weiss, 2013). This is a pro-inflammatory condition that enhances leukocyte infiltration into the vascular endothelium, causing a release of cytokines, tumor necrosis factor- $\alpha$  (TNF- $\alpha$ ) and plasminogen activator inhibitor type 1 (PAI-1), which directs mono- and leucocytes to the endothelium. Monocytes infiltrate the endothelial walls, phagocytize excess lipoprotein particles and thus become foam cells that are highly loaded with LDs that are enriched in cholesterol and arachidonic acid (Siegel-Axel et al, 2008). Cytokines secreted by foam cells cause endothelial proliferation and harden the vasculature, which increases the number of fibrin clots by PAI-1 inhibition. Subsequently, the risk of atherosclerotic plaque formation increases, which either clots the vessel or travels in the bloodstream to remote body parts and causes embolisms (Yuan et al, 2012). Macrophage LD formation is a result of known enzymes, such as ACAT (Acyl-coenzyme A cholesterol O-Acyltransferase) and DGAT (diacylglycerol-O-acyltransferase 1) (Walther & Farese, 2012), which were subsequently studied for their potential for pharmaceutical intervention in atherosclerosis and obesity treatment (Tomoda & Omura, 2007).

### 2.2.2 Lipid Droplets and Pathogens

Some infectious diseases can be tied to LD function, as the LDs are utilized by various pathogens. The life cycle and replication of hepatitis C virus (HCV), for example, strongly depends on the presence of LDs in liver cells (Herker & Ott, 2011). The virus uses LDs and ER membranes during viral RNA packaging, the secretion of the complete virus as part of the lipoproteins or as a store of HCV core proteins during virus assembly (Walther & Farese, 2012). The latter requires DGAT1 activity and

it was observed that blocked DGAT1 activity led to diminished viral replication. This might indicate a new therapeutic approach in HCV treatment (Herker et al, 2010). A similar LD dependent replication cycle was observed for the Dengue virus (Carvalho et al, 2012). Other pathogens, such as *Chlamydia trichomatis* (Cheng et al, 2014), *Mycobacterium tuberculosis* (Daniel et al, 2011) and *Mycobacterium leprae* (Mattos et al, 2010).

### 2.2.3 Lipid Droplets and Steatosis

LD proteins are closely related to the pathophysiology in the fatty liver diseases such as in nonalcoholic fatty liver disease (NAFLD; Goh & Silver, 2013). Lipid overstorage within the liver can be correlated to the prevalence of insulin resistance (Brown & Goldstein, 2008) and cancer (Hill-Baskin et al, 2009). FAAs from the diet or adipocyte lipolysis lead to an accumulation of neutral lipids in LD in hepatocytes and induce PPAR $\gamma$  expression that regulates the presence of a number of LD associated proteins. Among those proteins, especially members of the Perlipin (Plin) family are tightly regulated (reviewed by Okumura, 2011). Important regulative functions were associated with the concentration of the adipose differentiation-related protein (Plin2; McManaman et al, 2013) or the fat-specific protein 27 (FSP27; Xu et al, 2014). At the same time, LD associated lipase activities are also correlated with higher risks of NAFLD, as seen in mutation studies as ATGL (Wu et al, 2011) or PNLPA3 (He et al, 2010). As the presence of LDs is pivotal for the development of steatosis, LD modulation by small molecules might support new treatment strategies.

## CHAPTER 2:

This chapter summarized some aspects of the current knowledge and working models involved in the tightly regulated life cycle of LDs and additionally highlighted the pharmaceutical interest in LD modulators. It points to the necessity of new research tools which will lead to a better understanding of the cellular mechanisms involved. Since small modulators present a commonly used tool in academia, this project aimed for the detailed characterization of novel small molecules, which were identified in a previous cell based screen. The chosen approach for the target identification will be summarized in the following Chapter 3: History and Purpose of the Project.

## CHAPTER 3: HISTORY AND PURPOSE OF THE PROJECT

**CHARACTERIZATION OF NEWLY DISCOVERED INHIBITORS  
OF LIPID DROPLET FORMATION**

LDs are no longer regarded as static lipid deposits, but are acknowledged to be part of a tightly regulated network (see Chapter 2) whose interruption is related to a multitude of diseases (see Chapter 1). A better understanding of the molecular interplay of regulation is an important step towards a more complete view of metabolic diseases. This is especially motivating since currently only a limited number of chemical probes has been discovered for studying lipid storage *in vitro* and only few drugs reached approval for the treatment of the metabolic syndrome.

Up to date various approaches were undertaken in order to understand lipid regulation mechanisms with new sets of biological and chemical modulators. In the past, potential new modulators were aimed for in low and high throughput screens by pharmacological companies, as well as in academia. First regulatory leads were generated by analyzing the protein and lipid composition in LDs at given time points. Different proteome screens identified LD (subset) specific proteins (Beller et al, 2006; Cermelli et al, 2006)), while lipidome analysis indicated an additional regulatory function of the lipid compositions (Schmidt et al, 2013; Ivashov et al, 2013). Applying a genome-wide RNAi screen as a genetic tool, identified amongst others COPI as a key regulator of lipid storage in *Drosophila* cells (Beller et al, 2008; Guo et al, 2008), as well as an involvement of calcium signaling via SOCE (storage operated calcium entry) in flies (Baumbach et al, 2014) or *Wnt* signaling in flies (Pospisilik et al, 2010).

This PhD project focused on the detailed characterization of three novel small molecule that modulate lipid storage processes. My goal was to identify the respective (protein) target(s) in order to finally explain the LD reduced phenotype.

## 3.1 PART 1: CHARACTERIZATION OF THREE NOVEL LD MODULATORS

## 3.1.1 History in the Identification of Chemotype 1-3

The novel classes of small molecules, which were investigated in this thesis originate from a former quantitative high throughput screen (qHTS) performed at the NIH (Bethesda, USA). The screen identified small molecules that either increase or decrease the amount of stored lipids within cells without affecting their viability (NIH grant 1-R03-MH085686-01, Dr. Mathias Beller, Gottingen). The assay was performed in embryonic *Drosophila melanogaster* S3 cells (see Figure 5.A), which store a high number of LDs. Additionally, *Drosophila* is a well-accepted model system in research, based on a high homology between fly and human (disease) genes (Padmanabha & Baker, 2014).

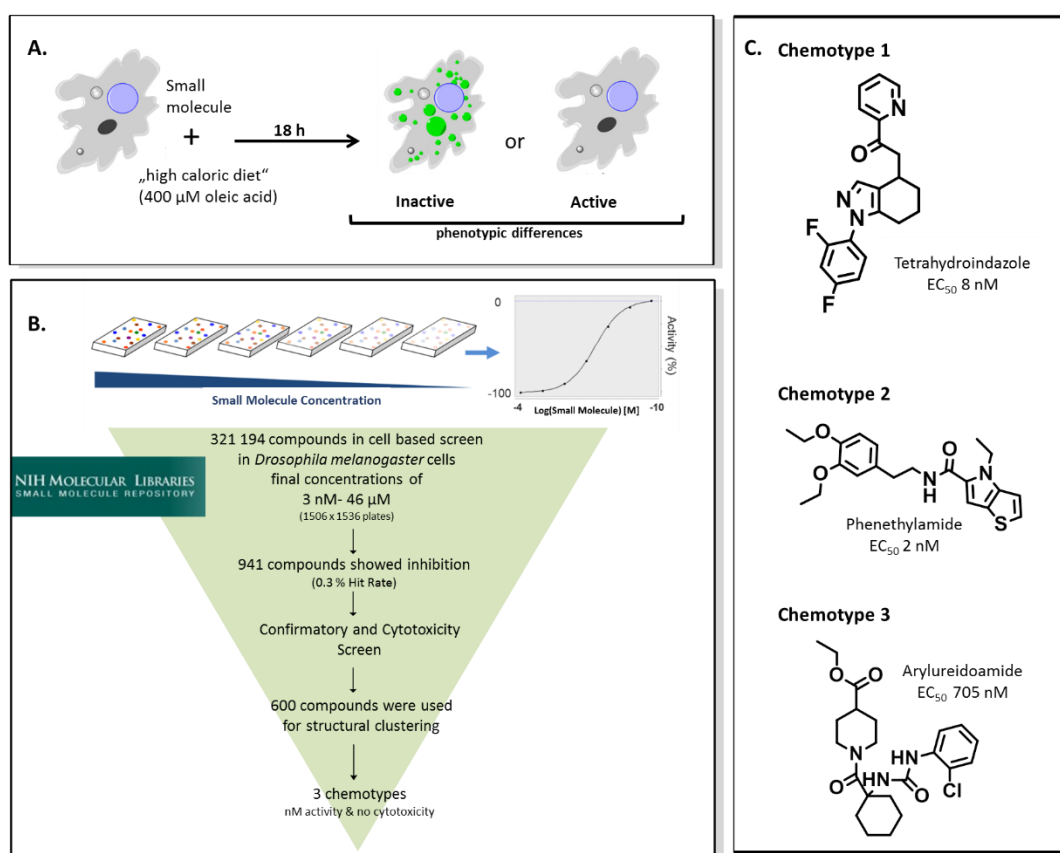


**FIGURE 5: Identification of small molecules that induce the LD reduced phenotype** **AI** Schematic summary of the cell based lipid droplet assay performed in *Drosophila melanogaster* S3 cells. Small molecule treatment occurred simultaneously to oleic acid feeding. Hits were classified as positive if the lipid droplets signal was decreased/ absent in comparison to untreated cells while the viability was simultaneously not affected. **BI** The initial qHTS screen led to the identification of three distinct classes of highly active small molecules that significantly reduced the amount of stored neutral lipids. **CI** Clustering of the most potent hits revealed three chemical independent scaffolds that resulted in the same LD reduced phenotype. These small molecules have low half maximal effective concentration ( $\text{EC}_{50}$ ) down to the nanomolar range. Derivatives of each small molecule series, were further investigated in this thesis.

The *Molecular Library Small Molecule Repository* (MLSMR; see <http://mli.nih.gov/mli/>) comprising >320,000 small molecules was screened in a quantitative ultra-high-throughput format at the NIH Chemical Genomics Center (Bethesda, USA) in a forward chemical genomic approach (see Figure 5.B). More than 600 highly potent small molecules that reduce cellular lipid stores were identified. These molecules were clustered according to their distinct chemical scaffolds. Three highly active chemical classes, here simply named Chemotype 1-3 were defined. The newly discovered small molecules are marked by high efficacies (EC<sub>50</sub> in low nM range) in the cellular LD assay and show a lack of cytotoxicity (see Figure 5.B). These three newly discovered distinct chemotypes are the foundation of this thesis. I aimed to further characterize the small molecules, investigate their mechanism of action and identify potential targets. This knowledge would increase the understanding of the tight regulation in lipid energy metabolism and would result in a new set of research tools.

### 3.1.2 Multidimensional Approach in Target Identification

In order to unravel the mechanism of action to explain the observed LD reduced phenotype upon small molecule treatment and to ultimately identify the direct (protein) target(s) I planned the small molecule characterization in a multidimensional experimental setup (see Figure 6).

The method of choice for target identification was a chemical affinity purification approach, using a modified derivative of the respective Chemotype as a chemical affinity reagent (Summarized in Chapter 4.2). Potential target candidates were concentrated out of bulk lysates and were analyzed via MS/MS. Metabolic labeling according to the established SILAC method (stable isotope labeling of amino acids in cell culture; Mann, 2014) allowed quantitative identification of potential target candidates. The proteins of interest were enriched by the active small molecule compared to the respective control derivative. Significantly enriched proteins were examined in further detail via direct enzymatic assays (if available) or for presence of a phenocopy introduced by either genetic interference or known chemical intercalators. The target validation for Chemotype 1 is summarized in Chapter 4.3. The subsequent Chapter 4.4 focuses on the validation of the protein target for Chemotype 2. Another aspect in the progress of target identification was the functional analysis of the chemotypes in different biological systems. These studies included the systematic analysis of the effects of the small molecule within different cell types as well as first *in vivo* experiments in flies (see Chapter 4.1.2.3). Other experiments focused on the characterization of the cellular lipid composition, the lipid uptake and the lipid mobilization upon compound treatment. Transcriptome studies via next generation sequencing of small molecule treated cells were additionally performed in the mechanism of action analysis. In the end, the different approaches of the functional characterization narrowed down likely affected pathways responsible for the strong phenotype.

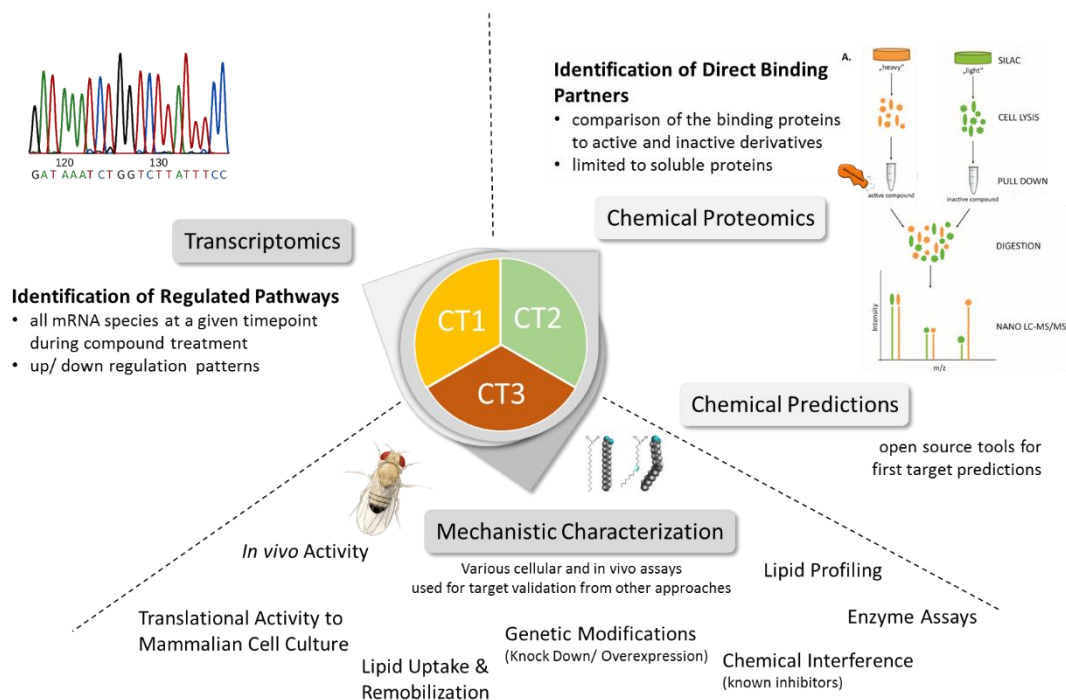


**FIGURE 6: Summary of the different levels of investigation in the target identification process.** The heart of the target identification approach is a combination of a quantitative chemical proteomic setup that allows the identification of soluble protein binders. The results are supported and validated by transcriptome analysis and computational predictions as well as a set of cell based experiments.

### 3.2 PART 2: ADAPTION OF LIPID DROPLET SCREENS

Currently only a limited number of small molecules is known for lipid storage modulation without the introduction of cytotoxic effects. In order to further discover potential modulators of LD storage, a library of natural product inspired compounds was screened for LD reduction. These small molecules with high similarity to naturally occurring compounds or secondary metabolites potentially have higher chances to constitute novel, highly potent small molecules.

Therefore, a high content screen (HCS) for lipid droplet reduction was established at the *Compound Management and Screening Center* (COMAS, Dortmund), which is the academic screening center affiliated to the Max Planck Society (MPG). COMAS combines the unique chemical compound library of the MPI of molecular physiology in Dortmund with small molecule libraries of commercial vendors.

On one hand it was intended to establish a standard screen for LD regulation in order to identify lipid droplet modulators aiming for tools in obesity. On the other hand, an additional LD-based screen for modulation of macrophage differentiation was planned to identify possible modulators of atherosclerosis by inhibiting foam cell generation.



## CHAPTER 4: RESULTS AND DISCUSSION- PART 1

### **4.1 FUNCTIONAL CHARACTERIZATION OF NOVEL LIPID DROPLET STORAGE INHIBITORS**

The three chemically independent small molecules were discovered in an assay following the classical forward chemical genetic design, which leaves the main task in target identification in order to explain the observed LD reduced phenotype on a molecular level. As the small molecules were discovered on a single cell level, complex sympathomimetic organismic causes are not assumed to be the primary mechanisms of action. Latter, however, are often targeted by known pharmacological modulators (see Chapter 1.1.2). Instead, direct interactions on cellular level is the speculated underlying mechanism of action. It is hypothesized that the newly identified chemotypes interact via direct (metabolic) enzyme or receptor modulation and thus trigger or disturb cellular signal transduction pathways or modulate transcriptional control.

In this chapter, the newly identified lipid storage modulators are functionally characterized to unravel their potential mechanism of action. In contrast to the focused chemical proteomic approach, which aims for the direct binding target (see Chapter 4.3), these investigations kept a general emphasis on potentially involved cellular mechanisms. This approach has the advantage that even classically not identifiable targets in proteomic studies, such as GPCRs or other transmembrane proteins, as well as non-protein targets, might move into the focus of investigation.

Remaining on the cellular level of investigation, various mechanisms of interaction can be hypothesized in order to explain the LD reduced phenotype in an environment containing high levels of free fatty acids (see summary in Figure 7). When the individual steps of the lipid droplet life cycle are reviewed independently in regard to the observed phenotype, the lack of cytotoxicity after Chemotype 1-3 treatment contradicts current knowledge. Not incorporated free fatty acids (FFAs) and lipid intermediates usually lead to cellular dysfunctions and cell death (Vigouroux et al, 2011). It can be speculated that the lack of lipotoxicity after Chemotype 1-3 treatment presumably relies on the highly dynamic and complex metabolic responses involved in cellular lipid storage: the tight, but flexible network is capable to compensate for inhibited enzymes or blocked pathways up to a certain level. However, observing such a stringent LD reduced phenotype at already low nanomolar inhibitor

concentrations, implies that a single enzyme at a key metabolic position might selectively be targeted. Alternatively, a well-defined cooperation of various enzymes in different pathways might be addressed at various sites, which enables the bypass of traditional feedback control mechanisms.

The mechanism of action studies of the Chemotypes, indirectly support the target identification process as not affected mechanism can be excluded, while potentially targeted pathways are highlighted. The physiological characterization of the different chemotypes will support the findings from chemical proteomic target identification (see Chapter 4.2) and leads the way to propose molecular targets.

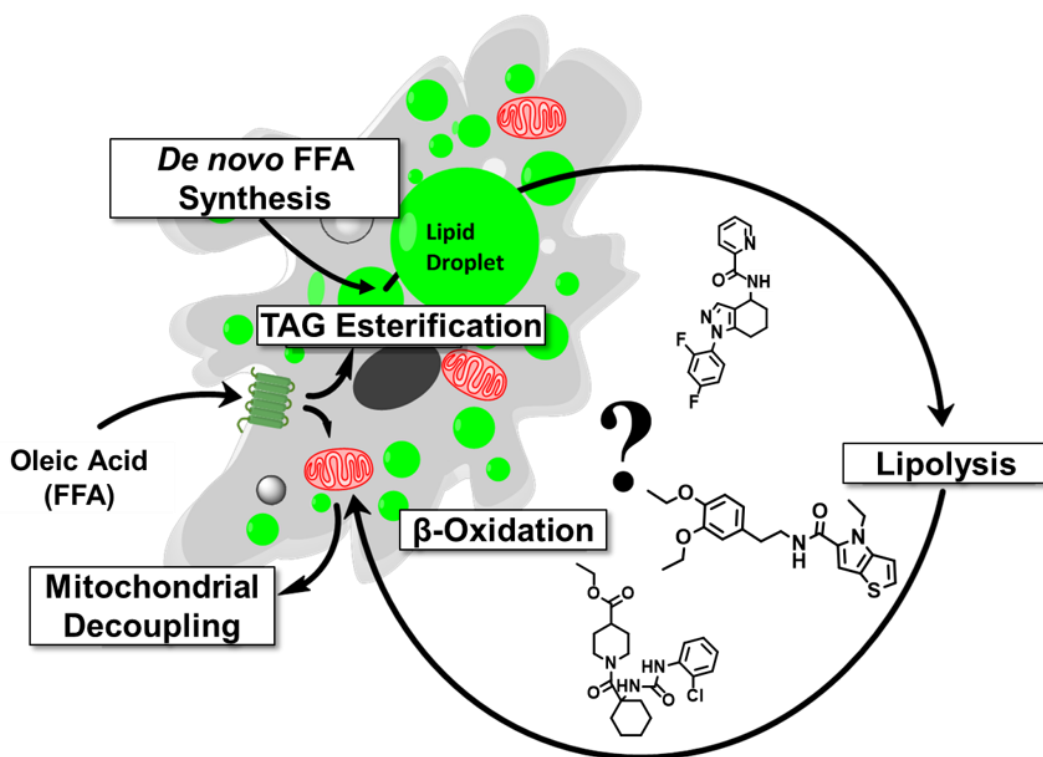


**FIGURE 7: Potentially targeted pathways affected by the newly discovered small molecule classes (Chemotype 1-3).** The LD reduced phenotype in an environment rich on free fatty acids (FFAs), can result from interference on various levels of the tightly controlled cellular lipid metabolism. The easiest explanation implies a direct block of the FFA uptake itself. Alternatively, the *de novo* TAG synthesis could be targeted as well as fatty acid esterification to form glycerol. A block at this level could either be caused by inhibition of the required CoA activation step of FFAs or by direct interference with enzymatic activities involved in the synthesis of neutral lipids. On the other hand, LDs could be temporarily formed, while the LD reduced phenotype results from excessive lipolytic activation. The increased FFA turnover is often paralleled by an increased level of  $\beta$ -oxidation in mitochondria. Which can either occur directly by shuffling entering FFAs immediately into mitochondria or delayed by an intermediate storage and subsequent increased lipolysis. In some cell types, especially brown adipose tissue (BAT), mitochondrial uncoupling leads to an increased energy consumption.

#### 4.1.1 CHEMICAL PROBES

The different chemical probes that were investigated in this thesis were all developed in the group of Dr. Mathew Boxer at the NIH (Bethesda, USA). The structural design, chemical synthesis and initial activity profiling by automated microscopy was done by the NIH working group. Only selected derivatives were examined in biological studies at the MPI in Dortmund and the HHU in Düsseldorf (see Supplemental Table 1+2, p.171-175). One major focus was devoted to structure activity relationship (SAR) studies of the distinct chemotypes in order to identify active and simultaneously stable derivatives for consecutive biological examination. Compound stability in regard to ADME characteristics (absorption, distribution, metabolism, and excretion) was investigated by Dr. Matthew Boxer (ongoing, not focused on in this thesis). Especially in regard to the chemical proteomic target identification approach, suitable positions for the attachment of biotin or free amine groups were explored. Additionally, clear-cut inactive probes were required as negative controls in biological experiments (see Chapter 4.2.2).

#### 4.1.2 CONFIRMATION OF BIOLOGICAL ACTIVITY

##### 4.1.2.1 Hit Validation by Secondary Assays

The original NIH HCS screen was performed in embryonic *Drosophila* S3 cells in a laser-based cytometry cellular assay. The fluorescence signal of the neutral lipid stain BODIPY<sup>®</sup> 493/503 was used as a proxy for the neutral lipid storage amount. The activities of promising small molecule lipid storage inhibitors were first confirmed by microscopy experiments. A concentration dependency of LD formation with decreasing small molecule concentration confirmed the high activities with EC<sub>50</sub> values in low nanomolar ranges (see Supplemental Figure 1, p.176). Secondary enzyme based assays validated the microscopic readout of the standard LD assay. The colorimetric assay relied on the hydrolysis of the glycerol backbone of TAGs as a reference for the total lipid concentration within the cell (ZenBio, Triglyceride Assay Kit). In Figure 8 the relative TAG levels of Chemotype 1-3 treated *Drosophila* S3 cells are summarized. Interestingly, even structures which did not show the LD reduced phenotype in previous microscopic assays revealed decreased lipid concentrations in the enzymatic assay. Systematic comparison of a subset of compounds confirmed the sensitivity discrepancy between the cell based LD-assay and the colorimetric TAG assay (see Supplemental Table 3, p.178). Nevertheless, both assays confirmed the reduction of neutral lipid storage amounts, which ruled out that any unspecific secondary effects such as quenching of the fluorescent dye by the administered small molecules are the cause of the LD reduced phenotype.

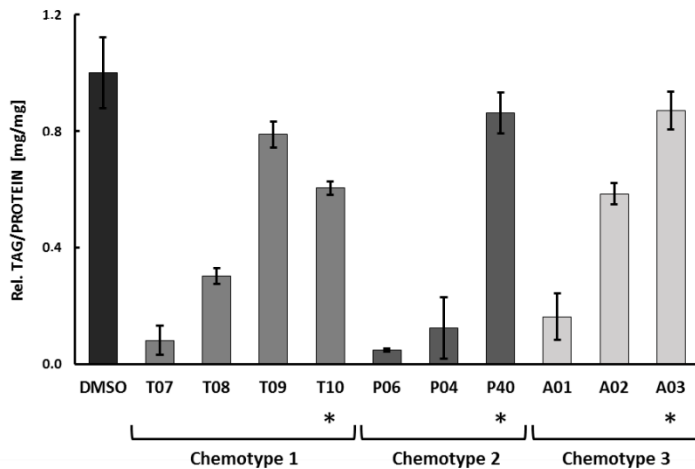


**FIGURE 8: The colorimetric TAG Assay (ZenBio, Triglyceride Quantification Kit) confirmed the reduced neutral lipid storage amounts in small molecule treated cells. *Drosophila* S3 cells were incubated in Schneider's Medium supplemented with 5% (v/v) FBS, 400  $\mu$ M OA and 5  $\mu$ M of the respective small molecule (0.2% (v/v) DMSO). The treated cells were incubated for 16 h. For TAG analysis, two replica plates were pooled at the cell lysis step, in order to increase the TAG amount. The TAG concentration (ZenBio) was normalized to protein levels (BCA) in triplicates. Small molecules marked by an asterisk were previously classified as inactive based on the microscopic LD assay readout.**

#### 4.1.2.2 Translational activity of Chemotype 1-3: Activity is not limited to *Drosophila* cells

In addition to the embryonic *Drosophila* S3 cells used in the primary screen, the investigated three Chemotypes demonstrate high lipid storage inhibitory activity in a broad range of fly cells, such as the embryonic *Kc167* or the neuronal *ML-DmBG3* cell lines. This observation points towards a target that is expressed in various fly tissues and at different developmental stages.

Additionally, all three chemotypes revealed activity in cell lines of a wide variety of species such as mouse (AML12, NIH-3T3, C3H/10T1/2), dog (MDCK), monkey (COS7) or human (HeLa, HEK293). As a consequence, the mechanism of action and probably also the molecular target appears to be evolutionary conserved in non-vertebrate and mammalian cells. The small molecule activity seems to be independent of the tissue, as the tested cell lines derive of different organs such as liver, kidney, undifferentiated adipocytes and ovary. Intriguingly, not all cell lines showed activity in the given experimental setup (PC12, THP-1, SH-SY5Y) (see Table 1 and Supplemental Figure 5, p.184). Unfortunately, activity mapping on basis of the origin of the tested cell lines did not reveal a distinct pattern in regard to a potential species or organ specificity. A distinct activity pattern might have helped in the progress of target identification.

The conserved activity of selected small molecule derivatives in different fly and mammalian cell lines (see Supplemental Figure 3, p.179), additionally emphasizes the strong predictive power of *Drosophila* cells as a biological test system. The high homology between human and *Drosophila* (disease) genes was demonstrated in various cases (Chien, 2002), making flies a valuable model system (Padmanabha & Baker, 2014).

As a summary, the observed translational activity of the Chemotype derivatives in different mammalian cell systems indicate an (evolutionary) conserved target. This increases the value of the small molecules as research tools and additionally allows a broader experimental setup in the process of target identification.

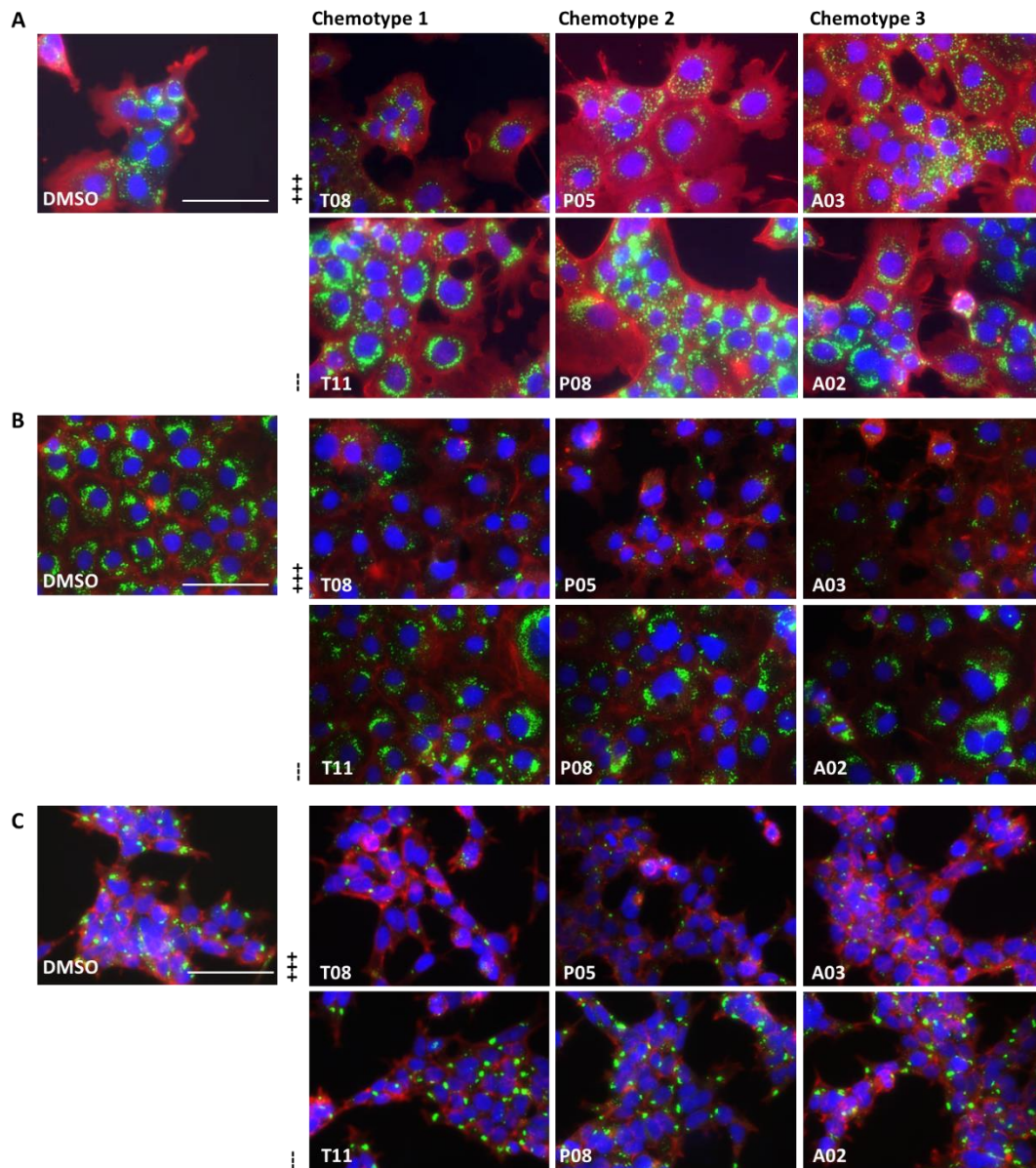


**FIGURE 9: Small molecule activity in selected mammalian cell lines.** Cells were treated with 5  $\mu\text{M}$  of the respective small molecule for 18 h in the presence of 400  $\mu\text{M}$  OA (or 200  $\mu\text{M}$  for AML12 cells) in the respective culture media with reduced FBS concentrations (5% (v/v)). Cells were stained with BODIPY<sup>®</sup>-493/503 (LDs, green), Hoechst 33342 (nuclei, blue) and phalloidin (actin, red). **AI** Murine AML12 hepatocytes, **BI** monkey COS7 kidney cells, **CI** human HEK293 kidney cells (+++ active derivatives; --- inactive control derivatives). Images were acquired with a Zeiss Axiovert Z.1 microscope at 40x magnification).

**TABLE 1: LD reduction in different insect and mammalian cell lines.** The cells were treated with 5  $\mu$ M Chemotype 2 for 18 h, stained for LDs and nuclei and visually examined for the presence of LDs. ( $\checkmark$  = LD reduction/active, ( $\checkmark$ ) = LD reduction but low original basal LD levels, x= LD remain present/ inactive).

Cell Line	Species	Species	Organ	Activity	LD induction
DGRC S3	<i>Drosophila melanogaster</i>	fruit fly	embryonic	$\checkmark$	Good
ML-DmBG3	<i>Drosophila melanogaster</i>	fruit fly	larval	$\checkmark$	good
Kc167	<i>Drosophila melanogaster</i>	fruit fly	embryonic	$\checkmark$	Good
NIH 3T3	<i>Mus musculus</i>	mouse	embryonic	$\checkmark$	moderate
C3H/10T1/2	<i>Homo sapiens</i>	human	embryonic	$\checkmark$	moderate
AML12	<i>Mus musculus</i>	mouse	liver	$\checkmark$	good
COS7	<i>Chlorocebus aethiops</i>	african green monkey	kidney	$\checkmark$	good
HEK 293	<i>Homo sapiens</i>	human	kidney	$\checkmark$	moderate
HeLa	<i>Homo sapiens</i>	human	cervix	( $\checkmark$ )	weak
CHO	<i>Cricetulus griseus</i>	hamster	ovary	( $\checkmark$ )	good
MDCK	<i>Canis familiaris</i>	dog	kidney	( $\checkmark$ )	moderate
HCT116	<i>Homo sapiens</i>	human	kidney	x	moderate
HepG2	<i>Homo sapiens</i>	human	liver	x	good
U2OS	<i>Homo sapiens</i>	human	bone	x	moderate
SW872	<i>Homo sapiens</i>	human	liposarcoma	x	moderate
THP-1	<i>Homo sapiens</i>	Human	monocytes	x	good

Not all of the tested cell lines (see Table 1) were suitable for LD analysis, since they either only reached low LD storage levels upon OA feeding or did not follow the required concentration dependency in LD formation in relation to the offered OA concentration. Consequently, it was not possible to distinguish a difference in LD formation upon small molecule treatment. Those cells were thus excluded from translational analysis.

Based on the broad use of murine AML12 hepatocytes as model system in obesity research (see Chapter 5.1) most subsequent experiments were performed in this cell line. AML12 cells show already at standard cultivation conditions high basal endogenous LD levels, which resulted in a lower signal-to-background ratio in the LD assay. Additionally, the cells showed decreased activities in the LD assay compared to the previously used *Drosophila* cells. In order to improve the readout the standard LD assay protocol was adapted in AML12 cells to a reduced OA feeding concentration of 200  $\mu$ M. This concentration was based on detail analysis of the OA concentration dependency and LD formation upon small molecule treatment (see Supplemental Figure 3, p.179). The necessity of an adapted assay protocol and the accentuated correlation illustrates the importance of the assay conditions for each respective cell line.

#### 4.1.2.3 *In vivo* activity: Activity is not limited to Tissue Culture Cells

In order to test whether the small molecule activity is not limited to tissue culture cells, but is also present in *in vivo* systems, adult flies were treated with small molecules supplied with the food. Subsequently, the overall organismic lipid storage amount was measured by an enzyme coupled colorimetric assay according to Hildebrandt et al, 2011. For this purpose, cohorts of eight male flies were fed with 7.5  $\mu\text{M}$  of the respective small molecule on a high caloric diet that based on a mixture of complex lipids for two days prior to homogenization and total lipid quantification (see Figure 10.A).

None of the three chemotypes indicated toxicity in flies. This finding on the one hand is in line with the lack of toxicity in cells, on the other hand it ensures small molecule uptake by the flies. Male flies averagely survive in 40-44 h without food intake (Zhukova & Kiseleva, 2011), thus the flies consumed the offered food and thus incorporated the small molecules. Unaltered food consumption was further supported in later experiments, where larval development was performed on food supplemented with small molecules (see Figure 11). However, several small molecules which were previously classified as LD storage inhibitors in the cellular LD assay, showed minimal or no changes in the total TAG content in whole male flies (see Figure 10). Only the Chemotype 2 derivative P04 significantly decreased the total neutral lipid level in flies. The derivative lowered the relative lipid level around 40% in comparison to DMSO treated cohorts.

A lack of activity translation from cells to the organisms can have numerous reasons and is a common problem for small molecules identified in biochemical or cell based assays. For example, bioavailability can be very low based on small molecule stability (Griffin et al, 2013), multi-drug resistance transporter mediated export (Chang, 2003) or cytochrome P450 enzyme mediated conversion of the small molecule to an inactive derivative (Guengerich, 2006). Importantly, however, several small molecules showed stable activity in both the cell based and the organismic assays. Small molecule stability, especially regarding ADME characteristics are important for later vertebrate model applications and have to be analyzed in a more detailed SAR study. Additional influential parameters which need to be considered at this point of investigation include food composition and treatment times and might need further optimization. At this stage, however, the very first positive *in vivo* activities are presented as a proof of concept and highlights that selected derivatives have the potential to intervene with lipid storage in whole organisms.

A closer examination of the derivative P04 with highest *in vivo* activity revealed that the lipid reduction was intensified, when the larval development was allowed in food containing 10  $\mu\text{M}$  of the active small molecule (see Figure 11). In this experimental setup the total amount of neutral lipids was reduced down to 20-30% of the DMSO control group.

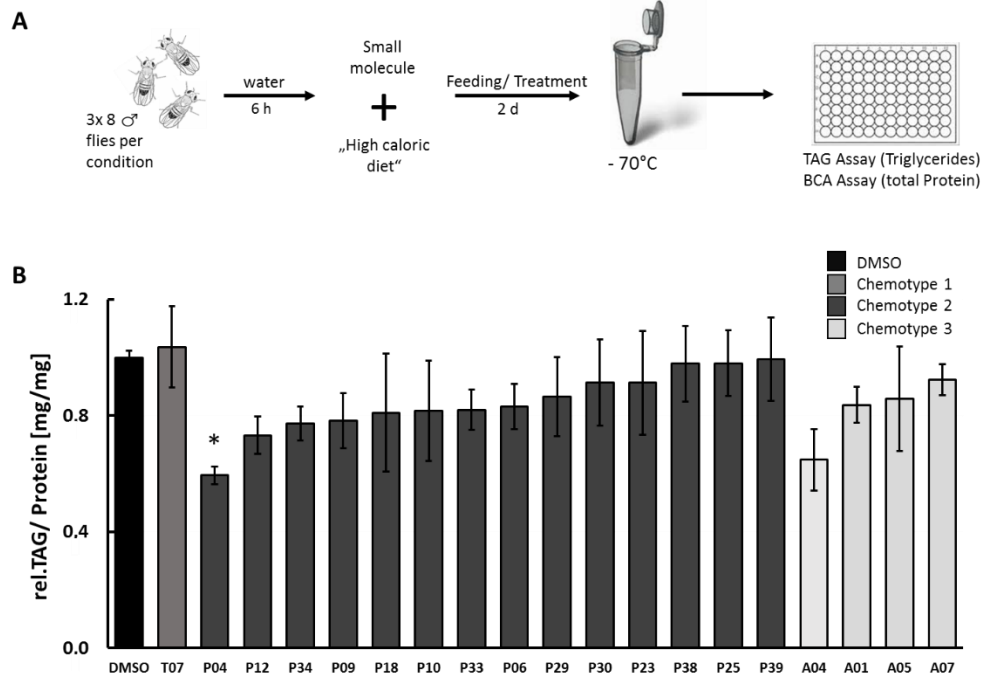


**FIGURE 10: Small molecule activity in whole flies. AI** The total TAG content in flies after small molecule treatment ( $7.5 \mu\text{M}$  on FFA rich media) was measured in a colorimetric assay (by Infinity TAG Kit, Thermo Fisher Scientific). Flies of the *w* genotype were starved for 6 h on a water only diet before the flies were transferred to vials containing Whatman filters soaked with a solution of 10% (w/v) sucrose, 5% (w/v) heat inactivated yeast extract and 0.4% (w/v) complex lipids (ClinOleic) in water supplemented with  $7.5 \mu\text{M}$  of the small molecule. The flies were incubated for two days and the filters were exchanged after 24 h, containing fresh small molecule and media. Each data point represents a triplicate cohort of eight virgin, male flies. **BI** The total neutral lipid content normalized to the protein content for the known active molecules of Chemotype 2 and Chemotype 3 highlighted the *in vivo* activity of P04 by a reduction of more than >25% of the lipid level compared to the control group.

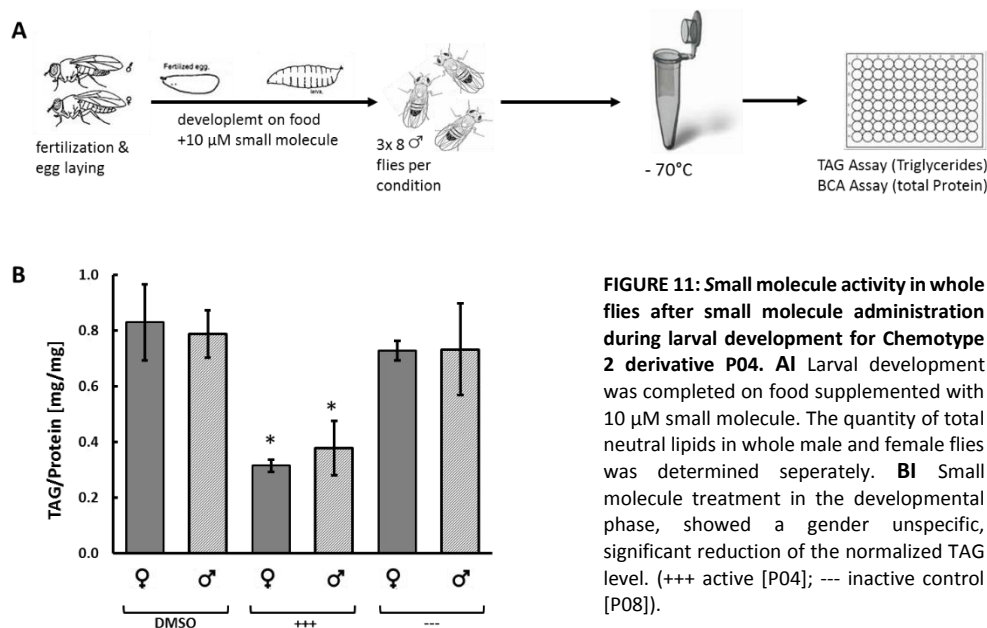


**FIGURE 11: Small molecule activity in whole flies after small molecule administration during larval development for Chemotype 2 derivative P04. AI** Larval development was completed on food supplemented with  $10 \mu\text{M}$  small molecule. The quantity of total neutral lipids in whole male and female flies was determined separately. **BI** Small molecule treatment in the developmental phase, showed a gender unspecific, significant reduction of the normalized TAG level. (+++ active [P04]; --- inactive control [P08]).



## 4.1.3 PHYSIOLOGICAL EXAMINATION OF THE PHENOTYPE

## 4.1.3.1 Onset of the LD reduced Phenotype

In the routine LD assay design, small molecule treatment was performed for 16-18 h. In order to follow the time dependent LD formation and thus define the onset of the small molecule interference, the treatment times were stepwise increased from 30 min to 10 h and the LD formation was monitored. These time course experiments, revealed that the treatment time can be decreased down to four hours in order to see first phenotypic changes between small molecule and DMSO treated cells (see Figure 12). This finding allowed the reduction of the treatment time in further experiments if required.

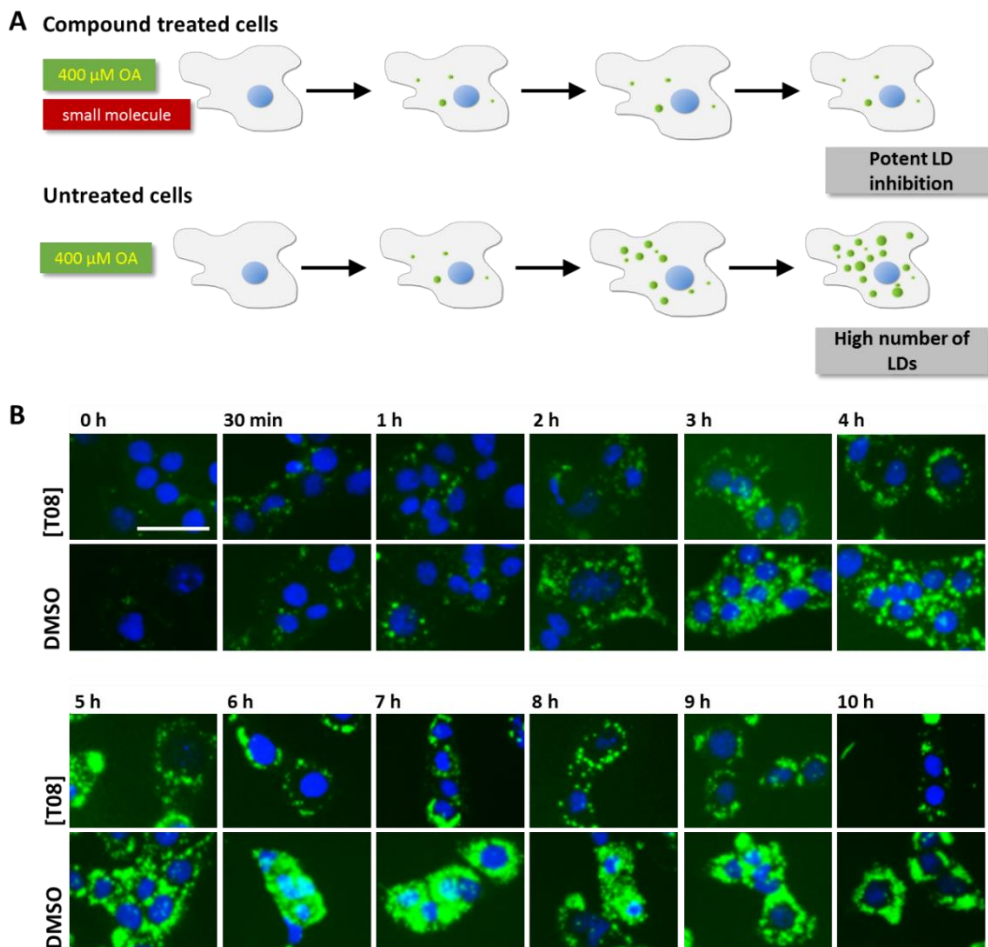


**Figure 12: LD formation with increasing treatment times in AML12 cells fed with 400  $\mu\text{M}$  OA and 5  $\mu\text{M}$  Chemotype 1 [T08].** **A** Schematic summary of the time course experiments **B** AML12 cells were treated with 5  $\mu\text{M}$  T08 for different time periods prior to fixation and staining of LDs (BODIPY<sup>™</sup> 493/503, green) and nuclei (Hoechst 33342, blue). The LD count was decreased already after 2-4 h in the small molecule treated cells in comparison to the respective DMSO control. Chemotype 1 is presented as representative for the other two Chemotypes, which show identical time course behavior towards LD formation. (Images: Zeiss Axiovert, 20x, blue: nuclei, green: lipid droplets).

The time dependency analysis of LD formation additionally revealed that no temporarily intermediate LDs were present at any time point of small molecule treatment. Temporal LDs would indicate an upregulated LD biogenesis or FFA incorporation into the LD, while simultaneously lipolysis is enhanced. This combination would speculatively lead to the LD reduced phenotype. Lipolytic activation is summarized in more detail in chapter 4.1.5.4.

#### 4.1.3.2 Binding Behavior

In order to investigate whether the LD reduced phenotype persists small molecule removal, the small molecule containing medium of treated cells was replaced by fresh, compound free media after 16 h incubation. In case that the LD reduced phenotype persists after small molecule removal, covalent target binding can be assumed. A rapid regeneration of LDs on the other hand supports a non-covalent interaction or alternatively rapid target protein turnover.

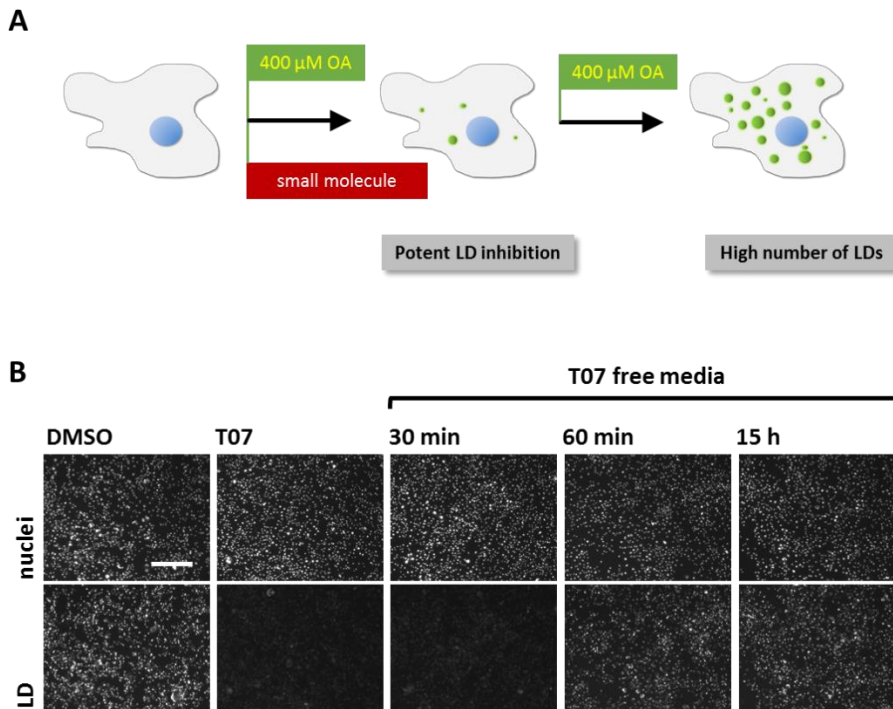


**FIGURE 13: Small molecule wash out experiments in *Drosophila* S3 of Chemotype 1. **A**** Schematic summary of the wash out experiments **B** *Drosophila* S3 cells were treated with 50 nM of the Chemotype 1 derivative T07 in serum reduced Schneider's medium (5% (v/v)) supplemented with 400  $\mu$ M OA for 16h. 0.2 % (v/v) DMSO was used as control. The small molecule containing medium was removed and the cells were washed twice with PBS buffer. Subsequently, fresh small molecule free medium containing 400  $\mu$ M oleic acid was added and the cultivation was continued. LDs were stained with BODIPY® 493/503 and nuclei with Hoechst 33342. The images were examined at the Zeiss Axiovert microscope, with 10x magnification (scalebar: 100  $\mu$ m). The here presented images show Chemotype 1 treated cells. Identical results were obtained for Chemotype 2 (data not shown).

Replacing the oleic acid rich media of small molecule treated cells after cultivation for 16 h with small molecule free media, resulted in fast regeneration of LDs (see Figure 13). Thus, these simple wash out experiments indicated a non-covalent or at least reversible small molecule interaction for all three chemotypes. The intermediate washing step was apparently sufficient to lower the concentration of the highly active small molecules below the respective  $EC_{50}$  level by dilution. In order to explain that the LD reduction was voided it can be assumed that the interaction between the target and the small molecule was disrupted in a concentration dependent manner. This led to the assumption that non-covalent binding was the underlying mechanism of the small molecule target interaction. Covalent target binding in contrast would have resulted in a prolonged LD reduced phenotype even after small molecule removal, since the active molecules cannot be washed off.

The non-covalent interaction was additionally confirmed by cell based replacement experiments. Chemotype 1 has a stereoselective activity: While the (+)- enantiomer is highly active, the (-)- enantiomer shows no LD reducing activity in the microscopic assay (additional information see Chapter 4.2.1). Applying an enantiomeric mixture containing an excess of the inactive isoform (10x) led to a restorage of LDs within cells (see Figure 14). The LD level of untreated cells was not reached, which indicates that either the applied excess of the inactive enantiomer was too low or alternatively that the inactive enantiomer still remained minor activity (see discussion in Chapter 4.2.1).

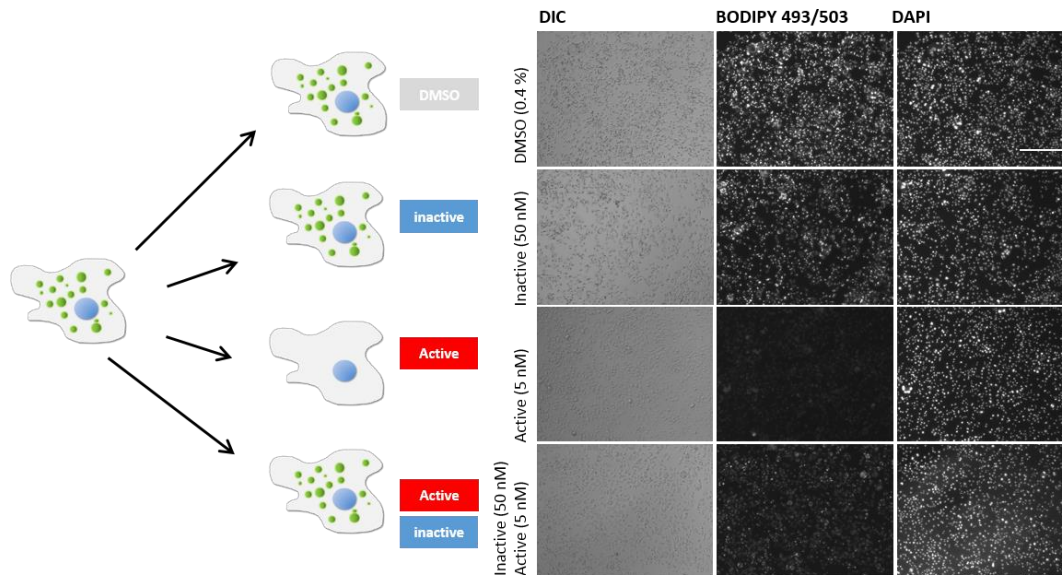


**FIGURE 14: Replacement experiments in *Drosophila* S3 cells confirm non-covalent interactions.** *Drosophila* S3 cells were treated with derivatives of Chemotype 1 (5 nM [T07], DMSO 0.4 % (v/v)) in Schneider's Medium (5% (v/v) FBS) containing 400 $\mu$ M OA. Additionally, increased concentrations of the inactive enantiomer (50 nM, [T07(-)]) was added in order to generate a competitive situation between the active and inactive derivatives. (Zeiss Axiovert microscope, 10x magnification, scalebar: 100  $\mu$ m)

#### 4.1.3.3 Cellular Location of Fluorescently Labeled Chemotypes

In order to examine the potential subcellular location of the small molecule- target interaction, fluorescent groups were attached to the examined chemotypes and microscopically analyzed upon cell treatment. The synthesis of the fluorescent derivatives was performed by the group of Dr. Boxer at the NIH (Bethesda, USA).

For Chemotype 1 a fluorescent BODIPY label [T06] was attached without affecting activity in the cell based LD assay. *Drosophila* S3 cells labeled with T06 show a small molecule accumulation within the cell. It was assumed that the labeled small molecule derivative is enriched in the endoplasmic reticulum (see Figure 15). The validity of this finding is questionable since, fluorescent probe accumulation within the ER might depend on passive accumulation of the hydrophilic molecules or active clearance of the incorporated chemical molecules.

Chemotype 2 was modified by a fluorescein tag [P03] and treated cells revealed also a cellular accumulation within the ER. Later colocalization studies indicated that Chemotype 2 accumulates in the ER (see Chapter 4.4.1.4, p.85). Chemotype 3 was not investigated by this approach due to a lack of suitable fluorescent probe. The chemical probe development is progress (Dr. Matthew Boxer, NIH).

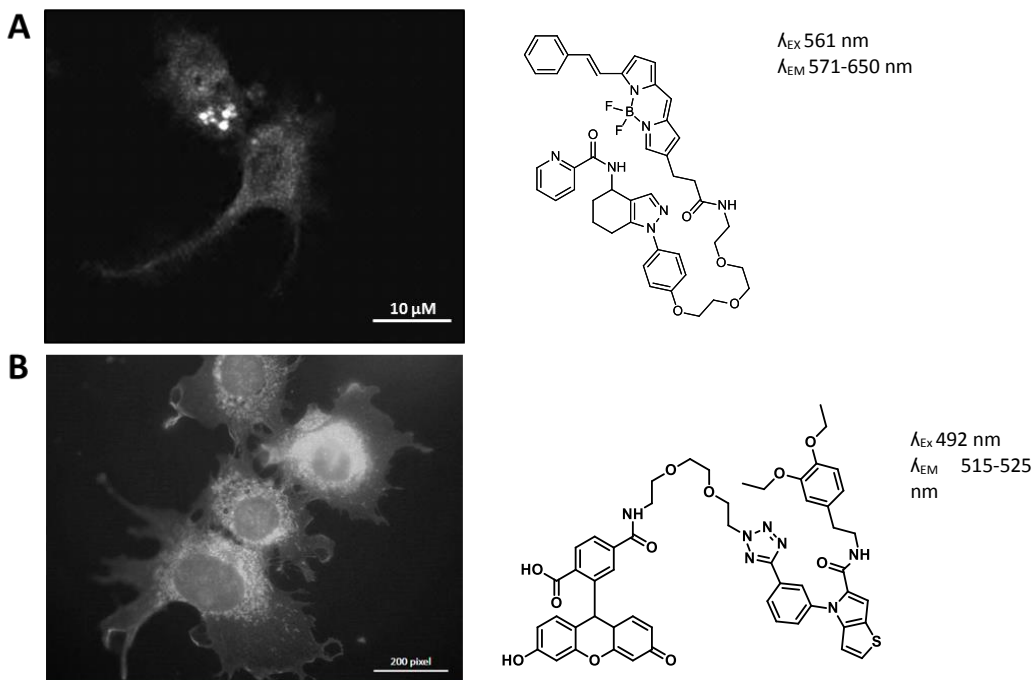


**FIGURE 15: Cellular localization studies of fluorescently labeled derivatives.** **AI** Viable *Drosophila* S3 cells were treated with 250 nM BODIPY-Chemotype 1 [T06] for 16 h. The cells were mounted without fixation or additional staining. Images were taken with a Leica SP5 Confocal microscope (digital zoom, scalebar: 10  $\mu$ M) **BI** Viable AML12 cells were treated with 10 nM Fluorescein-Chemotype 2 [P03] for 1 h. The cells were mounted with fixation or additional staining. The image was acquired at the Zeiss Observer Z1 (63x magnification, oil, scalebar: 200 pixel).

## 4.1.4 THREE CHEMOTYPES- ONE PHENOTYPE

## 4.1.4.1 Computational Target Prediction

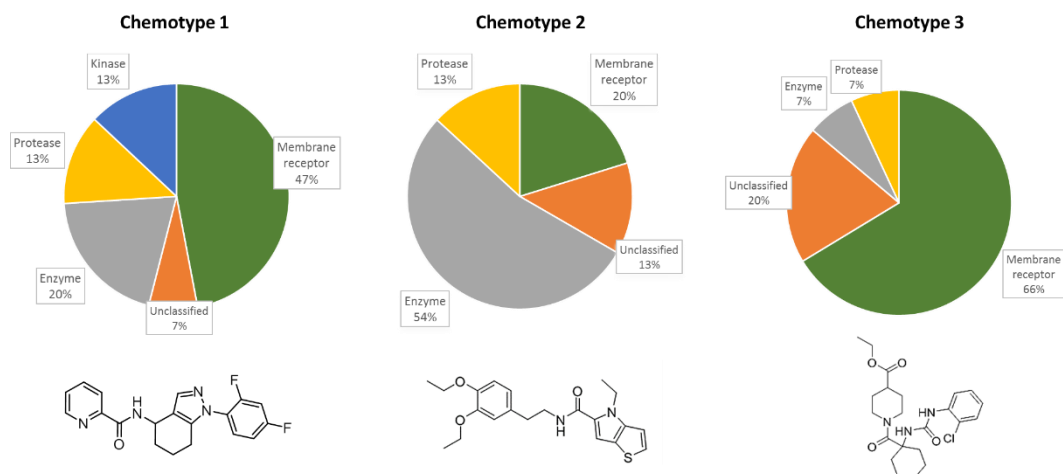


**FIGURE 16: Chemoinformatics based target prediction using the online prediction tool “Swiss Target Prediction” ([www.swisstargetprediction.ch/](http://www.swisstargetprediction.ch/)) based on the combination of 2D and 3D similarity search of the examined small molecules with 280.000 known small molecules against 2000 known targets. (green: membrane receptors; orange: unclassified proteins; grey: enzymes; yellow: proteases, blue: kinases).**

Computational based target predictions are a luring approach in order to obtain first ideas during target identification (Sliwoski et al, 2014). Potential protein targets of the respective chemotypes predicted by *Swiss Target Prediction* ([www.swisstargetprediction.ch/](http://www.swisstargetprediction.ch/); see Figure 16) and *SEA Analysis* ([www.sea.bkslab.org/](http://www.sea.bkslab.org/)) are summarized in the supplemental information (see Supplemental Table 4, p.181). The different algorithms led to a different set of predicted targets for the investigated three distinct Chemotypes (see Figure 16).

## 4.1.4.2 Transcriptome Analysis

The analysis of the transcriptome by RNA sequencing of the total mRNA moiety in small molecule-treated cells is not suitable to identify the direct interaction partner but might highlight up- or downregulated pathways in treated cells compared to controls. *Drosophila* S3 cells and murine AML12 cells, were treated in identical procedures and the expression pattern was analyzed by next generation sequencing. The data set included an active and inactive derivative of each chemotype, as well as the respective DMSO control. The cells were treated for 4 h and 16 h in order to see an early and late transcriptional response. Additionally, gene expression of OA fed cells was compared with cells cultured in standard medium lacking surplus FFAs. The respective RNA samples were analyzed at the National Institute of Diabetes and Digestive and Kidney Diseases (NIDDK, Bethesda, USA) and data analysis was performed by Dr. Kseniya Golovkina. Based on the complexity of the obtained results, it was decided to solely focus on the four hour time point: First phenotypic

differences in LD storage are known to appear after more than four hours of treatment time and it was assumed that the background of unspecific and secondary transcriptomic changes rise with increasing treatment times. Additionally, it was decided to only focus on the transcriptional analysis of treated *Drosophila* S3 cells. This decision was primarily based on first clustering analyses, which was more distinct in *Drosophila* S3 samples compared to the AML12 samples. But even if the murine cell line has around 5 fold more potentially regulated genes, the initial clustering was highly comparable between the different species (data not shown). Elaborated clustering of the *Drosophila* samples revealed five distinct groups of significantly regulated genes, which show altered expression between the different experimental conditions (see Figure 17). The two major clusters of regulated genes include genes relevant in fatty acid biosynthesis (Cluster 1) and genes involved in fatty acid oxidation (Cluster 5).

Cells cultured according to standard conditions show an apparent inversion of gene expression in Clusters 1-3 compared to cells on a high FFA diet (400  $\mu$ M OA). The concerned genes are mostly involved in (phospho-) lipid biosynthesis. Down regulation of *de novo* lipid synthesis genes is a likely response to the presence of external FFAs. The downregulated state of *de novo* lipid synthesis genes was observed throughout all samples treated with both 400  $\mu$ M OA and 1  $\mu$ M of the respective active and inactive control derivatives of the respective chemotypes.

The second pattern allows a differentiation between the expression profiles of active and inactive derivatives of the chemotypes. While the genes in clusters 2-4 are mostly downregulated in samples of cells treated with active derivatives, cluster 5 is specifically upregulated. An inversion of this pattern is observed in the respective samples of cells treated with the inactive control derivatives, which are highly similar to the expression profiles of untreated control cells. Cluster 5 combines genes involved in fatty acid metabolism, which indicates that all three chemotypes directly or indirectly affect pathways involved in  $\beta$ -oxidative processes. This observation explains the lack of lipotoxicity or cell death. Generally lipotoxicity is prevented by an either elevated oxidation of FFAs or by sequestering the surplus of FFAs as TAGs into LDs (Greenberg et al, 2011; Aon et al, 2014). As the LD storage is significantly reduced after small molecule treatment, an upregulation of  $\beta$ -oxidative mechanisms is a likely cellular response upon Chemotype 1-3 treatment.

Further, detailed GO-term analysis of the significantly regulated genes in cells treated with the respective active and inactive derivatives for each chemotype (by Dr. Kseniya Golovkina, NIDDK, USA), highlighted significant differences in regulated genes of the respective chemotypes. The active probe of Chemotype 1, for example, shows a specific clear-cut down regulation of genes in the undefined clusters 2 and 3. Some of those regulated genes are involved in nucleotide metabolism, vitamin and cofactor metabolism as well as starch metabolism. At the same time, selected genes in lipid biosynthesis are upregulated for Chemotype 1. In contrast to Chemotype 1, the chemotypes 2

and 3 do not show a significantly regulated specific metabolic response. Chemotype 2 shows some expression changes in DAG dependent protein kinases and GPCR signaling, while for Chemotype 3 many glutathione-S-transferases were upregulated. How these commonly and specifically regulated gene patterns match the observed LD reduced phenotype has to be examined in greater detail. The dataset will be further analyzed by Dr. Kseniya Golovkina in regard to the changes between active and inactive probes of the Chemotypes and the respective controls ( $\pm$  400 OA addition). In progress of this work, the transcriptome data is consulted for indirect target validation of Chemotype 1 in Chapter 4.3.

In summary, the transcriptome analysis highlighted that all three Chemotypes trigger an upregulation of genes involved in  $\beta$ -oxidation and fatty acid metabolic processes. This effect is more prone in Chemotypes 1 and 3. If this is primary cause by a target positioned directly  $\beta$ -oxidative metabolism, or if it is a secondary cellular response to the blocked LD storage in order to prevent lipotoxicity has to be analyzed in greater detail. Additionally, the specific changes in gene expression between the different chemotypes support the theory that the three distinct chemotypes likely target three individual targets.

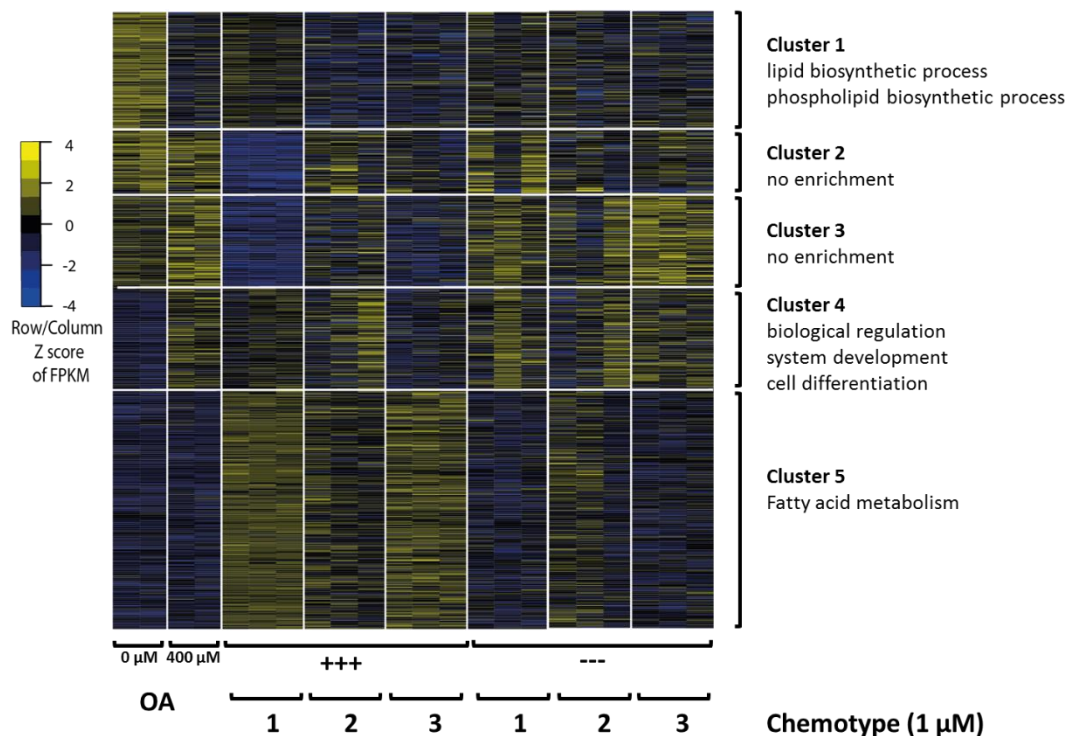


**FIGURE 17: Expression profiles of differentially expressed genes between treated and control samples in *Drosophila* S3 cells after 4 h treatment.** The cells were treated with the respective active and inactive control derivatives of the distinct Chemotypes at a concentration of 1  $\mu$ M in the presence of 400  $\mu$ M OA. The total RNA was isolated and analyzed by next generation sequencing. Differentially expressed genes were clustered according to their gene expression values. In the resultant heatmap, genes (rows) were arranged by the k-means method. Sequencing and data analysis was done by Dr. Kseniya Golovkina (NIDDK). (blue: upregulated genes, yellow: downregulated genes; +++ active derivatives; --- inactive derivatives; Chemotype 1 [T08; T11]). Chemotype 2 [P04; P08]; Chemotype 3 [A03; A02] [active/inactive]).

#### 4.1.5 METABOLIC CHANGES UPON SMALL MOLECULE TREATMENT IN CELLS

The results presented in this subchapter mainly focus on the Chemotype 2 derivative P04 as this small molecule showed the most defined expression profiles in the transcriptome analysis (see Chapter 4.1.4.2) which resulted in the privileged analysis of this chemotype. Additionally, it stands out by the highest activity of the investigated molecules (2 nM) and also shows *in vivo* activity.

#### 4.1.5.1 Analysis of affected Lipid Species revealed TAG Specificity

The readout of both the microscopic LD assay and the colorimetric TAG assay relied mainly on the presence or absence of neutral lipids. Whether other lipid species are also modulated cannot be estimated from these assays. Therefore, lipids were isolated from small molecule- treated cells and separated by thin layer chromatography (TLC). The qualitative analysis of the lipid extracts showed a significant decrease in TAG, while the other lipid species, such as sterylester, FFA and DAG/MAG remained unaltered (see Figure 18.A).

The unique TAG reduction was additionally confirmed in HPLC analyses of cellular lipid extracts (see Figure 18.B). Both murine AML12 and primate COS7 cell extracts were quantitatively analyzed for their respective lipid levels normalized to total protein after small molecule treatment. Again, only TAG was reduced, while phosphatidylcholine, cholesterylester and free cholesterol were not altered in comparison to the DMSO control.

Interestingly, the quantified TAG amount was never below the basal TAG level in cells cultured without OA supplementation (“unfed”). This is a possible explanation for the absence of cytotoxicity after small molecule treatment, as it can be assumed that a significantly lowered neutral lipid store below the endogenous lipid concentration would severely impact lipid dependent cellular processes. This is especially true in respect to the phospholipid moiety, since membranes are utterly important to keep cellular function either by compartmentalization of the intracellular space or by offering coating material for the neutral lipids in the hydrophilic cytosol. Especially the latter, would have been a potential cause for the lack of LDs upon small molecule treatment.

In summary, the lipid analysis highlighted that the LD reduced phenotype is confined to TAG. Additionally, it ruled out that decreased phospholipid levels are the primary cause for the LD absence. It was speculated that lipolysis is not likely targeted, as the basal level of stored LDs was never undercut. These results thus direct the mechanism of action hypothesis towards a likely block in lipid incorporation into LDs or increased  $\beta$ -oxidation. The latter hypothesis was supported by the transcriptome analysis which revealed a significant upregulation of genes involved in  $\beta$ -oxidation for all chemotypes (see Chapter 4.1.4.2).



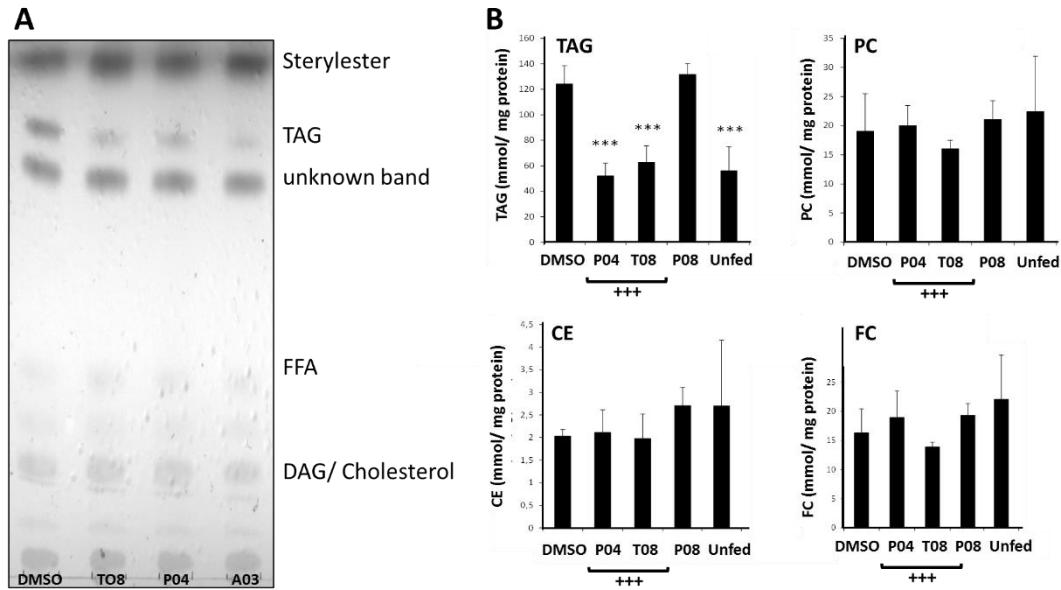


**FIGURE 18: Chromatographic analysis of lipid extracts from small molecule treated cells. A** Separation of triglycerides and sterylesters of small molecule treated AML12 cells in thin layer chromatography did only show a decrease in TAG. Lipids were separated by TLC in a solvent mixture suitable for neutral lipids [hexane/diethylether/ acetic acid (70:39:1)]. Lipids were stained by a cupric solution ((10% (w/v) CuSO<sub>4</sub>, 10% (v/v) phosphoric acid) and charring. (DMSO, Chemotype 1 [T08], Chemotype 2 [P04], c. Chemotype 3 [A03]) **B** HPLC analysis of lipid extracts in small molecule treated AML12 cells. [TAG: triacylglyceride; PC: Phosphatidylcholine; CE: cholesterylester; FC: free cholesterol, FFA: free fatty acids]. The HPLC analysis was performed by Dr. Thomas O. Eichmann, Universität Graz, Austria).

#### 4.1.5.1.1 No Effect in Cholesterylester Deposition by Chemotype 2

Classically, the core of adipocyte LDs predominantly consists of TAGs (see Figure 3.A, p.9), whereas many non-adipocytes LDs contain both TAG and cholesterol esters (CE) (Fujimoto & Ohsaki, 2006). CE are formed by an acyl-CoA cholesterol acyltransferase (ACAT) catalyzed reaction of the carboxylate group of a fatty acid and the hydroxyl group of cholesterol (Rogers et al, 2014a). CE metabolism has best been studied in macrophage foam cells (Li & Glass, 2002) and the cellular and extracellular CE levels are of medical relevance (Zhang & Porto, 2013) as CE concentrations were for example related to the risk of atherosclerosis (Lawrence Bachorik, 1997). Increased CE storage in LDs was related to a blocked protein translation either by autophagy or mTOR1 dependent pathways (Suzuki et al, 2012). While TAGs are degraded by a sequential reaction of ATGL, HSL and monoacylglycerol lipase (see Figure 3.C, p.9; Zechner & Madeo, 2009), the degradation of CE requires lysosomal lipase activity (Quimet et al, 2011). Nevertheless, it was speculated that CE hydrolysis requires effective TAG degradation as TAG forms a concentric layer on the CE surface (Czabany et al, 2008).

In order to test, whether cellular CE level change upon Chemotype 2 [P04] treatment NBD-cholesterol deposition studies were conducted in cells. AML12 cells were fed with high

concentrations of NBD-cholesterol (20 mM) which provoked LD formation of CE rich LDs (green). These LDs were not depleted after Chemotype 2 treatment (see Figure 19.A).

When OA and NBD-Cholesterol were provided simultaneously as external lipid sources, the formed LDs contained both TAG and NBD-cholesterol in untreated cells, which appeared yellow in the overlay (see Figure 19.B). Upon Chemotype 2 treatment, the TAG level was decreased, leaving NBD-cholesterol in the remaining lipid droplets (green). This discovery supports the previous finding of a confined change in TAG levels by TLC and HPLC analysis of lipid extracts from Chemotype 2 treated cells (see chapter 4.1.5.1.1). It additionally, allows the hypothesis that ACAT activity or cholesterol metabolism are likely not modulated by Chemotype 2.

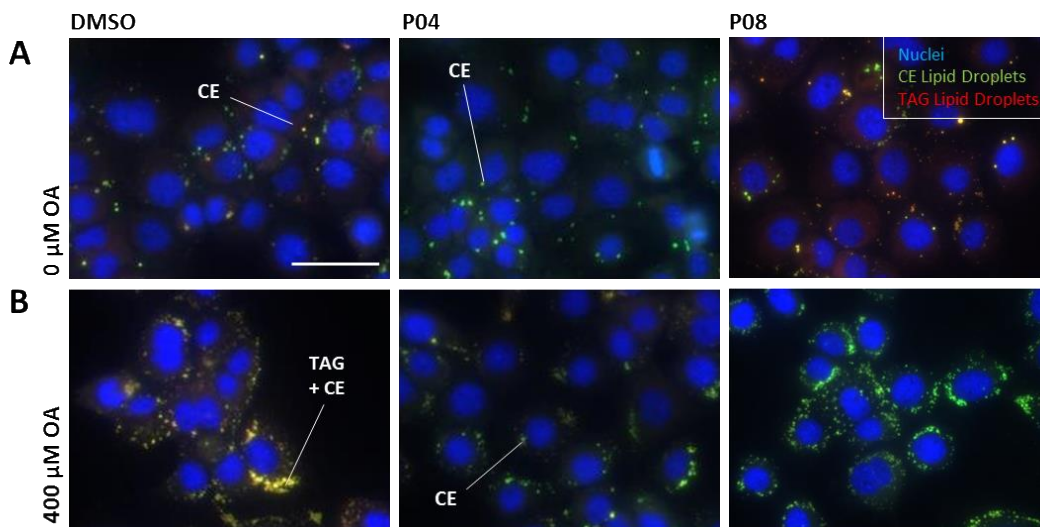


**FIGURE 19: Cholesterylester droplet formation is not altered upon Chemotype 2 [P04] treatment.** AML12 cells were treated with 20 mM NBD-Cholesterol, either in absence (A) or presence (B) of 400  $\mu$ M. The cells were fixed and stained for nuclei (Hoechst 33342, blue) and LDs (HCS LipidTox™ Deep Red). The different lipid species incorporated into the lipid droplets can be distinguished accordingly: the triglyceride moiety remains red, while NBD-cholesterylester containing droplets are green. LDs combining both lipids appear yellow in merged images (Images acquired with Zeiss Observer Z.1, 40x magnification; CE: cholesteryl ester; TAG: triacylglyceride; [P04] active derivative; [P08] inactive derivative).

#### 4.1.5.1.2 Exclusive Changes for DAG in Chemotype 2

The unique reduction in TAG upon small molecule treatment points to a target involved in TAG synthesis. The final step of TAG synthesis is catalyzed by the two well-known and evolutionary conserved enzymes diacylglycerol-O-acyltransferases 1 and 2 (DGAT1 and DGAT2). Both isozymes catalyze the final esterification of FFAs to an already existing diacylglycerol (DAG) (see Figure 4, p.11). Alternatively, the confined TAG reduction can be explained by targeting acyl-CoA synthetases (ACSL) and thereby blocking FA activation which is required for TAG synthesis. This hypothesis, however,

would presumably show indications of cytotoxicity due to the accumulation of free fatty acids (Drosatos & Schulze, 2013).

In theory, DGAT inhibition should lead to the temporal increase of the enzymatic educt: DAG. In standard lipid extractions of small molecule treated cells, however, DAG accumulation was not observed. However, slight modifications of the experiment revealed significantly increased DAG level in Chemotype 2 [P04] treated cells (see Figure 20). The DAG level decreased within the time of small molecule treatment. This strongly supports the hypothesis that one of the two DGAT enzymes might be the target for Chemotype 2. This hypothesis is reviewed in more detail in Chapter 4.4.4.

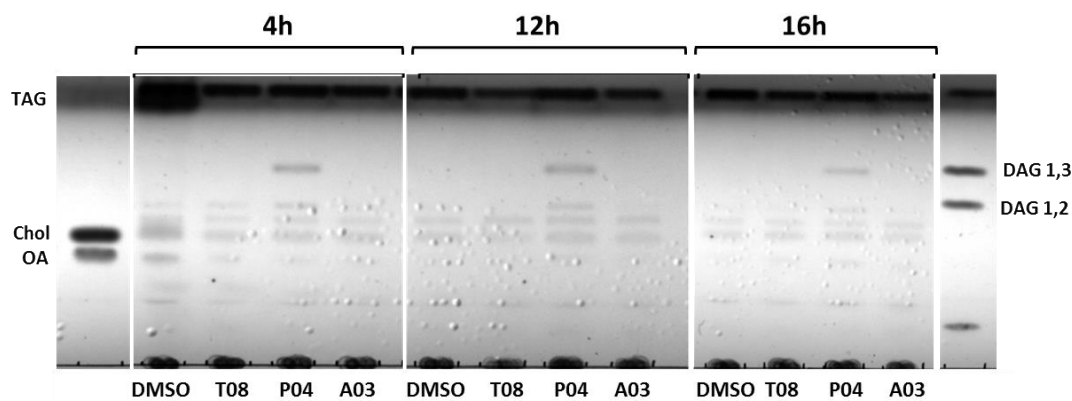


**FIGURE 20: Chemotype 2 [P04] treatment provokes a temporarily increase in sn-1,3 DAG levels.** *Drosophila* Kc167 cells were fed with 400  $\mu$ M OA overnight before 5  $\mu$ M Chemotype 2 [P04] in the presence of OA was added. The cells were harvested after different treatment times (4h, 12h, 16h) and the separated lipids were analyzed by TLC in a solvent suitable for mono-, di-, triglyceride separation [Chloroform/ Acetone/ Acetic Acid (45:5:0.5)]. Chemotype 1 [T08]; Chemotype 2 [P04], Chemotype 3 [A03]. The experiment were performed by M.Sc. Thomas Schlemper, HHU Düsseldorf, Germany (Masterarbeit Schlemper, 2014).

#### 4.1.5.2 Endogenous Lipid Storage is hindered by Chemotype 2

In the standard LD assay exogenous high concentrations of OA trigger the LD formation within cells. In order to study whether the endogenous lipid incorporation can be blocked by the small molecules as well, 3T3-L1 cells were differentiated and analyzed for a block of differentiation dependent LD formation. Differentiated 3T3-L1 cells generally show huge LDs without the need to a supply of exogenous FFAs. Yaqin Zhang (NIH, USA) could show that pre-adipocytes which were treated with 5  $\mu$ M P04 throughout the differentiation process lack these LDs (see Supplemental Figure 6).

In order to investigate whether a disrupted differentiation upon P04 treatment is the reason for the blocked LD formation from endogenous sources, the expression of different transcription factors which suit as proxies for the differentiation process was examined (see Figure 21). Generally,

adipocyte differentiation follows a precisely ordered and temporally regulated series of events (Gregoire et al, 1998). The two involved key transcription factors are C/EBP $\alpha$  (CCAAT/ enhancer binding protein alpha) and PPAR $\gamma$  (peroxisome proliferator activator receptor gamma). Additionally, two important metabolic proteins were checked for altered expression levels. AdipoQ encodes Adiponectin which is a regulator in glucose level and  $\beta$ -oxidation (Lopez-Jaramillo et al, 2014). Slc24a is a member of the glucose uptake transporter family (GLUT4).

Triggering the 3T3-L1 differentiation by dexamethasone, insulin and panthothenate in presence of the different Chemotypes, did not result in significant changes in the expression levels of the investigated marker genes as compared to the control cells. This indicates that pre-adipocytes are capable to turn into adipocytes, however, fail to store lipids.

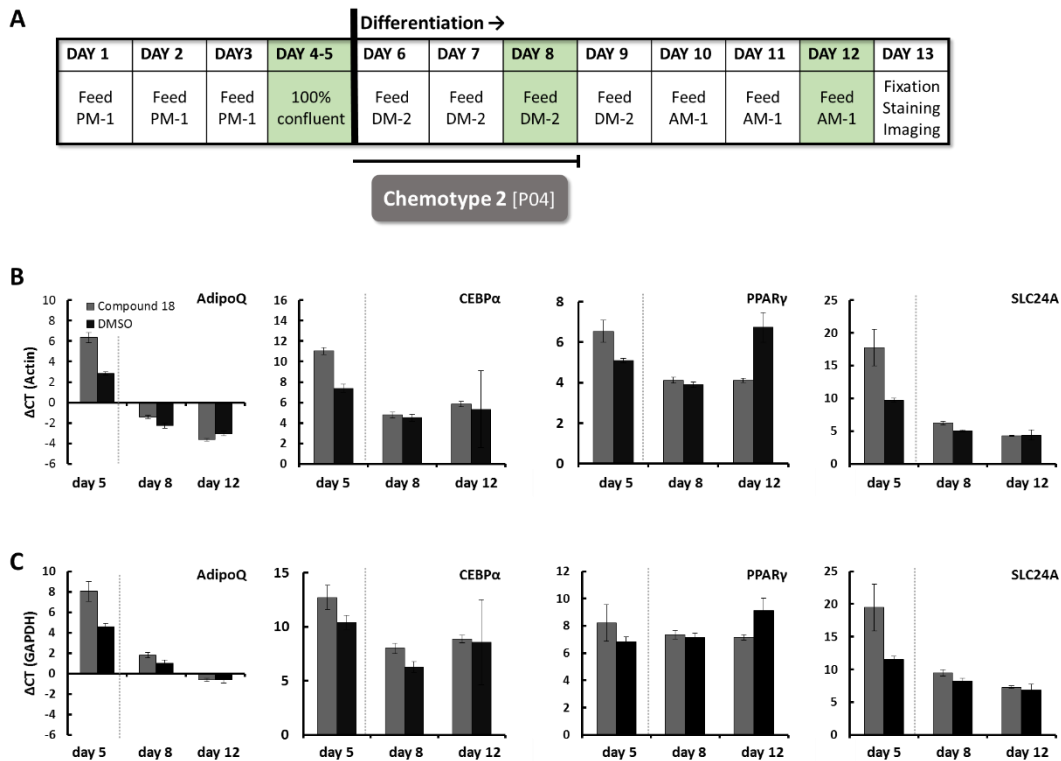


**FIGURE 21: Quantitative real time PCR analysis of differentiation markers involved in adipogenesis of 3T3-L1 cells** showed no significant changes between DMSO treated or Chemotype 2 [P04] treated cells throughout the differentiation process. **A** 3T3 cells were differentiated according to standard procedure (by Yaqin Zhang, NIH, USA). Total RNA was isolated at different time points throughout the experiment: day 5 (undifferentiated state), day 8 (stop of small molecule treatment) and day 12 (prolonged cultivation) in differentiated state. The relative expression level was determined for different expression markers by the  $\Delta$ CT method. **B** Actin normalization **C** GAPDH normalization (AdipoQ: Adiponectin; CEBP $\alpha$ : CCAAT/ enhancer binding protein alpha; PPAR $\gamma$ : peroxisome proliferator activator receptor gamma; Slc24a: glucose uptake transporter GLUT4).

#### 4.1.5.3 FFA uptake is not impaired by Chemotype 2

A block in lipid uptake was considered as the easiest explanation for the lack of LDs after small molecule treatment. Currently, different models explain the uptake of circulating, albumin bound

FFAs in living systems. In whole organisms FFAs either originate from postprandial FFA increase or from release from adipose tissue. In cellular experiments, FFAs are routinely administered with the culture medium in an albumin bound form at 400  $\mu$ M, representing circulating FFA plasma levels (Regensteiner et al, 2009). FFA can either be incorporated in cells driven by the transmembrane concentration gradient by a suggested flip-flop mechanism of non-ionized FFAs or by directed transport via membrane bound proteins with high affinity for fatty acids (Hamilton, 1998). Known transporters are the fatty acid translocase (FAT/CD36) (Bonen et al, 2004), the plasma membrane-associated fatty acid-binding protein (FABPpm) and members of the fatty acid transport proteins family (FATPs) (Anderson & Stahl, 2013).

Lipid Uptake inhibition was tested in a direct cellular FFA uptake assay based on the BODIPY-dodecanoic acid analog (QBT- Uptake Assay, Molecular Devices). Extracellular fatty acid analogs are quenched which is reversed upon fatty acid incorporation. Cellular fatty acid uptake can thus be followed by an increased fluorescence signal. The tested chemotypes did not inhibit the uptake of the BODIPY-analog in *Drosophila* S3 cells (see Figure 22). Additional competition experiments with unlabeled FFAs did support this finding (data not presented). Thus, blocked fatty acid uptake can be excluded as a cause of the LD reduced phenotype. This finding goes in hand with previous experiments that already suggested that lipid uptake is not impaired since endogenous LD formation was successfully blocked (see Chapter 4.1.5.2).

In contrast, AML12 cells did not respond to the QBT-assay format, presumably due to missing FATP transporters, which are dominantly found on differentiated adipocytes. As stated from the manufacturer, undifferentiated cells do not internalize the BODIPY-FFA or store it in LDs at assay conditions. It was assumed that *Drosophila* Kc167 cells were tested positive due to their embryonic character. However, radiolabeled FFA uptake measurements in mammalian cells by Dr. Thomas Eichmann (University of Graz, Austria) confirmed previous observations. Accordingly, a block in fatty acid uptake as a cause for the observed decreased lipid storage can be excluded.

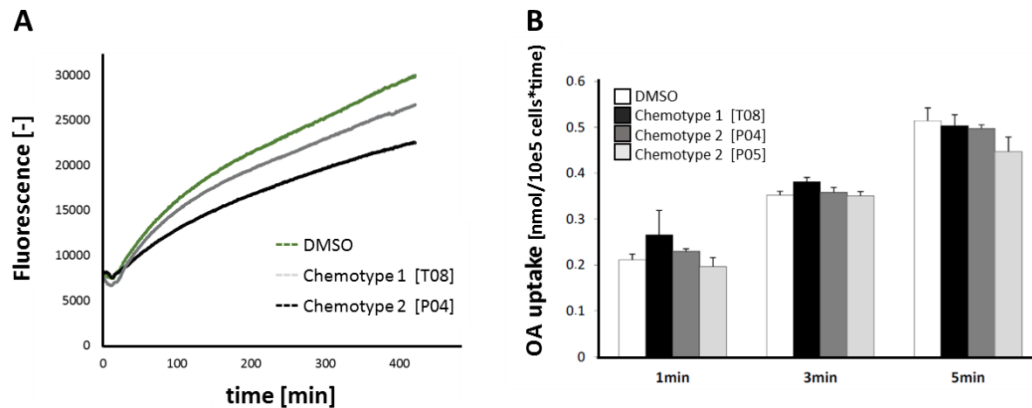


**FIGURE 22: FFA uptake assays confirmed that a blocked FFA is not the underlying cause for the observed LD reduced phenotype. A** Fluoresce/Quenching based QBT-Assay in *Drosophila* Kc167 cells did not show any significances in the uptake of fluorescently labeled FFAs between the DMSO control and active/ inactive derivatives of Chemotype 2. **B** The unaltered lipid uptake behavior of small molecule treated cells was confirmed in a radiolabeled assay in COS7 cells. The radiometric assay was performed by Dr. Thomas O. Eichmann (Graz University, Austria).

#### 4.1.5.4 Lipolysis is not activated by Chemotype 2

During lipolysis TAGs are hydrolyzed by lipases into their glycerol backbone and the respective FFA moieties. Both can be subsequently used for energy production via  $\beta$ -oxidation or as building blocks for membranes or hormones. Lipolytic signals are mostly endocrinologically coordinated: hormones such as epinephrine, norepinephrine, glucagon, growth hormones, testosterone or cortisol activate lipolysis via G-protein coupled receptor (GPCR) activation (Blad et al, 2012).

Lipolytic activation can be considered as a cause of the LD reduced phenotype in presence of the small molecules. This would imply a temporarily unaffected LD generation triggered by the high FFA concentrations, followed by an immediate enhanced lipolysis. This theory requires a direct processing of the lipolytically released FFAs, since an accumulation of FFAs or alternative lipid species induce cytotoxicity. Lipid analysis in cells, however, did not point to significant accumulations of lipid species compared to the controls (see 4.2.4.1).

In order to further investigate lipolytic activation, cells which already contain LD at the point of compound application were used in the LD assay. Lipolysis would consequently decrease the LD count as TAG are hydrolyzed. Chemotype 2 [P04] treatment, however, did not remobilize already existing LDs (see Figure 23). The LD count remained at the high initial lipid level of the respective controls. Additional indications against a lipolytic activation as a cause for the LD reduction were made during time course experiments by the absence of intermediate LDs (see Chapter 4.1.3.1.4, p.27).

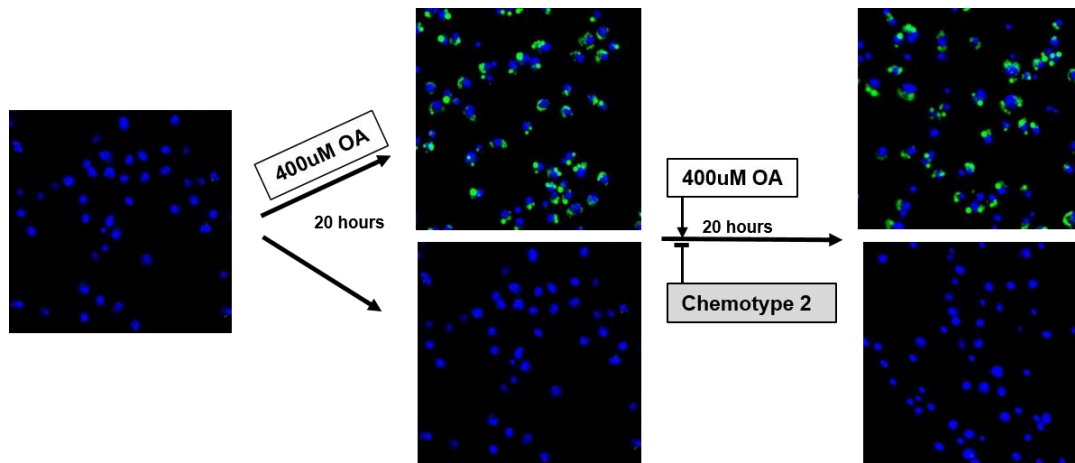


**FIGURE 23: LD remobilization assay in cells with already existing lipid droplets prior to Chemotype 2 [P04] treatment in order to test lipolytic activation.** *Drosophila* S3 cells were exposed to 400  $\mu$ M OA in order to increase the initial cellular LD concentration. The pre-fed cells were then treated with 5  $\mu$ M small molecule [P04] in the classical LD assay. If LDs were already present in the cells, the P04 did not induce the LD reduced phenotype. Similar effects were seen in AML12 and COS7 cells respectively, as well as with derivatives of the other phenotypes. (blue: nuclei; green: LDs)

The lack of the ability to remobilize existing LDs highlights that lipolytic activation is not increased by the small molecules and thus it is not considered as the primary cause of the observed LD reduced phenotype. Screening of selected derivatives of all chemotypes in pre-fed cells supported this finding (see Supplemental Figure 7, p.185). Only one derivative of Chemotype 1 and 3 each showed moderate properties for remobilization of existing lipids, but were not further followed.

#### 4.1.5.5 Elevated $\beta$ -oxidation is involved in the LD reduced Phenotype

Generally, incorporated FFAs are either stored in LDs or directly shuffled to energy production pathways where they are subsequently degraded. Stored lipids can be hydrolyzed in times of energy demand and the resultant FFA are again subjected to mitochondrial  $\beta$ -oxidation. In the following subchapter the  $\beta$ -oxidation process is under closer examination for a potential cause for the LD reduced phenotype. The transcriptome analysis (see Chapter 4.1.4.2) revealed that all three chemotypes provoke a common significant increase in gene expression levels of genes involved in  $\beta$ -oxidation. This result support the hypothesis that the target candidates are likely involved in  $\beta$ -oxidative processes themselves as a direct cause or trigger  $\beta$ -oxidation as an indirect cellular response in order to prevent lipotoxicity.

$\beta$ -oxidation occurs in the mitochondrial matrix. In order to investigate the mitochondrial distribution and mitochondrial counts within small molecule treated cells, metabolic active organelles were stained with a commercial MitoTracker™ stain (Life Technologies). This microscopy based analysis

revealed an increase in the mitochondrial signal for Chemotype 3, while no alteration were obvious for Chemotype 1 and Chemotype 2 (see Figure 24.A). Further analysis of Chemotype 3 indicated that this mitochondrial signal increase was specific for active derivatives (see Figure 24.B). As Chemotype 3 was not included in the chemical proteomic target identification approach (see Chapter 4.5), this finding was not further followed up. Nevertheless, an increased mitochondrial count can be considered as an underlying cause for the indicated elevated  $\beta$ -oxidation processes.

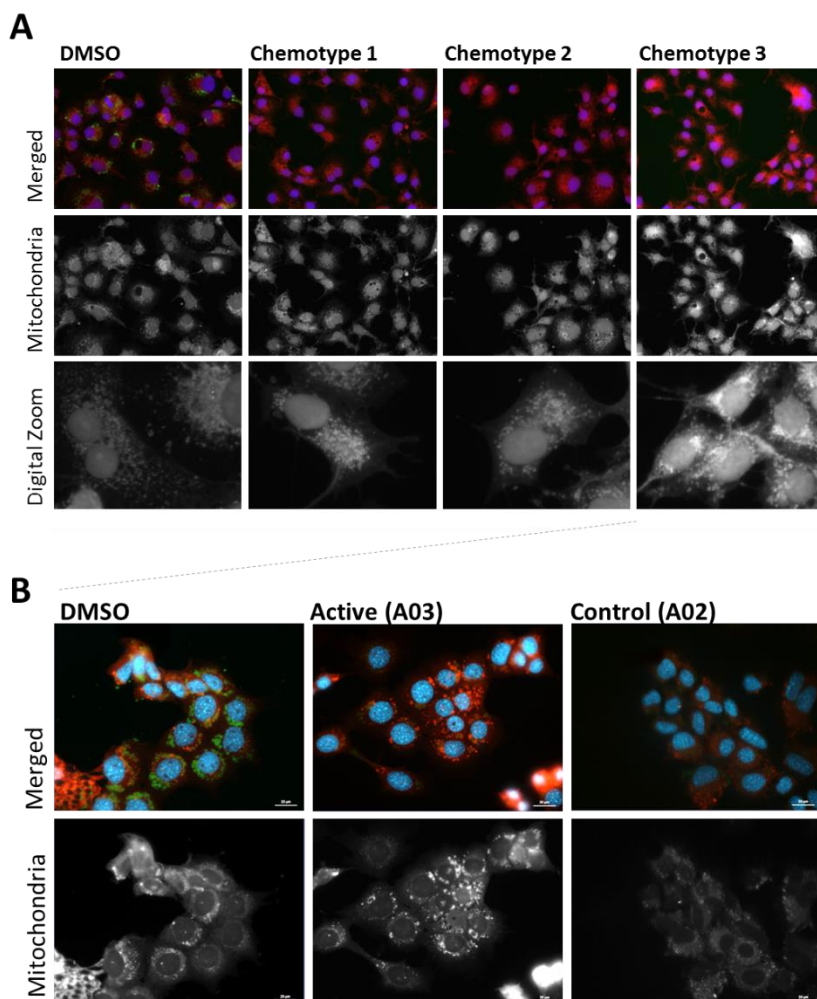


**FIGURE 24: Mitochondrial staining of small molecule treated AML12. AI** AML12 cells were treated with 1  $\mu$ M small molecule in the presence of 200  $\mu$ M OA for 18 h. Living cells were stained for mitochondria with MitoTracker™ Red (Invitrogen™). Cells were fixed and stained for nuclei (Hoechst 33342; blue) and LDs (BODIPY® 493/503; green). The images were acquired at the Zeiss Observer Z1, 40x. (Chemotype 1 [T08], Chemotype 2 [P04], Chemotype 3 [A03], 0.2% DMSO (v/v)). **BI** AML12 cells with active and inactive control derivatives of Chemotype 3. The images were acquired at the Zeiss Observer Z1, 63x, oil (scalebar: 20  $\mu$ M).



In order to further analyze the mechanistic involvement of  $\beta$ -oxidation the fatty acid derivative tetradecylthioacetic acid (TTA) that cannot be processed by  $\beta$ -oxidation due to the sulfur atom in the  $\beta$ -position (Tronstad et al, 2003) was applied as an external fatty acid substrate in the LD assay (see Figure 26.A). TTA showed a concentration dependent LD formation in cells (see Figure 26.B), however, high TTA concentrations led to a decreased cell number indicating cytotoxicity of free TTA. Literature descriptions confirmed apoptosis induction by TTA (Berge et al, 2003).

Surprisingly, when AML12 cells were fed with 200  $\mu$ M TTA as the sole external FFA source during small molecule treatment, differences in the TTA incorporation behavior were observed between Chemotype 1 and Chemotype 2 (see Figure 26.C). While Chemotype 1 only mildly reduced the ratio of LD per cell at high small molecule concentrations (5  $\mu$ M T08), Chemotype 2 showed a significant LD decrease per cell. This result suggest distinct modes of action of the two examined chemotypes. As Chemotype 1 lacks the ability to metabolize TTA, it can be assumed that this chemotype potentially is strongly dependent on a direct increase in  $\beta$ -oxidation. Direct shuffling of FFAs into  $\beta$ -oxidation is a likely explanation for the hindered LD formation in standard assay conditions. It additionally prevents cells exposed to high FFA concentration from lipotoxicity of the internalized FFAs. In case that the  $\beta$ -oxidation blocked, as seen by the nonprocessable TTAs, the phenotype is reversed as the TTAs are no longer processed by  $\beta$ -oxidation.

Chemotype 2 in contrast, shows even for the modified FFA a reduction of LD counts per cell. This indicates a  $\beta$ -oxidation independent process as a cause of the LD reduced phenotype upon small molecule treatment. The transcriptome analysis (see chapter 4.1.4.2) additionally indicated a lower extent of upregulated  $\beta$ -oxidative genes for Chemotype 2 treated cells compared to the other chemotypes.

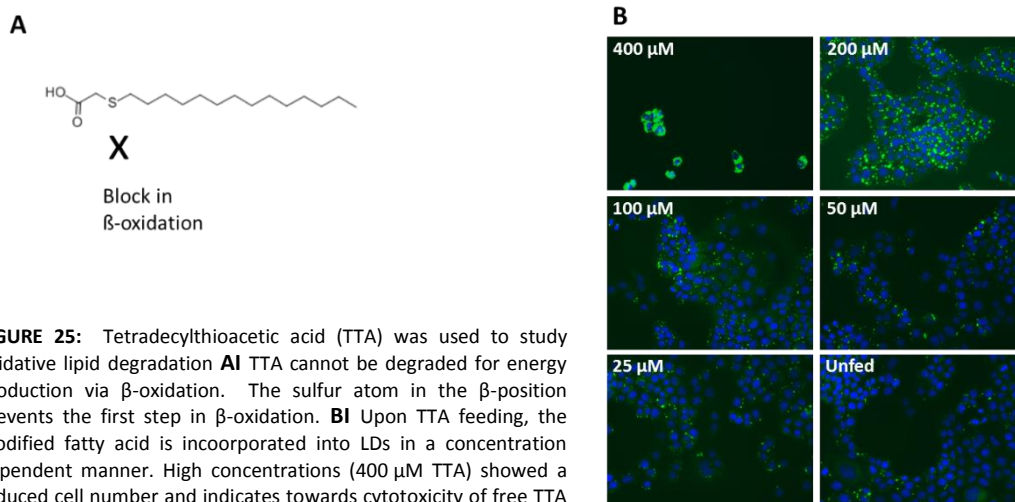


**FIGURE 25:** Tetradecylthioacetic acid (TTA) was used to study oxidative lipid degradation **A** TTA cannot be degraded for energy production via  $\beta$ -oxidation. The sulfur atom in the  $\beta$ -position prevents the first step in  $\beta$ -oxidation. **B** Upon TTA feeding, the modified fatty acid is incorporated into LDs in a concentration dependent manner. High concentrations (400  $\mu$ M TTA) showed a reduced cell number and indicates towards cytotoxicity of free TTA within the cell.

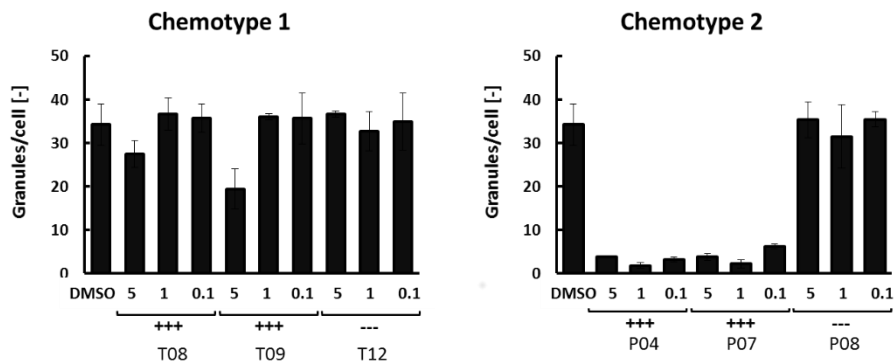


**FIGURE 26: Analysis for  $\beta$ -oxidation activation by Chemotypes 1+2 as a cause for the LD reduced phenotype.** AML12 cells were treated with 5  $\mu$ M small molecule in presence of 200  $\mu$ M TTA for 16 h. While the the average number of LDs/cell mildly changed in Chemotype 1 [T08-T09] treated AML12 cells, the TTA accumulation in LDs was disturbed in Chemotype 2 [P04-P07] treated cells.

#### 4.1.6 PATHWAYS INVOLVED IN LIPID STORAGE MODULATION

In the previous sub-chapters the direct molecular mechanisms of FFA uptake, lipid storage and lipid degradation for energy production were investigated. This subchapter in contrast focuses on the underlying signaling pathways, which might be involved in the metabolic regulation.

##### 4.1.6.1 Adipocyte Differentiation in undifferentiated Cells

The differentiation of LD free pre-adipocytes to LD loaded adipocytes is regulated by a number of pathways and transcription factors (Poulos et al, 2010). Previous experiments revealed that the adipocyte differentiation is not changed in Chemotype 2 treated differentiating 3T3-L1 adipocytes. Despite an apparently unaltered adipogenesis in pre-adipocyte model cells, the LD reduced phenotype was observed in the differentiated adipocytes (see Chapter 4.1.5.2).

Whether Chemotype 2 itself directly affects the differentiation process in the standard LD assay of undifferentiated 3T3-L1 cells, was closer investigated by qPCR analysis of the respective expression markers. The expression levels were examined at an early time point in the assay at 4h and 16h after small molecule application. Expression level analysis of selected differentiation markers showed no differences of the P04 and control samples (see Figure 27). Thus it was assumed that Chemotype 2 does not induce adipocyte differentiation in absence of the classical differentiation markers dexamethasone and IBMX.

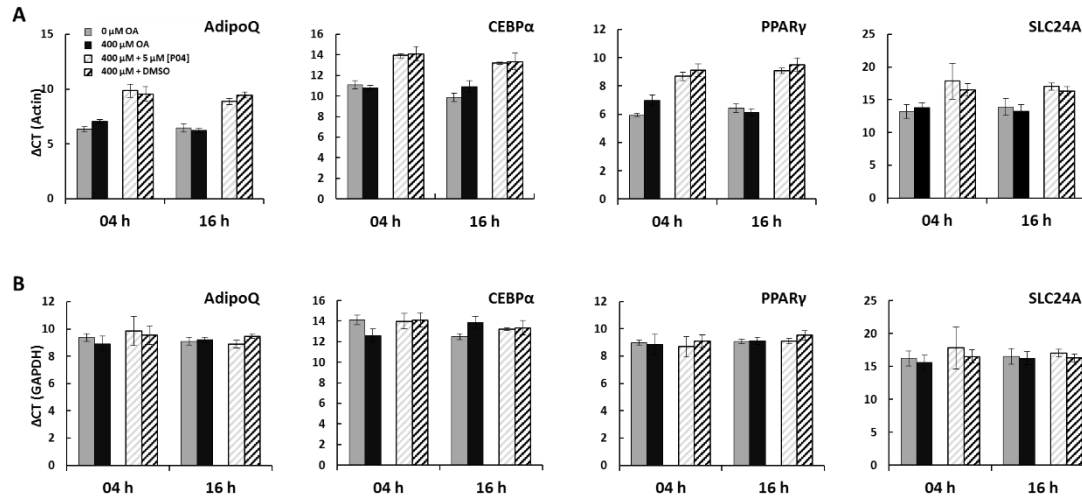


**FIGURE 27: Expression levels of undifferentiated 3T3-L1 pre-adipocytes in presence of oleic acid and Chemotype 2 in order to test for induction of adipogenesis by P04.** Undifferentiated 3T3-L1 cells were either solely treated with or without 400  $\mu$ M OA (filled bars) or with 5  $\mu$ M Chemotype 2 [P04] in presence of 400  $\mu$ M OA (shaded bars). Total mRNA was isolated and analyzed by quantitative PCR.  $\Delta$ CT was either determined for **AI** actin or **BI** GAPDH as a reference for relative changes for the expression level (AdipoQ: Adiponectin; CEBP $\alpha$ : CCAAT/ enhancer binding protein alpha; PPAR $\gamma$ : peroxisome proliferator activator receptor gamma; SLC24A: glucose uptake transporter (GLUT4) transporter gene family).

At the same time, it was tested whether the presence or absence of OA in the culture medium has any effects on adipogenesis of undifferentiated 3T3-L1 cells themselves (shaded bars in Figure 27). Undifferentiated 3T3 cells were cultured without any differentiation inducers and tested for the respective expression markers in qPCR. The expression level of the tested differentiation markers remained at constant levels (see Figure 27, filled bars). This confirms that the presence of OA does not induce adipocyte differentiation in 3T3-L1.

#### 4.1.6.2 *Wnt* and Hedgehog Signaling Pathways

Hedgehog (*Hh*) and wingless (*Wnt*) signaling pathways play an important role in embryonic development of many tissues and are also known to be involved in the control of fat levels in flies and mammals. In cultured cells hedgehog signaling blocks the differentiation of pre-adipocytes to white adipocytes (Pospisilik et al, 2010). Various members of the *Wnt* family inhibit adipogenesis as well, such as WNT10B which was shown to maintain 3T3-L1 cells in the undifferentiated state via PPAR $\gamma$  and c/EBP- $\alpha$  interaction (Ross et al, 2000). Based on these data, active and inactive derivatives of the newly identified LDSA small molecules were submitted for activity screening in the COMAS facility in Dortmund to address a possible modulation of *Wnt*/ or Hedgehog signaling (see Table 2 for *Hh* and Table 3 for *Wnt*).

Only Chemotype 1 showed moderate activation of the Hh pathway with an IC<sub>50</sub> value of 6.5 ± 1.5 μM without affecting cytotoxicity. The tested known inactive derivative, showed even decreased IC<sub>50</sub> values of 0.81 ± 0.1 μM, however, on costs of cytotoxicity. This weak sonic hedgehog activation is not likely to be the primary mechanism of action for the observed nanomolar phenotype in the cellular lipid droplet assay.

Both Wnt and Hh pathway were not prominently inhibited by any of the tested chemotypes. Therefore, it is unlikely that the small molecule phenotype is a result of altered Hh or Wnt signaling for any of the three tested chemical scaffold.

**TABLE 2: LDSA Small molecules show no prominent hedgehog activity modulation in a C3H/10T1/2 cell based osteogenesis HTS assay (performed by COMAS, Dortmund).**

Chemotype	Derivative	Activity <sup>1</sup>	IC <sub>50</sub> Sonic Hedgehog [μM]			IC <sub>50</sub> Cytotoxicity [μM]		
1	T08	active	7.35	7.71	4.33	inactive	inactive	inactive
	T09	active	> 10 μM	> 10 μM	7.90	inactive	inactive	inactive
	T12	inactive	0.77	0.94	0.73	7.58	4.81	4.86
2	P04	active	inactive	> 10 μM	9.09	inactive	inactive	inactive
	P05	active	inactive	inactive	inactive	inactive	inactive	inactive
	P08	inactive	7.47	8.95	8.88	inactive	inactive	inactive
3	A03	active	inactive	inactive	inactive	inactive	inactive	inactive
	A21	active	inactive	inactive	inactive	inactive	inactive	inactive
	A02	inactive	inactive	inactive	inactive	inactive	inactive	inactive

**TABLE 3: LDSA Small molecules show no Wnt pathway activity in a HEK293-FZ TOPFLASH cell based HTS assay (performed by COMAS, Dortmund).**

Chemotype	Derivative	Activity <sup>1</sup>	IC <sub>50</sub> Wnt Assay [μM]			IC <sub>50</sub> Cytotoxicity [μM]		
1	T08	active	inactive	inactive	inactive	inactive	inactive	inactive
	T12	inactive	> 30 μM	28,27	18,46	> 30 μM	> 30 μM	20,42
	P05	active	inactive	inactive	inactive	> 30 μM	> 30 μM	> 30 μM
2	P08	inactive	10,29	13,23	10,67	9,55	10,52	9,62
	A03	active	inactive	inactive	inactive	inactive	inactive	inactive
3	A02	inactive	inactive	inactive	inactive	inactive	inactive	inactive

<sup>1</sup>Activity in cell based LD assay (Kc167, AML12, COS7 and others)

#### 4.1.7 ATHEROSCLEROSIS MODELS

The differentiation of monocytes into LD loaded foam cells is an established model system to study the pathogenesis of atherosclerosis (see Chapter 5.2, p.100). All three chemotypes were tested in a THP-1 based differentiation assay for activity in either the differentiation process itself or the LD formation in differentiated foam cells. Both processes were not affected by the respective derivatives. The undifferentiated THP-1 cells differentiated in presence of PMA and active small molecule/DMSO into the adherent foam cells including LD formation upon OA treatment (see Figure 28.A). Differentiated THP-1 cells did not show significant alteration in LD count when OA and small

molecule were administered simultaneously (see Figure 28.B). Foam cell LDs show an enriched level of CE (Li & Glass, 2002). In chapter 5.1.5.1.1 it was shown that Chemotype 2 does not affect CE storage. Consequently, the lack of activity of the chemotypes in THP-1 cells can be speculated as a result of the altered lipid species in these cells. However, the detailed causes have to be further analyzed.

This finding indicate that the pathways involved in monocyte differentiation and subsequent foam cell formation are not targeted by the identified small molecule classes. In contrary, the newly discovered hits originating from the COMAS screens (see Chapter 5.2, p.100) target this mechanism. Indicating for a totally different mechanism of action.

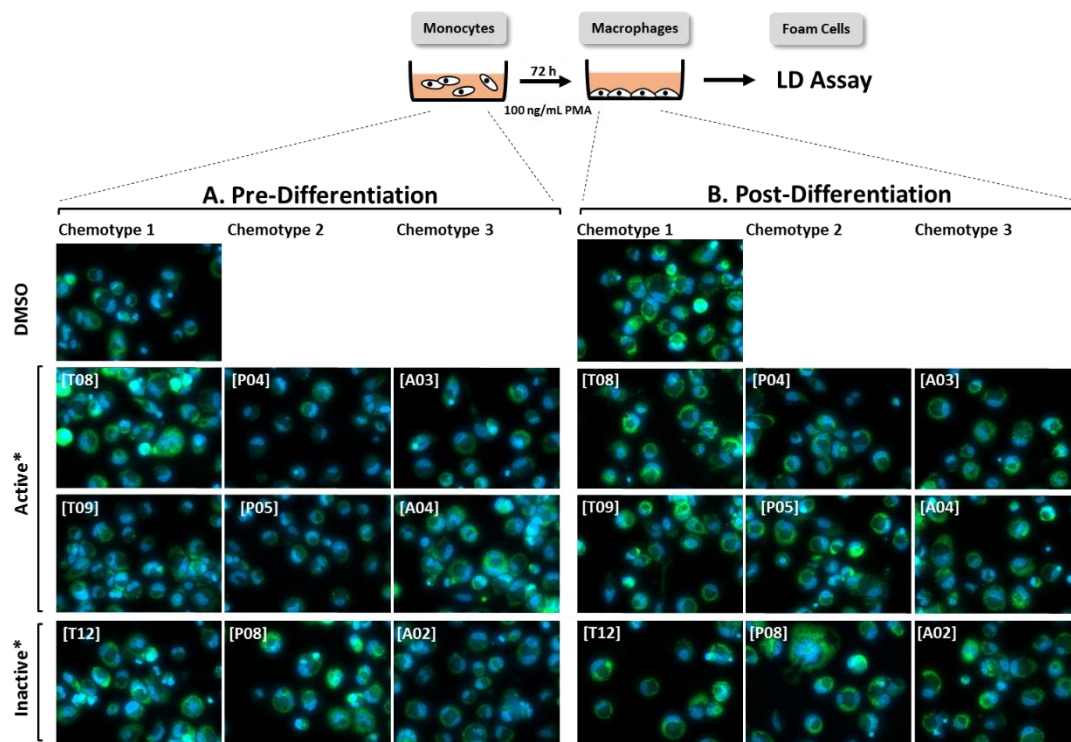


**FIGURE 28:** THP-1 cell based assay to study small molecule modulation in PMA dependent monocyte differentiation and foam cell generation. **A** 5 μM small molecules were added during the PMA differentiation step for 72 h. The cells were then fed with 400 μM OA in order to induce LD formation. **B** 5 μM small molecule was administered in presence of 400 μM OA to differentiated THP-1 cells. (blue: nuclei; green: LDs).

## 4.1.8 SUMMARY

Despite of the original identification of the three Chemotypes in a non-vertebrate cell based screen using *Drosophila* S3 cells, all three Chemotypes show a translational activity to different mammalian cell lines. This points to a conserved target. Chemotype 2 additionally showed in vivo activity in flies, where it successfully reduced the overall lipid stores without obvious toxic effects. A wide set of physiological experiments suggested that the Chemotypes most likely cause the LD reduced phenotype via different molecular targets, however, with a common upregulation in  $\beta$ -oxidation. LD reduction as a consequence of a blocked lipid uptake or an increased lipolysis were excluded for all Chemotypes.

Chemotype 2 additionally showed a unique temporal accumulation of DAG. This supports the hypothesis that the DGAT enzymes can be accounted for the lean phenotype. DGAT was further validated in Chapter 4.4 (p.79).

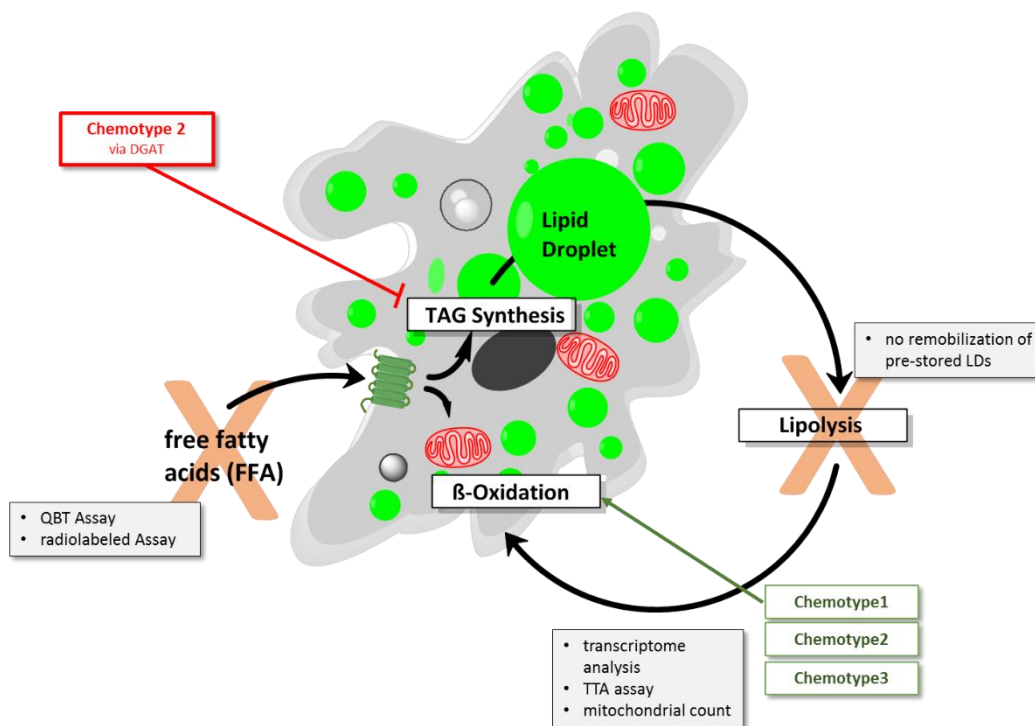


**FIGURE 29: Current hypothesis of potential Target and/or concerned Pathways.** Based on the functional small molecule characterization one of the DGAT isoforms is considered as a direct functional target of Chemotype 2. DGAT inhibition blocks the final step in TAG synthesis. The FFAs are then metabolized by an increased  $\beta$ -oxidation. Chemotypes 1+ 3 are considered to modulate proteins involved in an increased  $\beta$ -oxidation. Further direct target identification processes by chemical proteomics aim to name those.

## 4.2 CHEMICAL PROTEOMIC APPROACH FOR TARGET IDENTIFICATION

This chapter summarizes the optimization process of the experimental setup aiming at the identification of direct protein binding partners for two of the three investigated small molecules (Chemotypes 1+2). The chosen chemical proteomic approach (*pull-down*) is based on modified chemical probes which were exposed as chemical affinity reagents to a bulk mixture of potential interaction partners (see further explanation in Chapter 7.4, p.133). Proteins which interact specifically with the respective small molecule, were enriched out of bulk, soluble cell lysate. Isolated proteins were enzymatically digested and analyzed by means of qualitative and quantitative mass spectrometry. Statistical evaluation highlighted potential target candidates for the respective chemotypes, which were analyzed in greater detail in subsequent validation experiments (see Chapter 4.3-4.4). The underlying experimental considerations involved in the different optimization steps throughout the chemical proteomic approach for Chemotype 1 are summarized in Figure 30.

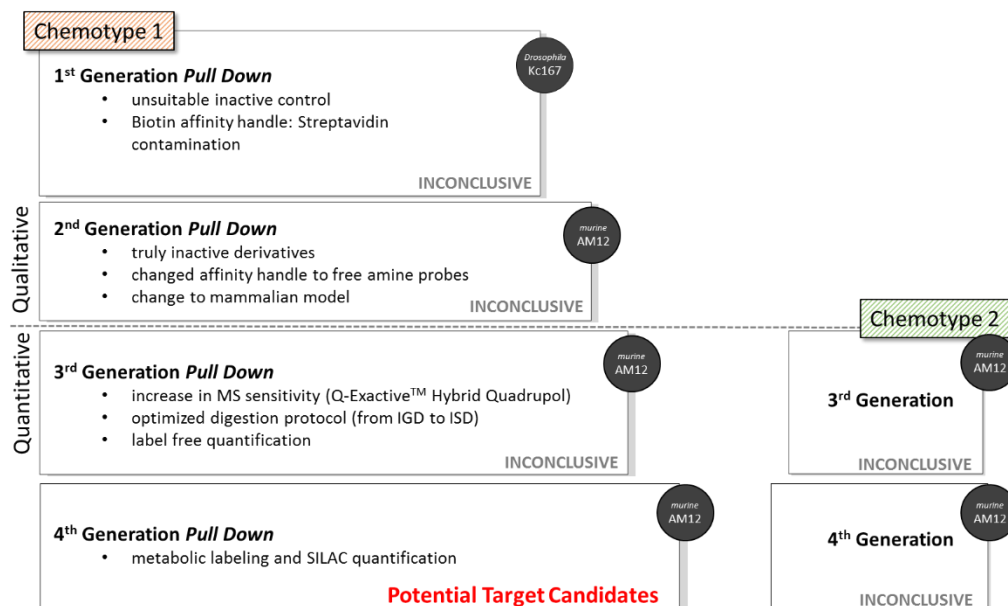


**FIGURE 30: Schematic summary of the process optimization workflow for the chemical proteomic target ID (*pull-down*).** The pull-down protocol was iteratively refined in different “generations” of pull-downs. The quantitative 3<sup>rd</sup> and 4<sup>th</sup> generations finally resulted in a coherent data set and allowed the identification of potential target candidates. (IGD: in-gel digest; ISD: in-solution digest; SILAC: stable isotope labeling of amino acids in cell culture).

#### 4.2.1 CHEMICAL PROBE OPTIMIZATION (1<sup>ST</sup> GENERATION)

The 1<sup>st</sup> generation affinity probes for Chemotype 1 [T01+T02] were based on a biotin linker attached to the terminal hydroxyphenyl moiety, without affecting activity in *Drosophila* S3 cells or murine AML12 cells (see Figure 31.A). The activity of Chemotype 1 strongly correlated with the stereochemistry. The positive enantiomer was 1000 times more active in reducing LD stores in the cell based LD assay. The enantiomers were used as active and control probe, respectively. In the optimization process, however, it was soon discovered that the originally considered inactive enantiomer retained little, but significant activity. This undesired property was only seen in the enzyme based colorimetric TAG assay (40% inhibition at 5  $\mu$ M assay concentration, see Figure 31.C), while the initial microscopic LD assay implied inactivity. The observed discrepancy between the two assays was discussed before (see Chapter 4.2.1). The remaining activity of the presumably inactive control probe was a major drawback in the qualitative experimental design. New truly inactive derivatives were required, since small molecules with even minor remaining activity might still be capable to bind the protein target.

Throughout the chemical proteomic setup, proteins that (specifically) interact with the investigated small molecule were identified by mass spectrometry. At this experimental stage, these proteins were solely evaluated in regard to their presence in the samples of the respective active and control probes in different experimental replicates. Potential target protein candidates were defined by enrichment in the active probe in comparison to the control sample as a consequence of specific protein- small molecule interactions. This qualitative experimental design highlights the importance of a truly inactive control probe as negative control. Falsely included proteins in the MS-based evaluation mislead the target definition and disparage the likelihood of successful target prediction. Thus, the target risks to bypass identification, even if it is present in the initial dataset.

The approximately 1000 fold activity difference between the enantiomers [T01+ T02] of Chemotype 1 handicaps successful identification of specific binders in the 1<sup>st</sup> generation qualitative proteomic setup. Most identified proteins were consequently found in both the active and control samples and thus were not considered as a potential target (see Supplemental Table 5, p.186). In total 205 different proteins were identified in the 1<sup>st</sup> generation pull- down. Of those 16 are preferentially enriched in the active probe. These proteins were identified in the active probe at least 3 out of 5 replicates and indicated enrichment in the active probe by a difference of >2 appearance counts.

In summary, the 1<sup>st</sup> generation of pull- down experiments highlighted the necessity of a new set of pull- down probes with a true negative control, as well as a method to quantify abundance of the identified proteins.

**1<sup>ST</sup> GENERATION:**

Enantioselective positive and negative probes were immobilized via biotin-streptavidin interaction on commercial neutravidin- agarose beads.

**MS-results:**

*inconclusive due to remaining activity of the control probe and a lack of quantitative MS- evaluation*



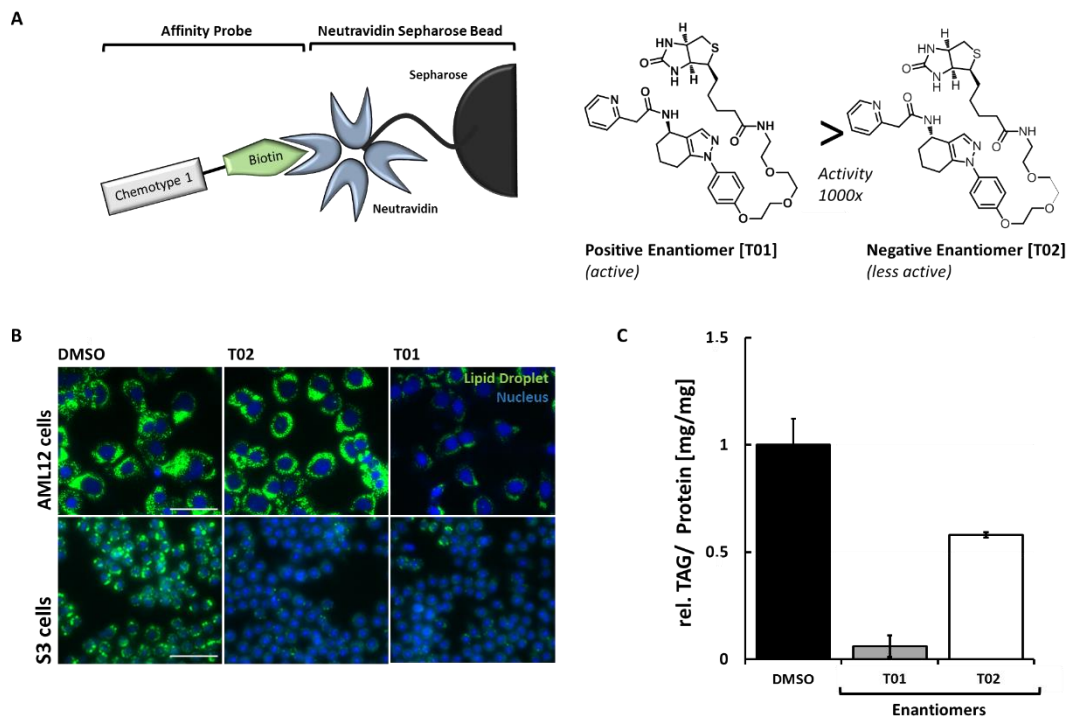


**FIGURE 31:** The 1<sup>st</sup> generation affinity probes for the chemical proteomic target identification approach for Chemotype 1 were based on a biotin linker attached to the terminal phenol moiety without affecting bioactivity. **A** The attached biotin allowed small molecule immobilization via streptavidin interaction in order to generate functional affinity beads. The resultant conjugate represents the basis for the affinity purification in the pull-down experiment [T01+T02]. **B** Stereochemistry affects the activity of Chemotype 1 as shown by the microscopic LD assay in murine AML12 and *Drosophila* S3 cells, respectively. **C** The negative enantiomer (inactive control probe) retained activity in the colorimetric TAG assay (40% inhibition), while the initial microscopic LD assay implied inactivity as LDs were absent.

#### 4.2.2 MODIFICATION OF THE AFFINITY TAG (2<sup>ND</sup> GENERATION)

In the 2<sup>nd</sup> generation pull-downs a truly inactive control probe [T04] for Chemotype 1 was introduced. Inactivity was gained by replacement of the pyridine group by a dimethyl-amine. This substitution resulted in a secured activity decrease in both in the microscopic- and the colorimetric lipid storage assay. The lack of a truly inactive control probe might at first appear as a “luxury problem”, as conventional probe optimization mostly directs to further activity gain. Nevertheless, a truly inactive control is of importance for the success of pull-down the experiment. The problem to identify truly inactive derivatives is a trade-off of the highly active small molecules with nanomolar EC<sub>50</sub> values.

The affinity probe T04 was additionally modified in regard to the functional group required for immobilization. In the 1<sup>st</sup> generation pull-down the small molecules were immobilized on agarose beads via the biotin- neutravidin interaction. The resultant high background of proteins identified in both active and control probes was speculated to be a result of endogenous biotin-binding proteins.

**2<sup>ND</sup> GENERATION:**  
Truly inactive probes were introduced as controls. The affinity linker was changed towards a free amine group and the biological system was changed to mammalian cell lysates (AML12 cells).  
**MS-results:**  
inconclusive as quantitative MS-data analysis was lacking

Another disadvantage of the neutravidin based immobilization was that neutravidin was digested itself in the trypsination step. High levels of these undesired peptides superimpose the respective  $m/z$  range, which bears the risk to miss the target peptides if those are separated within this range. Precautiously, the biotin was thus replaced with the smaller free amine group. This allowed covalent coupling of the examined derivatives of Chemotype 1 to commercial NHS-decorated magnetic sepharose beads via a succinimidyl ester formation (see Figure 32). The magnetic core additionally improved sample handling in respect of process time and washing conditions, as the beads can easily be separated in a magnetic field.

In the 2<sup>nd</sup> generation pull-down 875 different proteins were identified. This significantly increased number is probably not only based on the altered experimental setup but also the changed biological system. As the small molecule were identified as inhibitors of LD formation in *Drosophila* S3 cells, the first generation of pull-downs was carried out with *Drosophila* cell lysates. Translational activity in mammalian cells (see Chapter 4.1.2.2) supported the shift to AML12 cells, as these cells retain a broader application range in regard to later metabolic labeling compared to the less frequently used non-vertebrate cells. As the genome and proteome of AML12 cells is more complex (~30.000 protein coding genes) compared to *Drosophila* S3 cells (~14.000 protein coding genes), the magnitude of identified proteins was likely increased. This rise emphasizes the necessity to quantitatively evaluate the identified proteins in order to increase the likelihood for a successful identification of target candidates out of the complex lists with potential candidates.

Of the 875 identified proteins, 25 proteins were more often identified in the active sample [T03] of Chemotype 1 (see Supplemental Table 7, p.188). The proteins were present at least two out of three times in the active probe [T03] or showed an enrichment in the active probe [T03] compared to the inactive control probe [T04] by a difference of >2 counts. Thereof, three top candidates of this list are annexin A2 (ANXA2), the alpha-enolase (ENOA) and the FSHD region gene 1 protein (FRG1). These proteins were uniquely identified in the active probe in all individual replicates (n=3). Nevertheless, at this stage detailed target validation remained highly risky as it was likely that the target persisted in the non-specific protein moiety. Quantitative data analysis was therefore introduced in the next generation of pull-downs.

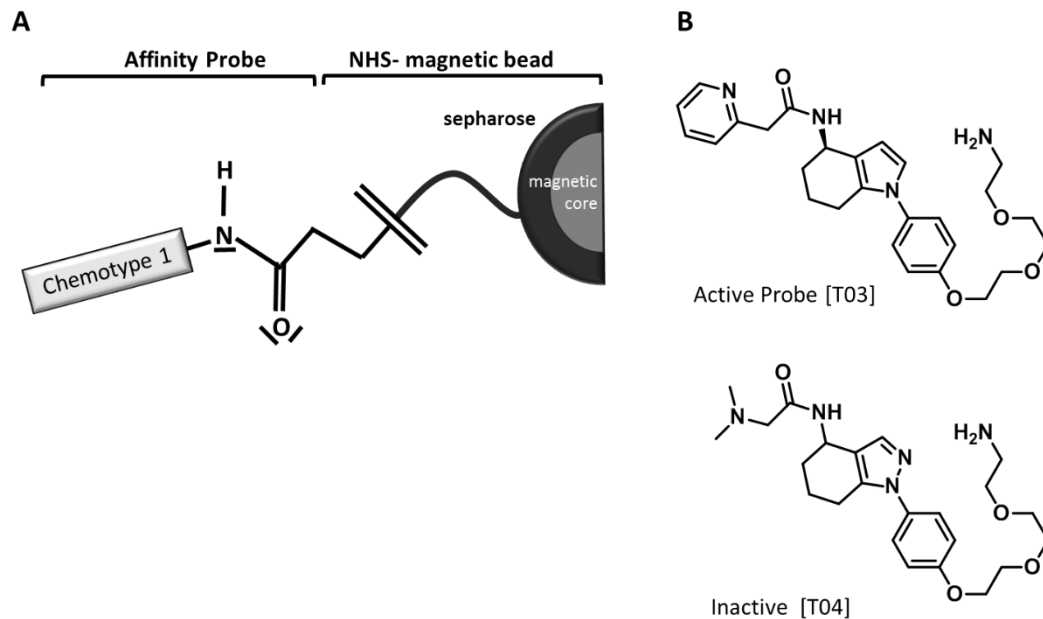


**FIGURE 32: New 2<sup>nd</sup> generation pull-down probes for Chemotype 1.** The new probes contain a free amine group [T03+T04], which replaced the previous biotin group [T01+T02]. This allowed covalent succinimidyl ester coupling to NHS sepharose beads.

#### 4.2.3 OPTIMIZED SAMPLE PREPARATION (3<sup>RD</sup> GENERATION)

Significant alterations in sample processing were introduced in the third generation pull-down. MS sensitivity was increased by a new Q Exactive™ Hybrid Quadrupole-Orbitrap Mass Spectrometer (Thermo Scientific). This on the one hand allowed measurement of more complex samples and was on the other hand required for label free quantification. A trade-off of the increased sensitivity was that the overall number of identified proteins drastically increased. The here introduced label free quantification approach allowed estimations of protein abundances on basis of the MS signal. The relative amount of each protein in the respective active and control sample was evaluated by means of the total peptide signal intensities in correlation to the original peptide concentration. In parallel, the peptides were identified according to their MS/MS pattern.

Prerequisite for this quantitative setup were significant changes in sample handling leaving the classical in-gel-digest (IGD) in favor of a direct digestion of the immobilized interacting proteins by in-solution digest (ISD) and consecutive STAGE tip peptide purification (Rappsilber et al, 2007). These overall procedural changes resulted in decreased sample preparation and measuring times, as the individual sample did not need additional fractionalization as required for IGD (see Figure 33). This improved the data quality due to a decreased sample to sample deviation.

In total, 1064 proteins were identified in three biological replicates consisting of three technical replicates each. Most proteins were identified in similar quantities in both samples and show a

**3<sup>RD</sup> GENERATION:**  
MS analytics reached new sensitivity levels by instrument changes (Quadrupole-Orbitrap). This allowed the change from IGD to ISD digest, which optimized sample preparation in quality and time and furthermore allowed label free quantification of the bound proteins.

**MS results:**  
*Target candidates*

correlation based on their similar MS values (see Supplemental Figure 8, p.189). Detailed analysis of one subset consisting of three technical replicates, revealed 45 proteins that were significantly enriched with the active probe (see Supplemental Table 8, p.190). However, when those proteins were compared with the additional biological replicates, most proteins failed re-identification. Only three proteins, were constantly identified with statistical significance (t-test; FDR 0.05,  $s_0 = 2$ ): the nucleotidase domain-containing protein (NT5DC1), the soluble epoxide hydrolase (EPHX2) and the sepiapterin reductase (SPR). The significant enrichment in all replicates strongly supports a potential selective interaction with the active derivative of Chemotype 1 [T03].

Nevertheless, most proteins among the proposed target candidates were solely identified by their absence in the respective negative controls. Only two proteins (Eif1a4 and Acad) were selected based on their significance values (t-test; FDR 0.05) as they were present in both samples (active and control) (see Supplemental Figure 8, p.189). This low number of quantitatively significantly enriched proteins might be due to the high variation between the different biological replicates. In order to further increase the data quality, it was decided to switch to metabolic labeling followed by quantitative SILAC analysis in the 4<sup>th</sup> and final generation of pull-downs.

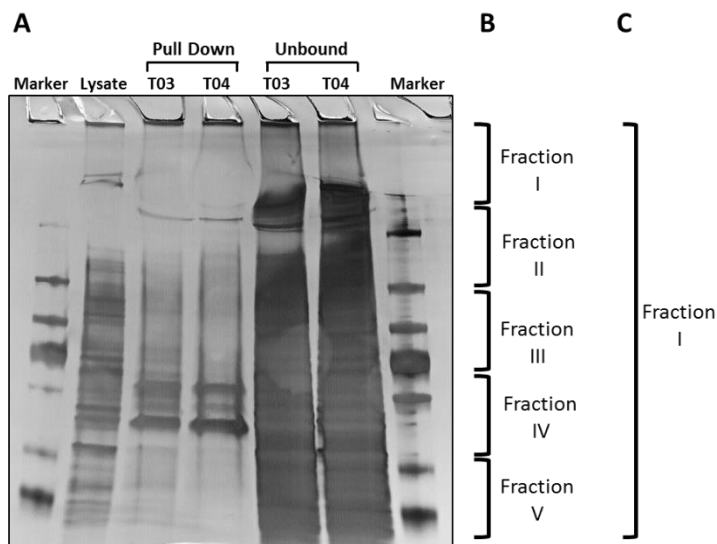


**FIGURE 33: In-gel digestion (IGD) and in-solution digestion (ISD) upon pull-down for Chemotype 1.** **AI** Traditional IGD designs are based on SDS-PAGE separation of all bound proteins towards the active [T03] and control [T04] small molecule derivatives. Ideally, the target protein is solely present or enriched in the active probe. **BI** Following the classical IGD protocol the complete protein moiety was analyzed by MS in five individual fractions. This leads to a rapid amplification in the number of processed samples and their respective analysis times. **CI** Changing to ISD of the bound protein moiety abandoned SDS-PAGE separation, since the complete sample was digested in one reaction directly on the beads.

#### 4.2.4 OPTIMIZATION BY METABOLIC LABELING (4<sup>TH</sup> GENERATION)

The final optimization step in the chemical proteomics based target identification approach was stable isotope labeling of cell culture cells (SILAC). The metabolic labeling of cells by the incorporation of the *heavy* amino acids  $^{13}\text{C}_6$  L-lysine and  $^{13}\text{C}_6^{15}\text{N}_4$  L-arginine into proteins results in a mass difference in comparison to peptides containing the *light* amino acids  $^{12}\text{C}_6$  L-lysine and  $^{12}\text{C}_6^{14}\text{N}_4$  L-arginine. The fixed shift of the respective  $m/z$  values was considered for protein quantification (Hanke et al, 2008; Mann, 2014). The SILAC procedure is schematically summarized in Supplemental Figure 14 (p.209).

In contrast to the employed label-free quantification approach, metabolic labeling had considerably higher accuracies as parallel sample preparation is allowed at early experimental stages. This minimizes sources of variability.

In total, 2546 proteins were identified in the SILAC approach. Therefore, target candidates were defined on basis of statistical evaluation of the SILAC distribution ratios of three independent technical replicates (see Supplemental Table 10, p.194). Among the specific binding proteins for the active derivative of Chemotype 1, several proteins which were already identified in the label free 3<sup>rd</sup> generation pull-down were enriched (FDR 0.05,  $s_0 = 2$ ). These recurrent proteins were NT5DC1, EPHX2 and SPR. Additionally, the deoxycytidine kinase (DCK), the pyridoxal kinase (PDXK) and the mitogen-activated protein kinase 9 (MAPK9; JNK2) moved into focus in this 4<sup>th</sup> generation pull-down. As a consequence high priority candidates were defined, which were closely examined for subsequent target validation (see Chapter 4.3).

#### 4.2.5 ALTERED EXPERIMENTAL SETUPS IN CHEMICAL PROTEOMICS

In order to overcome some of the limitations of the standard pull-down protocols, such as the high number of false positive proteins, several additional protocol modifications were tested in the early phases of pull-down protocol optimization. It was tried to elute the target protein specifically in a competitive situation with an excess of unlabeled “free” small molecules. Additionally, a sequential pull-down was performed. This approach assumes that the target protein is systematically depleted from the bulk lysate if the unbound fraction is sequentially administered to pristine small molecule decorated resin (Babu et al, 2009). Unspecific binders are assumed to remain at constant distribution ratios (active/ control) according to their randomized binding behavior. Specific binding proteins, in contrary, are assumed to show decreasing distribution ratios due to decreased concentration in the active probe as a consequence of specific interaction with the immobilized small molecule. The target protein remains immobilized and is thus excluded from further pull-downs with the unbound fraction. Both approaches remained inconclusive and were not continued (data not shown).

**4<sup>TH</sup> GENERATION:**  
SILAC allowed quantitative evaluation of the protein binders. The process additionally secured high data quality due to early sample multiplexing.

**MS-results:**  
*target candidates*

Two additional experimental setups: a two-tiered pull-down approach and cell lysates of cells that were treated with a high concentration of oleic acid were successfully introduced.

#### 4.2.5.1 Two-Tiered Pull-down: Chemotype Specificity

The project owns the exceptional situation that two chemically unrelated structures, which generate identical phenotypes by interference with presumably different molecular targets (see Chapter 4.1.4), were at the same time in the target ID process. This allowed an altered experimental setup, where the error-prone control derivatives were able to be omitted (see Chapter 4.2.1). Instead, both active probes of the distinct Chemotypes were used in a SILAC approach (Chemotype 1: T03; Chemotype 2 [P01]). The samples were combined after affinity purification and were processed simultaneously. This experimental setup allowed the identification of binding proteins that were specific for the respective chemical scaffold (see Figure 34). A prerequisite is the assumption that distinct proteins are targeted by the different chemotypes. Common targets will remain hidden among the high numbers of unspecific binders.

A general difference in binding behavior between T03 and P01 was indicated in the two-tiered pull-down approach (see Figure 34.A). Among the proteins specifically enriched in Chemotype 1 [T03], significant binders from previous classical affinity proteomic approaches for Chemotype 1 were validated (see Supplemental Table 13, p.198). Especially, the already prioritized proteins NT5DC1, DCK, EPHX2, MAPK9 and PDXK were identified among the Chemotype 1 specific binders. This supports the hypothesis that these proteins are likely specific binders of Chemotype 1 or alternatively highly robust false positive hits.

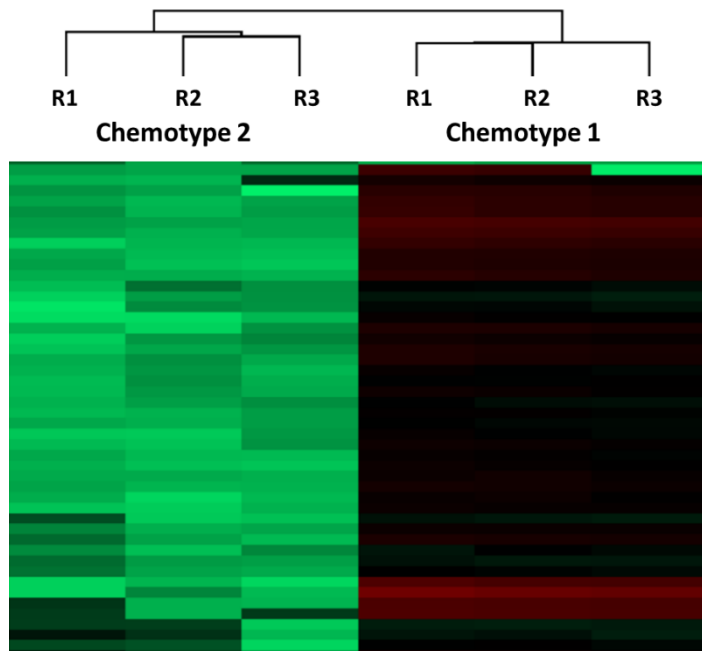


**FIGURE 34:** Schematic summary of the “two-tiered” pull-down approach in order to compare proteins that are enriched by the active probe of Chemotype 1 [T03] and the active probe of Chemotype 2 [P01]. AI Specific binders for Chemotype 1 and Chemotype 2 were plotted according to their respective SILAC ratios. The heatmap summarizes proteins that are highly enriched in T03 (green) and are identified in low intensities in P01 (red). (n=3, R= replicates, technical replicates, SILAC AML12 lysates, 4<sup>th</sup> generation pull-down conditions. The plot was generated by Perseus 1.5.0.31 based data analysis).

#### 4.2.5.2 Oleic acid induced Target Expression

In the classical LD assay, the small molecule is administered simultaneously with high concentrations of OA. Previous transcriptome analysis revealed that the presence of OA itself regulates the expression of genes. Especially genes involved in lipid biosynthetic pathways are downregulated in the presence of external OA sources (see Figure 17, p.33). As a consequence it was considered, that the target gene might be solely existent or enriched in presence of OA and thus lack identification under standard pull-down assay conditions.

In order to investigate this hypothesis, a new pull-down set was generated for Chemotype 1 [T03+T04]. The AML12 cells were therefore cultured in presence of 400  $\mu$ M OA for 24 h. Enriched proteins were evaluated by the label free quantification approach. The obtained proteins lists, however, remained inconclusive due to high statistical deviations between the different biological replicates (see Supplemental Table 12, p.197). Most probably, these deviation are related to the high lipid concentration in the final lysate. Nevertheless, previously defined high priority target candidates were again among the high ranked proteins which are significantly identified in the active probe (t-test; FDR 0.05): These proteins were NT5DC1, DCK and EPHX2 (see Supplemental Table 12, p.197).

## 4.2.6 PREDICTED TARGETS FOR CHEMOTYPE 1

The above summarized optimization processes in the chemical proteomic target identification approach highlighted four proteins that were significantly enriched with the active probe of Chemotype 1 [T03] in the late generation quantitative pull-downs (3<sup>rd</sup>-4<sup>th</sup> generation). The significance (t-test, FDR= 0.05, s0= 2) was consistent within replicates and altered experimental setups (see Table 4). This strongly indicates specific protein binding. The four high priority candidates NT5DC1, DCK, EPHX2 and SPR were considered for subsequent target validation (see Chapter 4.3).

Among those candidates, EPHX2 gained additionally attention as the transcriptome analysis of Chemotype 1 treated cells (see Chapter 4.1.4.2). *Ephx2* gene expression was significantly reduced in *Drosophila* S3 cells treated with 1  $\mu$ M active derivative of Chemotype 1 [T08] treatment for four hours (fold change= -0.65; p= 0.0005). Neither the inactive control derivative of Chemotype 1 [T11] nor probes for the other two chemotypes showed significant regulation of the *Ephx2* gene. This finding indicated that the soluble epoxide hydrolase was specifically downregulated in the active probe of Chemotype 1. Expression levels of all other target candidates were unchanged. Whether this observation is functionally based on Chemotype 1 activity has to be investigated in greater detail.

**TABLE 4: Definition of high priority target candidates for Chemotype 1.** Quantitative pull-down approaches (3<sup>rd</sup> and 4<sup>th</sup>), as well as modified pull-down approaches (OA induction and the specificity oriented two-tiered pull-down) showed a high consistency of significantly enriched proteins for the active derivative of Chemotype 1 [T03] in comparison to the control [T04]. The two highlighted proteins are significantly enriched in the active derivative in all compared experiments. (n.d. = not detected, n.s. = detected but not significant, only A: unique identification in the active probe).

Protein	Gene	4 <sup>th</sup> Generation SILAC ratio	3 <sup>rd</sup> Generation LFQ ratio	OA induced (3 <sup>rd</sup> ) LFQ ratio	Specificity (4 <sup>th</sup> ) SILAC ratio
<b>5-nucleotidase domain-containing P1</b>	<b><i>Nt5dc1</i></b>	<b>2.4 <math>\pm</math> 0.4</b>	<b>only A</b>	<b>only A</b>	<b>CT1</b>
Deoxycytidine kinase	<i>Dck</i>	2.8 $\pm$ 0.3	n.s.	only A	CT1
<b>Epoxide hydrolase 2</b>	<b><i>Ephx2</i></b>	<b>2.1 <math>\pm</math> 1.0</b>	<b>only A</b>	<b>only A</b>	<b>CT1</b>
Sepiapterin reductase	<i>Spr</i>	1.7 $\pm$ 0.7	only A	n.s.	CT1
Mitogen-activated protein kinase 9	<i>Mapk9</i>	2.1 $\pm$ 0.5	n.d.	n.s.	n.s.
Pyridoxal kinase	<i>Pdxk</i>	2.3 $\pm$ 1.0	n.s.	only A	n.s.

\*\* **SILAC ratio:** mean ratio of the peptide intensity in the active vs. the control probe in metabolically labeled AML12 cells (>1 indicates to a protein enrichment in the active probe)

## 4.2.7 PREDICTED TARGETS FOR CHEMOTYPE 2

In this chapter, the different optimization steps of the chemical proteomic approach were described in detail for Chemotype 1. Chemotype 2 was processed accordingly in the quantitative pull-down generations (3<sup>rd</sup> and 4<sup>th</sup>). However, no significantly enriched proteins were identified for the active probe of Chemotype 2 [P01] in the 3<sup>rd</sup> generation pull-down (data not presented). The consecutive 4<sup>th</sup> generation SILAC quantification pointed towards four enriched proteins, which do not have



known functions in lipid metabolism (see Supplemental Table 11, p.196). The enriched proteins are the A-kinase anchor protein 12 (Akap12), the Ras GTPase-activating protein binding protein (G3bp1), Nucleolin (Ncl) and a zinc finger domain protein (Prdm16).

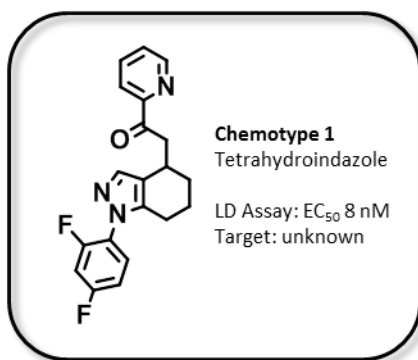
In contrast to Chemotype 1, there was no overlap between the proteins identified in the separate SILAC and the label free approaches. The proteins additionally were not enriched among the proteins that were identified as Chemotype 2 [P01] specific binders in the two-tiered pull-down approach. This lack of reproducibility might point to a non-identifiable protein in this chosen experimental setup. For example membrane proteins are likely excluded from the lysate based on the solubilization capacity of the homogenization buffer. As an alternative, the small molecule activity could involve non-protein targets (glycostructures, lipidations) or depend on the phosphorylation or ubiquitination state of the target for successful small molecule interaction. For Chemotype 2 the further target identification was therefore mainly based on the outcome of the functional characterization (see Chapter 4.1) which allowed a successful nomination of the diacylglycerol-O-acyltransferase 1 (DGAT1) as the functional target of Chemotype 2 (Chapter 4.4).

#### 4.2.8 SUMMARY

The chemical proteomics based identification of potential target proteins was the mainstay approach for direct target identification. The applied protocol was optimized in various means and it was revealed that early sample multiplexing and quantitative evaluation of the proteins identified by MS are utterly important in order to improve data quality and reliability. Nevertheless, a multitude of experimental conditions (pH, detergent concentration, incubation times and much more) must generally be considered to severely impact a successful target identification. As per definition the target protein is not known at this point of experiments a nostrum is not available. It solely can be trusted that the chosen conditions fulfill the parameters required for the particular protein of interest. Retrospectively, after the target is identified, it is possible to optimize the separate parameters if still desired which can be considered for an indirect target validation approach.

Chemotypes 1-2 entered the chemical proteomic experiment, while Chemotype 3 was excluded as a suitable affinity probe is currently lacking. The two investigated chemotypes showed distinct behavior in the performed experiments. For Chemotype 1, the late generation quantitative designs allowed the declaration of four high potential protein target candidates which were re-validated in independent pull-down setups. The here summarized target identification for Chemotype 1 highlights NT5DC, EPHX2, SPR and DCK as high priority targets. The target identification for Chemotype 2 remained inconclusive at this stage of chemical proteomic target identification.

## 4.3 TARGET VALIDATION FOR CHEMOTYPE 1



The optimization process in the affinity based chemical proteomic approach led to the identification of four high priority protein target candidates for Chemotype 1 (see Chapter 4.2). The proposed binding partners are the 5'-nucleotidase domain-containing protein 1 (NT5DC1), deoxycytidine kinase (DCK), soluble epoxide hydrolase (EPHX2) and sepiapterin reductase (SPR). All four proteins were coherently identified as significantly enriched with

the active pull-down probe for Chemotype 1 [P03] in different quantification approaches (see summarized information in Table 4, p.58). Additionally, these proteins were nominated as selective Chemotype 1 binders (see Chapter 4.2.5.1, p.56). This highlights the likelihood of an underlying specific protein- small molecule interaction or the identification of robust false positives.

In the following, different validation approaches are summarized focusing on high priority targets and selected low priority targets. These low priority target candidates lack significant enrichment with the active probe [T01 or T03], but own interesting functional properties which can be considered as a cause for the LD reduced phenotype. As the target identification solely based on the co-purification of proteins that interact with the small molecule, further functional (enzyme) modulation was concerned in the here summarized target validation process in direct or indirect assays if applicable.

### 4.3.1 HIGH PRIORITY TARGETS

#### 4.3.1.1 Nucleotidase Domain-Containing Protein (NT5DC1)

The 5'-nucleotidase domain-containing protein 1 (EC 3.1.3.-) dephosphorylates nucleoside monophosphates to produce nucleosides and inorganic phosphates. *Nt5dc1* gene silencing increased the intracellular availability of AMP/ATP and invoked AMPK activation (Kulkarni et al, 2011). Phosphorylated NT5DC1 subsequently promotes lipid oxidation and glucose transport by GLUT4 (McGee et al, 2008). In parallel, the glucose oxidation level was decreased since excess glucose was predominantly incorporated into glycogen or was metabolized via the lactate intermediate (Kulkarni et al, 2011). Therefore, AMPK is regarded as potential drug target in diabetes treatment (Coughlan et al, 2014). Inhibition of cytosolic NT5dc expression or its respective activity inhibition might also bypass the metabolic inflexibility seen in type 2 diabetes (Kulkarni et al, 2011).

The master regulator AMPK is thus potentially indirectly regulated by NT5DC1 activity. AMPK controls, among other processes, the lipid metabolism by inactivation of acetyl CoA carboxylase (ACC) via phosphorylation (Viollet et al, 2010). ACC catalyzes the rate-limiting step in malonyl-CoA synthesis which is a critical precursor for the biosynthesis of fatty acids (Ganguly, 1960). Additionally, it represents a potent inhibitor of long-chain fatty acyl-CoA transport for mitochondrial  $\beta$ -oxidation (Foster, 2012; Thupari et al, 2001). Knockdown of ACCs causes continuous fatty acid oxidation, increased energy expenditure and reduced fat mass (Viollet et al, 2010; Choi et al, 2007). Based on these reports, an impact of AMPK via NT5DC1 inhibition is in agreement with the LD reduced phenotype caused by Chemotype 1. This hypothesis is further supported by increased expression levels of different genes involved in FA oxidation, sucrose and nucleotide metabolism upon Chemotype 1 treatment as indicated in the transcriptome analysis (see Chapter 4.1.4.2).

Currently, no stable direct assays for NT5DC1 nucleotidase activity are known. This shifts the focus of NT5DC1 validation to the development of a suitable assay first and requires indirect validation approaches. Alternatively, alterations in AMPK activity can be analyzed by immunoblotting of AMPK and phospho-AMPK levels in Chemotype 1 treated cells. This approach was successfully applied for other indirect AMPK activators, such as resveratrol or the novel small molecules RSVA314 and RSVA405 (Vingtdeux et al, 2011; Shin et al, 2009).

RNA interference (RNAi) was applied as a method for target validation. It was assumed that the knock down of the target gene decreases the effective protein concentration and thus mimics the small molecule based enzyme inhibition. As a consequence, a phenocopy of the LD reduced phenotype was expected for the functional target. The RNAi mediated knock down of the fly NT5DC1 homolog CG2277 (32.3 % sequence identity) in *Drosophila* Kc167 cells, however, did not result in a phenocopy on basis of visual examination (see Figure 35.C). This finding is potentially based on the weak knock

#### NT5DC1

**Indications:**Label free (3<sup>rd</sup>):*Only A*Label free (3<sup>rd</sup>, OA):*Only A*Two-Tiered (3<sup>rd</sup>):*Chemotype 1**specific*SILAC (4<sup>th</sup>):2.8 $\pm$  0.4

Significant

**Hypothesis:**

Inhibition of AMPK

down efficiency (50% reduction on mRNA level). Increased dsRNA concentrations in knock down experiments (1 µg/ well in 384 format), however, led to cytotoxicity. This either indicates that NT5DC1 is required for essential cellular processes or that the high dsRNA amount was unspecifically toxic for the cells. Later protein level analysis of NT5DC1 revealed that the NT5DC1 protein remained present after a 4 day knock down (see Figure 35.D).

In order to validate NT5DC1 at protein level, it was aimed to prove binding specificity under competitive binding situations. It was assumed that high concentrations of unlabeled, soluble Chemotype 1 [T08] compete with the immobilized derivative for the respective target proteins. With increasing concentrations of [T08] the target protein is less likely solely immobilized at the beads but binds to the circulating excess small molecule. As a consequence, a concentration dependent target protein decrease should be detectable in immunoblotting. In order to validate this specificity of binding, the chemical proteomic setup was repeated (see methodical description in Chapter 7.4.1, p.133). The isolated proteins were analyzed via immunodetection of NT5DC1 protein (see Figure 35.A). Both *Drosophila* S3 and AML12 cell lysates contained detectable amounts of NT5DC1 protein. However, NT5DC1 protein was not enriched with the active probe [T03]. This contradicts the previous MS identification results. During immunodetection NT5DC1 was solely identified among the unspecific binding proteins in the unbound protein fraction. Increased competitor concentrations indicate a weak concentration dependency in the unbound fraction (Figure 35.A). This inverse effect might result from non-successful NT5DC1 elution from the beads. This would additionally explain the lack of identification in SDS-PAGE based pull-down evaluation, while NT5DC1 was significantly identified after tryptic digest directly at the beads. Additionally, sensitivity discrepancies between MS based and immunodetection may impact this observation.

In order to rule out that Chemotype 1 not only potentially mediates AMPK activity indirectly via NT5DC1 but also directly, an additional direct kinase activity assay was performed. The AMPK isoforms (A1, B1 and G1) were tested in the Z' Lyte™ Kinase Activity Assay (SelectScreen, Invitrogen™). No significant modulation was observed: AMPKa1 was inhibited by 8 ±2%, while the AMPKa2 isoform was inhibited by 12 ±2%.

As a consequence, NT5DC1 was not validated as the defined binding and functional protein target of Chemotype 1, even though the initial chemical proteomic approach strongly suggested this protein. With the applied set of experiments, it was not possible to securely validate or devalidate NT5DC1 as target. Nevertheless, it might be worth to further investigate the above formed hypothesis that Chemotype 1 might function as an indirect AMPK modulator via NT5DC1 dependent phosphorylation. A direct enzymatic assay would support secured functional target validation. Further, described but not yet understood indications also highlight NT5DC1 as an interesting cellular modulator in lipid metabolism: sequence homologies of the coding gene, for example can be related

with CG2277 in *Corynebacterium glutamicum* which is a predicted lipid transporter. However, an impaired lipid transport upon Chemotype 1 treatment was already employed as an unlikely target mechanism in previous QBT uptake studies (see Chapter 4.1.5.3).

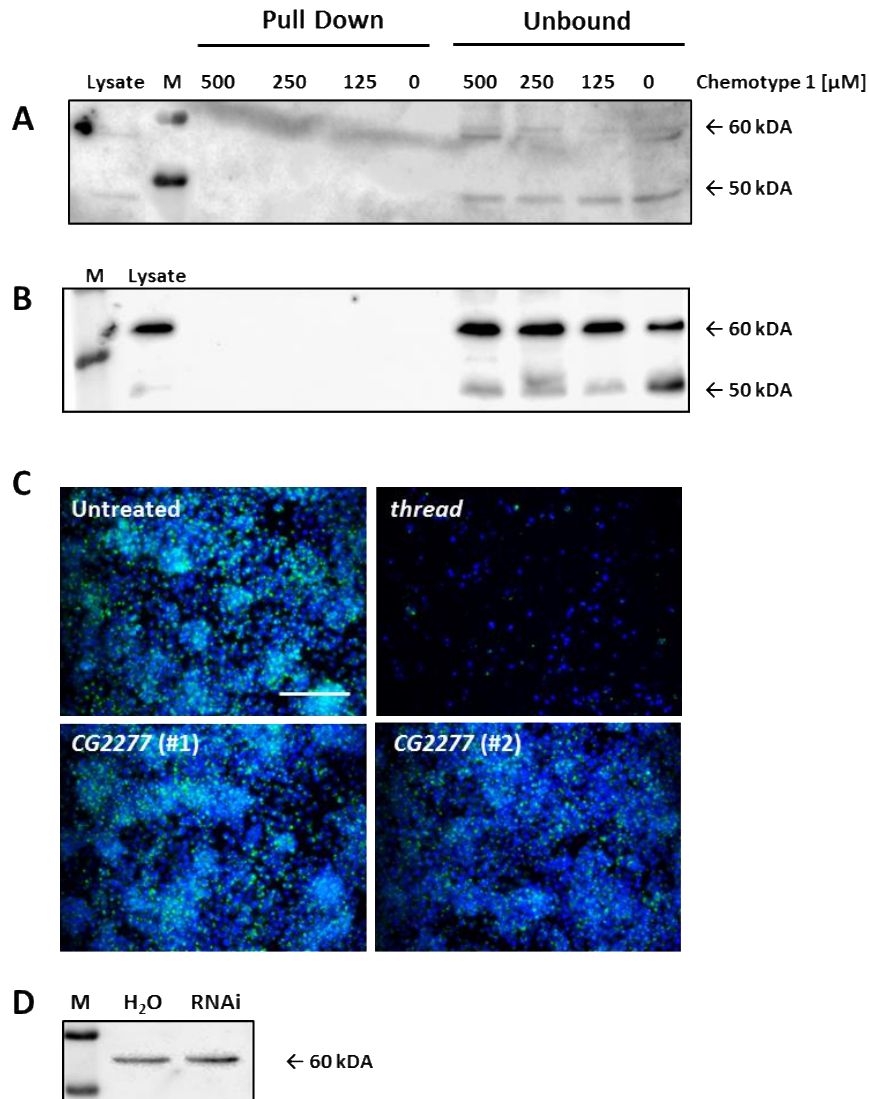


**FIGURE 35: Experiments to test if NT5DC1 is a potential target of Chemotype 1.** **AI** Detection of Nt5dc upon pull-down with probe T03 using immunoblotting. Pull-down was performed using AML12 cell lysates in the presence of different concentration of T08 (0- 500  $\mu$ M with constant DMSO concentrations). Enriched proteins were eluted by heating under denaturing conditions. Eluted and unbound proteins were resolved on SDS-PAGE, transferred to PVDF membrane and probed for NT5DC1 (Sigma, HPA030352). The secondary HRP- antibody conjugate was detected by ECL. **BI** Similar experiments to **AI** but using *Drosophila* Kc167 cell lysate (n=3). **CI** RNAi-mediated knockdown of *Nt5dc1*. *Drosophila* Kc167 cells were treated with 0.25  $\mu$ g dsRNA (384-well plate) for 4 days. Two independent dsRNA sequences targeting *Nt5dc1* (#1-2) were tested Cells were staining with DAPI and BODIPY<sup>®</sup>-493/505 to visualize DNA (blue) and LD (green). (Images: Zeiss Axiovert, 20x, scalebar = 100  $\mu$ m). **DI** Immunodetection of NT5DC1 in *Drosophila* Kc167 cells cultured according to above described knock down condition for dsRNA (#1).

#### 4.3.1.2 Deoxycytidine Kinase (DCK)

The deoxycytidine kinase (EC 2.7.1.74) is an essential nucleoside kinase critical for the production of nucleotide precursors for DNA synthesis in resting cells to assure the presence of deoxynucleotides for DNA repair and mitochondrial DNA synthesis. DCK phosphorylates both purine and pyrimidine deoxynucleosides either from ATP or UTP sources (Sabini et al, 2003). DCK activity is important for several small molecule- based therapies, since it is capable to convert a large number of therapeutic pro-drugs, such as anti-viral drugs used in HIV treatment or antineoplastic agents, into their *in vivo* active forms by phosphorylation (Sabini et al, 2007). As a consequence, mutations of DCK are considered to cause a failure in drug activation as reported for anti-viral and anti-cancer chemotherapeutic agents (Galmarini et al, 2001).

In the current literature there is no direct functional connection between DCK activity and lipid metabolism to form a mechanism of action hypothesis. In order to follow the potential physical interaction between DCK and Chemotype 1 as a cause for the observed LD reduced phenotype, two different enzyme assays were tested. However, as summarized in Figure 36.A neither the cell based DCK enzyme assay (Yu et al, 2010), nor in direct enzymatic activity studies (RECICE® dCK Assay, NovoCIB) resulted in a significant activity modulation by Chemotype 1 derivatives [T08, T09, T11] at the chosen assay conditions. In order to further investigate a potential modulation of DCK by Chemotype 1, the fly homolog *CG5452* (34.9% sequence identity) was knocked down in *Drosophila* Kc167 cells for 4 days (80% decreased expression level). The cells, however, did not show a phenocopy in the subsequent LD assay, even if the protein concentration was reduced (see Figure 36.G-H)

In order to test the binding of DCK to Chemotype 1 [T03], competitive pull- down experiments were performed. Purified recombinant DCK bound to the immobilized active derivative of Chemotype 1 (see Figure 36.B). Additionally, recombinant DCK was enriched in the active probe [T03] in a concentration dependent manner in competitive situations. Decreasing concentrations of DCK were immobilized in presence of increasing concentrations of an unbound competitor [T08] (see Figure 36.B). These results, however, were retracted when bulk cell lysate instead of pure recombinant protein was applied in an identical setup. DCK appeared mainly in the unbound protein fractions (see Figure 36.C-D). In order to further investigate the direct binding between Chemotype 1 and DCK microscale thermophoresis (MST) experiments with mCherry-labeled recombinant murine DCK were conducted. During this measurement the directed movement of particles is analyzed throughout a laser induced temperature jump (Jerabek-Willemsen et al, 2011). As the molecular movement is changed upon small molecule interaction, those differences can be considered for the respective binding constants. Current MST measurements did not support any kind of interaction between

#### DCK

**Indications:**

Label free (3<sup>rd</sup>):  
*Only A (n.S.)*

Label free (3<sup>rd</sup>, OA):  
*Only A*

Two-Tiered PD (3<sup>rd</sup>):  
*Chemotype 1  
specific*

SILAC (4<sup>th</sup>):  
2.8± 0.3  
(significant)

**Hypothesis:**

None

Chemotype 1 and DCK at the chosen assay conditions (see Figure 36.E). The fluorescence signal remained constant in a broad concentration range of Chemotype 1 (0.3 nM- 10  $\mu$ M).

In summary, the lack of functional modulation in enzyme activity and the absence of a phenocopy in the RNAi situation do not support DCK as the protein target of Chemotype 1. Currently, DCK is not securely validated, nor devalidated. As pure DCK weakly binds to Chemotype 1, this enzyme should still be considered in regard to potential pro-drug conversions in *in vivo* experiments.

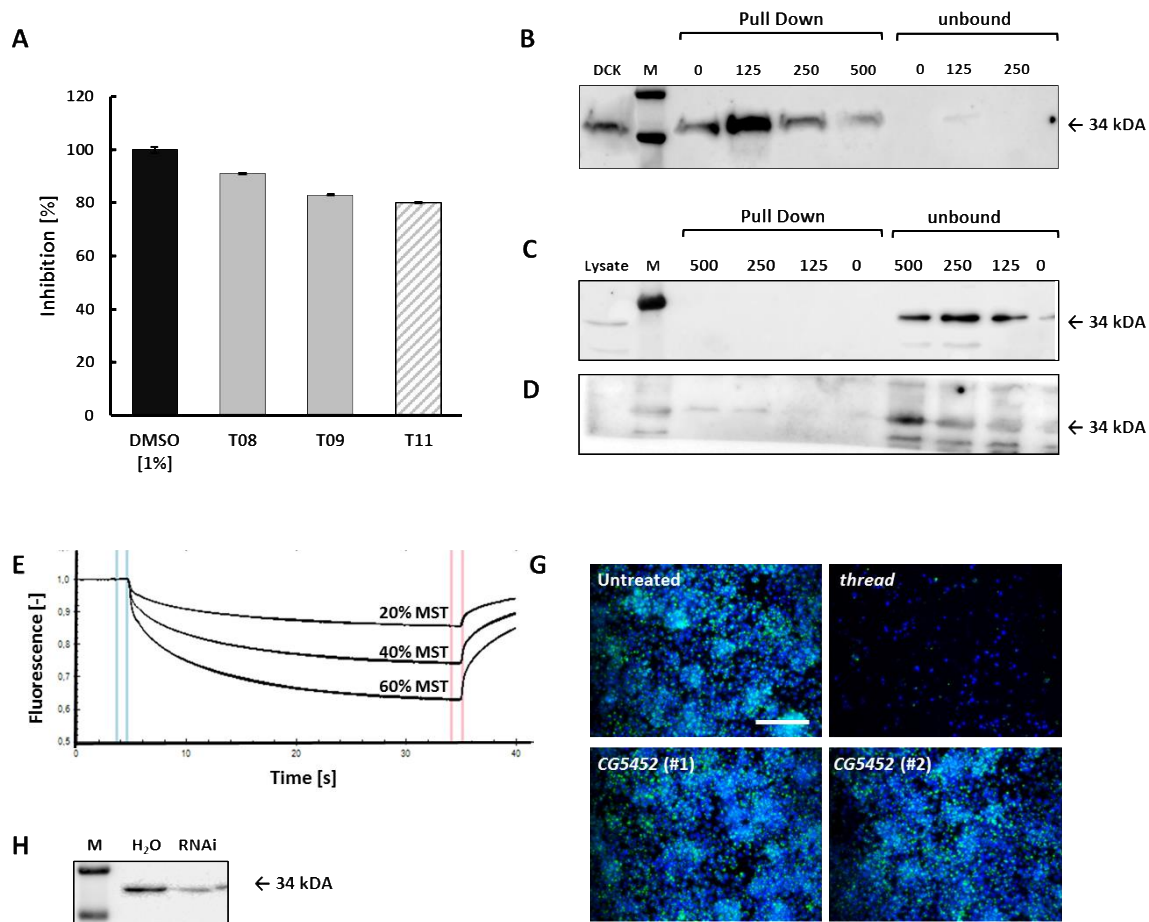


**FIGURE 36: Experiments to test if DCK is a potential target of Chemotype 1.** **AI** Influence of Chemotype 1 derivatives (10  $\mu$ M) on enzymatic activity (RECICE® dCK Assay, NovoCIB). The assay is based on an NADH readout in the phosphorylation progress of deoxyinosin. (black: DMSO control; filled grey bars: active derivatives of Chemotype 1; shaded grey bar: inactive control derivative of Chemotype 1; (n=2). **BI** Detection of recombinant murine DCK (300 ng per sample) upon pull-down with probe T03 by immunoblotting. The pull-down was performed using AML12 cell lysates in presence of different concentration of T08 (0-500  $\mu$ M at constant DMSO levels). Enriched proteins were eluted by heating under denaturing conditions. Eluted and unbound proteins were resolved on SDS-PAGE, transferred to PVDF membrane and probed for DCK (Thermo, PA5-21846). The secondary HRP- antibody conjugate was detected by ECL (n=2). **CI** Repetition of the pull-down with Chemotype 1 [T03] with murine AML12 lysates (0.5 mg total protein per sample) and **DI** *Drosophila* Kc167 lysates (0.5 mg total protein per sample). **EI** Microscale Thermophoresis (MST) did not reveal any binding of recombinant murine DCK-Cherry to Chemotype 1. (Concentration range: 0.3 nM- 10  $\mu$ M, MST power 20, 40, 60 %). **GI** RNAi-mediated knockdown of *Dck*. *Drosophila* Kc167 cells were treated with 0.25  $\mu$ g dsRNA (384-well plate) for 4 days. Two independent dsRNA sequences targeting *Dck* (#1-2) were tested. Cells were staining with DAPI and BODIPY®-493/505 to visualize DNA (blue) and LD (green). (Images: Zeiss Axiovert, 20x, scalebar = 100  $\mu$ m). **HI** Immunodetection of DCK in *Drosophila* Kc167 cells cultured in the above described knock down condition for dsRNA (#1).

#### 4.3.1.3 Soluble Epoxide Hydrolase (EPHX2)

The soluble, cytosolic epoxide hydrolase (EC 3.3.2.10) is an anti-parallel dimer with N-terminal lipid phosphate ester hydrolysis activity and a C-terminal epoxide hydrolase activity using epoxy fatty acids as endogenous substrate (Morisseau et al, 2012). EPHX2 is a potential therapeutic target for cardiovascular diseases (Imig & Hammock, 2009). Pharmacological inhibition of EPHX2 results in anti-hypertensive, neuroprotective and cardioprotective effects (Morisseau, 2013). EPHX2 is also linked to diabetes and the metabolic syndrome since the inhibition of EPHX2 reduces the risk of hepatic steatosis in mice fed on a high fat diet. This is due to a reduced systemic inflammation state (Liu et al, 2012b), which is mainly based on a NF- $\kappa$ B mediated transcriptional down-regulation of cyclooxygenase 2 (COX2) (Imig & Hammock, 2009). Additionally, EPHX2 inhibition reduces the food intake in obese mice (causing 32% body weight reduction) for unknown reasons and increases the metabolic rate ( $V[O_2]$  increase by 17%) (do Carmo, J M et al, 2012). The EPHX2 inhibition effects might result from mitochondrial uncoupling by the uncoupling protein 1 (UCP1). Uncoupling increases the energy expenditure at the same time as it prevents lipotoxicity by free fatty acids.

As EPHX2 is a bifunctional enzyme, Chemotype 1 was tested for both functional activities in different enzymatic assays. The N-terminal phosphatase activity of murine recombinant EPHX2 was analyzed in an AttoPhos® fluorescence assay (Morisseau et al, 2012); see Figure 37.A). The C-terminal epoxide hydrolase activity was either measured for human recombinant EPHX2 or alternatively in AML12 cell lysate using a modified protocol of the Soluble Epoxide Hydrolase Kit (Cayman Chemicals; see Figure 37.B). None of the performed EPHX2 enzyme assays showed a significant activity modulation of EPHX2 upon Chemotype 1 treatment.

The occurrence of a phenocopy was additionally examined in RNAi mediated knock down in *Drosophila* Kc167 cells. The fly EPHX2 homolog *CG15102* (26.6% identity) was targeted by two separate dsRNAs for 4 days. The *EPHX2* mRNA level was reduced by 80% compared to untreated control cells. Additionally, it was shown that the DCK protein level was reduced as a consequence of the RNAi mediated knock down (see Figure 37.F). The EPHX2 knock down, however, did not result in a phenocopy of the LD reduced phenotype in the standard LD assay (see Figure 37.E).

In order to analyze the direct binding of EPHX2 and the active derivative of Chemotype 1 the affinity purification was repeated. The enriched proteins were analyzed by immunoblotting. EPHX2 was identified in AML12 and Kc167 cell lysate, however, remained absent in the respective active probe [T03]. Instead EPHX2 was mainly identified in the unbound protein fractions (see Figure 37.D). A weak concentration dependency was observed within these fractions. A similar behavior was already observed for NT5DC1 (see 4.3.1.1, Figure 35, p.63).

#### EPHX2

##### Indications:

Label free (3<sup>rd</sup>):  
Only A

Label free (3<sup>rd</sup>, OA):  
Only A

Two-Tiered PD (3<sup>rd</sup>):  
Chemotype 1 specific

SILAC (4<sup>th</sup>):  
2.1  $\pm$  1.0

##### Hypothesis:

AI uncoupling via UCP  
BI reduction of food  
Intake (unknown)



Additionally, indirect validation approaches for EPHX2 were built on the hypothesis, that mitochondrial uncoupling is enhanced upon EPHX2 inhibition (do Carmo, J M et al. 2012). Generally, uncoupling is most important in brown adipose tissue, which is specialized in burning fat and is responsible for adaptive, non-shivering thermogenesis in mammals (Fedorenko et al, 2012). As non-adipocytes are investigated as model systems in this study, it was considered unlikely that the small molecules target brown adipocyte specific pathways. Nevertheless, the hepatocyte derived cells showed a weakly increased expression level of *UCP1* upon Chemotype 1 treatment compared to the respective DMSO control sample (see Figure 38.A). This did not seem to be a direct effect of the tested small molecule as the change on the expression level was seen for both active and inactive derivatives. Similar expression levels were also reached for derivatives of Chemotype 2 (data not shown). Thus, UCP1 dependent uncoupling is unlikely the primary cause for the lack of LDs upon Chemotype 1 treatment. Nevertheless, uncoupling might be unspecifically upregulated as a common response of all chemotypes. Image based examination of the mitochondrial membrane potential using the tetramethylrhodamine ethylester (TMRE) did additionally not indicate alterations in the membrane integrity of the mitochondria, as expected for UCP1 dependent uncoupled situation (see Figure 38.B). Another indicator pointing against EPHX2- dependent effects in the LD reduction is that EPHX2 is known to lower cholesterol and steroid levels, as observed in EPHX2 null mice (Luria et al, 2009). This contradicts the previous finding that Chemotype 1 did not introduce any significant changes in lipid classes despite of TAG, including cholesterol (see Chapter 4.1.5.1.1).

Apart from the proteomic based target identification, EPHX2 additionally gained attention in the analysis of the specifically regulated genes for Chemotype 1 during the transcriptome analysis (see Chapter 4.1.4.2). EPHX2 was significantly downregulated (-0.6 fold).

The present data do not indicate that EPHX2 modulation by Chemotype 1 is the underlying cause of the observed LD reduction phenotype, despite numerous considerable literature indications. In order to complete the validation, the far not tested conversion of epoxyeicosatrienoic acids (EETs) and linoleic acid epoxides (Zeldin et al, 1995) has to be assayed for a potential modulation by Chemotype 1.

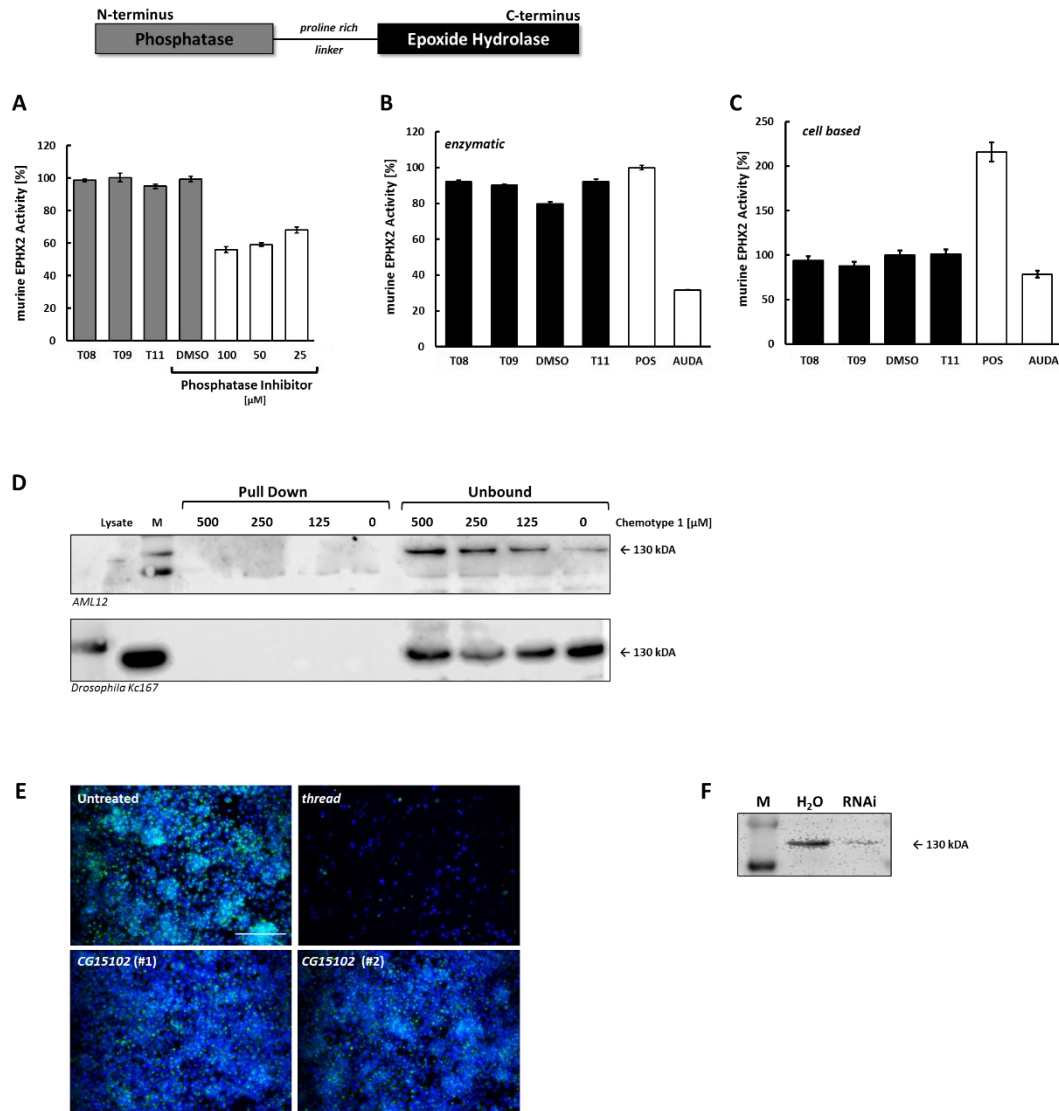


**FIGURE 37: Experiments to test if EPHX2 is a potential target candidate of Chemotype 1.** Different enzymatic assays for the N-terminal phosphatase activity and C-terminal epoxide hydrolase activity did not indicate an activity modulation by Chemotype 1 under the given assay conditions. **AI** The cell based AttoPhos® assay with murine recombinant EPHX2 did not show an activity change upon Chemotype 1 treatment, while the activity dropped as expected in the presence of complex phosphatase inhibitors (cComplete Phosphatase Mix). The assay was performed according to Morisseau et al, 2012. **BI** The C-terminal epoxide hydrolase activity was not affected either employing the murine or the human recombinant proteins. The soluble epoxide hydrolase assay (Cayman Chemicals) is based on the hydrolysis of a Fluor7 substrate (n=3). **DI** The Fluor7 based assay (Cayman Chemicals) was modified and repeated in AML12 cell lysate based assay. (n=3, AUDA is an inhibitor of EPHX2 exhibiting IC<sub>50</sub> values of 18 and 69 nM for the mouse and human enzymes, respectively.) **CI** Detection of EPHX2 upon pull-down with probe T03 using immunoblotting. Pull-down was performed using AML12 cell lysates in the presence of different concentration of T08 (0-500 µM at constant DMSO levels). Enriched proteins were eluted by heating under denaturing conditions. Eluted and unbound proteins were resolved on SDS-PAGE, transferred to PVDF membrane and probed for EPHX2 (Sigma, HPA023779). The secondary HRP- antibody conjugate was detected by ECL. **EI** RNAi-mediated knockdown of the EPHX2 homolog CG15102 in *Drosophila* Kc167 cells (0.25 µg dsRNA/well in 384-well plate format, knock down: 4 days). Two independent dsRNA sequences targeting CG15102 (#1-2) were tested. Cells were stained with DAPI and BODIPY®-493/505 to visualize DNA (blue) and LD (green). (Images: Zeiss Axiovert, 20x, scalebar = 100 µm). **FI** Immunodetection of EPHX2 in *Drosophila* Kc167 cells cultured in the above described knock down condition for dsRNA (#1).

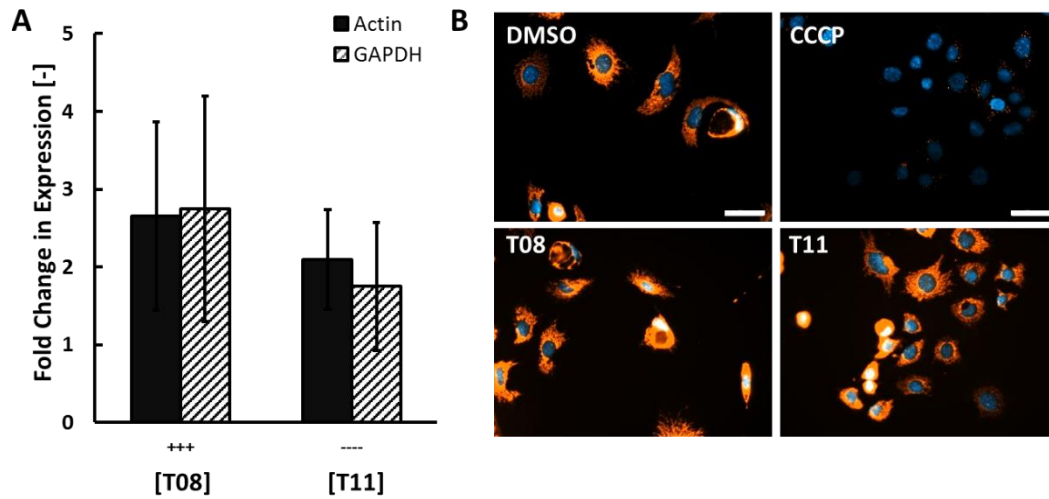


**FIGURE 38: Indirect test for EPHX2 as a potential target of Chemotype 1. AI** Uncoupling protein 1 expression analysis in Chemotype 1 treated AML12 cells (1 $\mu$ M, 18h). The active derivative [T08] was compared with a control derivative [T11]. The relative gene expression was determined for actin and GAPDH, respectively according to the  $\Delta\Delta$  CT method. **BI** Images of the mitochondrial membrane potential in AML12 cells treated with 1  $\mu$ M active [T08] and inactive control derivatives [T11] of Chemotype 1 after 18 h. The TMRE stain accumulates in active mitochondria (orange), while depolarized or inactive mitochondria have decreased membrane potential and fail to sequester TMRE. The protonophore CCCP (m-chlorophenylhydrazine) was used as control. 25  $\mu$ M CCCP was applied for 1 h. (blue: nuclei, orange: TMRE, Zeiss Microscope, 63x oil, scalebar: 50  $\mu$ m).

## 4.3.1.4 Sepiapterin Reductase (SPR)

Sepiapterin reductase (EC 1.1.1.153) belongs to the family of short-chain dehydrogenases/reductases (SCHAD). Members of this protein family were highlighted as a potential target class for Chemotype 1 during initial SciFinder similarity search target predictions.

SPR catalyzes the final reductions in tetrahydrobiopterin biosynthesis to form 5,6,7,8-tetrahydrobiopterin (THB, BH<sub>4</sub>). THB is an essential cofactor for many enzymatic reactions as it is the required educt for serotonin, dopamine and epinephrine synthesis. Especially serotonin pathways are often targeted in obesity treatment, mostly by suppression of appetite as seen for serotonin-norepinephrine reuptake inhibition by Sibutamin (Araújo & Martel, 2012) or stabilized vesicular neurotransmitter storage (reversed serotonin function) by Fenfluramine (Kaplan, 2010) (see summarized information in Chapter 1.1.2).

**SPR****Indications:**

Label free (3<sup>rd</sup>):  
Only A

Label free (3<sup>rd</sup>, OA):  
Not significant

Two-Tiered PD (3<sup>rd</sup>):  
Chemotype 1 specific

SILAC (4<sup>th</sup>):  
A/I = 4.75

**Hypothesis:**

Serotonin receptor modulation

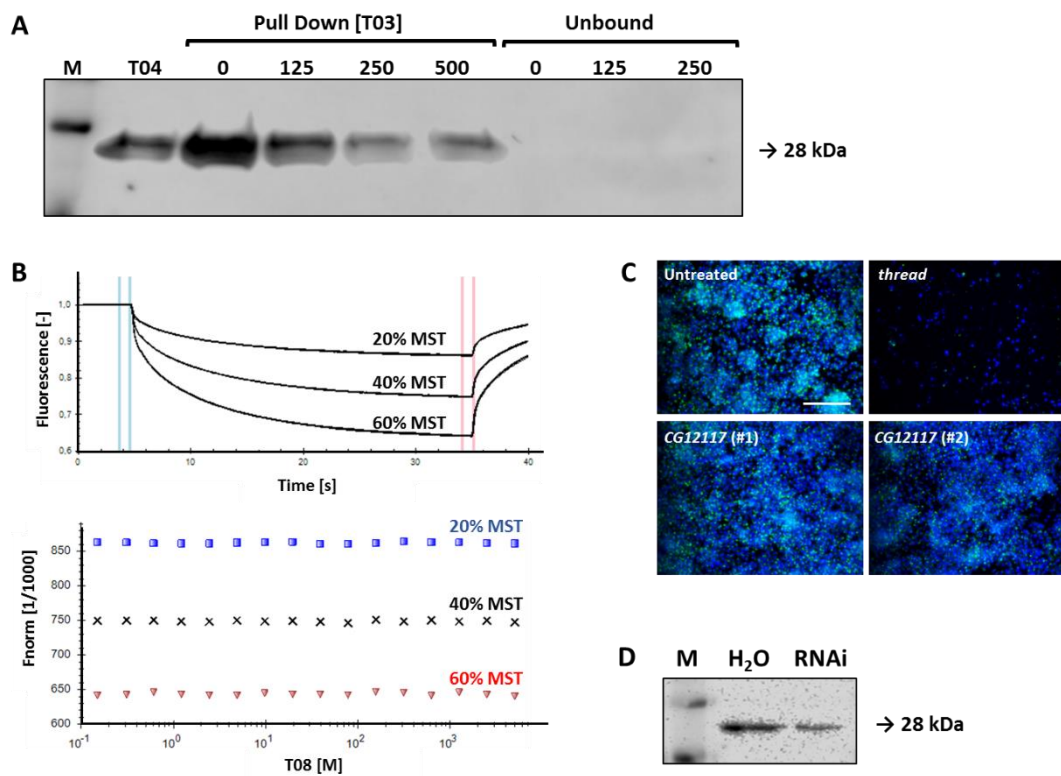


**FIGURE 39: Experiments to test if SPR is a potential target of Chemotype 1.** **AI** Competitive pull-down with recombinant murine SPR (300 ng per sample) showed that SPR binds to both active [T03] and control [T04] derivatives of Chemotype 1, with preference towards the active probe supporting the proteomic data. The concentration dependent binding indicates a specific small molecule SPR interaction, since increasing concentrations of free Chemotype up to 500 μM show a competitive decrease of SPR in the bound fraction. **BI** Microscale Thermophoresis, however, did not support specific binding of mCherry-SPR and Chemotype 1 [T08]. **CI** RNAi-mediated knockdown of the fly homologue *CG12117* of SPR. *Drosophila* Kc167 cells were treated with 0.25 μg dsRNA (384-well plate) for 4 days. Two independent dsRNA (#1-2) were tested. Cells were staining with DAPI and BODIPY®-493/505 to visualize DNA (blue) and LD (green). (Images: Zeiss Axiovert, 20x, scalebar = 100 μm). **DI** Immunodetection of SPR in *Drosophila* Kc167 cells cultured in the above described knock down condition for dsRNA (#1).

SPR was consistently identified in different chemical proteomic setups with Chemotype 1 [T03]. Repetition of pull-down experiments with immunodetection confirmed the enrichment of recombinant murine SPR in active probes of Chemotype 1 (see Figure 39.A). Under competitive conditions introduced by increasing excess of unlabeled, active derivative of Chemotype 1 [T08], a concentration dependent replacement of SPR from the solid phase was detected (see Figure 39.A). Direct binding of recombinant SPR towards T08 was not confirmed in MST measurements of recombinant mCherry-SPR (see Figure 39.D).

The RNAi mediated knockdown of the SPR fly homolog *CG12117* (31.8% sequence identity) in *Drosophila Kc167* cells did not alter the number of stored LDs within treated cells (see Figure 39.C). This finding is potentially based on the weak knock down efficiency (50% reduction on mRNA level). Increased dsRNA concentrations in knock down experiments (1 µg/ well in 384 format), however, led to cytotoxicity. This either indicates that SPR is required for essential cellular processes or that the high dsRNA amount was unspecifically toxic for the cells. The protein level was not significantly reduced in the RNAi mediated knock down for 4 days. Consequently, the RNAi experiments need optimization in efficiency for further target validation.

In summary, it was not possible to securely validate or devalidate SPR as the direct target of chemotype 1.

#### 4.3.2 LOW PRIORITY TARGETS

##### 4.3.2.1 Hydroxyacyl-CoA Dehydrogenase (HCD-2, Scully)<sup>7</sup>

The 3-Hydroxyacyl-CoA Dehydrogenase (HCD-2) was identified in among potential binding candidates in the 1<sup>st</sup> generation pull-down, which employed probes of the enantiomeric pair of Chemotype 1 [T01+T02] in *Drosophila* lysates. HCD-2 was identified three out of four times in both probes. Due to the remaining activity of the inactive probe (see chapter 4.2.1) and the lack of a quantitative readout during MS identification, it was not possible to exclude HCD-2 as a potential target candidate at that point of investigation. Additional initial indications to HCD-2 were based on SciFinder target predictions, which suggested an interaction of Chemotype 1 with members of the short-chain dehydrogenase/reductase superfamily (SCHAD).

The mitochondrial and LD associated HCD-2 protein catalyzes the oxidation of a wide variety of fatty acids, alcohols and steroids in the third reaction of the mitochondrial β-oxidation cascade (oxidation

#### HCD-2

##### Indications:

Qualitative (1<sup>st</sup>):  
A/I= 3/3 appearances  
(n=5)

SILAC (4<sup>th</sup>):  
not identified

##### Hypothesis:

β-oxidation

<sup>7</sup> Alias: 3-Hydroxyacyl-CoA Dehydrogenase, 7-β-hydroxysteroid dehydrogenase; estradiol 17-β-dehydrogenase; testosterone dehydrogenase; 3-hydroxy-2-methylbutyryl-CoA dehydrogenase activity

of 3-hydroxyacyl-CoA to 3-ketoacyl-CoA) (Dellomonaco et al, 2011). Mutations in HCD-2 disturb mitochondrial fatty acid oxidation, amino acid metabolism and insulin secretion (Heslegrave & Hussain, 2013). HCD-2 knockout mice have a slightly reduced body weight following a high-fat diet due to an elevated body temperature (Schulz et al, 2011). Decreased HCD-2 enzyme activity was correlated with weight gain (Rogers et al, 2014b) and an altered acyl-CoA metabolism (Shafqat et al, 2003).

Immunoblot detection of pull-down samples based on the 1<sup>st</sup> generation probes [T01+T02] confirmed the mass spectrometry results. HCD-2 was specifically enriched out of bulk *Drosophila* Kc167 cell lysates by the active derivative of Chemotype 1 [T01], while it remained absent in the unbound fractions (see Figure 40.A). However, the amount of extracted proteins remained equal in the active [T01] and the control [T02] derivatives. This equal distribution matches with the result of qualitative MS analysis, where HCD-2 was identified in identical quantities with both active and control samples. Applying competitive conditions by an excess of unmodified, active Chemotype 1 [T08] resulted in a minor concentration dependent replacement of HCD-2 protein. This supports the specificity of a general interaction with both Chemotype 1 derivatives at the given 1<sup>st</sup> generation pull-down conditions. However, when the biotin group was substituted with a free amine group in the 2<sup>nd</sup> pull-down generation, this finding was inverted (Figure 40.B). Pull-downs depending on [T03] and [T04] did not indicate an interaction of HCD-2 and the respective modified derivatives anymore. The lack of HCD-2 in the free amine labeled affinity probes [T03+T04] was confirmed throughout the later pull-down generations, as HCD-2 was not identified amongst the significant binders in mass spectrometric results anymore.

In order to test for a potential impact of HCD-2 inhibition on LD formation, the known HCD-2 inhibitor glycyrrhetic acid (GA) (Seckl et al, 1993) was included in the standard LD assay to test for a potential phenocopy. GA treated *Drosophila* Kc167 cells did not mimic this phenotype upon GA treatment (Figure 40.C), nor did an RNAi based knock down of the HCD-2 fly gene *CG7113* (Figure 40.E). The knock down efficiency as well as the protein level upon 4 day knock down were not determined. Thus the RNAi experiments need further emphasis for further target (de)validation.

A lysate-based enzymatic HCD-2 assay in HEK293 lysates, however, showed weak inhibition of HCD-2 dependent oxidation of [1,2,6,7-<sup>3</sup>H]-cortisol by compound [T08] (Figure 40.D). Yet, an inhibition of 50% at 20  $\mu$ M was not considered to be the primary targeted protein for the LD reduced phenotype.

As a result of the negative indications, HCD-2 was excluded from the potential target candidates. Nonetheless, structurally and functionally closely related proteins might still be involved in the generation of the observed LD reduced phenotype.

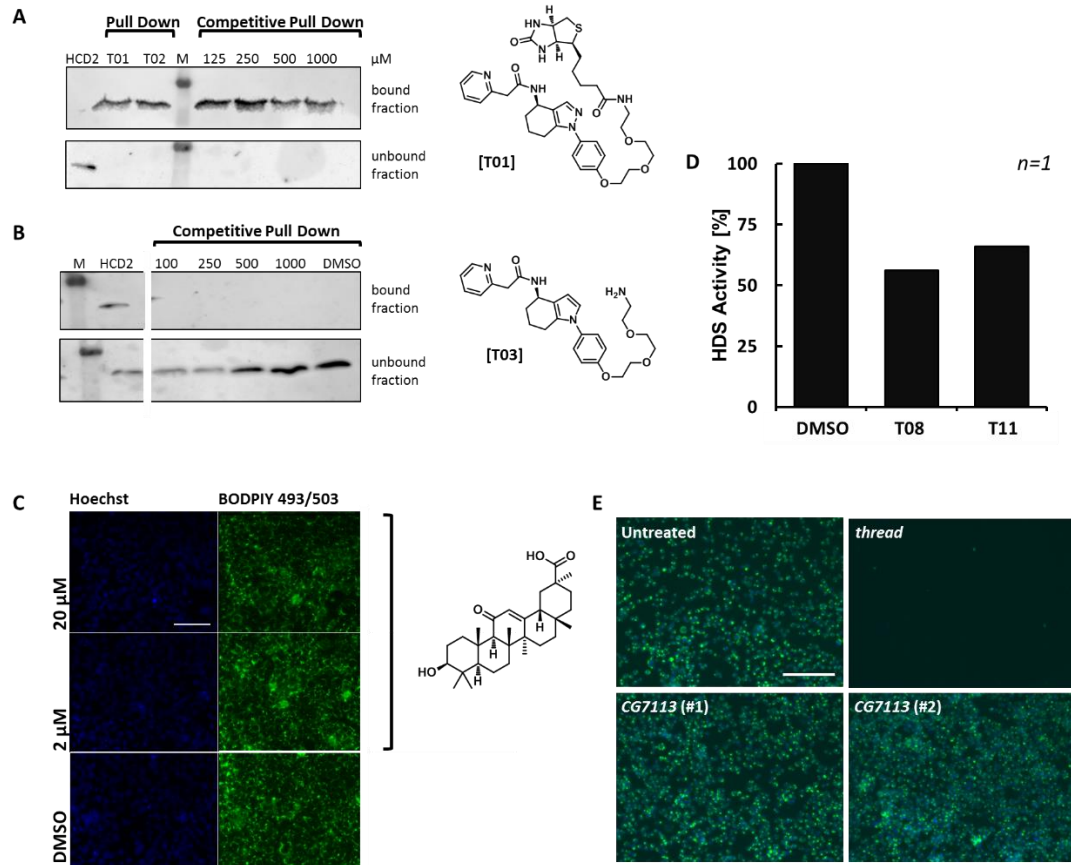


**FIGURE 40: Experiments to test if SPR is a potential target of Chemotype 1.** **AI** In the first generation of pull-down probes [T01+T02] HCD-2 was identified in the bound protein fraction. Detection of HCD-2 upon pull-down with probe [T01] using immunoblotting. Pull-down was performed using *Drosophila* Kc167 cell lysates in the presence of different concentration of [T08] (0-1000 μM, 0.2% (v/v) DMSO). Enriched proteins were eluted by heating under denaturing conditions. Eluted and unbound proteins were resolved on SDS-PAGE, transferred to PVDF membrane and probed for HCD-2 (Origene, #6598P1). The secondary HRP- antibody conjugate was detected by ECL. **BI** Repetition with the 2<sup>nd</sup> generation pull-down probes [T03+T04], employing a free amine group for covalent immobilization via succinimidyl ester formation. **CI** *Drosophila* Kc167 cells treated with glycyrrhetic acid (GA) in the standard LD protocol for 16 h. **DI** HCD-2 enzyme activity in HEK293 cell lysates by radiolabeled measurement of the oxidation of [1,2,6,7-<sup>3</sup>H]-cortisol. 20 μM of the respective derivatives were tested in collaboration with Dr. Odermatt (University of Basel). **EI** RNAi-mediated knockdown of the fly gene CG7113 (HCD-2). *Drosophila* Kc167 cells were treated with 0.25 μg dsRNA (384-well plate) for 4 days. Two independent dsRNA sequences (#1-2) were tested. Cells were staining with DAPI and BODIPY®-493/505 to visualize DNA (blue) and LD (green). (Images: Zeiss Axiovert, 20x, scalebar = 100 μm).

## 4.3.2.2 Pyruvate Kinase (PKM)

Pyruvate kinase was found as a potential target candidate for Chemotype 1 in the first generation of qualitative pull-downs. In five experiments PKM was identified four times in the active samples [T01] and three times in the control [T02]. The pyruvate kinase catalyzes the last step of glycolysis and is thus important for ATP production. Altered PKM activity is generally linked to tumor metabolism and was defined as the Warburg effect (reviewed by (Granchi et al, 2014)). Aerobic glycolysis is a central mechanism to provide cancer cells with not only energy, but also building blocks for macromolecule synthesis, such as carbohydrates, proteins, lipids and nucleic acids (Vander Heiden, Matthew G. et al, 2009; Zhang & Du, 2012). The pyruvate kinase is thus at the nexus for glycolytic modulation and it was considered that PKM inhibition by Chemotype 1 might induce the LD reduced phenotype. Based on this key position, PKM inhibitors moved into pharmaceutical focus as a potential new target in cancer therapy (Gupta et al, 2014).

**PKM****Indications:**

Qualitative (1<sup>st</sup>):  
A/I= 4/3 counts  
(n=5)

Qualitative Fly (1<sup>st</sup>):  
*present*

SILAC (4<sup>th</sup>):  
n.d.

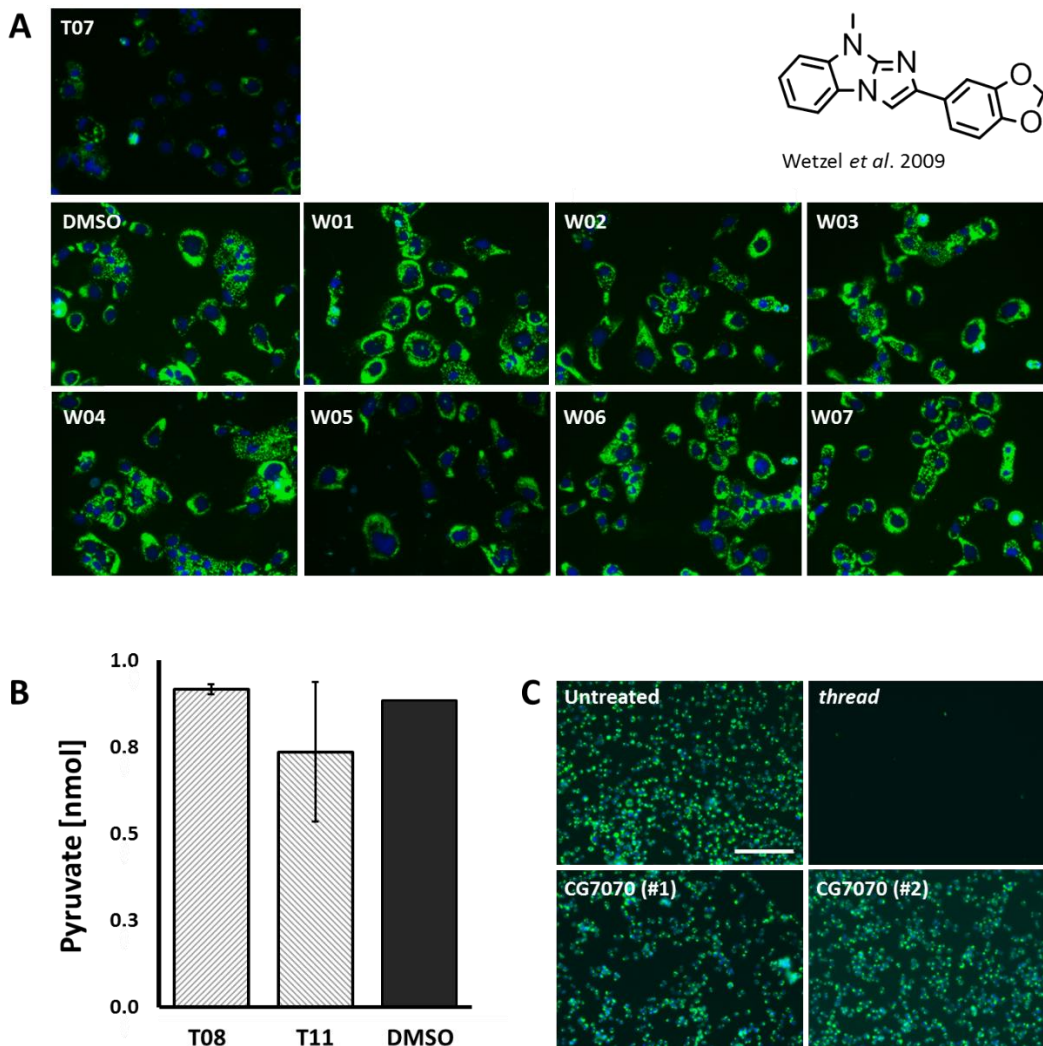




**FIGURE 41: Experiments to test if the pyruvate kinase as a potential target of Chemotype 1.** **AI** Effect of known pyruvate kinase inhibitors (Wetzel et al, 2009) in the LD assay. AML12 cells treated with 20  $\mu$ M of the inhibitors [W01- W06] or activator [W07] in presence of 400  $\mu$ M OA. The cells were fixed and stained for LDs (green) and nuclei (blue) (Images: Zeiss Axiovert, 40x). **BI** PKM dependent conversion of phosphoenolpyruvate (PEP) and ADP to pyruvate and ATP was evaluated in an AmplexRed<sup>®</sup> based assay (BioVision). *Drosophila* Kc167 cell lysate was incubated with 5  $\mu$ M active Chemotype 1 [T08] and the respective control [T11] (n=4). **CI** RNAi-mediated knockdown of the *drosophila* pyruvate kinase *CG7070*. *Drosophila* Kc167 cells were treated with 0.25  $\mu$ g dsRNA (384-well plate) for 4 days. Two independent dsRNA sequences (#1-2) were tested. Cells were stained with DAPI and BODIPY<sup>®</sup>-493/505 to visualize DNA (blue) and LD (green). (Images: Zeiss Axiovert, 20x, scalebar= 100  $\mu$ m).

In order to examine whether PKM activity is affected by Chemotype 1, a set of known PKM inhibitors was tested in the standard LD assay in AML12 cells. These inhibitors were identified by Stefan Wetzel using a chemoinformatic approach based on the scaffold hunter software (Wetzel et al, 2009). None of the tested inhibitors showed a reduction of the LD count at 20  $\mu$ M. An RNAi based reduction of the enzyme protein level additionally did not reveal any changes in the phenotype. The knock down efficiency and the protein level were not securely validated. Functional inactivity of Chemotype 1 [T08] was supported by a direct PKM enzyme assay (see Figure 41). Consequently, PKM is not considered as the direct protein target of Chemotype 1.

#### 4.3.2.3 Mitogen-activated Protein Kinase 9 (MAPK9)<sup>8</sup>

In the final generation (4<sup>th</sup>) of pull-downs for Chemotype 1, MAPK9 was significantly increased in the active probe (FDR 0.05). MAPK9 was identified as a new regulator in TAG homeostasis and lipid droplet metabolism in an RNAi-based kinase screen in HeLa cells (Grimard et al, 2008). The screen showed, that different siRNA sequences targeting MAPK9 increased the level of cellular TAG in MAPK9 abridged cells. An identical effect was seen after treatment with the known inhibitor SP600125 (Grimard et al, 2008). The phenotype was considered to be the result of decreased lipase activity (Grimard et al, 2008). This finding is in agreement with reports which relate MAPK9 inhibition to obesity (Tuncman et al, 2006) and atherosclerosis (Ricci et al, 2004). Some contradictive results, however, were reported in regard to different isoforms in different disease models (Hirosumi et al, 2002). For example, mice lacking MAPK8 (JNK1) are known to resist diet induced obesity, while MAPK9 (JNK2) knockout mice do not show alterations as compared to the control groups (Hirosumi et al, 2002). MAPK9 knock down in macrophages, however, can be linked to decreased arteriosclerosis levels, which was not seen for MAPK8 (Ricci et al, 2004). As cholesterol levels change upon MAPK9 modulation, MAPK9 was considered as a potential target for hypercholesterolemia (Nagelin et al, 2009; Osto et al, 2008).

#### MAPK9

##### Indications:

Label free (3<sup>rd</sup>):  
n.D.

Label free (3<sup>rd</sup>, OA):  
n.S.

Two-Tiered PD (3<sup>rd</sup>):  
*Chemotype 1 specific*

SILAC (4<sup>th</sup>):  
2.1  $\pm$  0.5

##### Hypothesis:

Lipase activity

<sup>8</sup> Alias: JNK2; SAPK; p54a

Based on the literature reports, Chemotype 1 could act as a MAPK9 activator, resulting in an increased lipase activity and might thus be responsible for the lean phenotype of the Chemotype 1 treated cells. This hypothesis, however, contradicts the previous finding that lipolytic activity was not affected by Chemotype 1 (see Chapter 4.1.5.4). In contrast to Chemotype 1 which only renders cellular TAG levels, MAPK9 is known to intervene with more lipid species than solely TAG (Grimard et al, 2008). This lack of lipid specificity indicates against a MAPK9 activation upon Chemotype 1 treatment.

In order to test for phenocopy or an opposite phenotype *MAPK9* gene expression was reduced by two separate dsRNAs targeting the fly homolog of MAPK9 which is called *CG5680* (75.9% sequence homology) by RNAi- based knock down in *Drosophila* Kc167. Neither the knock down efficiency nor the MAPK9 protein level upon 4d knock down was examined. The LD formation was analyzed via the standard LD assay. According to the literature (Grimard et al, 2008) an increased LD storage phenotype would have been expected. Additionally, the known MAPK9 inhibitor SP600125 was tested for LD modulation. Simultaneous treatment with SP00125 and 1  $\mu$ M active derivative of Chemotype 1 [T08] resulted in a weak but not significant increase in LD formation. However, the determination of increased lipid levels with the standard assay remains limited, as a clear-cut readout as in the LD absence situation is not given. Further enzyme based TAG analysis has to be conducted for secure evaluation.

Additionally, direct kinase binding of three obesity and arteriosclerosis relevant MAPK isoforms (MAPK8-10) was tested in a commercial Lantha™ kinase binding and Z'LYTE™ activity screen (SelectScreen Kinase Profiling, Life Technologies). The screening results are summarized in Figure 42.B-C. None of the tested isoforms indicated preferential binding to Chemotype 1 [T08] or showed significant activity modulation.

MAPK9 is additionally described to be downregulated in atherosclerosis (Ricci et al, 2004). MAPK9 depleted macrophages are suppressed in foam cell formation. Foam cells are characterized by a high number of LDs and are responsible for the formation of atherosclerotic plaques (Ricci et al, 2004). Previous studies, however, revealed that the foam cell formation in THP-1 cells is not affected in presence of Chemotype 1 (see Chapter 4.1.7).

In summary, Chemotype 1 dependent functional modulation of MAPK9 is not expected as the primary cause for the LD reduced phenotype. MAPK9 activation by Chemotype 1, however, remains currently not validated or securely devalidated.

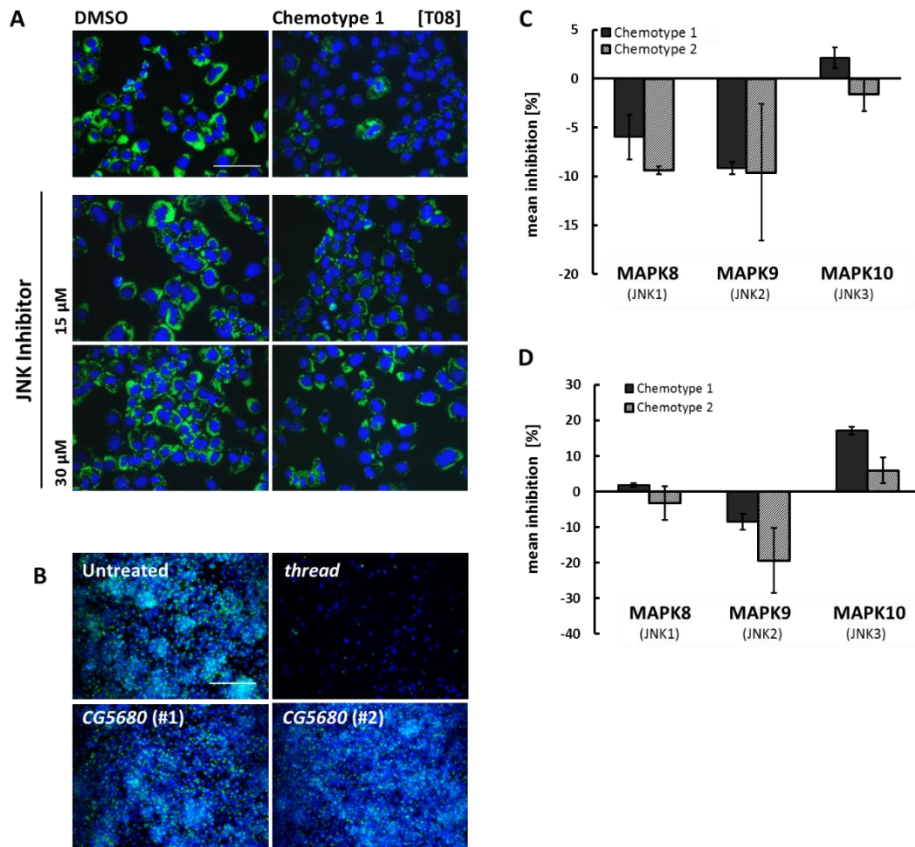


**FIGURE 42: Experimental test if MAPK9 is a potential target of Chemotype 1.** **AI** Inhibition of MAPK9 (JNK2) by the known inhibitor SP600125 did not show a significant increase in stored LD in treated AML12 cells. Simultaneous treatment with SP600125 and active derivative of Chemotype 1 (1  $\mu$ M, [T08]) resulted in a weak increase in LD formation compared to the Chemotype 1 [T08] treated state alone. Small molecule treatment was allowed for 16 h. **BI** RNAi-mediated knockdown of the MAPK9. *Drosophila* Kc167 cells were treated with 0.25  $\mu$ g dsRNA (384-well plate) for 4 days. Two independent dsRNA sequences targeting *CG5680* (#1-2) were tested. Cells were staining with DAPI and BODIPY<sup>®</sup>-493/505 to visualize DNA (blue) and LD (green). (Images: Zeiss Axiovert, 20x, scalebar = 100  $\mu$ m). **CI** The Lantha™ Binding Assay (SelectKinase, Life Technologies) indicated no binding preferences toward the tested MAPK isoforms. 5  $\mu$ M Chemotype 1 [T08] was tested. **DI** The Z'Lyte Activity Assay (SelectKinase, Life Technologies) showed a minor decrease in MAPK9 activity for Chemotype 1 (10%, [T08]) and Chemotype 2 (19% [P04]).

#### 4.3.3SUMMARY

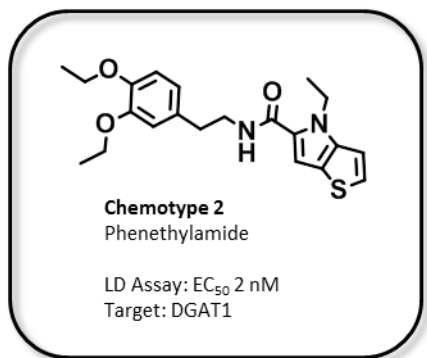
The affinity chromatographic chemical proteomic approach led to the identification of four high priority protein candidates for Chemotype 1: NT5DC1, DCK, EPHX2 and SPR. Different working models were built on the basis of published literature. These models would present new strategies for pharmacological lipid storage modulation apart from the traditional strategies (see Chapter 1.2). The new modulators would thus be important new research tools and might help to unravel currently unknown pathway connections involved in the complex regulatory network of lipid metabolism.

Despite of the prominent enrichment of several candidate targets in the chemical proteomic approach (see Chapter 4.2), none of the highlighted proteins could so far be validated as the direct functional protein target of Chemotype 1. However, the target candidates were also not securely devalidated. The investigated proteins might own uncharacterized, neomorph enzymatic functions, which were not considered in the progress of target validation. Therefore, target validation has to be extended in order to securely validate or devalidate the functional protein target(s). Especially, NT5DC1 and EPHX2 are interesting candidates to follow up. Both proteins were not only statistically highly significant enriched by active derivative of Chemotype 1, but those proteins are additionally easily functionally linked to the observed LD reduced phenotype. Additionally, these proteins share the same HAD-like domain (HAD: haloacid dehalogenase-like hydrolases) and are therefore classified in the same HAD-superfamily which generally includes phosphatases, P-type ATPases and phosphoglucomutases (EMBL-EBI, InterPro web interface). Whether this shared structure is relevant for functional target binding has to be further examined.

In case that the high priority targets will be securely devalidated, non-significant binders of the identification process might be additionally considered for further validation. As statistical significance failed for those proteins, the candidates have to be rationally selected by their physiological function. This, however, generates the classical needle-in the haystack situation and results in time and cost intensive procedure of functional characterization. Optionally, the target identification might be repeated with altered conditions. Currently, proteins which are insoluble or degraded at the chosen experimental conditions bypass identification. The same is true if the successful small molecule target interaction requires the temporal presence/absence of protein modifications such as glycosylations, phosphorylation or lipidations. This highlights one additional bottleneck of the chosen chemical proteomic approach, which bases on the assumption that the target belongs to the class of proteins. Alternative biomolecular targets, such as carbohydrates, nucleic acids or lipids are ignored. However, these classes might as well be involved in the direct interaction with Chemotype 1 in order to cause the observed LD reduced phenotype.

In case that Chemotype 1 targets a membrane protein or ion channel, the chances for successful identification via the proteomic approach at the chosen conditions are small. As membrane proteins and ion channels have high pharmacological potential, they are often approached in pharmacological interventions. The examination of known GPCRs and ion channels in obesity for potential modulation by Chemotype 1 is an alternative investigative level in target ID, which has to be considered next, in order to shed some light on the currently unresolved target identification process for Chemotype 1.

## 4.4 TARGET VALIDATION FOR CHEMOTYPE 2



In this thesis a chemical proteomic approach was chosen to identify the direct protein target of the investigated novel lipid storage modulators. This experimental setup, however, remained inconclusive for Chemotype 2 (see Chapter 4.2.7). Different proteins were highlighted during protocol optimization, but could not be confirmed in different pull-down approaches. Nevertheless, the systematic and functional characterization of

Chemotype 2 (see Chapter 4.1) resulted in the hypothesis that one or both diacylglycerol-O-acyltransferase (DGAT) enzymes could be the cause for the LD reduced phenotype following Chemotype 2 treatment. The initial hypothesis was mostly based on the prominent position of DGATs in the final step of TAG synthesis as both DGAT enzymes present the nexus of both major lipid synthesis pathways (see Figure 44.A). This hypothesis was supported by chemo-informatic target prediction relying on the open source SEA software (Similarity Ensemble Approach; [sea.bkslab.org/](http://sea.bkslab.org/)). The SEA algorithm predicts potential target proteins based on the set-wise chemical similarity comparison among their ligands (Keiser et al, 2007). DGAT1 was listed with high respective E-values at the top ranks of potential hits (see Supplemental Table 15, p. 205). These theoretical indications were experimentally supported by the previously observed unique change in TAG levels upon small molecule treatment, while no other examined lipid species were altered (see Chapter 4.1.5.1). Additional support of DGATs was an observed unique accumulation of diacylglycerol (DAG), which is the direct educt of the diacylglycerol-O-acyltransferase catalyzed reaction. The DAG accumulation was unique for Chemotype 2 treatment (see Chapter 4.1.5.1.2).

Two DGAT enzymes (DGAT1 and DGAT2) are known to catalyze the committing step in TAG synthesis by esterification of an acyl-CoA fatty acid to an existing diacylglycerol. The two enzymes catalyze the

same reaction, however, do not have redundant functions and own different sequences with distinct structure predictions (Qi et al, 2012; Liu et al, 2012a). Membrane spanning domains locate both enzymes primarily to the ER-membrane (Stone et al, 2009), but not in overlapping ER regions (Shockey et al, 2006). DGAT2 additionally was found on LDs upon lipid loading (Kuerschner et al, 2008; Wilfling et al, 2013) and was predicted to be involved in LD expansion (Xu et al, 2012). These different localizations were considered in different hypothesis for the respective enzyme functions. It was speculated that the ER bound DGAT1 isoform is responsible to form a new set of small LDs (Wilfling et al, 2013; Thiam et al, 2013) by re-esterification of preferentially exogenous Acyl-CoAs to DAG that was generated by intracellular lipolysis (Ohsaki et al, 2014; Wendel et al, 2013). DGAT2 in contrast, mostly adds *de novo* synthesized fatty acids to glycerol and was claimed to react upstream of DGAT1 (Wurie et al, 2012; Qi et al, 2012).

It is widely accepted that the two DGAT enzymes act via different pathways in a not totally resolved mechanism. Knock out studies support the different functions. DGAT1<sup>-/-</sup> mice are healthy and resist diet induced obesity (Chen et al, 2002), while DGAT2<sup>-/-</sup> mice die shortly after birth and exhibit severe skin barrier abnormalities (Stone et al, 2004). Both knock out models were reported to remain lean, but only DGAT2<sup>-/-</sup> mice had altered TAG levels under standard feeding conditions.

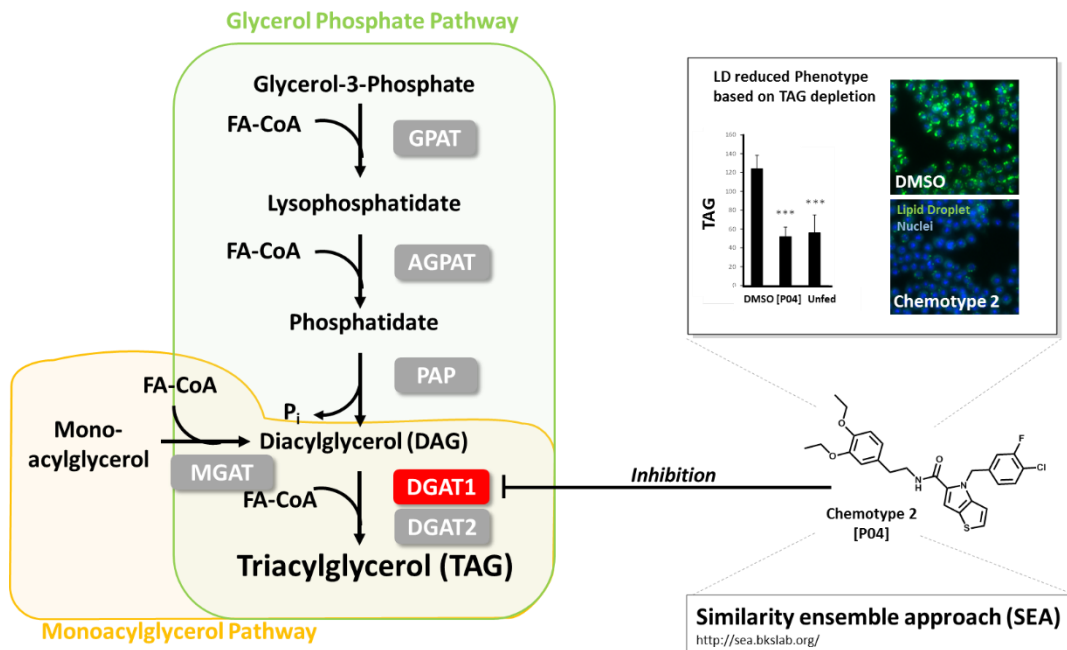


**FIGURE 43: Target hypothesis for Chemotype 2.** A direct interaction of Chemotype 2 [P04] with DGAT1 was hypothesized as the underlying cause for the observed LD reduced phenotype in the cell based assay. The monoacylglycerol and the glycerol phosphate pathway are both linked by DGAT1 function. Based on different physiological indications, we speculated that Chemotype 2 might function as DGAT1 inhibitors and thus blocks the committing step in the esterification of external free fatty acids to DAG. (Schematic pathway modified according to a figure in Yen *et al.*, 2008).

#### 4.4.1 DGAT1 VALIDATION BY DIFFERENT APPROACHES

#### 4.4.1.1 Chemotype 2 inhibits DGAT1 Enzyme Activity

In order to test the potential influence of Chemotype 2 on DGAT1 activity, the incorporation of radiolabeled fatty acids into TAG was quantified in COS7 cells that either expressed mouse DGAT1 or DGAT2. These experiments were performed in collaboration with Dr. Thomas O. Eichmann from the University of Graz. He could show that 5  $\mu\text{M}$  Chemotype 2 [T04] successfully inhibit DGAT1 enzyme activity. An activity decrease by more than 90% was detected in those assays. The respective DGAT2 activity was not affected (see Figure 44.B).

This selective inhibition of DGAT1 supports the hypothesis, that the two DGAT isoforms have distinct modes of actions within the lipid synthesis pathways. The here newly identified specific DGAT1 inhibitor might help to decipher the underlying mechanisms and thus presents a valuable new research tool.

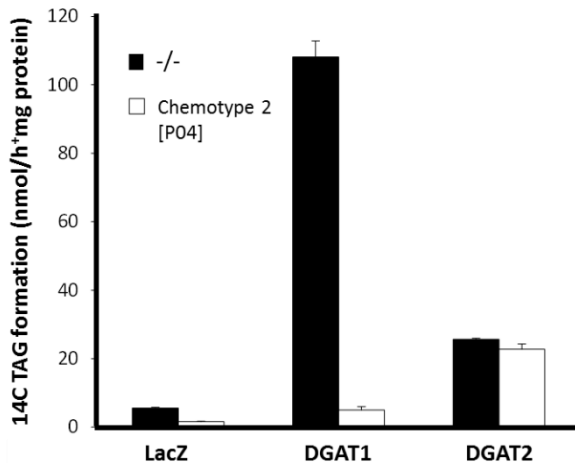


**FIGURE 44: DGAT1 is a potential direct target of Chemotype 2 [P04].** Bulk lysates of DGAT1 or DGAT2 overexpressing COS7 cells were treated with 5  $\mu\text{M}$  Chemotype 2 [P04] in presence of DAG and radiolabeled acyl-CoA FA. The specific inhibition of the DGAT1 isoform (> 90%) was shown based on the scintillation counts of the formed TAG product. (Collaboration with Dr. Thomas O. Eichmann, University of Graz, Austria).

#### 4.4.1.2 *In vivo* Epistasis Experiments highlight DGAT1 Dependency

In order to test whether the Chemotype 2 induced block of DGAT1 activity is sufficient to explain the lean phenotype of small molecule treated flies, whole fly epistasis experiments were performed. For this purpose, different lean mutants were treated with Chemotype 2. Flies with a mutation in the perlipin homolog *LSD-2* [-/-] (lipid storage droplet 2) and *midway* [-/-] (DGAT1 homolog) were therefore examined in regard to their total TAG storage levels. Generally, both *LSD-2* and *midway* mutants show a reduction in TAG by affecting presumably different pathways. *LSD-2* reduces lipid stores by a most likely DGAT1 independent mechanism as it is assumed to promote lipolysis (Teixeira et al, 2003; Gronke et al, 2003).

Both *LSD-2* and DGAT1 show a reduction of the lipid levels in *Drosophila* (see Figure 45.B-C). Upon Chemotype 2 treatment the *LSD-2* [-/-] flies showed a further decrease in neutral lipid stores compared to the untreated knock out flies (see Figure 45.B). This synergetic effect of *LSD-2* and Chemotype 2 [P04] strongly indicates a target independent of *LSD-2* and its downstream targets. *Midway* [-/-] flies remained identical neutral lipid levels in both untreated and Chemotype 2 treated flies (see Figure 45.C). This observed lack of synergy strongly supports the previously hypothesized DGAT1 dependent pathway modulation by Chemotype 2 and suggests that the Chemotype 2 induced leanness is due to DGAT1 inhibition. It additionally highlights the potential of *Drosophila* as a suitable model system for the initial small molecule identification and later target validation progresses, since genetic proof of concept experiments can be easily introduced.

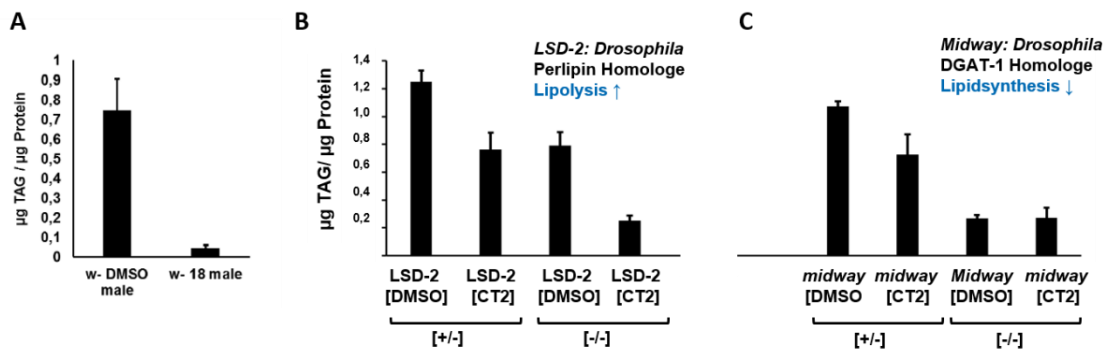


**FIGURE 45: *In vivo* validation of DGAT1 inhibition by Chemotype 2 [P04] as a cause for the observed LD reduced phenotype.** TAG level of male w<sup>-</sup> flies which completed their development on media containing 10 µM Chemotype 2 [P04]. The TAG level was measured by a colorimetric enzyme coupled assay (Infinity TAG reagent) and was normalized to the protein concentration (BCA assay). **AI** w<sup>-</sup> flies show reduced TAG levels upon 10 µM small molecule treatment without affecting the viability over the experimental time. **BI** *LSD-2* [-/-] mutants show a lipid reduced phenotype compared to heterogeneous flies. The decrease in relative TAG can be further decreased by 10 µM Chemotype 2 [P04] treatment. **CI** In contrary, the lipid level of [-/-] *midway* mutants (*Drosophila* DGAT1 homolog) cannot be further decreased by parallel treatment with 10 µM Chemotype 2 [P04]. The fly experiments were performed by Petra Kolkhof, HHU Düsseldorf, Germany.



#### 4.4.1.3 DGAT1 is not significantly identified in the Chemical Proteomic Approach

The direct target identification of Chemotype 2 remained inconclusive in the chemical proteomic approach (see Chapter 4.2.7). In the final SILAC experiments (4<sup>th</sup> generation), potential target candidates were summarized on the basis of the quantitative evaluation ratios, but all failed reproduction in separate experimental replicates. These high sample to sample variations hindered successful statistical evaluation. The lack of significantly enriched proteins in the active sample might depend on solubility problems of the target protein, especially if GPCRs or membrane proteins are targeted. Alternatively, the protein of interest might lack the active binding conformation (non-optimal buffer conditions, detergents, pH, salt, missing cofactors) or is simply absent in the lysate due to a lack of expression, as for example speculated for oleic acid induced genes before (see Chapter 4.2.5.2, p.57). The lack of DGAT1 solubility at the applied assay conditions explains retrospectively the absence of the target protein in the generated candidate hit lists: it was shown that overexpressed DGAT-His was absent in the traditional lysate used in the target ID process (see Figure 46.A).

Manual in-depth analysis of the generated SILAC lists revealed that DGAT1 peptides were identified at low levels. DGAT1 was exclusively identified among the proteins binding to Chemotype 2 [P01] and was not present in experiments with Chemotype 1 [T03]. However, the peptide count was below the standard filter settings (<2 identified peptides) and were thus routinely excluded from any further evaluation at an early stage. Manual inspection of predicted DGAT1 peptides confirmed that DGAT1 is present in both experiments with active and inactive derivatives of Chemotype 2 (see Supplemental, p.178). These peptides, however, were only identified by single hits. Thus, DGAT1 was not considered for further analysis (Standard filter setting: >2 peptides). The second isoform, DGAT2, was neither identified in the manual examination of the MS datasets for both Chemotype 1 and Chemotype 2. This weakly supports the assumption of direct DGAT1 interaction for Chemotype 2.

With the intention to increase the likelihood of DGAT1 peptide identification, a new set of pull-down replicates was analyzed by focused MS analysis. Already during mass acquisition the peptides were sorted in regard to their respective m/z values of expected DGAT1 peptides. This directed mass acquisition is sometimes used in order to increase the sensitivity for expected peptides (Carrillo et al, 2005). Preliminary results of the DGAT1 focused MS analysis, however, did not lead to an increased number of quantifiable DGAT1 peptides in any sample (data not shown). As a consequence, MS based target identification and validation failed for Chemotype 2.

In order to validate the hypothesized DGAT1- Chemotype 2 interaction in the chemical proteomic approach immunodetection was conducted. This semi-quantitative approach supported weak binding of murine recombinant DGAT1 under pull-down conditions (see Figure 46). Hek293 cells overexpressing DGAT1-His, however, did not show a significant preference of DGAT1-His towards

the active probe of Chemotype 2 (55 kDa). Surprisingly, also DGAT2 showed a weak signal at the respective protein size of (44 kDa). This indicates a weak interaction between Hid-tagged DGAT2 and Chemotype 2 *in vitro*. Most importantly, the experimental parameters require optimization in terms of an increased solubility of the membrane bound DGAT enzymes. Currently, DGAT1 is hardly present in the soluble extract (see Supplemental Figure 12, p.207). As expected, experimental repetition with membrane extracts increased the initial DGAT1 concentration in the lysate. As a tradeoff, the high detergent concentration speculatively impaired protein folding in a way that successful interaction with Chemotype 2 in pull-down conditions was hindered. As a consequence DGAT1-His was not identified in the respective eluates (see Supplemental Table 16, p.207). In order to validate DGAT by the chosen affinity based purification approach, further in-depth protocol optimization has to be performed. A suitable approach could implement DGAT1 expression on microsomes as a possibility to investigate the native enzyme.

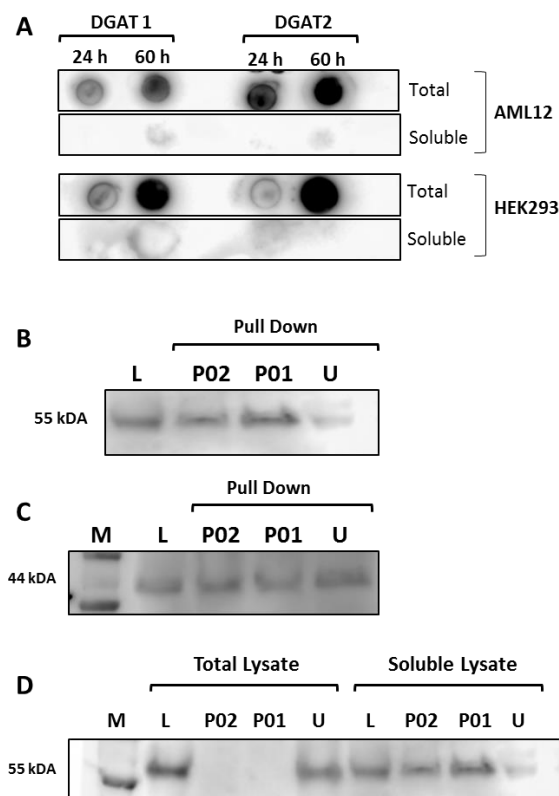


**FIGURE 46: Binding studies with recombinant murine DGAT1-His (55 kDa) and murine DGAT2-His (44 kDa) in an affinity purification approach to Chemotype 2 [P01].** Hek293 cell lysate (1 mg total protein per sample) from cells overexpressing the respective DGAT construct were used in standard pull-down experiments. The bound proteins were unspecifically eluted by boiling in denaturation buffer and were subsequently separated in SDS-PAGE. The His-tag of the recombinant protein was used for immunodetection based on the ECL reaction of the HRP-conjugated secondary antibody. **AI** Dotblot of DGAT1-His and DGAT2-His overexpression in AML12 and Hek293 cells. The cells were transfected and cultured for 24h and 60h respectively. Total cell lysates based on the direct lysis in detergent rich SDS-Sample loading buffer without any centrifugation steps. Soluble lysates only contain mild detergent concentrations and the insoluble membrane fraction is removed by centrifugation. Recombinant DGAT enzymes were detected by immunoblotting targeting the His-Tag. Both DGAT isoforms were enriched in the detergent rich total lysate (includes membrane fraction), while both enzymes remained absent in the soluble lysate. **BI** Recombinant DGAT1-His, **CI** recombinant DGAT2-His, **DI** Pull-down with DGAT1-His in regard to the cell lysate composition. Total membrane lysate (high detergent concentrations) and the standardly used soluble cell lysate were compared. DGAT1 Interaction with Chemotype 1 was only observed at low detergent concentrations. (M: SDS-PAGE protein marker (Fermentas), L: lysate; active [P01], control [P02] U: unbound protein fraction of the active probe)

#### 4.4.1.4 Subcellular Localization Indicate a Compound Accumulation in the ER

In previous physiological studies with a fluorescein labeled derivative of Chemotype 2 [P03] (introduced in Chapter 4.1.4), it was shown that this derivative was preferentially found in the endoplasmic reticulum (ER). This observation was supported by colocalization studies of the fluorescein derivative in cells overexpressing the ER pDsRed2-ER (Clontech), which initiates the expression of a protein that localizes within the ER membrane (see Figure 47). The physiological localization of the fluorescein derivative of Chemotype 2 [P03] could either be explained by unspecific ER accumulation based on the intrinsic cellular degradation machinery or indicate a specific DGAT1 interaction. Both DGAT isoforms predominantly localized in the endoplasmic reticulum (Wurie et al, 2012). In order to test the hypothesis of a direct interaction between the small molecule and DGAT1, direct binding studies were required. The *in situ* proximity ligation assay (DuoLink) was therefore considered as the assay design allows binding studies in cells.

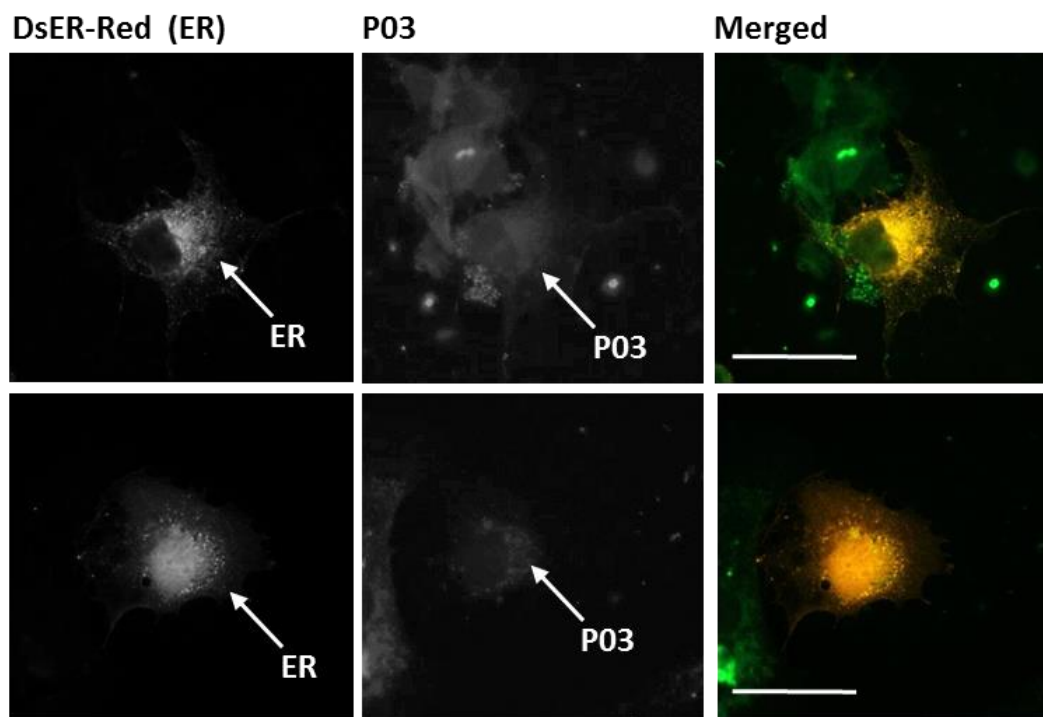


**FIGURE 47: The fluorescein labeled Chemotype 2 derivative is enriched in the ER.** pDsRed2-ER (Clontech) transfected AML12 cells were treated with 20 nM labeled Chemotype 2 [P03] for 1 h. For pDsRed2 positive cells a colocalization with fluorescein-Chemotype 2 was shown. (Images acquired with Zeiss Observer Z1, 63x oil, scalebar 50  $\mu$ m, red: endoplasmic reticulum, green: Fluorescein-Chemotype 2, yellow: overlay).

#### 4.4.1.5 A Physiological Binding Assay Demonstrates direct interaction between DGAT1 and Chemotype 2

Different membrane spanning domains are assumed for both DGAT isoforms (Lopes, José L. S. et al, 2014). These hydrophobic domains hinder sufficient production and purification of functional, recombinant DGAT protein. Purified protein, however, is required for direct biophysical binding studies such as fluorescence polarization (FP; Wendy & Simeonov, 2011), MicroScale Thermophoresis (MST; Jerabek-Willemsen et al, 2011) or isothermal titration calorimetry (ITC; Falconer & Collins, 2011). One way to circumvent the solubility problem is the microsomal expression of the DGAT isoforms, which was successfully described in the literature (Cao et al, 2011). Nevertheless, microsomal purification is still not the optimal direct method for validation of direct interaction still requires an artificial environment of the investigated membrane proteins. For that reason, the hypothesized interaction was analyzed in an image based *in vitro* setup by a modified proximity ligation assay (PLA, DUOLINK® Technologies).

The PLA assay can be performed under nearly native conditions in cells and only requires the presence of the endogenous or overexpressed, recombinant protein in a cellular environment and a modified small molecule suitable for antibody detection. The assay principle relies on a polymerase based signal amplification that only occurs when the respective interactors are in close proximity to each other (max. 30-40 nm). The close proximity is considered as an indicator for direct interaction. In the here chosen experimental setup, recombinant murine DGAT1 or DGAT2 overexpressing cells were treated with a fluorescein- labeled derivative of Chemotype 2 [P03] (see Figure 48.A). Specific PLA amplification signals were seen as red dots in microscopic images. The PLA signal was significantly enriched in the presence of DGAT1-His, while the respective DGAT2-His and untransfected control cells showed only isolated PLA amplification signals (see Figure 48.B). Image segmentation supported significant differences (see Figure 48.C). This finding, strongly suggests an interaction of DGAT1 with Chemotype 2.

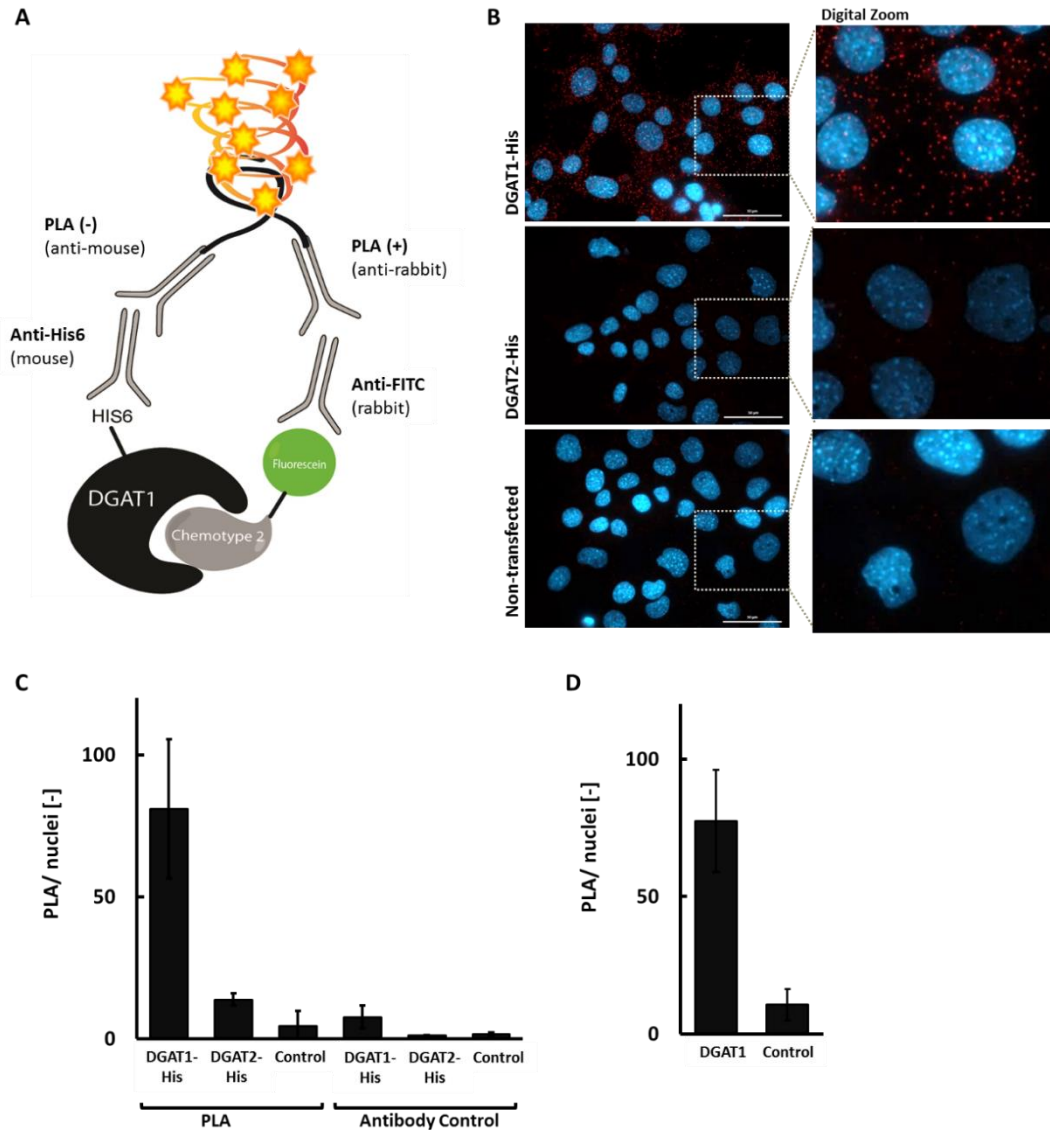


**FIGURE 48: *In vitro* binding of a fluorescein labeled derivative to DGAT1 in a proximity ligation assay (PLA).** **A** Schematic summary of the PLA assay (Duolink®PLA® Technology). AML12 cells were transfected with murine DGAT1-His and DGAT2-His for 48 h. Fixed cells were incubated first with a fluorescein labeled active derivative of Chemotype 2 and subsequently with primary antibodies either recognizing the His-tag of the recombinant protein or the fluorescein tag of Chemotype 2 [P03]. Specific secondary PLA antibodies which carry complementary oligonucleotides allowed a later ligation of the nucleotides if the probes were in close proximity. A rolling circle amplification connects and amplifies the nucleotide sequence. Addition of fluorescence labeled complementary single stranded oligonucleotides align with the amplification. As the signal requires a close proximity of the analyzed probes, this method can be used as a cell model for small molecule and target interaction. **B** mDGAT1-His and mDGAT2-His expressing AML12 cells and untransfected control cells were tested in a PLA setup for interaction between the small molecule [P03] and the His-tagged DGAT isoforms. A specific signal was detected in DGAT1-His samples whereas PLA signals were lacking in the respective DGAT2-His and non-transfected controls. Unspecific binding of the secondary antibodies was tested in separate antibody controls. AML12 cells overexpressing recombinant DGAT isoforms treated in these controls support the specificity of the signal (images not shown). **C** Image segmentation based on the PLA signal in cells expressing recombinant DGAT-His isoforms. The average PLA signal count was normalized to the nuclei count per image. **D** PLA experiment based on endogenous DGAT1 detected by a primary DGAT1 antibody (Abcam, ab54037) compared to the secondary antibody control. (Images were acquired at the Zeiss Observer Z1, 63x oil, scalebar: 100  $\mu$ m, blue: DAPI, red: PLA amplification signal).

#### 4.4.2 REMAINING QUESTIONS REGARDING DGAT1 SPECIFICITY

In the previous section the hypothesis that Chemotype 2 is able to directly interact with DGAT1 and furthermore effectively inhibits functionality was substantiated. The specificity of Chemotype 2 for DGAT1, but not for DGAT2, is seen both in direct binding and functional enzyme assays. This finding raised questions in regard to the not yet totally elucidated cooperation of the distant, but synergistically acting DGAT isoforms. The next subchapter focuses on some questions which occurred in the course of the target identification and validation process.

##### 4.4.2.1 DGAT1 and DGAT2 Expression in Non-Adipocytes

The two DGAT enzymes play distinct but synergistic roles in TAG synthesis necessary for LD formation. The current data indicate that Chemotype 2 uniquely affects DGAT1, while DGAT2 function is not altered. DGAT1 inhibition in the absence of DGAT2 would thus present one possible explanation. In order to examine this hypothesis, the expression levels of both enzymes in non-adipocytes were compared. DGAT1 and DGAT2 are considered to be ubiquitously expressed in eukaryotic cells (Turchetto-Zolet et al, 2011). Nevertheless, different tissues show variations in the respective DGAT1 and DGAT2 expression levels (proteintlas.org). Expression levels of murine DGAT1 are especially high in brown and white adipose tissue and peak additionally in placenta, uterus, epidermis, the adrenal gland, liver, kidney and testis (www.biogps.org). DGAT2 also shows increased levels especially in BAT and WAT, but additionally in the intestine and granulocytes, as well as in the mammary gland, the adrenal gland, bone and testis (www.biogps.org). During previous activity studies of Chemotype 2, different cells of different origins were tested in the LD droplet assay (see Chapter 4.1.2.2, p.22). The specimen set, however, was too small to determine a correlation between small molecule activity and cell type. Liver and kidney cells, which are considered rich on DGAT1 mRNA, however, show a good phenotypic response upon Chemotype 2 treatment, while the tested intestinal or bone derived cells rich in DGAT2 did not show a LD reduced phenotype. In order to examine the potential cause for the DGAT1 dependent effect in the presence or absence of DGAT2, the expression levels were analyzed in cells with known sensitivity to Chemotype 2. Surprisingly, the DGAT1 and DGAT2 expression levels were in similar relative concentration ranges (see Figure 49). This rules out that the presence or absence of both isozymes is responsible for the selective inhibition of DGAT1 in non-adipocytes. This observation is in agreement with literature descriptions for the DGAT1 specific commercial inhibitor A-922500 (Zhao et al, 2008). It was shown that TAG formation in A-922500 [1 $\mu$ M] treated HepG2 cells was successfully inhibited even in the presence of both isozymes (Qi et al, 2012).

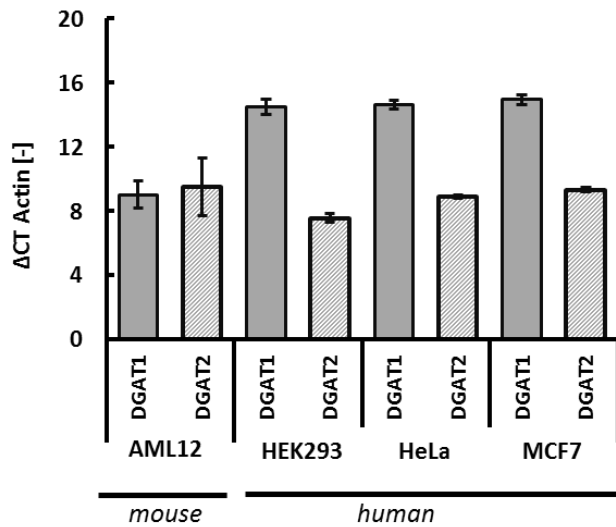


**FIGURE 49: DGAT1 and DGAT2 expression profiles in cell lines with known activity for Chemotype 2.** Total RNA was isolated from untreated mammalian cells fed with 200  $\mu$ M OA. The total RNA was analyzed by quantitative real-time PCR towards the relative expression of DGAT1 and DGAT2 levels in correlation to  $\beta$ -Actin. Both enzymes were expressed. The murine cell line showed no differences in the abundance of the respective DGAT1 and DGAT2 RNA species, while differences were measured in human cell lines.

#### 4.4.2.2 Diacylglyceride (DAG) Species

Both DGAT isoforms catalyze the esterification of acyl-CoA fatty acids with existing diacylglycerol which results in the formation of complete TAG species which are stored in LDs. Consequently, an educt accumulation would have been expected as a consequence of DGAT1 inhibition, but was not reported in DGAT1 depletion studies. Generally, it is assumed that constant DAG and acyl-CoA levels are beneficial in regard to lipotoxicity (Chen et al, 2002). This is in argument with the observed lack of DAG accumulation in this study.

Slight alterations in the standard LD storage assay, however, changed this result: Pre-fed cells which already store lipids at the point of small molecule treatment, show a temporal accumulation of DAG. This observation was unique for Chemotype 2 (see Figure, p.37). We hypothesize that the temporal DAG accumulation is realized by the high number of LDs in pre-fed cells. The hydrophobic organelles might temporarily be able to ingest the DAG species and thus prevent the usual DAG consuming pathways or lipotoxic effects. A similar phenotype characterized by the DAG accumulation is seen upon hormone sensitive lipase (HSL) knock out (Morak et al, 2012).

Detailed analysis of the temporarily accumulated DAG indicated that both *sn*-1,2 and *sn*-1,3 DAG intermediates were present upon Chemotype 2 treatment, with an enhanced concentration of *sn*-1,3 DAG. The formation of this diester was considered as a result of ATGL mediated lipolysis of the existing LDs, as ATGL has a strong preference for the hydrolysis of FA esters at the *sn*-2 position of the glycerol backbone (Eichmann et al, 2012). If the re-esterification is simultaneously blocked by DGAT1 inhibition DAG consequently accumulates. Currently, it is not resolved which DAG isomers are preferred substrates for DGAT1 or DGAT2 (Eichmann et al, 2012). It is assumed that the *sn*-1,2

DAG is preferably used as the substrate for glycerophospholipid biosynthesis (Hiramane & Tanabe, 2011) and functions as a potent activator of protein kinase C (Boni & Rando, 1985). In contrast, the *sn*-1,3 DAG is the preferred substrate for HSL-mediated degradation or re-esterification and re-storage of the generated TAG in LDs. Especially the re-esterification of external FFAs was associated with the DGAT1 specific function (Qi et al, 2012; Ohsaki et al. 2014). As the standard LD assay is performed at high FFA concentrations (400  $\mu$ M OA), a DGAT1 mediated block might offer a direct explanation for the LD reduced phenotype. DGAT2, on the other hand, was predicted to mainly re-esterify FFAs from *de novo* synthesis (Qi et al, 2012; Ohsaki et al. 2014), which is known to be downregulated on mRNA level upon Chemotype 2 treatment (see Chapter 4.1.4.1). This hypothesis would coherently explain, why a LD reduced phenotype is observed at the given experimental conditions even when only one of two enzymes which are known to catalyze the same reaction is selectively inhibited.

#### 4.4.3 OUTLOOK

The validation process for Chemotype 2 sustained the hypothesis that DGAT1 is a likely direct target of this small molecule. The validated inhibition of DGAT1 activity is a conclusive mechanism to block the TAG synthesis including preferably external FFAs. As DGAT1 catalyzes the final step of TAG synthesis, a DGAT1 specific inhibition is a likely cause for the observed LD reduced phenotype. Chemical modulation of DGAT1 was in the focused of academic and pharmacological research during the last decade (DeVita & Pinto, 2013). Its unique mechanistically position as the committing step in TAG synthesis, makes it a luring target candidate in obesity and diabetes therapies and the metabolic syndrome (Birch et al, 2010). A multitude of potential inhibitors was thus developed (see Supplemental Figure 10, p.206) and reached different stages in clinical trials. Most clinical studies, however, were stopped as a consequence of skin abnormalities and (severe) gastrointestinal adverse side effects, such as nausea, diarrhea and vomiting (reviewed by (DeVita & Pinto, 2013).

Since the novel discovered Chemotype 2 shows a distinct chemical scaffold compared to the currently described DGAT1 inhibitors, it might be speculated that this molecule is able to target DGAT1 by alternative mechanisms. This raises the perspective that the currently described side effects might be minimized. Conversely, most of the observed adverse effects are assumed as a direct consequence of DGAT1 inhibition itself, since the symptoms are highly similar to the ones observed in DGAT1 deficient humans (Ables et al, 2012; DeVita & Pinto, 2013). As a consequence, the scope of pharmacological applications especially for long term use as required in obesity treatment is extenuated. Nevertheless, Chemotype 2 has high potential to become a valid research

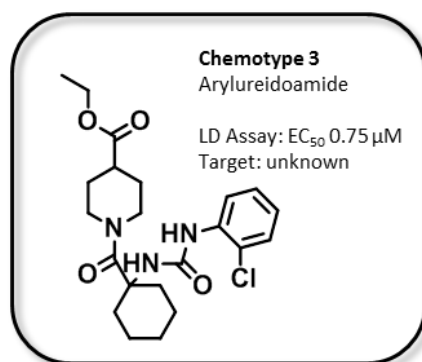


tool and thus might help to further investigate and further understand the cooperation of the known DGAT isoforms in the complex metabolic network. Chemotype 2 additionally might be able to shed some light to the yet not totally elucidated progress of LD formation and degradation and might help to discover novel connections between currently unrelated enzymes of different pathways.

Leaving the metabolic potential of DGAT1, a diversified interest in DGAT1 was claimed in distinct research areas. Starting at the DGAT1 dependent hepatitis C virus replication as a lead for new therapy approaches (Herker et al, 2010), ranging over increased DGAT1 dependent oil concentrations in algae and plants as broadly concerned in commercial raw oil production (Andrianov et al, 2010) to increased yields in dairy production. A QTL analysis of German milk cows showed a relationship between milk yield, fat content and protein content, depending on genetic variants of DGAT1 and mutations in different milk cow lines (Thaller et al, 2003). The importance of DGAT1 and LDs was generally related to lactating mammary glands as an important enzyme required for secretion and nutritional transfer to the offspring. For instance, homozygous females for a DGAT mutation show impaired ability to nurse their babies presumably to a lack of LDs for milk production (Cases et al, 2004).

The presented data point out the importance and widespread interest in DGAT1 inhibitors. Detailed analysis of Chemotype 2 as a new research tool applicable in different research fields, will help to further characterize the newly discovered DGAT1 inhibitor.

## 4.5 TARGET IDENTIFICATION FOR CHEMOTYPE 3



The arylureidoamide scaffold of Chemotype 3 is the chemical class with the lowest activity in the initial LD based assays ( $EC_{50}$  0.74  $\mu$ M). In ongoing SAR studies by Dr. Matthew Boxer, the activity was increased to 250 nM (data not shown). The chemical affinity probe optimization required for proteomic studies is not completed at the current state of investigations. Accordingly, this probe did not enter the chemical proteomic target identification

process. As a consequence, this chemotype was not analyzed in extensive detail in this thesis.

Unmodified, active derivatives of Chemotype 3 were used in physiological experiments in order to gain information of the underlying mechanism of action (see Chapter 4.1). As the previously investigated other Chemotypes, Chemotype 3 derivatives also showed activity in insect and mammalian systems as well as *in vivo* activity in *Drosophila* flies. Additionally, it was indicated that neither lipid uptake nor lipolysis were affected by derivatives of this small molecule. Transcriptome data analysis indicated towards increased  $\beta$ -oxidation and first indications point toward an increased number of mitochondria in cells treated with Chemotype 3. This effect was not seen in the respective experiments with Chemotype 1 and Chemotype 2. The underlying cause, however, has to be examined in more detail in order to name the direct interaction partner.

## CHAPTER 5: RESULTS AND DISCUSSION- PART 2

### 5.1 ADAPTION OF LD BASED SCREENS

Currently, only a limited number of small molecules are known to efficiently modulate lipid storage without introducing cytotoxic effects. Especially peripherally acting small molecules which do not affect neuroendocrine modulation are lacking. The investigation of cellular proteins involved in lipid storage currently mainly focuses on known key players in lipid synthesis (e.g. DGAT1 Inhibitor: PF-04620110; Dow et al, 2011) or lipolysis (ATGL Inhibitor: Atglistatin, Mayer et al, 2013). In order to further discover potential modulators in LD storage, two new HCS lipid droplet screens were established at COMAS (*Compound Management and Screening Center, Dortmund*). The COMAS compound library presents a unique collection of natural product derived small molecules. It was proposed that this widespread collection of small molecules with high similarity to naturally occurring compounds and secondary metabolites, yields higher probabilities to identify novel, highly active small molecules involved in LD storage processes apart from currently literature described lipid storage modulators.

Two screens were thus introduced into the screening routine at COMAS, which are now able to be executed in regular intervals with the newly submitted small molecules accepted in the COMAS compound collection. Both screens concentrate on lipid storage inhibition with discrete medical relevance and potential application as research tools. On the one hand, a “standard” LD assay in a mouse hepatocytes was established in order to identify lipid droplet modulators relevant in obesity and steatosis research, as well as for potential pharmacological intervention (see results in Chapter 5.1). On the other hand, an additional HCS LD- based screen was introduced in order to investigate the inhibition of macrophage differentiation. This screen aimed at the identification of possible modulators of arteriosclerosis by inhibiting foam cell formation (see results in Chapter 5.2).

### 5.1 HCS LIPID DROPLET SCREEN IN AML12 CELLS

The AML12 cell line ( $\alpha$ -mouse liver 12, ATCC: CRL-2254<sup>™</sup>) originates from hepatocytes of a transgenic mouse expressing human TGF  $\alpha$ . This cell line was chosen based on its potentially broad range of scope: the identified small molecules might not only modulate LD storage in classically non-adipocyte cells, but also might be able to deplete undesired lipid storage in nonalcoholic fatty liver disease (NAFLD). NAFLD has been linked to obesity and diabetes with still remaining unclear causes (Rosso et al, 2014). AML12 cells are a long established system to study lipid droplet formation and were used in different screening approaches either to identify small molecules that stimulate lipid droplet formation or to antagonize oleic acid induced lipid droplet formation (McDonough et al, 2009).

The LDs found in AML12 cells are homogenously distributed all over the single cell and have distinct characteristics in size and globular shape, which are suitable for automatic image processing required in HCS campaigns. One general disadvantage of liver cell based screens, thus including AML12 cells, are known high levels of cell to cell heterogeneity. In literature it is speculated that this mixed cellular population is beneficial in order to diminish cytotoxicity as some cells within this population are capable to incorporate the toxic free fatty acids (Herms et al, 2013). One hypothesis is that the heterogeneity relies on stochastic gene expression as a reflection of differently transcribed or translated genes (Shahrezaei & Swain, 2008). However, this heterogeneity might lead to an altered cellular response throughout the treated population and thus might impact the determined global activity. The heterogenic LD accumulation, was not further considered in the here summarized experimental design. Instead, solely the overall LD accumulation was analyzed. Nevertheless, the obtained dataset can still be evaluated in regard to further cellular characteristics, including cell to cell heterogeneity, if this additional information is required. Maximized output can be gained, when the LD shape or potential clusters within single cells are focused in more detail. Especially single cell analysis allows the identification of subpopulations within the treated cells. This in-depth data analysis was not required at this point, but remains feasible with the stored dataset.

### 5.1.1 Setup of the HCS LD Screen in AML12 cells

The HCS LD screen was designed according to the forward chemical genomic approach, aiming for phenotypic changes regarding the abundance of LDs in the presence of small molecules. In this AML12 based screen, an internal sub-library of more than 12.000 small molecules of the COMAS compound collection was screened in a single dose concentration. The small molecules were added at the same time as the oleic acid was administered thus directing the screen into the search for OA uptake and lipid droplet formation inhibitors. In order to keep the number of false positive hits at a minimal level, a low initial screening concentration of 10  $\mu$ M was chosen in the primary screen. Only small molecules which did not show any cytotoxicity and reduced the number of lipid droplets by more than 50% and simultaneously did not affect the cell number, determined by the nuclear count, were considered for the subsequent  $IC_{50}$  determination.  $IC_{50}$  values were determined for eight different concentrations in the range between 78 nM- 10  $\mu$ M in triplicates. The cytotoxicity was tested at identical conditions in parallel based on the ATP production of viable cells in a CellTiterGlo<sup>®</sup> luminescent assay.

To adapt the LD assay to the 384-well format and the available equipment of the COMAS facility the semi-automated screening protocol as summarized in Table 5 was established. This involved an automated small molecule administration step by the ECHO acoustic dispenser, semi-automated plate handling and the ImageXpress<sup>™</sup> HCS System (Molecular Devices). The listed conditions are based on process optimization in respect to multiple parameters such as the initial cell number, concentrations of staining solutions, incubation times and minimal amount of required manual handling steps. One critical point in process optimization was the plate washer setup during step 8 in order to avoid cell loss by harsh washing conditions. The implemented assay can now be performed in 3 ½ work days in the laboratory and another 2 ½ days for automated imaging and simultaneous image processing.

A total number of 12.118 small molecules was screened in the here presented setup, resulting in 28x 384 well plates. Each plate contained 32 control wells of DMSO treated cells in presence and absence of 200  $\mu$ M OA. DMSO- treated cells without oleic acid feeding were used to determine the basal level of endogenous LD formation (negative control).

TABLE 5 HCS LD Screening Protocol in AML12 cells to identify modulators of lipid storage.

STEP	① ②	③ ④ ⑤	⑥ ⑦ ⑧ ⑨	⑩	Day 1	Day 2	Day 3	Day 6
	Adaption		Treatment + OA feeding		Staining		Imaging & Data Analysis	
Step	Step	Description						
1	cell seeding	800 AML12 cells per well, in 20 $\mu$ L DMEM: F12 (1:1) medium, 10% (v/v) FBS in Corning 384-imaging plates (#3712) administered semi-automatically by MultiDrop Dispenser						
2	adaption	incubation over night 37°C, 5% CO <sub>2</sub>						
3	small molecule administration	small molecule administration by ECHO acoustic dispenser Screen: 30 nL; 10 $\mu$ M, single dose IC <sub>50</sub> : 30 nL; 78 nM- 10 $\mu$ M, triplicates Controls: DMO control (0.1% (v/v), Column 11) Basal LD level in unfed cells (-200 $\mu$ M OA, DMSO (0.1% (v/v)), column 12)						
4	FA feeding ("high fat diet")	200 $\mu$ M oleic acid in DMEM:F12 (1:1) medium, 5% (v/v) FBS (10 $\mu$ L) administered semi-automatically by MultiDrop Dispenser						
5	treatment	incubation over night 37°C, 5% CO <sub>2</sub>						
6	staining	add-on staining 30 $\mu$ L 3x Fixation and Permeabilization solution including BODIPY®493/503 (1:1000) and Hoechst 33342 (1:500) administered semi-automatically by MultiDrop Dispenser						
7	incubation	1h at room temperature						
8	washing	3x PBS washing Semiautomatic with ElxWasher (BioTek)						
9	centrifugation	2min, 800 rpm centrifugation and plate cleaning (30% (v/v) ethanol) (manually)						
9	detection	automated imaging at 20x magnification BODIPY® 493/503 (Ex 488 nm, Em 493-598 nm; FITC filter) Hoechst 33342 (Ex 405 nm, Em 410-496 nm; DAPI filter) ImageXpress XL (Molecular Devices), automated by Orbitor RS Microplate Mover (Thermo)						
10	analysis	automated image segmentation MetaXpress™ Systems						

### 5.1.2 Evaluation of the HCS LD Screen in AML12 cells

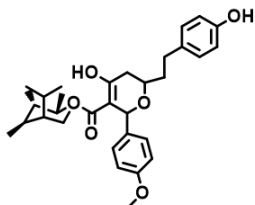
The first pilot screen and subsequent IC<sub>50</sub> determination experiments resulted in a hit rate of 2%. These initial experiments suffered from low data quality in image processing which was mainly caused by focusing problems during automated image acquisition. A changed batch of 384-well plates in the primary screen resulted in a higher image quality and better segmentation results. Among the identified small molecules, five compounds introduced a significant reduction of LD deposition in both the pilot and the primary screen (see Table 6).

**TABLE 6: Comparison of AML12 screening hits in the small pilot screen and the final primary screen.** AML12 cells were incubated with 10  $\mu\text{M}$  of small molecule in presence of 200  $\mu\text{M}$  OA for 16 h. The increased data quality in the primary screen in comparison to the pilot screen was reached by a changed batch of screening plates.

Internal ID	Pilot Screen (IC <sub>50</sub> )		Primary Screen (IC <sub>50</sub> )	
	LD [ $\mu\text{M}$ ]	Cytotoxicity [ $\mu\text{M}$ ]	LD [ $\mu\text{M}$ ]	Cytotoxicity [ $\mu\text{M}$ ]
100075	7.76 $\pm$ 7.76	20.30 $\pm$ n.D.	>10	inactive
100370	1.59 $\pm$ 1.59	9.79 $\pm$ n.D.	2.52 $\pm$ 1.04	> 10
100372	0.47 $\pm$ n.D.	3.76 $\pm$ n.D.	3.68 $\pm$ 1.1	> 10
100959	7.79 $\pm$ 7.79	Inactive	< 5	Inactive
100960	7.74 $\pm$ n.d	inactive	< 5	inactive
103084	7.74 $\pm$ n.d	Inactive	> 10	inactive
335672	7.00 $\pm$ 0.34	Inactive	> 10	inactive

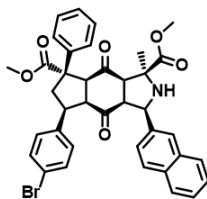
The primary screen identified 96 small molecules which led to a decrease in formed LDs without affecting viability of the tested AML12 cells. In the secondary IC<sub>50</sub> screen, only ~ 25% of the initial hit candidates (26 derivatives) were confirmed with good to moderate IC<sub>50</sub> values (< 10  $\mu\text{M}$ ) and the required lack of cytotoxicity. The confirmed hits of the primary LD screen in AML12 cells are summarized in Table 7.

**TABLE 7: Hits in the AML12 HCS lipid droplet screen (AML12-Hit).** Hits from the primary screen were re-screened for IC<sub>50</sub> determination. Only small molecules without cytotoxic effects were included in the evaluation. Highlighted small molecules in grey boxes, were also previously identified in the pilot screen with comparable IC<sub>50</sub> values.



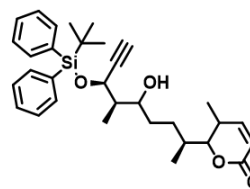
**AML12 Hit\_1**

LD- IC<sub>50</sub>: 0.98 ± 0.39 μM  
Cytotoxic IC<sub>50</sub>: inactive



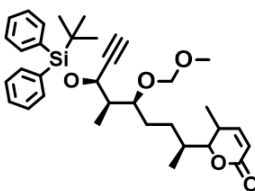
**AML12 Hit\_2**

LD- IC<sub>50</sub>: 2.40 ± 0.48 μM  
Cytotoxic IC<sub>50</sub>: inactive



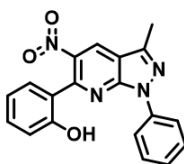
**AML12 Hit\_3**

LD- IC<sub>50</sub>: 2.52 ± 1.04 μM  
Cytotoxic IC<sub>50</sub>: >10 μM



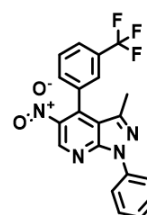
**AML12 Hit\_4**

LD- IC<sub>50</sub>: 3.68 ± 1.1 μM  
Cytotoxic IC<sub>50</sub>: >10 μM



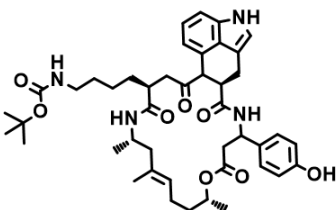
**AML12 Hit\_5**

LD- IC<sub>50</sub>: 4.85 ± 0.57 μM  
Cytotoxic IC<sub>50</sub>: inactive



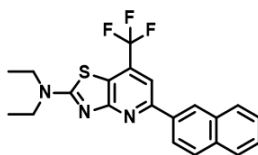
**AML12 Hit\_6**

LD- IC<sub>50</sub>: 5.79 ± 1.63 μM  
Cytotoxic IC<sub>50</sub>: inactive



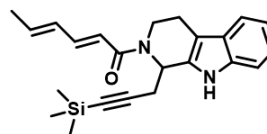
**AML12 Hit\_7**

LD- IC<sub>50</sub>: 6.52 ± 0.27 μM  
Cytotoxic IC<sub>50</sub>: inactive



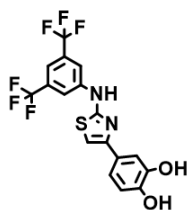
**AML12 Hit\_8**

LD- IC<sub>50</sub>: 6.88 ± 1.60 μM  
Cytotoxic IC<sub>50</sub>: inactive



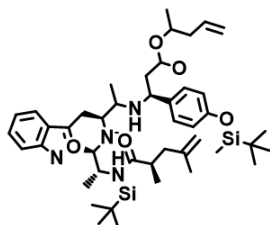
**AML12 Hit\_9**

LD- IC<sub>50</sub>: 7.62 ± 1.22 μM  
Cytotoxic IC<sub>50</sub>: inactive



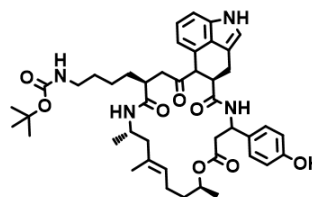
**AML12 Hit\_10**

LD- IC<sub>50</sub>: 8.05 ± 0.58 μM  
Cytotoxic IC<sub>50</sub>: >10 μM



**AML12 Hit\_11**

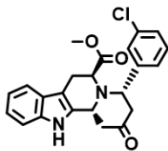
LD- IC<sub>50</sub>: 8.21 ± 1.44 μM  
Cytotoxic IC<sub>50</sub>: inactive



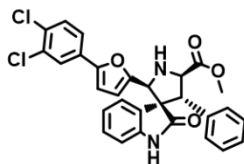
**AML12 Hit\_12**

LD- IC<sub>50</sub>: 9.22 ± 0.18 μM  
Cytotoxic IC<sub>50</sub>: inactive

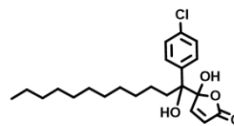




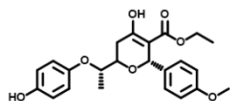
**AML12 Hit\_13**  
LD- IC<sub>50</sub>: 9.84± 0.05 μM  
Cytos IC<sub>50</sub>: >inactive



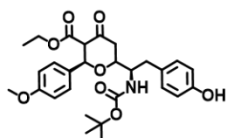
**AML12 Hit\_14**  
LD- IC<sub>50</sub>: >10 μM  
Cytos IC<sub>50</sub>: inactive



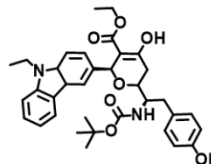
**AML12 Hit\_15**  
LD- IC<sub>50</sub>: > 10 μM  
Cytos IC<sub>50</sub>: inactive



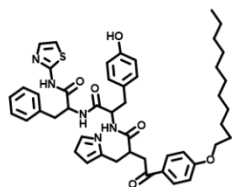
**AML12 Hit\_16**  
LD- IC<sub>50</sub>: > 10 μM  
Cytos IC<sub>50</sub>: >inactive



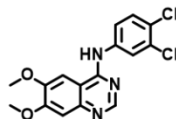
**AML12 Hit\_17**  
LD- IC<sub>50</sub>: >10 μM  
Cytos IC<sub>50</sub>: inactive



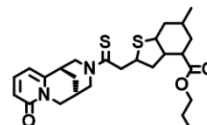
**AML12 Hit\_18**  
LD- IC<sub>50</sub>: > 10 μM  
Cytos IC<sub>50</sub>: inactive



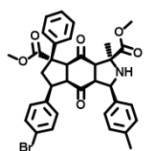
**AML12 Hit\_19**  
LD- IC<sub>50</sub>: > 10 μM  
Cytos IC<sub>50</sub>: >inactive



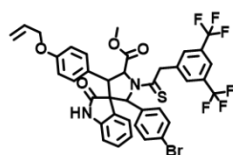
**AML12 Hit\_20**  
LD- IC<sub>50</sub>: >10 μM  
Cytos IC<sub>50</sub>: inactive



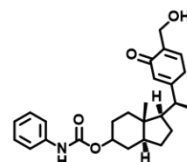
**AML12 Hit\_21**  
LD- IC<sub>50</sub>: > 10 μM  
Cytos IC<sub>50</sub>: inactive



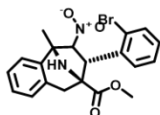
**AML12 Hit\_22**  
LD- IC<sub>50</sub>: > 10 μM  
Cytos IC<sub>50</sub>: >inactive



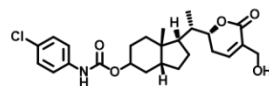
**AML12 Hit\_23**  
LD- IC<sub>50</sub>: >10 μM  
Cytos IC<sub>50</sub>: inactive



**AML12 Hit\_24**  
LD- IC<sub>50</sub>: > 10 μM  
Cytos IC<sub>50</sub>: inactive



**AML12 Hit\_25**  
LD- IC<sub>50</sub>: > 10 μM  
Cytos IC<sub>50</sub>: >inactive



**AML12 Hit\_26**  
LD- IC<sub>50</sub>: >10 μM  
Cytos IC<sub>50</sub>: inactive

## 5.2 HCS LD ASSAY FOR MODULATORS IN FOAM CELL LD STORAGE

As previously described in Chapter 2.2.1, LD formation within macrophages impacts the development of coronary artery disease, as the accumulation of TAGs and especially cholesterol esters within LDs leads to the production of foam cells and atherosclerotic plaques (McDonough et al, 2009). Macrophagic LDs are additionally implicated in the etiology of tuberculosis (D'Avila et al, 2006). To identify novel modulators which are able to block lipid storage in foam cells, a sublibrary of more than 10.000 small molecules of the COMAS compound collection was screened in a HCS format in order to identify potential chemical inhibitors.

### 5.2.1 Setup of the HCS Assay for the Detection of Inhibitors in Foam Cell LD Storage

The established THP-1 human monocyte cell line was chosen as a cellular model for foam cell generation in the HCS screen. The cells originate from a patient with monocytic leukemia and can be easily converted into macrophage like cells by the addition of phorbol myristate acetate (PMA). Undifferentiated THP-1 cells proliferate in suspension and become adherent by administration of 100 nM PMA (Tsuchiya et al, 1982) after 2-3 days of incubation. Differentiated cells show the flattened appearance reminiscent of human monocyte derived macrophages, which are the precursors of foam cells. The formed foam cells are characterized by a large amount of cytosolic LDs in presence of high amounts of free fatty acids or free cholesterol. Oleic acid incubated THP-1 cells show a concentration dependent LD formation (see Supplemental Figure 13, p.208). The formed LDs show an evenly shaped morphology suitable for automated image processing.

To identify small molecules with an inhibitory potential of lipid deposition, THP-1 cells were cultured in suspension, which is an excellent characteristic for the initial steps in high-throughput processing. The differentiation into the macrophage phenotype was induced by 100 nM PMA in a 384 well format. Visual confirmation of cell adherence served as a proxy for the differentiation process, which usually was completed after three days. In the following, 400  $\mu$ M OA was added to load the cells with LDs. In order to screen for modulators, small molecules of the tested COMAS sublibrary were added simultaneously with the oleic acid. This procedure was chosen, since the screen intended to identify modulators in the actual lipid storage process and not in the differentiation process itself. Latter could be tested by slight modification of the assay protocol, if the compounds and the PMA are added simultaneously.

The general assay design is comparable to the parameters described before for the "standard" LD assay (see Chapter 4.1.2) and only includes one additional differentiation step (see Table 8).

**TABLE 8: HCS LD Screening Protocol in THP-1 cells** in order to identify inhibitors of lipid storage dependent foam cell differentiation within the COMAS compound collection.

STEP	Step	Description
①② Day 1		
	Differentiation	
③④⑤ Day 4	Treatment + OA feeding	
⑥⑦⑧⑨⑩ Day 5	Staining	
⑪ Day 8	Imaging & Data Analysis	
<b>1</b>	cell seeding	5000 THP-1 cells in RPMI 1640 medium, 10% (v/v) FBS in Greiner 384-imaging well plates (#781092) (administered semi-automatically by MultiDrop Dispenser)
<b>2</b>	differentiation	addition of 100 nM PMA incubation for 3 days 37°C, 5% CO <sub>2</sub>
<b>3</b>	small molecule administration	small molecule administration by ECHO acoustic dispenser screen: 30 nL; 10 μM, single dose IC <sub>50</sub> : 30 nL; 78 nM-10 μM, triplicates controls: DMO control (0.1% (v/v)) Basal LD level in unfed cells (-200 μM OA, DMSO (0.1% (v/v)))
<b>4</b>	FA feeding (high caloric diet)	400μM oleic acid in DMEM:F12 (1:1) medium, 5% (v/v) FBS. (administered semi-automatically by MultiDrop Dispenser)
<b>5</b>	treatment	incubation over night 37°C, 5% CO <sub>2</sub>
<b>6</b>	staining	add-on staining 10 μL fixation and permeabilization solution including BODIPY®493/503 (1:1000) and Hoechst 33342 (1:500) (administered semi-automatically by MultiDrop Dispenser)
<b>7</b>	incubation	2h at room temperature
<b>8</b>	washing	3x PBS washing (50 μL) (by ElxWasher (BioTek) in combination with F5-robot arm for automation)
<b>9</b>	centrifugation	2min, 800 rpm centrifugation and plate cleaning (30% ethanol) (manually)
<b>10</b>	detection	automated imaging at 20x magnification BODIPY® 493/503 (Ex 488 nm, Em 493-598 nm; FITC filter) Hoechst 33342 (Ex 405 nm, Ex 410-496 nm; DAPI filter) ImageXpress XL (Molecular Devices), automated by Orbitor RS Microplate Mover (Thermo)
<b>11</b>	Analysis	automated image segmentation MetaXpress™ Systems

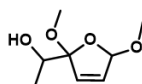
### 5.2.2 Evaluation of the HCS LD Screen in differentiated THP-1 Cells

More than 10,000 small molecules were screened at a concentration of 10  $\mu$ M. The signal to background level reached 20-30 and the  $z'$ -value of the assay was 0.5. In total 12 hits were identified which reduce the number of stored LDs without resulting in the cytotoxicity (see Table 9). This equals a hit rate of 0.1 %. Overall, the differentiated THP-1 cells were relatively sensitive upon small molecule treatment and many of the test substances were cytotoxic.

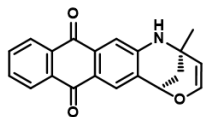
Interestingly, a link between the identified hits for LD reduction in differentiated THP-1 cells and purmorphamine- induced osteogenesis via hedgehog (Hh) was established during later internal database comparison. Ten out of twelve hits identified in the THP-1 screen showed weak to moderate activity in a previous purmorphamine- induced osteogenesis screen performed in COMAS (see boxed structures in Table 9). The COMAS Hh screen focused on the smoothed driven osteogenesis in multipotent murine C3H/10T1/2 cells. These cells are a well-accepted model in adipocyte differentiation as well, but follow another differentiation mechanism apart from the known PPAR $\gamma$  dependent adipose differentiation inducers (Konieczny & Emerson, C P Jr, 1984).

Simultaneous modulation of adipogenesis and Hh pathway was described in literature. Hh is among others a key regulator in adipogenesis (James et al, 2010). For example, a genome-wide transgenic RNAi screen performed in adult *Drosophila* flies identified hedgehog to be involved in the differentiation of adipocytes (Pospisilik et al, 2010). Hedgehog activation blocks white, but not brown adipocyte differentiation. This effect is mainly mediated by Gli dependent activation of anti-adipogenic factors (Ddit3, Gilz, Hes1, Ncor2, Nrf2), which subsequently block activity of PPAR $\gamma$  and CEBP members (Pospisilik et al, 2010). Consequently, osteogenesis and adipogenesis differentiation pathways are commonly described in an inverse correlation: either osteogenic programming is activated at the expense of adipogenesis, or vice versa (Beresford et al, 1992). These literature descriptions however contradict the THP-1 screening hits as most identified small molecules show an inhibition of the puromycin induced Hh activation at the same time as LD reduction. As a consequence, it can be speculated that a pathway that is independent of adipocyte differentiation is targeted.

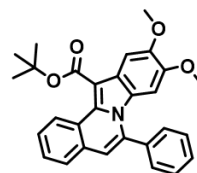
**TABLE 9: Screening hits in the HCS lipid droplet assay for lipid storage modulators in foam cell.** Hits from the primary screen in differentiated THP-1 monocytes to foam cells were re-screened for IC<sub>50</sub> determination. PMA differentiated THP-1 cells were treated with 78 nM – 10 μM small molecule in presence of 400 μM OA in triplicates. Only small molecules without cytotoxic effects in a secondary cytotoxicity assay were included for evaluation. The identified small molecules show an additional activity in a C3H/10T1/2 osteogenesis assay mediated by hedgehog signals (grey boxes). Hit 5 (filled grey box) was additionally identified in the AML12 LD screen. (significance on Hh signaling evaluated in percent (%) inhibition (primary screening results) and/or pIC<sub>50</sub> (secondary screening results)).



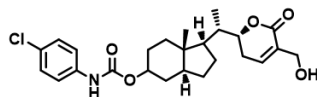
**THP-1-Hit\_1**  
LD- IC<sub>50</sub>: 1.36 ± 0.15 μM  
Cytox IC<sub>50</sub>: 5.73 ± 1.64 μM  
Hh: inactive



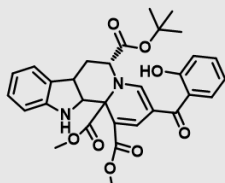
**THP-1-Hit\_2**  
LD- IC<sub>50</sub>: 2.76 ± 0.56 μM  
Cytox IC<sub>50</sub>: inactive  
Hh: 33 % (pIC<sub>50</sub>: 5.4 μM)



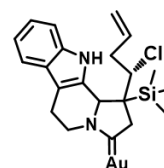
**THP-1-Hit\_3**  
LD- IC<sub>50</sub>: 3.39 ± 2.55 μM  
Cytox IC<sub>50</sub>: inactive  
Hh: 11 % (pIC<sub>50</sub>: n.D.)



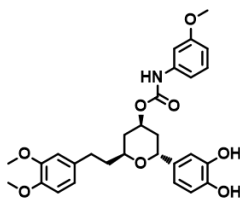
**THP-1-Hit\_4**  
LD- IC<sub>50</sub>: 3.82 ± 0.16 μM  
Cytox IC<sub>50</sub>: inactive  
Hh: n.D. (pIC<sub>50</sub>: 5.6 μM)



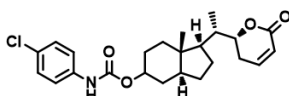
**THP-1-Hit\_5**  
LD- IC<sub>50</sub>: 3.92 ± 2.01 μM  
Cytox IC<sub>50</sub>: inactive  
Hh: 11 % (pIC<sub>50</sub>: 5.4 μM)



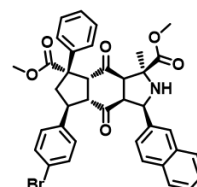
**THP-1-Hit\_6**  
LD- IC<sub>50</sub>: 5.89 ± 3.44 μM  
Cytox IC<sub>50</sub>: inactive  
Hh: inactive



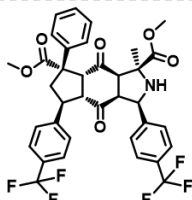
**THP-1-Hit\_7**  
LD- IC<sub>50</sub>: 6.52 ± 2.29 μM  
Cytox IC<sub>50</sub>: inactive  
Hh: inactive



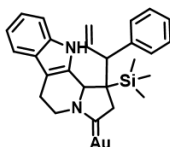
**THP-1-Hit\_8**  
LD- IC<sub>50</sub>: 6.62 ± 1.47 μM  
Cytox IC<sub>50</sub>: inactive  
Hh: n.D. (pIC<sub>50</sub>: 5.40 μM)



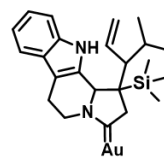
**THP-1-Hit\_9**  
LD- IC<sub>50</sub>: 7.25 ± 2.38 μM  
Cytox IC<sub>50</sub>: inactive  
Hh: 26 % (pIC<sub>50</sub>: n.D.)



**THP-1-Hit\_10**  
LD- IC<sub>50</sub>: > 10 μM  
Cytox IC<sub>50</sub>: inactive  
Hh: 11 % (pIC<sub>50</sub>: n.D.)



**THP-1-Hit\_11**  
LD- IC<sub>50</sub>: >10 μM  
Cytox IC<sub>50</sub>: inactive  
Hh: n.D. (pIC<sub>50</sub>: 5.9 μM)



**THP-1-Hit\_12**  
LD- IC<sub>50</sub>: > 10 μM  
Cytox IC<sub>50</sub>: inactive  
Hh: n.D. (pIC<sub>50</sub>: 5.72 μM)

## 5.3 SUMMARY

## 5.3.1 Identification of Compound 100960 as a potential LD storage modulator

The comparison between the AML12 and THP-1 HCS LD assays led to the identification of compound 100960 as a promising candidate for a novel lipid storage inhibitor ( $IC_{50}$  AML12: 7.7  $\mu$ M/  $IC_{50}$  THP-1: 3.9  $\mu$ M). The small molecule additionally scored as an inhibitor in a previous Hh driven osteogenesis screen carried out by the COMAS facility. Nonetheless, Compound 100960 cannot be classified as a “frequent-hitter” of HTS, as it might be assumed from the listing above. The small molecule was included in a wide range of screening campaigns at COMAS and remained inactive in those assays thus indicating specificity in the three pathways.

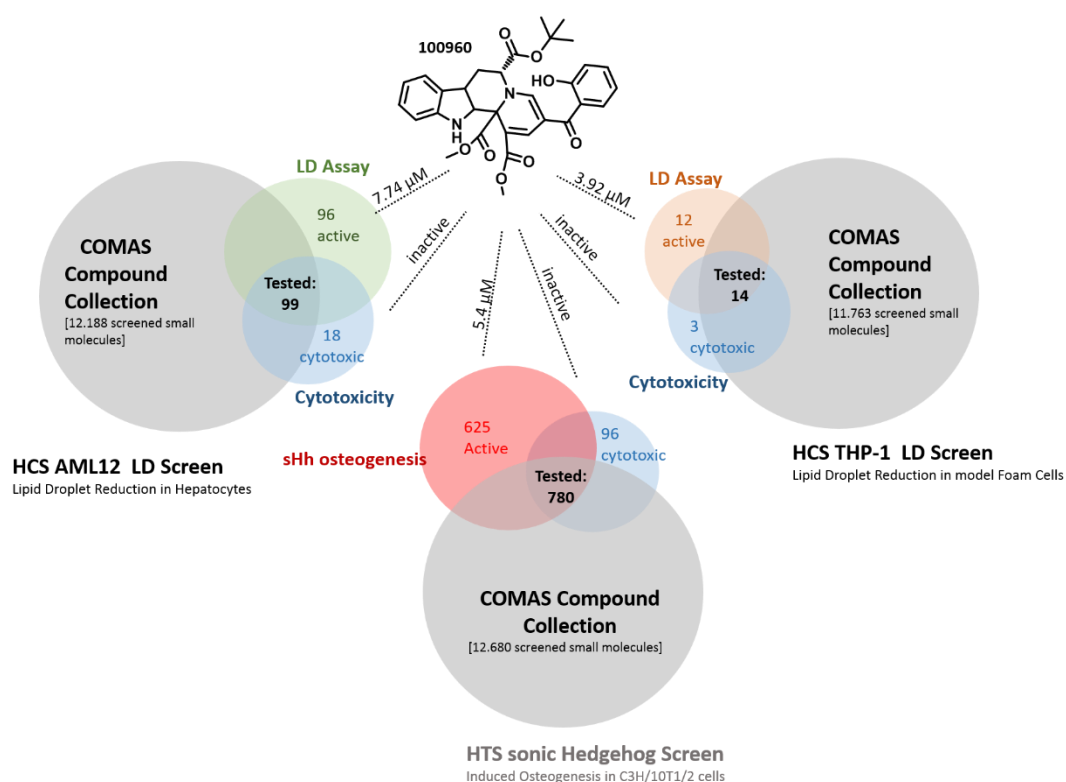


**FIGURE 50: Summary of the COMAS Screening off LD-reducing compounds.** The established HCS for LD modulations employing AML12 or THP-1 cells identified Compound 100960 as an inhibitor of lipid droplet storage. Internal database comparisons additionally identified the structure as a hedgehog driven osteogenesis inhibitor. (Big grey circles represent the tested small molecules of the respective primary screens; smaller colored circles summarize the  $IC_{50}$  measurements and regarding the revalidation and cytotoxicity data. Cytotoxic small molecules were excluded from further analysis.)

### 5.3.2 A Modified Screening Setup would allow directed Assays

As the presented screens were both designed in a classical forward chemical genomic approach, the underlying mechanism of action remains unclear. The experimental setup was solely focused on the identification of small molecules inducing LD reduced phenotypes without any pre-selection of potential involved pathways or targets. This “black box” setup, leaves the main task in later target identification. Target identification connected with an SAR study would be the consecutive next steps for the further characterization of the discovered small molecules in the different assays.

For further screening campaigns, small adaptations in the established assay protocol would additionally allow a directed screen to specific targets. By introduction of stably, genetically modified cell lines for known key players in lipolysis or TAG synthesis, the targeted pathway would be defined already at the first stage of screening which facilitates the consecutive target identification. A directed screen for lipolytic stimulators would for example implement a cell line with a stable overexpression of adipocyte triglyceride lipase (ATGL). Excess of ATGL would cause increased lipolysis and would result in cells with reduced numbers of LDs in the untreated state. Small molecules with ATGL inhibitory activity would rescue the native, LD rich phenotype and increase the level of stored triglycerides. Small molecules which support LD accumulation might lead to new tools in cachexia research and treatment. This or alternative directed setups would ease the progress of the target identification and validation significantly. However, reversed experimental designs base on the rational decision for a relevant and druggable target, as trade-off, only modulators for known (drug) targets acting via the established mechanism of action theories can be targeted, thus limiting the range of action and the scientific and pharmacological potential.

## CHAPTER 5:

This chapter summarized the introduction of two stable HCS Lipid Droplet based assays at COMAS, which are now applicable for routine screening campaigns in the future. First screens of the in-house COMAS sublibrary containing 12.000 small molecules, identified 26 small molecules which reduce the amount of LDs in AML12 cells without cytotoxic effects. Additional 12 small molecules were able to block foam cell generation in THP-1 cells. Among those hits, especially Compound 100960 stood out as it showed activity in both LD assays ( $IC_{50}$  AML12: 7.7  $\mu$ M/  $IC_{50}$  THP-1: 3.9  $\mu$ M) as well as in a previous hedgehog assay ( $IC_{50}$ : 5.4  $\mu$ M). It might possess particularly interesting properties as a tool compound to understand the link between the involved adipogenesis pathways.

## CHAPTER 6: MATERIAL

### 6.1 LABORATORY EQUIPMENT

Agarose Gel Chamber	BioRad, München, GER
BioPhotometer	Eppendorf, Hamburg, GER
Cell Counter, Countess™	Life Technologies™, Darmstadt, GER
Centrifuge 5415R, Eppendorf	Eppendorf, Hamburg, GER
Centrifuge, Minispin, Eppendorf	Eppendorf, Hamburg, GER
ECHO acoustic dispenser	LABCYTE™, California, USA
Elx405 Select Deep Well Microplate Washer	BioTek, Friedrichshall, GER
F5 Robot System	Thermo Scientific, Schwerte, GER
Gellogic 200 Imaging System	KODAK, Rochester, USA
iCycler Thermal Cycler (iQ5)	BioRad, München, GER
ImageXpress Micro XLS Widefield High Content Screening System	Molecular Devices, California, USA
Incubator Nuaire DHD Autoflow, NU5510E	Nuaire, Fernwald, GER
Incubator, (Drosophila)	Memmert, Nürnberg, GER
INFORS HT Minitron Standard, Bacterial Incubator	INFORS HT, Bottminge, CH
Leica SP5 Confocal Microscope	Leica, Solms, Germany
Liquid handling station Freedom EVO100	Tecan, Männedorf, GER
LTQ Orbitrap XL™ Hybrid Ion Trap-Orbitrap MS	Thermo Scientific, Schwerte, GER
Magnetic racks	Life Technologies™, Darmstadt, GER
Magnetic Stirrer	IKA®Werke, Staufen, GER
MiniProtean 3 Gelelektrophorese System	BioRad, München, GER
Monolith NT.115, MST	NanoTemper Tech., Munich, GER
Mr. Frosty™ Freezing Container	Thermo Scientific, Schwerte, GER
Multidrop™ Combi Reagent Dispenser	Thermo Scientific, Schwerte, GER
NanoDrop 2000c UV-Vis Spectrophotometer	Thermo Scientific, Schwerte, GER
Odyssey® Fc imaging System	LI-COR Biosciences, Bad Homburg, GER
Orbitor RS Microplate Mover	Thermo Scientific, Schwerte, GER
pH-Meter	Mettler Toledo, Giessen, GER
Plate Reader, Tecan Infinite M200	Tecan, Crailsheim, USA
PYREX® vials	Corning Incorporated, New York, USA
Q-Exactive™ Hybrid Quadrupol MS	Thermo Scientific, Schwerte, GER
Shaker/ Thermomixer comfort	Eppendorf, Hamburg, GER
SpeedVac	Eppendorf, Hamburg, GER
Sterile Bench, Mikroflow	NuncNalgene, Rochester, USA
Sterile Bench, Nuaire	NuAire, Fernwald, GER
Trans blotting chamber	BioRAD, München, GER
Vortex Genie 2	Roth, Karlsruhe, GER
Waterbath (Memmert)	Hettich AG, Bäch, GER
xCELLigence RTCA DP	ACEA Bioscience, San Diego, USA
Zeiss Observer Z.1, inverse, fluorescence microscope	Zeiss, Jena, Germany
Zeiss, VisiTron Systems, automated microscope	Zeiss, Jena, Germany

*\*All further laboratory equipment equates the usual standard.*



## 6.2 CONSUMABLES

12- well plates (Falcon)	#353043	Corning Incorporated, New York, USA
24-well plates (Falcon)	#353047	Corning Incorporated, New York, USA
384-well imaging Plates	#3826	Corning Incorporated, New York, USA
384-well imaging Plates	#3701	Corning Incorporated, New York, USA
6-well plates (Falcon)	#353046	Corning Incorporated, New York, USA
96-well imaging Plates, high resolution	#5241	Zellkontakt, Nörten, GER
96-well imaging Plates, screening	#3340	Corning Incorporated, New York, USA
96-well plates (Falcon)	#353072	BD Falcon™, New York, USA
AeraSeal™	#BS-25	Excel scientific Inc., Victorsville, USA
Aqua Poly/Mount	#53023	Polysciences, Warrington, USA
Carl Zeiss™ Immersol™ Immersion Oil	#12-070-394	Thermo Fisher Scientific, Schwerte, GER
Cell culture flasks (various sizes)	#353136	BD Falcon™, New York, USA
Cell scraper, big	#831831	Sarstedt, Newton, USA
Cell scraper, small	#353085	BD Falcon™, New York, USA
Corning® bottle-top vacuum filters	#CLS430049	Corning Incorporated, New York, USA
Countess Counting Slides	#C10283	Invitrogen, Carlsbad, USA
Cover Slips	#P231.1	Carl Roth GmbH, Karlsruhe, GER
DNA Loading Dye, 6x	# R0611	Thermo Fisher Scientific, Schwerte, GER
DNA Zap	#9891G	Amnion®, USA
Eppendorf Uvette®	#634-1922	Eppendorf, Hamburg, GER
Filter, syringe filter	#831826001	Sarstedt, Nümbrecht, GER
FINNTIP, 10 µL	#9900370	Thermo Fisher Scientific, Schwerte, GER
FINNTIP, 50 µL	#9900377	Thermo Fisher Scientific, Schwerte, GER
Gradient Protein Gel (4-20%)	#84713	Pierce, Thermo Fisher, GER
iCycler iQ® PCR Plates, 96 well	#2239441	BIORAD, UK
Immobilon® FL- Transfer Membrane (PVDF)	#IPFL00010	Thermo Fisher Scientific, Schwerte, GER
Incidur®	#3186407	Ecolab, Wien, AUT
Kuvettes, Standard	#67.742	Sarstedt, Nümbrecht, GER
Kyro Vials	#72.379.005	Sarstedt, Nümbrecht, GER
Lumitrac 600, white	#2015-09	Corning Incorporated, New York, USA
Microscope slide (Super Frost)	#36053500	Diagonal, Münster, GER
Mini-PROTEAN®TGX™ Gels (4-20%)	#456-1094	BIORad, München, GER
MULTIWell™, E-Plate 16 (RTCA)	#0569830001	ACEA Bioscience, San Diego, USA
Mycoplasma-ExSpray	#PK-CC91	PromoKine, Heidelberg, GER
Neubauer Counting Chamber	# PC72.1	Carl Roth, Karsruhe
Parafilm	#PM-996	Roth, Karsruhe, GER
PCR Sealers™, Microseal® 'B' Film	#00253112	BIORAD, UK
Petri dishes	#83.1800	Sarstedt, Nümbrecht, GER
Pipette Tipps, filter	#F171403	Gilson
Pipettes, pasteur	#747715	BRAND,
Scalpel	#5518075	Braun, Melsungen, GER
SIL G-25 UV254 plates	# 809022	Macherey-Nagel, Oensingen, SUI
Small volume spin columns	# 84868	Thermo Fisher Scientific, Schwerte, GER

Sterican needles (various sizes)	#various	Braun, Melsungen, GER
Syringes (1, 5, 20, 50 mL)	#various	Braun, Melsungen, GER
Test Tubes (0.5, 1.5, 2 mL)	# T9661	Eppendorf, Hamburg, GER
Test Tubes (15, 50 mL)	# T9661	Sarsted, Nümbrecht, GER
Test Tubes (low protein bind, 1-5 mL)	#0030.108.11	Eppendorf, Hamburg, GER
TLC Silica Gel plates	#1.05748.000	Merck, Hohenbrunn, GER
Trypan Blue Solution	#T10282	Life Technologies™, Darmstadt, GER
Whatmann 3 MM Paper		Schleicher & Schüll, Dassel, GER

*\*All further laboratory equipment equates the usual standard.*

### 6.3 CHEMICALS

<sup>13</sup> C <sub>6</sub> L-Lysine-2 HCl	#89988	Thermo Scientific, Rockford USA
<sup>13</sup> C <sub>6</sub> <sup>15</sup> N <sub>4</sub> L-Arginine-HCl	#89990	Thermo Scientific, Rockford USA
Acrylamid/N,N-Methylenbisacrylamid	#A1672	AppliChem GmbH, Darmstadt, GER
Agarose	#15510-027	Invitrogen, Carlsbad, USA
Ampicillin, soldium salt	#10460050	GERBU Biotechnik, Heidelberg, GER
AttoPhos® AP Fluorescent Substrate	# TB280	Promega, Madison, USA
blasticidin	#15205	Sigma Aldrich, St.Louis, USA
Bovine Serum Albumin, (BSA) fatty acid free	#A8806	Sigma Aldrich, St.Louis, USA
Chloramphenicol	#3886.2	Roth, Karlsruhe, GER
cOmpete protease Inhibitor, EDTA free	#11873580001	Roche, Mannheim, GER
Coomassie Brilliant Blue, G-250	#17524	Serva, Heidelberg, GER
DAKO®Fluorescent Mounting Medium	#53023	DAKO Corporation Capintaria, USA
DMSO	#20385	Serva, Heidelberg, GER
DMSO, cell culture grade	#EMR385100	Biozol, Eching, GER
DTE	#10070025	GERBU Biotechnik, Heidelberg, GER
DTT	#1008	GERBU Biotechnik, Heidelberg, GER
EDTA	#1034.1000	GERBU Biotechnik, Heidelberg, GER
Ergocalciferol	#E5750	Sigma Aldrich, St.Louis, USA
Formaldehyd	#A0877.0500	AppliChem, Darmstadt, GER
HEPES (Ultrapure)	#1009.0250	GERBU Biotechnik, Heidelberg, GER
High Capacity Neutravidin® Agarose Resin	#29202	Thermo Scientific, Rockford USA
Imidazole	#8.14223.0250	Merck, Hohenbrunn, GER
Iodacetamid	#122270250	ACROS Organics, Geer, BEL
Kanamycin sulfate	#1091	GERBU Biotechnik, Heidelberg, GER
Ketokonazole	#K1003	Sigma Aldrich, Steinheim, GER
NHS MagSepharose™	#28-9513-80	GE Healthcare, Buckinghamshire, UK
Nonfat dried milk powder	#A0830	AppliChem, Darmstadt, GER
NP-40 Alternative	#492016	Calbiochem®, Darmstadt, GER
Oleic acid	#4954	Calbiochem®, Darmstadt, GER
Oriole™ Fluorescent Gel Stain	#161-0495	BioRad, München, GER
Orlistat	#04139	Sigma Aldrich, Steinheim, GER
PBS Tablets	#AK-1029P-I	Jena BioScience, Jena, GER

PhosStop, Phosphatase Inhibitor Cocktail	#04906845001	Roche, Mannheim, GER
PIPES	#P6757	Sigma Aldrich, Steinheim, GER
Ponceau S	#P7170-1L	Sigma Aldrich, Steinheim, GER
SlimFast Schoko	#72768	SlimFast, Messel, GER
Streptavidin Magnetic Beads	#514205	NewEngland Biolabs, Frankfurt, GER
TEMED	#35925	Serva, Heidelberg, GER
TFA	#T6508	Sigma Aldrich, Steinheim, GER
TRIS	#48552.2	Roth, Karlsruhe, GER
Triton® X-100	# 39795.02	Serva, Heidelberg, GER
Tween®-20	#BP337	Fisher BioReagents®, NJ, USA
Zinc sulfate heptahydrate	#16301.1	Roth, Karlsruhe, GER

\* Further Chemicals not listed in this table where supplied from Sigma-Aldrich (Steinheim), Fluka (Neu-Ulm), Merck (Darmstadt), Riedel-de-Haen (Seelze), Roche (Mannheim), Roth (Karlsruhe) or Serva (Heidelberg).

#### 6.4 FLUOROPHORES

Alexa Fluor® 488 Phalloidin	#A12379	Life Technologies™, Darmstadt, GER
BODIPY® 493/503	#D3922	Life Technologies™, Darmstadt, GER
BODIPY® 558/568 C <sub>12</sub>	#D3835	Invitrogen™, Eugene, USA
CellTracker™ Red CMTPX	#C34552	Life Technologies™, Darmstadt, GER
DAPI	#D1306	Life Technologies™, Darmstadt, GER
ER-Tracker™ Green (BODIPY®FL glibenclamide)	#E34251	Life Technologies™, Darmstadt, GER
GelRED™	# S420	GeneOn AG, Hamburg, GER
HCS LipidTox™ Deep Red neutral Stain	#H34477	Life Technologies™, Darmstadt, GER
Hoechst 33342, Trihydrochloride	#H1399	Life Technologies™, Darmstadt, GER
LysoTracker® Red DND-99	#L7528	Life Technologies™, Darmstadt, GER
MitoTracker® Deep Red 633	#M22426	Invitrogen™, Darmstadt, GER
MitoTracker® Deep Red FM	#M22426	Life Technologies™, Darmstadt, GER
MitoTracker® Red FM	#M22425	Life Technologies™, Darmstadt, GER
NBD-Cholesterol	#N-1148	Life Technologies™, Darmstadt, GER
NHS-Flourescin	#46410	Thermo Scientific, Rockford USA
SYTOX®Green nucleic acid stain	#S7020	Life Technologies, Darmstadt, GER

## 6.5 BUFFER &amp; SOLUTIONS

## 6.5.1 Buffers in Molecular Biology

HBSS	<p>Component A:</p> <p>260 mg <math>\text{CaCl}_2 \times 6 \text{ H}_2\text{O}</math></p> <p>100 mg <math>\text{MgCl}_2 \times 6 \text{ H}_2\text{O}</math></p> <p>48 mg <math>\text{MgSO}_4</math></p> <p>400 mg KCl</p> <p>Component B:</p> <p>60 mg <math>\text{KH}_2\text{PO}_4</math></p> <p>90 mg <math>\text{K}_2\text{HPO}_4</math></p> <p>1100 mg Glucose</p> <p>* Both components are prepared separately to avoid precipitation and then mixed 1:1.</p> <p>* pH adjustment is not necessary.</p>
PBS	<p>137 mM NaCl</p> <p>2.7 mM KCl</p> <p>10 mM <math>\text{Na}_2\text{HPO}_4</math></p> <p>2.0 mM <math>\text{KH}_2\text{PO}_4</math></p> <p>pH 7.4</p>
TAE	<p>40 mM Tris/ Acetic Acid (pH 7.5)</p> <p>20 mM Na- Acetat</p> <p>1 mM EDTA</p>
TBS	<p>10 mM Tris/HCl, pH 7.4</p> <p>150 mM NaCl</p>
TBS-T	<p>10 mM Tris/HCl, pH 7.4</p> <p>150 mM NaCl</p> <p>0.1% (v/v) Triton-X100</p>

## 6.5.2 Buffers in Cell Biology

Lysis Buffer (mainly soluble Proteins)	<p>50 mM PIPES</p> <p>50 mM NaCl</p> <p>5 mM <math>\text{MgCl}_2</math></p> <p>5 mM EGTA</p> <p>0.1% (v/v) NP40</p> <p>0.1% (v/v) Triton X-100</p> <p>0.1% (v/v) Tween-20</p> <p>Protease Inhibitor Cocktail</p> <p>pH 7.4</p>
Fixation- Buffer	3.7 % Formaldehyd in PBS
HEPES Running Buffer	<p>12 g/L Tris</p> <p>23.8 g/L HEPES</p> <p>1.0 g/L SDS</p> <p>pH 8.0</p>

Oleic acid Stock solution (12.5 mM)	14 % (w/v) fatty acid free BSA 78 µL oleic acid stock in 0.1 M Tris, pH 8.3 incubation at 37°C for 1 h sterilfiltration 0.22 µm sterile filter store at 4°C
Permeabilization- Buffer	0.1% (v/v) Triton X-100 in PBS
PLA® Assay Buffer A	0.15 M NaCl 0.01 M Tris 0.05 % (v/v) Tween-20 pH 7.4 (0.22 µM filter)
PLA® Assay Buffer B	0.2 M Tris 0.1 M NaCl pH 7.5 (0.22 µM filter)
QBT- Base Buffer	10 mL HBSS Buffer (10x) 3 mL HEPES Buffer (1M) 88 mL H <sub>2</sub> O 200 mg fatty acid free BSA

### 6.5.3 Buffers and Solutions in Protein Biochemistry

Blocking Buffer	10 mM Tris 150 mM NaCl 0.05 % (v/v) Tween-20 pH 7.5  Blocking substances: 1-5% (w/v) dry milk powder, BSA or SlimFast Schoko depending on experimental setup.
Coomassie Destaining Solution	30% (v/v) methanol 10% (v/v) acetic acid
Coomassie Staining Solution	0.25% (w/v) coomassie brilliant blue G-250 45% (v/v) methanol 10% (v/v) acetic acid
Coomassie Staining Solution, colloidal	Solution A: 2% (v/v) ortho phosphoric acid 10% (w/v) ammonium sulfate Solution B: 5% (w/v) coomassie brilliant blue G-250 Mix: 78% (v/v) solution A 2% (v/v) Solution B 20% (v/v) methanol
Fixing Solution for Zink-Imidazol Stain	50% (v/v) methanol 5% (v/v) acetic acid
Imidazol-SDS Solution	0.2 M Imidazol 0.1% (w/v) SDS

NanoTemper Buffer	50 mM Tris-HCl 150 mM NaCl 10 mM MgCl <sub>2</sub> (optimal: 0.05% (v/v) Tween-20)
SDS Running Buffer (10x)	2.5 M Glycin 250 mM Tris 35 mM SDS
SDS Sample Buffer (5x)	50% (v/v) glycerol 250 mM Tris (pH 6.8) 350 mM SDS 500 mM DTE 360 µM Bromphenol blue
SDS Separating Gel (12%, 20 mL) <i>(modified from Harlow and Lane; 1988)</i>	6.60 mL H <sub>2</sub> O 8.00 mL acrylamide mix (30%) 5.00 mL Tris (1.5 M, pH 8.8) 0.20 mL SDS (10%) 0.20 mL ammonium persulfate (10%) 0.008 mL TEMED
SDS Stacking Gel (5%, 5mL ) <i>(modified from Harlow and Lane; 1988)</i>	3.40 mL H <sub>2</sub> O 0.83 mL acrylamide mix (30%) 0.63 mL Tris (1.0 M, pH 6.8) 0.05 mL SDS (10% (w/v)) 0.05 mL ammonium persulfate (10% (w/v)) 0.005 mL TEMED
Silver Developer Solution	3% (w/v) Na <sub>2</sub> CO <sub>3</sub> 0.05% formaldehyde
Silver Sensitizer Solution	0.02% (w/v) Sodium Thiosulfate
Silver Staining Solution	0.1% (w/v) AgNO <sub>3</sub>
Silver Termination Solution	0.05 M EDTA
Transfer Buffer	14.41 g/L glycin 3.03 g/L Tris 20% (v/v) MeOH
Zink Sulfate Solution	0.2 M zinc sulfate in H <sub>2</sub> O

#### 6.5.4 Buffers and Solutions in Proteomics

Block A Solution	0.5 M Ethanolamine, 0.5 M NaCl, pH 8.3
Block B Solution	0.1 M Sodium Acetate, 0.5 M NaCl, pH 4.0
IGD Alkylation Buffer	55 mM Iodacetamid in 25 mM NH <sub>4</sub> HCO <sub>3</sub>
IGD Digestion Solution	0.01 µg/mL trypsin (proteomic grade) in 25 mM NH <sub>4</sub> HCO <sub>3</sub>
IGD Reduction Buffer	50 mM DTT in 25 mM NH <sub>4</sub> HCO <sub>3</sub>
IGD Wash Solution I	25 mM NH <sub>4</sub> HCO <sub>3</sub> / Acetonitril (3:1)
IGD Wash Solution II	25 mM NH <sub>4</sub> HCO <sub>3</sub> / Acetonitril (1:1)
LYS-C Reduction/ Denaturation Buffer	8M urea in 50 mM Tris, pH 7.9

LYS-C Alkylation Buffer	50 mM chloracetamide in RD-Buffer
LysC Buffer	50 $\mu$ M Tris, pH 7.5
STAGE Elution Buffer	0.1 % (v/v) formic acid, 80% (v/v) acetonitrile in H <sub>2</sub> O
STAGE Equilibration Buffer	0.1 % (v/v) formic acid in H <sub>2</sub> O
STAGE Reducing Buffer	0.05 M iodacetamide in urea buffer [always fresh]
STAGE Urea Buffer	8 M urea in 0.1 M Tris HCl (pH 8.5), 5 $\mu$ g/mL trypsin [always fresh]

### 6.5.5 Buffers and Solutions in Enzyme Assays

AttoPhos <sup>®</sup> Stock Solution (100x) ( <i>AttoPhos<sup>®</sup> Assay</i> )	16.7 mM AttoPhos <sup>®</sup> Substrate (Promega) in water (250 $\mu$ L aliquots were stored at -20°C)
Reaction Buffer ( <i>11<math>\beta</math>-HSD Assay</i> )	400 $\mu$ M NADP <sup>+</sup> or NADPH 30 nM [3H]-labeled substrate HSD1: [1,2,6,7-3H]-cortisone (American Radiolabeled Chemicals) HSD2: [1,2,6,7-3H]-cortisol (Amersham Biosciences) 25 nM unlabeled cortisol (HSD2) or 200 $\mu$ M unlabeled cortisone (HSD1) 0-200 $\mu$ M inhibitor in TG1 buffer
Reaction Buffer ( <i>AttoPhos<sup>®</sup> Assay</i> )	25 M Bis-Tris HCL (pH 7.0) 0.1 mM MgCl <sub>2</sub> 0.1 mg/mL BSA
TG1 Buffer ( <i>11<math>\beta</math>-HSD Assay</i> )	20 mM Tris-HCl (pH7.4) 1 mM EGTA 1 mM MgCl <sub>2</sub> 100 mM NaCl 20% (v/v) glycerol

## 6.6 MEDIA

### 6.6.1 Mammalian Cell Culture Medium

Dexamethasone	D4902-25MG	Sigma Aldrich, Steinheim, GER
DMEM (high glucose)	#P04-03550	PAN BioTech, Aidenbach, GER
DMEM/ F12 (1:1) for SILAC	#88215	Thermo Scientific, Schwerte, GER
DMEM/F12 (1:1)	#P04-41250	PAN BioTech, Aidenbach, GER
Fetal bovine serum (FBS) (Lot 441F1615K)	#10270	GIBCO-Invitrogen, Darmstadt, GER
Insulin-Transferrin-Selenium Stock	#11074547001	Roche, Mannheim, GER
Leibovitz's-L15	#E15-821	PAA, Pasching, AUT
McCoy's 35A	#P04-05500	PAN BioTech, Aidenbach, GER
MEM-NEAA (100x)	#P08-32100	PAN BioTech, Aidenbach, GER
PMA	#P8139	Sigma Aldrich, Steinheim, GER
Penicillin- Streptomycin Solution	#P06-07100	PAN BioTech, Aidenbach, GER
RPMI-1640	#P04-16500	PAN BioTech, Aidenbach, GER
Sodium Pyruvate	#P04-43100	PAN BioTech, Aidenbach, GER

## 6.6.2 Preadipocyte Differentiation Medium

PM-1 (Preadipocyte Differentiation Medium)	# PM-1-L1	Zen-Bio Inc, N Carolina, USA
DM-2 (Differentiation Medium)	# DM-2-L1	Zen-Bio Inc, N Carolina, USA
AM-1 (Adipocyte Medium)	# AM-1-L1	Zen-Bio Inc, N Carolina, USA

## 6.6.3 Insect Cell Culture Medium

Fetal bovine serum (FBS), for Insect culture	# 10270	PAN BioTech, Aidenbach, GER
Penicillin- Streptomycin Solution	#P06-07100	PAN BioTech, Aidenbach, GER
Schneiders Medium	#217720-024	GIBCO-Invitrogen, Darmstadt, GER
Schneiders Medium	#P04-91500	PAN BioTech, Aidenbach, GER

\* Charge (P120909) of the FBS is important for sufficient cell growth

## 6.6.4 Bacterial Culture Medium

LB Medium	0.5% (w/v) yeast extract 1% (w/v) tryptone 0.5% (w/v) NaCl
-----------	--

LB Agar Plates	0.5% (w/v) yeast extract 1% (w/v) tryptone 0.5% (w/v) NaCl 1.5% (w/v) agar
----------------	---

## 6.6.5 Drosophila Fly Food

Complex Drosophila Food <i>(by the department of Prof. Klein, Uni Düsseldorf)</i>	0.5% (w/v) agar-agar 7.1% (w/v) corn grain 0.95% (w/v) soy flour 1.68% (w/v) dry yeast 4% (w/v) treacle 4.5% (w/v) malt extract 1.5% (v/v) nipagin (10% in ethanol) 4.5% (v/v) propionic acid
--	--

HFD Drosophila Food	0.624% (w/v) agar agar 8.0% (w/v) polenta 1.0% (w/v) soy flour 1.8% (w/v) dried yeast 2.2% (w/v) treacle 1.5% (w/v) malt extract 1.5% (v/v) nipagin solution (10% in ethanol) 0.63% (v/v) propionic acid 10% (w/v) coconut oil
---------------------	--



## 6.7 ORGANISMS

## 6.7.1 Mammalian Cell Lines

Cell line	Organism	Organ	Morphology	Medium
3T3-L1	<i>Mus musculus</i>	embryo	fibroblast	DMEM+ 10% (v/v) FBS DMEM/F12+ 10% (v/v) FBS 0.005 mg/ml insulin 0.005 mg/ml transferrin
AML12	<i>Mus musculus</i>	liver	hepatocyte	5 ng/ml selenium 40 ng/ml dexamethasone NO further NAA, SP
CaCo-2	<i>Homo sapiens</i>	colon	epithelial	DMEM+ 10% (v/v) FBS
CHO	<i>Cricetulus griseus</i>	ovary	epithelial-like	F12 + 10% (v/v) FBS
COS7	<i>Cercopithecus aethiops</i>	kidney	fibroblast	DMEM+ 10% (v/v) FBS
HCT116	<i>Homo sapiens</i>	colon	epithelial	DMEM+ 10% (v/v) FBS
HEK293	<i>Homo sapiens</i>	embr. Kidney	epithelial	DMEM+ 10% (v/v) FBS
HeLa	<i>Homo sapiens</i>	Cervix	epithelial	DMEM+ 10% (v/v) FBS
HT29	<i>Homo sapiens</i>	Colon	epithelial	DMEM+ 10% (v/v) FBS
MDCK	<i>Canis familiaris</i>	kidney	epithelial-like	DMEM+ 10% (v/v) FBS
SW872	<i>Homo sapiens</i>	liposarcoma	fibroblast	Leibovitz + 10% (v/v) FBS
THP-1	<i>Homo sapiens</i>	periph. Blood	monocyte	RPMI-1640+ 10% (v/v) FBS
U2-OS	<i>Homo sapiens</i>	bone	epithelial	McCoy's + 10% (v/v) FBS

\* all media contain Penicillin (1000 U/mL) and Streptomycin (1 mg/mL).

\*\* if not differently declared the mammalian cell culture media contain non-essential amino acids (NAA, 1x) and sodium pyruvate (SP, 1mM/mL) as additional additives.

\*\*\* DMEM medium contains high glucose levels (4.5 g/L)

## 6.7.2 Insect Cell Lines

Cell line	Organism	Specificity	Reference & Source	Medium
DGRC S3	<i>Drosophila melanogaster</i>	late embryonic cell line generated shortly before hatching	(Affleck & Walker, 2008), obtained by Dr. M. Beller via DGRC	Schneiders Medium+ 10% (v/v) FBS
ML-DmBG3-c2	<i>Drosophila melanogaster</i>	L3 larvae with neuronal characteristics	(Ui et al, 1994) obtained by Dr. M. Beller via DGRC	Schneiders Medium+ 10% (v/v) FBS
Kc167	<i>Drosophila melanogaster</i>	embryonic cell line with plasmatocyte like expression profile	(Cherbas et al, 2011). obtained by Dr. M. Beller	Schneiders Medium+ 10% (v/v) FBS

\* all media contain Penicillin (1000 U/mL) and Streptomycin (1 mg/mL)

\*\* charge (P120909) of the FBS is important for sufficient cell growth

\*\*\* detailed information of the respective cell lines at flybase.org

## 6.7.3 Bacterial Strains

Omnimax™ 2 T1	F' {proAB lacIq lacZΔM15 Tn10(TetR) Δ(ccdAB)} mcrA Δ(mrr hsdRMS-mcrBC) Φ 80(lacZ)ΔM15 Δ(lacZYA-argF)U169 endA1 recA1 supE44 thi-1 gyrA96 relA1 tonA panD
BL21-DE3	fhuA2 [lon] ompT gal (λ DE3) *dcm+ ΔhsdS λ DE3 = λ sBamHI ΔecoRI-B int1::PlacUV5::T7 gene1) i21 Δnin5

## 6.7.4 Drosophila Fly Strains

Name	Internal Stock ID	Genotype	Referenz
<i>w-</i>	65	<i>w[1118]</i>	DGRC RNAi library
<i>Actin5C</i>	75	<i>actin5C-Gal4 / CyO, ftz lacZ</i>	obtained from Dr.Ralf Pflanz
<i>Lsd-2</i>	125	<i>Lsd-2[51] / FM7i</i>	Beller et al., 2010
<i>Mdy</i>	62	<i>w*; mdy[QX25] cn[1] bw[1] / CyO float. (Chromosome 1;2)</i>	Bloomington Drosophila Stock Center

## 6.8 ENZYMES

Trypsin recombinant, Proteomics Grade	#03708969001	Roche Diagnostics, Mannheim, GER
Trypsin EDTA (1%)	#P10-023100	PAN BioTech, Aidenbach, GER
Lys-C Protease, MS Grade	#90051	Thermo Scientific, Schwerte, GER
<i>Pfu</i> DNA Polymerase (recombinant)	# EP0501	Thermo Scientific, Schwerte, GER
Restriction enzymes	# various	Fermentas, St. Leon-Rot, USA

## 6.9 PROTEINS

MAPK9 Protein (human, recombinant)	#H00005601-P01	Abnova, Taiwan, TW
Hmgcl Protein (human, recombinant)	#H00003155-P01	Abnova, Taiwan, TW
DCK Protein (human, recombinant)	#H00001633-P01	Abnova, Taiwan, TW
EPHX2 Protein (mouse, recombinant)	#10011670	Cayman Chemicals, MI, USA
EPHX2 Protein (human, recombinant)	#H00002053-P01	Abnova, Taiwan, TW
SPR Protein (human, recombinant)	#228-11455-2	RayBiotech, Norcross, GA
NT5DC1 Protein (human, recombinant)	#H00221294-P01	Abnova, Taiwan, TW

## 6.10 ANTIBODIES

## 6.10.1 Primary Antibodies

Antibody	Origin	Number	Manufacturer
Anti-ABAD/HADH2	goat	#6598P1	OriGene Technologies, Rockville, USA
Anti- SPR	rabbit	#HPA039505	Atlas Antibody, Stockholm, SE
Anti- DCK2	rabbit	#PA5-21846	Thermo Scientific, Rockford, USA
Anti- EPOX2	rabbit	#HPA023779	Sigma Aldrich, Steinheim, GER
Anti- JNK 172/3	rabbit	#NBP1-19873	Novus Biologicals, Oakville, CA
Anti-GFP	mouse	# G6795	Sigma Aldrich, Steinheim, GER
Anti-DGAT1	rabbit	#ab54037	Abcam®, Cambridge, USA
Anti-DDK	mouse	#TA50011	OriGene Technologies, Rockville, USA
Anti-Tubulin	mouse	# F2168	Sigma Aldrich, Steinheim, GER
Anti-GAPDH	rabbit	# G9545	Sigma Aldrich, Steinheim, GER
Anti-GaPDH	mouse	# G8795	Sigma Aldrich, Steinheim, GER
Anti-HMGCL	rabbit	#GTX109096	GeneTex, Irvine, USA
Anti-NT5DC1	rabbit	#HPA030352	Sigma Aldrich, Steinheim, GER
Anti-FITC	rabbit	# 711900	Invitrogen™, Darmstadt, GER
Anti-FlagTag	rabbit	# 2368	CellSignaling Technology®, Danvers, USA
Anti-FITC	rabbit	# 711900	Invitrogen™, Darmstadt, GER
Anti-FITC (F4)	mouse	# sc-65218	Santa Cruz Biotechnology, Dallas, USA

## 6.10.2 Secondary Antibodies

Antibody	Reactivity	Number	Manufacturer
PLA®Anti-Mouse MINUS	mouse	#DUO92004	Sigma Aldrich, Steinheim, GER
PLA®Anti-Rabbit PLUS	rabbit	# DUO92002	Sigma Aldrich, Steinheim, GER
Anti-Goat-HRP	goat	#sc-2033	Santa Cruz Biotechnology, Dallas, USA
Anti-mouse-Alexa594	mouse	# A11005	Invitrogen™, Darmstadt, GER
Anti-goat-Alexa594	rabbit	# A11012	Invitrogen™, Darmstadt, GER

## 6.11 KITS &amp; STANDARDS

## 6.11.1 Commercial Kits

BCA Assay Kit	# 23227	Pierce, Schwerte, GER
Bradford Assay Dye Reagent Concentrate	#500-0006	BIORad, München, GER
CellTiter-Glo® Luminescent Viability Assay	#G7571	Promgea, Madison, USA
Duolink® In Situ Detection Reagents Orange	# DUO92007	Sigma Aldrich, Steinheim, GER
Effectene Transfection Reagent	# 301425	Qiagen, Hilden, GER
FuGENE® 6 Transfection Reagenz	#E2691	Promgea, Madison, USA
Infintiny Triglyceride Kit	# TR-22421	Thermo Fisher Scientific, Schwerte, GER
Isocitrate Dehydrogenase Activity Assay Kit	# K756-100	BioVision, San Francisco, USA
MEGAscript® T7 Transcription Kit	#AM1333	Invitrogen™, Darmstadt, GER
MitoPT® TMRE Assay Kit	#9102	Immunochemistry Technologies, USA
MycoAlert™ Mycoplasma Detection Kit	#LT07-318	Lonza, Basel, CH
Pierce™ BCA™ Protein Assay	# PI-23221	Thermo Fisher Scientific, Schwerte, GER
Pyruvate Kinase Activity Assay Kit	# K709-100	BioVision, San Francisco, USA
QBT™ Fatty Acid Uptake Assay Kit	# R8132	Molecular Devices, Sunnyvale, USA
Qiagen® Plasmid Mini Purification Kit	#12125	Qiagen, Hilden, GER
QIAquick® Gel Extraction Kit	#28704	Qiagen, Hilden, GER
QIAquick® PCR Purification Kit	#28104	Qiagen, Hilden, GER
QuantiFast SYBR® Green PCR Kit	# 204054	Qiagen, Hilden, GER
QuantiTect Reverse Transcription Kit	#205311	Qiagen, Hilden, GER
Rneasy Mini Kit	#74104	Qiagen, Hilden, GER
Soluble Epoxide Hydrolase Cell-Based Assay	# 600090	Cayman Chemicals, MI, USA
SuperSignal® West, Femto	#34096	Thermo Fisher Scientific, Schwerte, GER
SuperSignal® West, Pico	#1859674	Thermo Fisher Scientific, Schwerte, GER
Triglyceride assay kit	#TG-1-NC	ZenBio, Raleigh, USA

## 6.11.2 Protein and DNA Standards

GeneRuler™ 1 kb DNA Ladder	#SM0312	Thermo Fisher Scientific, Schwerte, GER
GeneRuler™ 100 bp DNA Ladder plus	# SM0321	Thermo Fisher Scientific, Schwerte, GER
PageRuler™ Plus Prestained Protein Ladder	# 26619	Thermo Fisher Scientific, Schwerte, GER
PageRuler™ Unstained Protein Ladder	# 26614	Thermo Fisher Scientific, Schwerte, GER

## 6.12 OLIGONUCLEOTIDES

## 6.12.1 Sequencing

T7 kurz	AAT ACG ACT CAC TAT AGG
T7 terminator	GCT AGT TAT TGC TCA GCG G
SP6	GAT TTA GGT GAC ACT ATA G
T3	AAT TAA CCC TCA CTA AAG GG

## 6.12.2 RNA Interference

Protein	Organism	Chemotype	DRSC		ID	Sequence	size [bp]
ACT1	<i>Drosophila</i>	Chemotype 1	DRSC25024	FWD	CG4027	gtaatacgactcactataggTGTGACGAAGAAGTTGCTGC	170
	<i>Drosophila</i>	Chemotype 1	DRSC25024	REV	CG4027	gtaatacgactcactataggTCATCACCCACGTACGAGTC	
ACT1	<i>Drosophila</i>	Chemotype 1	DRSC17723	FWD	CG4027	gtaatacgactcactataggGAGGCCCCGCTGAACC	500
	<i>Drosophila</i>	Chemotype 1	DRSC17723	REV	CG4027	gtaatacgactcactataggCCGCAAGCTCCATTCC	
DCK	<i>Drosophila</i>	Chemotype 1	DRSC29240	FWD	CG5452	gtaatacgactcactataggTCCAGCGTATTGTACATGCC	345
	<i>Drosophila</i>	Chemotype 1	DRSC29240	REV	CG5452	gtaatacgactcactataggAAGAACGACATTTGCTGCT	
DCK	<i>Drosophila</i>	Chemotype 1	DRSC41562	FWD	CG5452	gtaatacgactcactataggAGGTGCCTTGCCTTTAAACAT	251
	<i>Drosophila</i>	Chemotype 1	DRSC41562	REV	CG5452	gtaatacgactcactataggGGGTCGCCAGATAAACCATTA	
EPHX2	<i>Drosophila</i>	Chemotype 1	DRSC06530	FWD	CG15102	gtaatacgactcactataggGGAATGAGTTGGTACATAA	515
	<i>Drosophila</i>	Chemotype 1	DRSC06530	REV	CG15102	gtaatacgactcactataggCAAAAAGTGGATTCGGTGTG	
EPHX2	<i>Drosophila</i>	Chemotype 1	DRSC25496	FWD	CG15102	gtaatacgactcactataggGGATTCATGCCAACGAAC	372
	<i>Drosophila</i>	Chemotype 1	DRSC25496	REV	CG15102	gtaatacgactcactataggGTGGTCAGGAGAGGGATGAA	
HCS2	<i>Drosophila</i>	Chemotype 1	DRSC27026	FWD	CG7113	gtaatacgactcactataggCAGGTTCAATGTGATCCGTC	442
	<i>Drosophila</i>	Chemotype 1	DRSC27026	REV	CG7113	gtaatacgactcactataggCAGGTCCAAGACAGTGCTCA	
HCS2	<i>Drosophila</i>	Chemotype 1	DRSC20369	FWD	CG7113	gtaatacgactcactataggACGAGGTGCCAAGGAG	484
	<i>Drosophila</i>	Chemotype 1	DRSC20369	REV	CG7113	gtaatacgactcactataggAGGGCGGCCAGCATAG	
IDH3A	<i>Drosophila</i>	Chemotype 1	DRSC28303	FWD	CG12233	gtaatacgactcactataggGCCAGAAAGTCCCAGAAAT	207
	<i>Drosophila</i>	Chemotype 1	DRSC28303	REV	CG12233	gtaatacgactcactataggGCCACATGTGACAGAGAAAT	
IDH3A	<i>Drosophila</i>	Chemotype 1	DRSC19446	FWD	CG12233	gtaatacgactcactataggAAGTTCGGCATCCACAG	380
	<i>Drosophila</i>	Chemotype 1	DRSC19446	REV	CG12233	gtaatacgactcactataggATGTTGCGCTTGTGCACC	
MAPK9	<i>Drosophila</i>	Chemotype 1	DRSC03499	FWD	CG5680	gtaatacgactcactataggTTCCTCAGCATCATACCA	271
	<i>Drosophila</i>	Chemotype 1	DRSC03499	REV	CG5680	gtaatacgactcactataggATTAGGTACACCATCACCCCTC	
MAPK9	<i>Drosophila</i>	Chemotype 1	DRSC36595	FWD	CG5680	gtaatacgactcactataggAAATGTAACCCATGCCAAGC	473
	<i>Drosophila</i>	Chemotype 1	DRSC36595	REV	CG5680	gtaatacgactcactataggTTTAGAGTGACAGTCCGCTT	
NT5DC1	<i>Drosophila</i>	Chemotype 1	DRSC08561	FWD	CG2277	gtaatacgactcactataggTTGCCTTGCAGTAGACC	500
	<i>Drosophila</i>	Chemotype 1	DRSC08561	REV	CG2277	gtaatacgactcactataggCGCTCGCTATTGGATTACT	
KPYK	<i>Drosophila</i>	Chemotype 1	DRSC20372	FWD	CG7070	gtaatacgactcactataggGATTGCGTCATGTTGTCTGG	336
	<i>Drosophila</i>	Chemotype 1	DRSC20372	REV	CG7070	gtaatacgactcactataggCAGTCCACGGTAGAGATGGG	
KPYK	<i>Drosophila</i>	Chemotype 1	DRSC16806	FWD	CG7070	gtaatacgactcactataggACGGTCTGATCTCACTGATT	515
	<i>Drosophila</i>	Chemotype 1	DRSC16806	REV	CG7070	gtaatacgactcactataggGGCCACATCAGAGATCTCA	
scully	<i>Drosophila</i>	Chemotype 1	DRSC15718	FWD	CG5112	gtaatacgactcactataggGGTGAACAAGTGGATTGAGTC	503
	<i>Drosophila</i>	Chemotype 1	DRSC15718	REV	CG5112	gtaatacgactcactataggGCACGTCCTTCCACTCA	

## 6.12.3 Quantitative PCR

Target		Orientation	Sequence
ADIPONECTIN	<i>human</i>	FWD	GGTGAGAAGGGTGAGAAAGGA
	<i>human</i>	REV	TTTCACCGATGTCTCCCTTAG
ADIPQ	<i>mouse</i>	FWD	ATCTGACGACACCAAAAGGGCT
	<i>mouse</i>	REV	CTCCTTCTGCCAGGGGTT
CEPBA	<i>mouse</i>	FWD	TGGAACAGCTGAGCCGTGAA
	<i>mouse</i>	REV	CGAGTCCGGCTCAGAGGAAG
CEPBA	<i>human</i>	FWD	AGTTCCTGGCCGACCTGT
	<i>human</i>	REV	CCCGGGTAGTCAAAGTCG
DCK	<i>mouse</i>	FWD	CGACCCGAGTCGTGCAA
	<i>mouse</i>	REV	GATGGCTCGAATATGCTGCT
DGAT1	<i>mouse</i>	FWD	TCGTGGTATCCTGAATTGGTG
	<i>mouse</i>	REV	AGGTTCTCTAAAATAACCTTGCATT
DGAT1	<i>human</i>	FWD	GCTGTGGTCTTACTGTTGAGTC
	<i>human</i>	REV	GGTAGGAGAAGAGCTTGAGGAAG
DGAT2	<i>mouse</i>	FWD	GGCGTACTTCCGAGACTAC
	<i>mouse</i>	REV	TGGTCAGCAGGTTGTGTGTC
DGAT2	<i>human</i>	FWD	TACAGCAGGTGATCTTTGAGG
	<i>human</i>	REV	GGCGAAACCAATATACTTCTG

EPHX2	<i>mouse</i>	FWD	CCCGGCTACGGATGGTCTC
	<i>mouse</i>	REV	TCCCACTCGGAGCATCAGGT
FABP4	<i>mouse</i>	FWD	TGAAAGAAGTGGGAGTGGGCT
	<i>mouse</i>	REV	GCCCCGCCATCTAGGGTTAT
GAPDH	<i>mouse</i>	FWD	TGGAGGACAAATCCCCCTGT
	<i>mouse</i>	REV	CGGGAAGGCAGGGTATCAGG
GLUT4	<i>mouse</i>	FWD	TTCACGTTGGTCTCGGTGCT
	<i>mouse</i>	REV	TAGTCTATGGCTGGAACCCG
GLUT4	<i>human</i>	FWD	CTGTGCCATCCTGATGACTG
	<i>human</i>	REV	CGTAGCTCATGGCTGGAAC
KPYK	<i>mouse</i>	FWD	TTGCGTGTGCAGTTGCAAGA
	<i>mouse</i>	REV	TTGGGGTACTTCTGTTGGGCTTC
LPL	<i>mouse</i>	FWD	GGATCCGAGTGAAAGCCGGA
	<i>mouse</i>	REV	TGTCCAGTGTACCCAGACTT
NT5DC1	<i>mouse</i>	FWD	TCTGCAGAAGGGCCTGTTCC
	<i>mouse</i>	REV	CGCTTAGTAGACGGGTGCCA
PDXK	<i>mouse</i>	FWD	CCACGAAAAGAAGCAGCGAA
	<i>mouse</i>	REV	CAGCAGCTGCAGTGGATAGG
PPARY	<i>mouse</i>	FWD	GTGCCTTCGCTGATGCACTG
	<i>mouse</i>	REV	ATCGCACTTGGTATTCTTGAGC
SCULLY	<i>mouse</i>	FWD	CGCACATACGGTCACACTGC
	<i>mouse</i>	REV	CCAGGGAAACGGCGTTCTTG
SPR	<i>mouse</i>	FWD	CCATGGTGACGCTTCTGGGA
	<i>mouse</i>	REV	CCTCCGTTTTGGCCGTTTCC
THREAD	<i>mouse</i>	FWD	TCGTCAAATCTAACGCAACGG
	<i>mouse</i>	REV	CTGAAGTCGAAACTTGACGGCT
UCP1	<i>human</i>	FWD	TGCCCAACTGTGCAATGAA
	<i>human</i>	REV	TCGCAAGAAGGAAGTACCAA
UCP1	<i>mouse</i>	FWD	CCTGCCTCTCTCGAAACAA
	<i>mouse</i>	REV	TGTAGGCTGCCCAATGAACA

\*\*\* all primers were designed with the NCBI primer design freeware (<http://www.ncbi.nlm.nih.gov/tools/primer-blast/>). Primers ideally span an exon junction and have a melting temperature around 60°C.

### 6.13 PLASMIDS

mCherry-DCK	pOPIN(n)Cherry	Provided by DPF (Campain 91-62)
mCherry-SPR	pOPIN(n)Cherry	Provided by DPF (Campain 91-66)
mDGAT1-His	pCDNA/ HisMaxC	Provided by Dr. Thomas O. Eichmann, University of Graz
mDGAT2-His	pCDNA/ HisMaxC	Provided by Dr. Thomas O. Eichmann, University of Graz

### 6.14 SOFTWARE

CellProfiler	Version 2.0.0	CellProfiler & Broad Institute
EnsoChemLab	Version 5.0.1	enso Software GmbH, Erbach, Germany
Fiji- ImageJ	Version 2.0.0	Imagej open-source platform
Image Studio™	Version 2.0	LI-COR Biosciences GmbH, B.H., Germany
iQ5™ Optical Systems Software	Version 2.0	Optical System Software,
KODAK MI Imaging Software	Version 4.05	KODAK, Rochester, USA
MaxQuant	Version 1.4.1.2	MaxQuant; Cox & Mann, 2008
MetaMorph Offline	Version 7.7.0.0	Molecular Devices, Biberach, Germany
MetaXpress	Version 5.0.0.26	Molecular Devices, Biberach, Germany
NT Control Software	Version 2.0.1.26	NanoTemper Tech., Munich, GER
Perseus	Version 1.5.0.31	MaxQuant; <a href="http://www.perseus-framework.org">www.perseus-framework.org</a>
RTCA Data Analysis Software	Version 1.0.0.1304	ACEA Biosciences Inc, San Diego, USA
Tecan i-control	Version 3.4.2.0	Tecan AG, Männedorf, CH

## CHAPTER 7: METHODS

### 7.1 METHODS IN MOLECULAR BIOLOGY

#### 7.1.1 Cultivation of Bacteria

*Escherichia coli* was grown and stored following standard procedures as described in (Ausubel, 1995). If not described otherwise, Luria Broth (LB) media (see Chapter 6.6) was used as standard cultivation medium. It was sterilized by autoclaving (121°C, 20 min). Afterwards, the required antibiotics were added by syringe sterile filtration (0.2 µm), reaching final concentrations of 0.1 mg/mL ampicillin and chloramphenicol or a final concentration of 0.05 mg/mL kanamycin. Bacteria were grown in an incubation shaker (INFORS HT) at 37°C at 220rpm.

#### 7.1.2 Storage of Bacteria

Glycerol cultures of the respective *E.coli* strains were used for long term storage. Therefore, the (transformed) bacteria containing the plasmid of interest were plated on LB media plates containing the respective antibiotic as a selection marker. After overnight incubation at 37°C one part of the bacterial solution was mixed with an equal part of sterile glycerol (final concentration 50%). The glycerol samples were subsequently stored at -80°C.

#### 7.1.3 Heat Shock Transformation of Bacteria

The heat shock protocol for introducing pDNA into *E.coli* (Hanahan, 1983) was standardly used. Isolated pDNA (100 ng) was mixed with competent OmiMAX™ *E.coli* cells (100 µL) and was incubated on ice for 20 min. The heat shock was done in a water bath at 42°C for 90 s. The cells were subsequently cooled for another 2 min on ice, before adding pre-warmed LB media (final 1 mL). An additional cultivation step in selection marker free LB media at 37°C for 1h allowed bacterial recovery. The cell suspension was then plated on LB-Agar plates including the appropriate selection markers (ampicillin 0.1 mg/ mL; kanamycin 0.05 mg/mL) for an overnight cultivation.

#### 7.1.4 Plasmid DNA Isolation from Bacteria

For standard procedures pDNA was isolated from *E.coli* using the QIAprep® Spin Miniprep Kit according to manufacturer's advices. The pDNA intended for transfections of mammalian cells was purified by the QIAfilter® Plasmid Midi/Maxi Kit (Qiagen), respectively.

### 7.1.5 Determination of DNA and RNA Concentration

DsDNA, dsRNA as well as ssRNA concentrations were estimated by measuring the absorbance of samples diluted in (RNase free) H<sub>2</sub>O at 260 nm using the NanoDrop 2000c UV-Vis Spectrophotometer (Thermo Scientific). A linear correlation of nucleic acid and absorbance following Lambert-Beer law was assumed:  $A_{260} = 1.0$  is equivalent to 50 µg/mL dsRNA and dsDNA, while a concentration of 40 µg/mL is estimated for RNA (Barbas et al, 2007).

The quality of the nucleotide samples was estimated by the  $A_{260/280}$  ratios and should range around 1.8 for pure DNA and for 2.0 for RNA.

### 7.1.6 pDNA and dsRNA Verification via Agarose Gel Electrophoresis

The specificity of the total plasmid size, plasmid fragment size after restriction, the size of PCR amplicates or the size of synthesized dsRNA were estimated via agarose gel electrophoresis. DNA was separated in 1% agarose gels supplemented with 0.00001% GelRED™ (v/v) in TAE buffer (40 mM Tris/ acetic acid (pH 7.5), 20 mM sodium acetate, 1 mM EDTA) using a horizontal agarose gelectrophoresis system (BioRad). The samples were mixed with loading buffer (6x Loading Dye orange, Fermentas) in an appropriate dilution and was separated at 100V for 45-60 min. The gel was evaluated using the GelLogic200 imaging system (KODAK) and KODAK-Mi Software for analysis. The final size was estimated with help of the Gene Ruler 1 kb DNA ladders (Fermentas).

### 7.1.7 Plasmid Verification by Sequencing

Plasmid fragments were routinely checked for mutations by sequencing. This was performed by StarSEQ with the V-mix\* approach (<http://www.starseq.com/>) using T6 or Sp6 primers respectively.



## 7.2 METHODS IN CELL BIOLOGY

### 7.2.1 Mammalian Cell Culture

Culturing mammalian cells requires the utmost accordance to principles established for sterile working routine in order to protect the samples of bacterial or fungal contaminations. This implicates that only sterile equipment, media and solutions were used in a sterile environment using the cell culture approved work benches equipped with the correct air flow and appropriate HEPA filters. Additionally, all media contained penicillin (1000 U/mL) and streptomycin (1 mg/mL). All cell culture strains used were approved for safety class S1.

The generated waste (solid and liquid) was collected and sterilized by autoclaving (121°C, 20 min).

#### 7.2.1.1 Handling cryo-conserved Probes (thawing & freezing)

In order to thaw aliquots of mammalian cells from long term liquid nitrogen storage, the vial containing the cells was shortly put into a 37°C water bath under constant agitation. In order to minimize the DMSO toxicity of the storage medium, the cells were immediately diluted in 10 mL of the respective cultivation medium containing 10% (v/v) FBS and all required additives. The cells were then pelleted (5min, 800 rpm) and again resuspended in fresh culture medium. This cell suspension was then transferred to a 25 cm<sup>2</sup> culture vessel and was cultured at 37°C and 5% CO<sub>2</sub> if not mentioned otherwise. After max. 24 h the non-adherent cells were removed by media exchange. Depending on the cell line, a defined number of passages had to pass before the cells grew with a stable doubling time.

If a cell line was aimed to be conserved by cryo conservation, the cells (80% confluency, 75 cm<sup>2</sup> tissue culture flask) were detached either by trypsination (see 7.2.1.2) or by mechanical force (pipetting, cell scraping) to get a homogeneous solution. The cells number was determined (see 7.2.1.3) and the respective number of cells (usually 1.0x 10<sup>6</sup> mammalian cells or 1-2x 10<sup>7</sup> *Drosophila* cells per kryo vial) was resuspended after centrifugation (5 min, 1000 rpm) in culture medium containing an increased percentage of FBS (according to ATCC recommendations) and DMSO (10% (v/v)). The freezing occurred in a specialized freezing device ("Mr. Frosty", Thermo Fisher Scientific), which guaranteed a controlled temperature decrease of -1°C per minute. The vessel is first placed at -20°C for 30 min and was then moved to -70°C overnight, before the vials were transferred to the vaporous phase of the liquid nitrogen tank for long term storage.

### 7.2.1.2 Passaging mammalian Cells

Depending on the cell line, the cells were passaged after reaching a confluency of 75- 90%. Usual dilution rates ranged from 1:5 to 1:20. Detachment was induced by tryptic digestion. Therefore, cells were washed in pre-warmed PBS and incubated with Trypsin/EDTA (1 mL) for 1-5 min. The tryptic digest was stopped by addition of fresh, FBS containing culture medium. The cell number was counted and the desired cell number was transferred to a new culture vessel containing the respective culture medium including FBS and all additional additives (see Chapter 6.6.1).

If tryptic digestion for detachment was not applicable, Cell Dissociation Solution (Sigma Aldrich) or mechanical force by cell scraping were used.

### 7.2.1.3 Determining the Cell Number

The cell number was traditionally determined using the Neubauer Counting Slide. The cover slip was moistened and pressed to the racks of the normalized Neubauer slide. A 1:10 dilution of cells was injected and the number of the quadrants was counted, averaged and multiplied with the respective chamber factor (here  $1 \times 10^4$ ) and dilution factor (here 10).

Alternatively, an automated counting device (Countess™, Invitrogen™) was used according to the manufacturer's instructions. This device was not applicable for determining the number of insect cells, since the cell dimensions were below the instruments size recognition thresholds.

For determination of cell viability, the cells were mixed with an equal amount of Trypan Blue staining solution. Considering the additional dilution factor, the cell number was determined by the methods described above. Live cells with intact cell membranes remain colorless, while dead and apoptotic cells are colored blue. The percentage of viable cells was agreed to be above 90% for experimental conduction in order to rule out cell stress dependent artefacts in cell based assays or a decrease in growth rate during sub-cultivation.

### 7.2.1.4 Routine Check for Mycoplasma Contaminations in Cell Culture

Since mycoplasma contaminations are fast spreading and might have a severe impact on the assay credibility, all cultured cells were routinely checked for mycoplasma contaminations using the MycoAlert™ Kit (Lonza) according to manufacturer's descriptions. Therefore media of highly confluent cells (> 80%) was used for the luminescence- based assay.

In order to keep the mycoplasma contamination risk low, benches and equipment were routinely cleaned with Mycoplasma-ExSpray (PromoKine).

### 7.2.2 Insect Cell Culture

The *Drosophila* cell lines (see 6.7.2) were routinely cultivated in 25 cm<sup>2</sup> cell culture vessels at 25°C without the need of CO<sub>2</sub> regulation. Either Gibco or PAA provided the required Schneider's medium, which was supplemented with heat inactivated (30 min, 56°C), 10% FBS (v/v) and penicillin (100 U/mL) and streptomycin (100 µg/mL).

Since the *Drosophila* cell lines used (S3, Kc167) were only weakly adherent trypsination was not required. Cell detachment was performed solely by weak shear forces by pipetting or if necessary by cell scraping. The cells were passaged into a fresh culture vessel when a confluency of 90-95% was reached. Experiments were performed with cells in passages 6- 45. Cells increasing this passages showed aberrant growth behavior.

### 7.2.3 Generation of Cell Lysates

Total soluble protein lysate of (treated) cell culture cells was generated from cells reaching 90- 95% confluency. Cells were washed twice with ice cold PBS and were then detached by trypsin. The cell pellet (5 min, 1200 rpm) was washed again with PBS in order to remove the remaining trypsin (5min, 1200 rpm) and was then resuspended in lysis buffer (50 mM PIPES, 50 mM NaCl, 5 mM MgCl<sub>2</sub>, 5 mM EGTA, 0.1% (v/v) NP40, 0.1% (v/v) Triton X-100, 0.1% (v/v) Tween-20, protease inhibitor, pH 7.4). The mixture was incubated on ice for 40 min to allow sufficient levels of membrane permeabilization. Additionally, mechanical shear forces for additional cell lysis were generated by pressing the lysate ten times threw a small diameter needle. Subsequently, cell debris was removed by centrifugation (20 min, 12.000 rpm, 4°C). The total protein count of the supernatant was determined according to the Bradford protein assay. Samples were subsequently snap frozen in liquid nitrogen or constantly kept on ice for consecutive experiments. Lysates were stored long-term at -80°C.

Total lysates which contain membrane fractions were generated by direct lysis of washed cell culture cells in SDS-sample loading buffer (50% (v/v) glycerol, 250 mM Tris (pH 6.8), 350 mM SDS, 500 mM DTE and 360 µM bromphenol blue). For normalization the initial cell count was consulted, since standard protein concentration methods are not applicable at strong denaturation conditions.

#### 7.2.4 Transfection of Mammalian and Insect Cells

In order to temporarily introduce plasmid DNA into mammalian and *Drosophila* cells FuGENE® 6 reagent (Promega) was used. Therefore, cells were seeded into well plates. After an adaption phase (minimum 6 h; usually overnight) in the respective medium, the cells was treated with a reagent mixture according to the manufacturer's instructions (see Table 10).

Cells were fixed (see 7.2.8.1) or lysed (see 7.2.3) after 48- 64 h. The cells were fed with 400  $\mu\text{M}$  oleic acid after 24 h if LD formation was of interest.

**TABLE 10: FuGene® 6 Instructions** regarding reagent and pDNA concentrations for mammalian and insect cell transfection.

Well number	FuGENE® reagent/ well volume (advised range)	DNA/ well Used (advised range)	Total Volume
96	0.5 $\mu\text{L}$ (0.15-0.6 $\mu\text{L}$ )	0.2 $\mu\text{g}$ (0.04-0.2 $\mu\text{g}$ )	7.5 $\mu\text{L}$ (2- 10 $\mu\text{L}$ )
24	2.5 $\mu\text{L}$ (0.75- 3.0 $\mu\text{L}$ )	0.8 $\mu\text{g}$ (0.2- 1.0 $\mu\text{g}$ )	40 $\mu\text{L}$ (10-50 $\mu\text{L}$ )
12	5.0 $\mu\text{L}$ (1.5- 6.0 $\mu\text{L}$ )	1.6 $\mu\text{g}$ (0.4- 2.0 $\mu\text{g}$ )	80 $\mu\text{L}$ (20-100 $\mu\text{L}$ )
6	15 $\mu\text{L}$ (4.5- 18 $\mu\text{L}$ )	5.0 $\mu\text{g}$ (1.2- 6.0 $\mu\text{g}$ )	250 $\mu\text{L}$ (60-300 $\mu\text{L}$ )

In order to generate *Drosophila* cell lines which constantly express the protein of interest, the cells were co-transfected with an additional vector for selection. Therefore,  $1 \times 10^6$  cells were seeded into a 25  $\text{cm}^2$  culture vessel. After 20 h the expression vector (2  $\mu\text{g}$ ) and the selection vector pCoBlast (50 ng) were transfected using the Effectene Transfection Reagent (Qiagen) according to the manufacturer's instructions (140  $\mu\text{L}$  EC buffer, 16  $\mu\text{L}$  Enhancer, 20  $\mu\text{L}$  Effectene). The cells were incubated for three days in Schneider's medium, additionally containing 10  $\mu\text{g}/\text{mL}$  blasticidin as the respective selection marker.

#### 7.2.5 Adipocyte Differentiation

3T3-L1 differentiation was performed according to the instructions of ZenBio (#ZBM0009.02). The used buffers were obtained from ZenBio. 3T3-L1 cells were cultured to confluency in PM-1 medium. Two days post-confluency, differentiation was induced by DM-2 medium. This medium contains, biotin, panthothenate, human insulin, dexamethasone, isobutylmethylxanthine and a PPAR $\gamma$  agonist. The differentiation occurs during 2-3 days. Differentiated cells were cultured in AM-1 medium until further experimental procedure. The adipocyte medium contains biotin and panthothenate.

### 7.2.6 Generating an AML12- SILAC Cell Line

In order to label AML12 cells consistently with *light* or *heavy* amino acids for *stable isotope labeling of amino acids in cell culture* (SILAC), the cells were grown in separate SILAC approved media (excluding L- lysine and L-arginine; Invitrogen™). Those were supplemented either with *light* isotopes  $^{12}\text{C}_6$  L-lysine and  $^{12}\text{C}_6^{14}\text{N}_4$  L-arginine or *heavy* isotopes  $^{13}\text{C}_6$  L-lysine and  $^{13}\text{C}_6^{15}\text{N}_4$  L-arginine, respectively. To limit the off-side lysine and arginine source, the FBS was dialyzed accordingly. Dexamethasone and ITS stock solution required for AML12 growth, were added according to routine procedure. Initially, the cells were diluted to the minimal required number of cells, in order to allow as many replications as possible without the necessity of passaging (here  $1.4 \times 10^6$  cells per  $75 \text{ cm}^2$  culture vessel).

After more than six doubling times, a fully labeled cell population was assumed. In order to verify the incorporation rate, an aliquot of the cells was lysed following standard protocols (see 7.2.3) and mixed in equal total protein concentrations of *light* and *heavy* lysates. The incorporation was then analyzed by Nano-LC-MS/MS (see 7.3.4). If the metabolic labeling was successful and in 1:1 incorporation ratios, the lysates were approved for quantitative chemical proteomics experiments (see Chapter 7.4).

In order to diminish the biological variety, the *light* and *heavy* AML12 cell culture lines were handled in identical procedures. In order to minimize the biological variance, SILAC lysates were pooled.

### 7.2.4 RNAi Knock Down in *Drosophila* cells

dsRNA (synthesized as described in 7.5.4) was introduced according to the bathing protocol described by the DRSC (<http://www.flyrnai.org/DRSC-PRR.html>). On the first day, *Drosophila* Kc167 cells ( $10 \mu\text{L}$  serum free medium; 7000 cells) were plated a 384 well plate containing a defined concentration of dsRNA in RNase free water. The plates were centrifuged (2 min, 800 rpm, RT). After an incubation period (30 min, RT), complete Schneider's medium ( $40 \mu\text{L}$ , 10% (v/v) FBS) was added and the plates were centrifuged again. The plates were sealed with an air permeable AeraSeal™ foil (Excel Scientific Inc) and incubated in a humidified chamber for four days at  $25^\circ\text{C}$ . At day three, oleic acid ( $400 \mu\text{L}$ ) was added to induce the LD formation. Finally, the cells were then either fixed (see 7.2.8.1) for imaging or lysed (see 7.2.3) or qPCR (see 7.5.3).

In case of 96 well plates, the cell number was increased to 16.000 cells per well in initially  $20 \mu\text{L}$  SFM and a total volume of  $100 \mu\text{L}$  during the cultivation period.

For the analysis of the *Drosophila* GPCR RNAi sub-library (DRSC, Harvard Medical School) the plates were processed according to the dsRNA protocol described above. The protocol was adapted to the

half-automated plate handling using COMAS facilities. The cells were then seeded by the Multidrop™ Combi Reagent Dispenser with a small seeding cassette.

In all performed RNAi knock out experiments *thread* (*th*) was used as a positive control. A successful *thread* knock down kills the cells due to the wildtype function of thread as apoptosis inhibitor, which can be easily quantified (Lisi et al, 2000).

### 7.2.7 Cell Treatment with Biological Active Small Molecules

If not declared otherwise, the small molecules were solved in DMSO. Cells were plated into the required culture vessel (96-well plate, 6-well plate ± coverslips, petri-dishes and others) in a cell number that allows a confluency of 75- 90% at the end of the experiment. After an initial adaption phase for ~24 h the cells were treated. Therefore, the medium was fully replaced by a media solution containing 5% (v/v) FBS (if not noted otherwise) and the desired concentration of small molecule/ DMSO and oleic acid (final concentration of 400 μM). Small molecule treatment was allowed for 18 h, before cells were harvested for protein isolation (see 7.2.3) or preserved by fixation for imaging (see 7.2.8).

### 7.2.8 (Immune-) Fluorescence Staining of Cells

#### 7.2.8.1 Fixing Cells

Cells intended for (immune-) fluorescence staining were plated either in 96-well imaging plates (black wall, clear bottom; Corning), 384-well imaging plates (black wall, clear bottom; Corning) or in standard 24-well plates on cover slides. Cells were carefully washed with PBS in order to remove remaining media and were then preserved by adding Fixation Buffer (3.7 % Formaldehyde in PBS) for 5- 10 min. The Fixation-Buffer was replaced by Permeabilization Buffer (0.1% (v/v) Triton X-100 in PBS) for another 5 min. Cells were washed trice with PBS in order to remove remaining buffer.

#### 7.2.8.2 Staining Cells with Fluorescent Dyes

Fluorescent dyes for direct staining of cellular compartments and structures were used according to the manufacturer's instructions. Washed cells were either directly stained for the requested amount of time or were first prepared for staining by fixation and permeabilization, if required. After completing the staining, the cells were washed trice with PBS for 5 min at soft agitation to remove the unbound dye.

*Lipid Droplets* were stained in fixed and permeabilized cells either by the green BODIPY® 493/503 neutral lipid stain (Invitrogen™, stock 1 mg/mL in ethanol, 1:2000 in PBS, 1-2 h, RT) or HCS LipidTOX™-Red (Invitrogen™, stock 1 mM in DMSO, 1:500 in PBS, 1 h, RT).

*Nuclei* were stained by the blue benzimidazole Hoechst33342 (Invitrogen™) in live cells as well as in fixed cells (stock 1 mg/mL in ethanol, 1:500-1:1000 in PBS; 1-2 h).

*Actin* was stained by Alexa Fluor® 488 Phalloidin in fixed and permeabilized cells (Invitrogen™ stock 300 U/mL, 1:500 in PBS).

*Mitochondria* were stained in living cells by incubation in the presence of 200 nM MitoTracker™ Red or MitoTracker™ Deep Red solution (stock: 1 mM in DMSO) at the desired assay conditions for 45 min. The dye was removed by washing thrice in PBS before the cells were finally fixed, permeabilized and stained for additional organelles.

#### 7.2.8.3 Staining Cells with Antibodies

Fixed cells (see 7.2.8.1) were blocked (2% (v/v) BSA in PBS-T) for 1 h in order to minimize unspecific binding. The primary antibody was diluted according to manufacturers instructions (commonly PBS-T/ 2% (w/v) BSA, if not noted otherwise). Cells were incubated for 1h at room temperature (alternatively at 4°C overnight). The antibody was removed and stored at -20°C for reuse. The cells were washed thrice for 10 min with PBS-T/2% (w/v) BSA. The secondary antibody fluorescent conjugate was then added (1:500 in PBS-T/2% BSA) and incubated for 1 h at room temperature. The unbound antibody was removed by washing thrice with PBS for 10 min. The cells were mounted and preserved by curbing with nail polish. The probes were handled and stored protected from light.

#### 7.2.8.4 Mounting of Cells

Fluorescently stained cells (see 7.2.8.2-3) were washed three times for 5 min with PBS at soft agitation in order to reduce the remaining dye. If the cells were plated in multi-well plates, an adequate volume of PBS was allowed to remain per well in order to keep the cells in a liquid solution. Plates were sealed with aluminum tape and stored at 4°C until microscopy.

Cells plated on coverslips were carefully removed and subsequently mounted in a drop of Aqua-Poly/Mount (Polyscience). The cover slides were allowed to dry protected from light at room temperature. Slides were then stored at 4°C until microscopy.

### 7.3 METHODS IN PROTEIN BIOCHEMISTRY

#### 7.3.1 Purification and Isolation of Proteins

Cloning and Expression of recombinant proteins was performed by the Dortmund Protein Factory (DPF) according to standard protocols. mCherry-DCK (project 91\_62) and mCherry-SPR (project 91\_66) were expressed in bacterial campaigns of the DPF.

#### 7.3.2 Protein Concentration Determination

Routine protein concentration determination was performed using the Bradford method (Bradford, 1976) with the commercial Bradford reagent (Bio-Rad Laboratories) in the linear range of a BSA regression (20-150  $\mu\text{g}$  protein or rather 200-1500  $\mu\text{g}/\text{mL}$ ). The absorbance was measured at 595 nm using the cuvette based BioPhotometer (Eppendorf).

If Bradford was not applicable due to high detergent concentrations or a high number of samples, a BCA assay was performed (Pierce). BSA was used as reference (20- 2000  $\mu\text{g}/\text{mL}$ ). The absorbance was measured at 562 nm using the cuvette based BioPhotometer (Eppendorf).

#### 7.3.3 Concentration of Proteins Solutions

Proteins in solutions were concentrated by chloroform precipitation (Wessel & Flugge, 1984). The proteins were diluted in four sample volumes methanol, were separated (10s, 9000 rpm) and supplemented by an additional sample volume chloroform. Then, three sample volumes  $\text{H}_2\text{O}$  were added. After mixing the two phases vigorously, the proteins were allowed to settle and the organic phase was removed. The protein phase was washed with three sample volumes methanol. After final phase separation (2 min, 9000 rpm), the organic phase was fully removed and the protein were dried at room temperature.

Alternatively, the protein solutions were concentrated with the help of the membrane filter concentrators (AMICON) in regard to the respective required cut-offs. The concentrator units were used according to the manufacturer's advice including a buffer exchange for > 3 times.

#### 7.3.4 SDS- Polyacrylamide Gel Electrophoresis (SDS-PAGE)

For standard protein separation SDS-PAGE was performed (Laemmli, 1970) using the MiniProtean 3 Gelelektrophoresis system (BIORAD) system. The composition of the gel matrices are summarized in 6.5.3. The proteins were mixed with 6x SDS loading buffer (50% (v/v) glycerol, 250 mM Tris (pH 6.8), 350 mM SDS, 500 mM DTE, 360  $\mu\text{M}$  bromphenol blue) prior to loading onto the gel. If desired,



reducing conditions were generated by addition of 20% (v/v)  $\beta$ -mercaptoethanol to the sample buffer. Reduced and non-reduced protein samples were denatured at 100°C for 5- 10 min prior gel loading. The protein separation was conducted in gel-running buffer (2.5 M glycine, 250 mM Tris, 35 mM SDS) at 40 mA per gel for 1 h at room temperature. Protein size was estimated in reference to the PageRuler™ Plus Prestained Protein Ladder (Thermo Fisher Scientific).

For proteomics experiments involving in gel digestion steps (see 7.4.2), commercial gradient gels (4-20%) were used. Gels were supplied by either Pierce (Gradient Protein Gel) or BIORAD (Mini-PROTEAN®TGXTM Gels).

### 7.3.5 Protein Visualization in PAGE

#### 7.3.5.1 Coomassie Protein Staining

The SDS gel was incubated in Fixing Solution (10% (v/v) glacial acetic acid, 40% (v/v) ethanol) for 15 min and subsequently transferred into Coomassie Staining Solution (0.25% (w/v) coomassie brilliant blue G-250, 45% (v/v) methanol, 10% (v/v) acetic acid) and was stained for 2 h (optional overnight). Afterwards the SDS gel was de-stained in De-Staining Solution (30% (v/v) methanol, 10% (v/v) acetic acid) until the background was clear. The gel was subsequently imaged using the Gellologic 200 Imaging System (KODAK) and KODAK-Mi software. Alternatively, the gel was processed for IGD (see 7.4.2).

#### 7.3.5.2 Silver Staining

The SDS gel was fixed for 1 h (10% (v/v) glacial acetic acid, 40% (v/v) ethanol). The fixing solution was then washed off by 30% ethanol (2x 20min) and an additional washing step in water (1x 20 min). The gel was then sensitized (0.02% sodium thiosulfate) for 1 min. The gel was transferred into a new washing container and was washed in water (3x 20s). Then, ice cold Staining Solution (0.1% silver nitrate) was added. After 20 min the gel was washed in water (3x20 s) and the bands were visualized by addition of Developing Solution (3% Na<sub>2</sub>CO<sub>3</sub>, 0.05% formaldehyde). As soon as the desired band intensity was reached, the reaction was stopped by addition of Termination Solution (0.05 M EDTA). The gel was then subsequently imaged using the Gellologic 200 Imaging System (KODAK) and KODAK-Mi software. This method is not compatible with MS/MS analysis.

### 7.3.5.3 Zinc- Imidazole Staining

In order to use the MS- compatible zinc imidazole based precipitation for protein visualization (Fernandez-Patron et al, 1998), the SDS gel was fixed for 20 min under constant agitation (10% (v/v) glacial acetic acid, 40% (v/v) ethanol) and subsequently washed with water (2x 10 min). The gel was then incubated in Imidazole Solution for 15 min (0.2 M imidazole, 0.1% (w/v) SDS). Bands were rapidly visualized 30-60 s after addition of Zinc Sulphate Solution (0.2 M zinc sulphate). The gel was washed thrice in water and subsequently imaged using the Gellogic 200 Imaging System (KODAK) and KODAK-Mi software or processed for IGD (see 7.4.2).

### 7.3.5.4 Oriole™ Fluorescence Staining

The SDS gel was shortly washed in water (2x 5 min) and then directly placed into a new incubation vessel containing 50 mL Oriole™ Fluorescent Staining Solution (BIORAD). After a minimum of 30 min incubation time (no more than 2 h) the washed gel (1x 5 min, H<sub>2</sub>O) was ready to be imaged using UV detection in the Gellogic 200 Imaging System (KODAK) and KODAK-Mi software.

### 7.3.6 Electrophoretic Transfer of Proteins (Blotting)

In a process also known as “western blotting” (Towbin et al, 1979) the proteins separated in acrylamide gels by SDS-PAGE (see 7.3.5) were transferred to a PVDF membrane in an electrical field. The semi-dry electrotransfer was performed in a horizontal BIORAD Trans Blotting chamber, by assembling a sandwich consisting of two layers of filter sheets, followed by the gel and the membrane, closed by two filter sheets again. All layers were first soaked in freshly prepared Transfer Buffer (14.41 g/L glycine, 3.03 g/L Tris, 20% (v/v) MeOH). The transfer occurred at 5.5 mA/cm<sup>2</sup> membrane at a constant voltage (25V) for 70 min.

### 7.3.7 Immunodetection of immobilized Proteins

The protein bearing membrane was blocked for 1 h with Blocking Buffer (routinely 2% (w/v) dry milk powder in 10 mM Tris, 150 mM NaCl, 0.05 % (v/v) Tween-20, pH 7.5; alternative blocking reagents are listed in 7.5.3). The target specific primary antibody was incubated for 1 h at room temperature at constant agitation (optionally overnight at 4°C) in the respective buffers described by the manufacturers. Unbound antibody was removed by washing thrice with Blocking Buffer for 10 min. Then the secondary antibody was added (1:10.000; Blocking Buffer containing 1% (w/v) dry milk powder) and incubated for 1 h at room temperature at constant agitation. The membrane was washed twice in Blocking Buffer and once in PBS to decrease the detergent concentration.

The signal was detected depending on the properties of the bound secondary antibody. The enzymatic HRP signal was detected using the SuperSignal Pico/Femto Chemiluminescent Substrate (Pierce) according to the manufacturer's instructions. The resulting chemiluminescence was quantified using the Odyssey® Fc Imaging System (Li-COR® Bioscience) with adequate exposure times.

Alternatively, when Li-COR® antibodies or antibodies with a fluorescent tag were used, the fluorescence was directly quantified by the Odyssey® Fc Imaging System (Li-COR® Bioscience) using the appropriate filter sets.

## 7.4 METHODS IN CHEMICAL PROTEOMICS FOR TARGET ID

### 7.4.1 Affinity Chromatography based Binding Partner Identification (Pull-down)

Affinity chromatography as a tool for the detection and quantification of interactions between small molecules and their target proteins is an experimental setup in target ID studies (Draczkowski et al, 2012). Generally the small molecule of interest is modified by introduction of an affinity reagent, which is commonly either biotin (see 7.4.1.1) or a free amine group (see 7.4.1.2). The biotin probe can then be easily bound to (magnetic) streptavidin sepharose beads. Alternatively the free amine group can be covalently coupled to N-hydroxysuccinimid decorated beads.

Mixing this chemically decorated affinity beads with bulk cell lysates allowed specific protein interactions out of the complex sample of interest. Unspecific binders were removed by subsequent washing, while the specific interaction of the small molecule causes it to remain predominantly immobilized. The bound protein fraction was either directly digested on the beads (see 7.4.2.2; ISD) or unspecifically eluted by boiling in detergent rich buffers and subsequent SDS-PAGE separation (see 7.4.2.1, IGD). For both strategies, the proteins were identified by means of their peptide fingerprint and collision induced peptide sequencing in LC-MS/MS analysis (see 7.4.3).

Since the final quantification method of the peptides in form of Nano-LC-MS/MS is a highly sensitive method, the number of contaminants had to be kept minimal. For this reason, all experiments described in the following subchapter were performed in a designated proteomic room. The samples were handled in a safety cabinet to minimize keratin contamination. Low protein binding filter tips and reaction tubes were routinely used.

#### 7.4.1.1 Biotin-based Pull- down

High Capacity Neutravidin Agarose Beads (Pierce) were equilibrated at room temperature. The beads (100  $\mu$ L of a 1:3 slurry) were packed in low volume spin columns (Thermo Fisher Scientific) and were washed three times with two column volumes (cv) PBS (1000 rpm, 1 min). The biotinylated derivative in PBS was then added (40  $\mu$ L, 200  $\mu$ M) and the biotin-streptavidin interaction was allowed during an incubation period of 1 h at room temperature and constant agitation (shaker, 200 rpm). Alternatively, magnetic sepharose beads (NewEngland Biolabs) were used (250  $\mu$ L resin; 1 mL 10  $\mu$ M biotin sample in PBS). The beads were separated in a magnetic field using specialized magnetic racks for 1 mL reaction tubes (Life Technology).

Unbound biotinylated small molecules were removed by subsequent washing with 500  $\mu$ L Lysis Buffer (50 mM PIPES, 50 mM NaCl, 5 mM MgCl<sub>2</sub>, 5 mM EGTA, 0.1% (v/v) NP40, 0.1% (v/v) Triton X-100, 0.1% (v/v) Tween-20, protease inhibitor, pH 7.4). A total protein concentration of 1 mg was applied in form of bulk cell lysate (prepared as described in 7.2.3). Specific protein-small molecule bonds were allowed to be formed during an incubation period of 2h at 4°C. Unbound protein was washed off by washing trice with lysis buffer. The sample was either further processed for IGD (see 7.4.2.1) or ISD (see 7.4.2.2).

#### 7.4.1.2 NHS based Pull- down

25  $\mu$ L NHS activated magnetic Sepharose (GE Healthcare) was equilibrated with ice cold HCl (1 mM; 5 min). The solution was immediately replaced by the active/ inactive small molecules carrying a free amine group for linkage. The reaction was performed at room temperature over 1h in a rotation wheel. Successful coupling was checked via TLC in methanol in DCM (10% (v/v)). Spots were visualized under UV light after staining with KMnO<sub>4</sub> Solution (9 g KMnO<sub>4</sub>, 60 g K<sub>2</sub>CO<sub>3</sub>, 1 mL NaOH (1% (v/v))). The released succimidine concentration increased over time if the reaction was successful.

Residual active groups were quenched in a blocking and alkylation sequence with Block Solution A (0.5 M ethanolamine, 0.5 M NaCl, pH 8.3) and Block Solution B (0.1 M sodium acetate, 0.5 M NaCl, pH 4.0) for a total number of 3 cycles (each step 5 min). Only the second cycle was altered by a prolonged incubation with Block Solution A for 15 min. The beads were then equilibrated in lysis buffer (5 min, RT) and bulk protein lysate was added (1 mg total protein) and incubated (2 h, 4°C). Unbound protein was removed by washing once with lysis buffer and thrice in PBS (5 min, RT). The sample was either further processed for IGD (see 7.4.2.1) or ISD (see 7.4.2.2).

#### 7.4.1.3 Quantitative setup for Pull- down by SILAC

While the standard non-quantitative pull- down approaches, as well as the label free evaluation require two independent samples for the active and the inactive derivative of the test substance, quantitative pull- down strategies based on SILAC allow mixing of samples at a certain point. This diminishes measuring inaccuracies by variances in sample handling up to a certain level. A schematic summary of the SILAC procedure is given in Supplemental Figure 14, p.209).

In the SILAC process the labeled lysates (see 7.2.6) were applied for the standard pull- down by NHS based (see 7.4.1.2) immobilization of the active and the inactive small molecules. Hence the protein loaded beads were combined in the last step of the pull- down process, it was utterly important to start with identical total protein concentration in the separate *light* and *heavy* samples. Later during the SILAC evaluation the mass difference ( $\Delta 6$  Da) of metabolically labeled proteins were used for quantification. Specific binders towards the active probe were considered to have a significant aberration from the abundant binders. This is summarized by SILAC ratios: a ratio  $A/I = 1$  indicates an abundant binder, a ratio  $A/I > 1.0$  indicates an enrichment in the active derivative. Different replicates of SILAC experiments were statistically evaluated by t-test in order to securely identify significantly enriched proteins in the respective active probe.

#### 7.4.2 Sample Preparation for MS/MS analysis

##### 7.4.2.1 In-Gel Digest (IGD)

Proteins isolated from the affinity purification based on immobilized small molecules (see 7.4.1) were mixed with concentrated SDS-sample buffer (50% (v/v) glycerol, 250 mM Tris (pH 6.8), 350 mM SDS, 500 mM DTE, 360  $\mu$ M bromphenol blue). The denatured samples (95°C for 5-10 min) were separated by SDS-PAGE (see 7.3.4) and stained by mass spectrometry compatible staining methods (see 7.3.5).

Each line in the SDS-gel was fractionated into five gel slices which were transferred into separate reaction vials and minced into slices of 1-2 mm. The gel slices were incubated with 200  $\mu$ L IGD Wash Solution 1 (25 mM  $\text{NH}_4\text{HCO}_3$ / acetonitrile (3:1)) at 37°C for 1 h. The gel slices were additionally washed with 200  $\mu$ L IGD Wash Solution 2 (25 mM  $\text{NH}_4\text{HCO}_3$ / acetonitrile (1:1)) at 37°C for 15 min. The Wash Solution was removed and the gel slices were first reduced in 200  $\mu$ L IGD Reducing Buffer (45 min, 37°C; 50 mM DTT in 25 mM  $\text{NH}_4\text{HCO}_3$ ) and subsequently alkylated in IGD Alkylation Buffer (1h, RT, darkness: 50 mM DTT in 25 mM  $\text{NH}_4\text{HCO}_3$ ). The slices were washed again twice in 200  $\mu$ L IGD Wash Buffer 2, before they were dehydrated by adding 50  $\mu$ L acetonitrile (15 min). The shrunken gel slices were then allowed to dry at room temperature (~30 min). Rehydration with IGD Digestion

Solution (0.01 µg/mL trypsin (proteomic grade) in 25 mM NH<sub>4</sub>HCO<sub>3</sub>) allowed a good admission of the included trypsin. Tryptic digest took place overnight at 30°C in a thermal shaker at constant agitation.

The resulting tryptic peptides were mobilized by sonication (30 min, 0°C, max. amplitude). The supernatant was transferred into a new vial. The gel slices were fully dehydrated by 100 µL acetonitrile (> 30 min, RT), which was then combined with the supernatant from the previous step. The liquid was removed by vacuum centrifugation (~2h, max speed, RT) and samples were submitted for Nano-LC-MS/MS analysis.

#### 7.4.2.2 Trypsin based In-Solution Digest (ISD)

Proteins bound to the immobilized small molecules during affinity purification (see 7.4.1) can be directly digested by trypsin. Therefore 100 µL Urea Buffer (8 M urea in 0.1 M Tris HCl (pH 8.5), 5 µg/mL trypsin) was added (1h, RT, overhead rotation). The supernatant was transferred into a new reaction tube, while the beads were subsequently treated with Alkylation Buffer for 2 min at room temperature at constant agitation (0.05 M iodacetamide in urea buffer). The supernatants were combined and incubated overnight at 37°C under constant shaking. The digest was stopped by 2 µL conc. TFA.

#### 7.4.2.3 LYS-C and Trypsin based In-Solution Digestion (ISD)

Proteins bound to the immobilized small molecules during affinity purification (see 7.4.1) were directly denatured and reduced by addition of 50 µL Buffer RD (8M urea in 50 mM tris, pH 7.9) for 30 min at room temperature at constant agitation. Subsequent alkylation took place in presence of a final concentration of 5 µM chloracetamide (10x stock: 50 mM chloracetamide in DR Buffer) for another 30 min at room temperature and agitation. The proteins were then digested by Lys C (1µg per sample) during an incubation of 1 h at 37°C. The supernatant was transferred into a new reaction vessel and was later combined with the supernatant of an additional tryptic digest (1 µg, 1h, 37°C). The combined supernatant was then supplemented with another 2 µg of trypsin and was digested overnight at 37°C at constant agitation. The digest was stopped by addition of 2 µL conc. TFA.

#### 7.4.3.4 Stop and Go Extraction Tip (STAGE) based Peptide Purification

For purification of soluble peptides, self-packed microcolumns in pipet tips with C18 Empore (2215-C18) filters were used following the descriptions of the Mann Group (Rappsilber et al, 2007). The C18 material was activated by washing with 100 µL methanol and was then equilibrated with STAGE Equilibration Buffer (0.1 % (v/v) formic acid in H<sub>2</sub>O) by applying 100 µL buffer twice. The sample was loaded and passed by centrifugation (5 min, 5000 rpm). Salts and detergents were removed by

washing twice with Equilibration Buffer. The C18 tip was transferred into a new reaction tube and the peptides were eluted in STAGE Elution Buffer (0.1 % (v/v) formic acid, 80% (v/v) acetonitrile in H<sub>2</sub>O). The liquid was removed by vacuum centrifugation (~2h, max speed, RT) and samples were submitted for Nano-LC-MS/MS analysis.

#### 7.4.3 Peptide Identification via Nano-LC-MS/MS

The resulting peptides from the tryptic digest (see 7.4.2) were first separated by nano-HPLC and subsequently identified by MS and MS/MS either using an Ultimate 3000 nano-HPLC MS/MS (Dionex, Idstein) or a Q Exactive™ Hybrid Quadrupole-Orbitrap Mass Spectrometer (Thermo Scientific). MS analysis and data evaluation was performed in cooperation with Dr. Petra Janning (MPI Dortmund).

In the first step, the dried peptides were resuspended in 20 µL TFA and solved by sonication (15 min, max. amplitude). Insoluble particles were separated by centrifugation (15000x g, 1min). A fraction (10 µL) was desalted and concentrated in a Nano-(U)HPLC system suitable for flow-rates of 300 nL/min using the UltiMate™ 3000 RSLCnano system (Dionex) equipped with a nano-HPLC Acclaim PepMap RSLC C18 (2 µm, 100 Å, 75 µm ID × 25 cm, nanoViper, Dionex), a pre-column cartridges (Acclaim PepMap100 C18, 5 µm, 100 Å, 300 µm ID × 5 mm, Dionex) and a nano-spray emitter (Standard Coated SilicaTip™ Emitter, 360 µm OD, 20 µm ID, 10 µm Tip ID, 10.5 cm, New Objective, USA) in a linear gradient (start: 96.8% formic acid (0.1%), 3.2% formic acid (0.1%) in acetonitrile, end: 62% formic acid (0.1%), 38% formic acid (0.1%) in acetonitrile) at a constant flow rate of 300 nL/min at a column temperature of 40°C.

High performance mass spectrometry for high resolution MS and MS/MS measurements were routinely performed at a Q Exactive™ Hybrid Quadrupole-Orbitrap Mass Spectrometer (Thermo Scientific) equipped with a nano-spray ion source (e.g. Nanospray Flex Ion Source, Thermo Scientific). The spray was generated with 2.1 kV and a mass range of m/z 300-1650 was analyzed in a full scan MS with a resolution of 70000 units in a one micro-scan mode using automated gain control (AGC) of  $3 \times 10^6$  units and a maximum injection time (IT) of 20 ms. Up to ten high energy dissociation (HCD) MS/MS scans with a resolution of 17500 units of the most intense at least double charged ions were analyzed (AGC:  $1 \times 10^5$ , IT: 120 ms, isolation window: 3 m/z, normalized collision energy (NCE): 25, ratio of 0.1%, intensity threshold:  $8.3 \times 10^2$ , dynamic exclusion: 20s). Both full scale and fragmentations spectra were recorded.

#### 7.4.4 MS and MS/MS Data Evaluation and Statistical Analysis

The data was either analyzed on the basis of the MOWSE score (molecular weight search) based MASCOT analysis (Koenig et al, 2008) or alternatively by the Andromeda algorithm based open source software MaxQuant (Cox & Mann, 2008).

The SwissProt data base (Version 56.7) was checked for peptides resulting from full tryptic digest, while allowing mis-digestions and based on  $[M+2H]^{2+}$  MS/MS ions, using a filter for identification of the applied host (*Mus musculus* (mouse), *Drosophila melanogaster* (fruit fly) or *Homo sapiens* (human), respectively). Carbamidomethylation was set as a fixed protein modification, while methionine oxidation was set as a flexible modification.

Only proteins with significances of  $p < 0.001$  (FDR 1%) were used for analysis, relying on measurement precision of 5 ppm for peptide mass and 0.5 Da for MS/MS data.

##### 7.4.4.1 Qualitative Data Analysis

Qualitative MS analysis based on the Ultimate 3000 nano-HPLC MS/MS (Dionex, Idstein). The obtained proteins were compared in regard their counts in the respective probes. In a dataset of 5 independent replicates, which were at least identified 3 out of 5 times in the active probe with a difference of  $>2$  counts to the inactive probe were considered as likely specific binders.

##### 7.4.4.2 Label Free Data Analysis

Qualitative MS analysis based on the Q Exactive™ Hybrid Quadrupole-Orbitrap Mass Spectrometer (Thermo). The MASCOT search was performed according to the above described parameters.

Further data analysis was performed with MAXQuant (version 1.5.1.2; Cox & Mann, 2008) and PERSEUS (Version 1.5.0.31) first by filtering of the original proteins lists by means that proteins which were not confirmed in a reverse database were removed, as well as proteins which were solely identified by one side chain and proteins from non- murine origin. Furthermore, the proteins had to be present in at least 2 out of 3 replicates of the positive control. Median and arithmetic mean of  $\log_2$  (LFQ intensity) values were calculated. If the protein was absent in the control probe (inactive) an artificial numerical value was introduced. The ratio (Active/Inactive) was evaluated in two t-test separately (FDR 0.05,  $s_0 = 2$ ). The classical significance A gives no weight to signal intensity, while Significance B is weighted. This weighting is important as the width of the bulk distribution of logarithmic ratios depends on the protein intensity. High abundant proteins show more focused distribution, than low abundant proteins. To overcome this, the signal intensity is binned in order to



calculate significance B separately (Eidhammer et al, 2013). Significantly enriched proteins in the active probe were considered as specific for the respective probe.

#### 7.4.4.3 SILAC based Data Analysis

Qualitative MS analysis based on the Q Exactive™ Hybrid Quadrupole-Orbitrap Mass Spectrometer (Thermo). The MASCOT search was performed according to the above described parameters.

Further data analysis was performed with MAXQuant (version 1.5.1.2; (Cox & Mann, 2008)) and PERSEUS (Version 1.5.0.31) first by filtering of the original proteins lists by means that proteins which were not confirmed in a reverse database were removed, as well as proteins which were solely identified by one side chain and proteins from non murine origin. The HL ratio (heavy light ratio) was normalized and log-transformed ( $\log_2$ ). Each replicate contained a label switch (R1: Active = Heavy; R2: Active = light), therefore the respective sample was inverted and evaluated by t-tests (FDR 0.05,  $s_0=2$ ). Significance A and B were considered for evaluation (see above).

### 7.5 METHODS IN TRANSCRIPTOMICS

Working with RNA, especially with the highly sensitive ssRNA species, required cleaning of the workspace, pipettes and all material used with the DNAZap™ (Life Technology) to avoid contaminations as well as RNA degradation by abundant RNases. Additionally, RNase free filter pipette tips and reaction tubes were routinely used. RNA samples were solved in RNase free water provided by the different kit manufacturers.

### 7.6 METHODS IN TRANSCRIPTOMICS

#### 7.5.1 Isolation of total RNA

Total mRNA was isolated from (treated) cell culture cells using the RNeasy Mini Kit (Qiagen). Adherent cells were directly lysed in a 6-well tissue culture plate. First the cells were washed twice with ice cold PBS, then snap frozen by floating the plate in liquid nitrogen and subsequently lysed with the provided RLT buffer. The succeeding RNA isolation was done using the QiaShredder™ spin columns (Qiagen) according to the manufacturer's instructions. RNA concentration was determined by measuring the UV absorbance (see Chapter 7.1.5).

### 7.5.2 cDNA Preparation

Complementary DNA (cDNA) was generated from the isolated RNA using the QuantiSript® Reverse Transcription Kit (Qiagen) including an initial gDNA elimination step by applying gDNA wipeout concentrate for 2 min at 42°C. This step was followed by the reverse transcription reaction (42°C for 15 min) by adding the required mastermix. The reaction was inactivated (95°C for 3 min). The cDNA products were either controlled by agarose gel electrophoresis (see Chapter 7.1.6) or were used for quantification by real time PCR (see Chapter 7.5.3).

### 7.5.3 Quantitative Real-Time PCR (qPCR)

Primer for the sequences of interest were designed with the help of the NCBI Primer-BLAST tool with respect to the standard parameters in qPCR primer design (Li & Brownley, 2010). The here chosen parameters were a  $T_m$  of ~62°C, a CG content of ~55%, a length of 70-150 bp while optimally including an exon-intron boundary. Primers were tested using the qPCR cycle program (see below), using a test reaction consisting of 10 µL Phusion Flash High Fidelity PCR Mastermix, 20 ng template and 0.5 µM each primer. The product size was verified with agarose gel electrophoresis.

Quantitative real time PCR allows the determination of the relative and absolute concentration of a RNA species out of the total RNA pool at a given time point. Here the QuantiFast® SYBR Green PCR Kit (Qiagen) was used according to the manufacturer's instructions starting with 100 ng cDNA template for each sample and 0.5 µM of each respective primer. The samples were measured in triplicates. Real time quantification of the SYBR green signal was performed by the iQ5™-Thermo-Cycler (BioRad) and the respective iQ5™ Optical System Software (BioRad). A two-step real time cycling program was applied: after an initial activation step (95°C, 5 min), 40 cycles of denaturation (95°C, 10 s) and a combined annealing/ extension (60°C, 30 s) were performed. The specificity of the generated products was checked by melting curve analysis and eventually additional agarose gel electrophoresis.

Standardly, normalization occurred to both GAPDH and actin and data was evaluated by the  $\Delta CT$  or  $\Delta\Delta CT$  method, respectively.

#### 7.5.4 DsRNA Synthesis for RNAi knock down in *Drosophila* Cell Culture Cells

Double stranded RNA (dsRNA) for RNAi knock down in *Drosophila* cell culture was generated following the adapted protocol from the Harvard *Drosophila* Screening Center (DRSC) (<http://www.flyrnai.org/DRSC-PRS.html>).

First, the gene of interest was amplified by a touch-up PCR using primers introducing a T7 sequence (TAATACGACTCACTATAGGG) at both 5'ends of the intended fragment. The PCR product was designed to span an intron-exon boundary, if possible, and to have a size between ~150-600 bp. Primers were calculated by NCBI Primer-Blast or were chosen from the DRSC database if applicable. The used primer sets are summarized in Chapter 7.12. Each touch-up PCR reaction consisted of 1.5  $\mu$ L Taq Polymerase LC (Fermentas), 1.0  $\mu$ L dNTP Mix (2 mM each; Fermentas), 5.0  $\mu$ L Taq Puffer (10x, including  $(\text{NH}_4)_2\text{SO}_4$ ; Fermentas), 4.0  $\mu$ L  $\text{MgCl}_2$ , 35  $\mu$ L  $\text{H}_2\text{O}$ , 1.0  $\mu$ L genomic *drosophila* DNA (w-), and 2  $\mu$ L of the respective primer Mix (100 pmol/ $\mu$ L stock). Amplification occurred according to the following gradient PCR protocol: An initial denaturation step of 94°C for 5 min was followed by three cycles of 95°C, 57°C and 72°C for 30 s each. During the next steps the temperature was gradually increased by 1.5°C at each cycle for a total number of 10 cycles. Each cycle consist of a denaturation step at 94°C for 30 s, an annealing step at 57°C for 30 s and an elongation step at 72°C for 90 s. The following amplification was continued for 35 cycles consisting of a denaturation step at 94°C for 30 s and a subsequent elongation step for 90 s and a final elongation step for 10 min, before the reaction was cooled to 4°C. The purity of the T7-sequence containing PCR constructs was checked via agarose gel electrophoresis.

DsRNA required for the knock down process was produced by an *in vivo* transcription PCR products from the previous step in an *in vitro* transcription using the MEGAscript® T7 Transcription Kit (Invitrogen™) according to the manufacturer's instructions. However, the reaction scale was reduced by a factor two. The transcription was done over 16 h at 37°C. Remaining genomic DNA was subsequently removed by in-solution DNase Treatment (provided with the kit) for 15 min at 37°C. The generated RNA was then purified using the RNeasy® Mini Kit (Qiagen). The dsRNA was eluted in RNase free water and controlled by agarose gel electrophoresis (see Chapter 7.1.6) and  $A_{260}$  spectroscopy (see Chapter 7.1.5) for quality and concentration respectively.

### 7.5.5 Transcriptome Analysis by Next-Generation-Sequencing

Isolated and purified total mRNA from *Drosophila* S3 and mouse AML12 cell culture cells treated with the corresponding bioactive small molecules or DMSO, respectively, was sent to NIDDK (Bethesda, USA) and analyzed by Dr. Kseniya Golovkina in the group of Dr. Brian Oliver.

## 7.6 METHODS TO STUDY PHYSICAL BINDING

### 7.6.1 MicroScale Thermophoresis (MST)

MST measurements were performed in the Monolith NT.115 instrument (NanoTemper Technologies, Munich). In order to avoid precipitates all buffers and solutions were centrifuged prior to use (5min, 13.000 rpm). To measure the equilibrium binding constants between the unmodified small molecule and a fluorescently labeled protein (e.g. Cherry-DCK), the compound was diluted 16 times in PBS (factor two; final concentration 10  $\mu$ M- 0.3 nM) at steady protein levels (final concentration 25  $\mu$ M). The DMSO concentration was also constant at 0.2% (v/v). The samples were transferred to K002 Monolith™ Standard Untreated Capillaries and were subsequently measured at RT for temperature jumps at different MST powers (20%, 40%, 60%). Data was evaluated with the Monolith Detection software.

### 7.6.2 Proximity ligation Assay (PLA)

An *in situ* PLA assay was performed by adaption to the Duolink® PLA® Technology (Sigma Aldrich®) using the Duolink® Orange Detection Kit. This setup enabled the investigation of the interaction between a labeled small molecule and the cellular target protein candidate (see Supplemental Figure 20, p.212). Cells growing on cover slips (10 mm) were transfected with the respective constructs (see Chapter 7.2.4) and cultured for 48 h in the presence of 400  $\mu$ M OA. The cells were fixed and permeabilized according to standard conditions (see Chapter 7.2.8). The cells were incubated with Fluorescein-Chemotype 2 (20 nM P03 in PBS) for 1h at room temperature in the dark at constant agitation. Cells were washed thrice in PBS and blocked with PLA® Blocking Solution (two drops per slide). The blocking solution was washed off with PBS (3x 2 mL, 5 min). The primary antibodies detecting the small molecule and protein target were incubated in PBS-T + 1% (w/v) BSA (e.g. 1:200 anti-His, mouse and 1:200 anti-FITC, rabbit) for 1-1.5 h at RT in the dark at constant agitation. PBS-T washed cells were then incubated in a pre-heated humidity chamber at 37°C without agitation with a mixture of the diluted PLA® specific antibodies in the supplied antibody diluent (e.g. 1:5 Duolink® PLA® Anti-Rabbit PLUS and Duolink® PLA® Anti-Mouse PLUS). The antibody solution was removed and the cells were washed in PLA Buffer A (2x 5 min). Subsequently, the PLA® Ligase solution was

added (40  $\mu$ L of a 1:5 mixture in ultra-pure water). The sample was incubated in a pre-heated humidity chamber for 30 min at 37°C. The ligation mixture was removed from the cover slips and the cells were washed twice in PLA Buffer A (2x 2 min). The PLA<sup>®</sup> Polymerase (0.5  $\mu$ L in 40  $\mu$ L PLA<sup>®</sup> Amplification Solution) was added and amplification was allowed to take place in a pre-heated chamber for 100 min at 37°C in the dark. The Amplification-Polymerase solution was removed from the slides and the samples were washed twice in PLA<sup>®</sup> Buffer B (2x 10 min) and once with 0.01x PLA<sup>®</sup> Buffer B containing Hoechst<sup>®</sup> 33342 for nuclear staining (1:1000). The slides were then completely dried at room temperature in the dark. The samples were mounted in DAKO<sup>®</sup>Fluorescent Mounting Medium. Images were acquired at the Zeiss Observer Z.1 at 63x magnification (oil).

The images were segmented with Fiji ImageJ (Version 2.0.0). The cell number (30-60 cells per image) was related to the number respective of PLA signal points. The average ratio of six images was considered for data analysis. Evaluation quality might increase if cell membrane markers are used. That would allow the estimation of PLA signal per cell.

## 7.7 METHODS IN LIPID ANALYSIS

### 7.7.1 Lipid Droplet Assay

The standard LD assay involved plating the cells in 96-well imaging plates (Corning<sup>®</sup>) on day one (AML12 2800 cell/well, HeLa 4500 cells/well, Hek293 4200 cells/well, Kc167 100.000 cells/well) for initial adaption. On day two the complete media was replaced by serum reduced medium (5% (v/v) FBS) containing the desired concentration of the test substance/ DMSO (0.02% (v/v)) and oleic acid (400  $\mu$ M final concentration). After 18 h treatment the cells were fixed, permeabilized and stained for LDs and Nuclei (see 7.2.8) and were subsequently imaged.

#### 7.7.1.1 HCS LD Assay for Lipid Storage Modulators

The automated LD assay in AML12 cells performed at *COMAS Screening Facility* was performed according to an add-only protocol in order to minimize the number of liquid handling steps. Therefore, 800 AML12 cells were automatically seeded in a total volume of 20  $\mu$ L in 384-well plates (Corning<sup>®</sup>) by the Multidrop<sup>™</sup> Combi Reagent Dispenser (Thermo Scientific) using a small dispensing cassette. On day 2 the small molecules of the COMAS library were sonically added by the ECHO Acoustic Dispenser (LABCYTE<sup>™</sup>) at single point measurements of 10  $\mu$ M (30 nL). For IC<sub>50</sub> determination small molecule dilution (10  $\mu$ M- 78 nM) were added in triplicates. Oleic Acid (final concentration 200  $\mu$ M) was then semi-automatically added by the Multidrop<sup>™</sup> Combi Reagent

Dispenser (Thermo Scientific). Small molecule treatment took place for 24 h. Cells were then fixed and permeabilized by addition of 10  $\mu\text{L}$  of 2x Perm-Fix Solution (9.4% (v/v) formaldehyde in 0.25% (v/v) PBS/ Triton X-100,) was applied by the Multidrop<sup>TM</sup> Dispenser. Cells were subsequently stained for LD (BODIPY<sup>®</sup> 493/503, 1:1000) and Nuclei (Hoechst 33342, 1:500). The staining solution was removed using the semi-automated ELx405 Select Deep Well Microplate Washer (BioTek) and washed three times with PBS (3x 60  $\mu\text{L}$ ). 40  $\mu\text{L}$  PBS was finally left per well and the plates were sealed with aluminium foil. Imaging was performed using the ImageXpress Micro XLS Widefield High Content Screening System and MetaXpress<sup>®</sup> (Molecular Devices).

Automated image segmentation for data evaluation was performed by the granularity program by MetaXpress<sup>®</sup> (Molecular Devices). As a reference for LDs (FITC channel), the corresponding signal was in a range between 0.7 - 6  $\mu\text{m}$  (2-18 pixels) and an intensity of >150 units above the background. Nuclei were respectively evaluated from pictures acquired in the DAPI channel with a size between 8-40  $\mu\text{m}$  (25-123 pixels) and an intensity above background by >100 graylevel units.

#### 7.7.1.2 HCS LD Assay for Modulators in Foam Cell LD storage

The automated LD assay in THP-1 cells including a differentiation step from soluble, undifferentiated THP-1 monocytes to LD loaded, adherent foam cells, was performed following a similar protocol to the one described in 7.7.1.1. The differentiation was introduced on day two by addition of PMA (100 nM). On day three after differentiation oleic acid (final concentration 400  $\mu\text{M}$ ) and the small molecules (10  $\mu\text{M}$ , single point measurement) were added.

Automated image segmentation for data evaluation was performed by the granularity program in MetaXpress<sup>®</sup> (Molecular Devices). As a reference for LDs (FITC channel), the corresponding signal was in a range between 0.7- 6  $\mu\text{m}$  (2-18 pixels) and an intensity >500 units above the background. Nuclei, were respectively evaluated from pictures acquired in the DAPI channel with a size between 8-40  $\mu\text{m}$  (25-123 pixels) and an intensity above background >100 graylevel units.

#### 7.7.2 Determination of Triglyceride Content

The triglyceride content of cells was measured in a colorimetric cell based assay (Triglyceride Assay Kit; Zenbio) following a modified protocol. Cells were grown and treated with small molecules as described in Chapter 7.2. Two identically treated 96-well plates were pooled in the initial lysis step in order to increase the TAG quantity in the samples. TAGs were then hydrolyzed by lipases contained in the kit reagent and the released glycerol was quantified by the following enzymatic reaction, first forming G1P (glycerol-1-phosphate) and then DAP (dihydroxyacetone phosphate). This

reaction initiates H<sub>2</sub>O<sub>2</sub> production which then reacts with the quinoeimine dye to a product with absorbance maximum at 540 nm. The absorbance correlates with the released amount of glycerol and can be quantified using the Infinite®2000 reader (Tecan) in the linear range of a glycerol standard curve. Samples were normalized to their protein content using a BCA assay (see 7.3.2). All samples were measured in triplicates.

Alternatively, TAG content was estimated by HCS imaging using cell profiler for image segmentation, thus allowing the relative quantification of the TAG content to a DMSO or unfed cell, respectively.

Additionally the TAG content was determined by HPLC measurements in Collaboration with Dr. Thomas O. Eichmann from the University of Graz (see 7.7.7).

### 7.7.3 Lipid Uptake Assay

*Principle:* The uptake of a fluorescently tagged FA was measured by the QBT™ Fatty Acid Uptake Assay Kit (Molecular Devices) in 96 well format. A BODIPY® 500/512 C1 fatty acid analog was quenched as long as it remained extracellular, while a fluorescence signal at 515 nm can be detected upon internalization. The BODIPY label does not affect the native uptake behavior and is activated inside the cell by acyl-CoA attachment and can thus be incorporated into di- and triglycerides.

*Assay:* Cells were plated in a 96 well plate (8000 AML12 cells/well) and cultured for ~24 h. The medium was replaced by serum reduced medium (5% (v/v) FBS) containing 5 µM bioactive small molecule, which was incubated for 3 h. The cells were then starved for 30 min in serum free medium. To start the measurement of QBT™ reagent solved in QBT Base Buffer (10 mL HBSS Buffer (10x), 3 mL HEPES Buffer (1M), 88 mL H<sub>2</sub>O and 200 mg fatty acid free BSA) containing the bioactive small molecule (5 µM) was added. The absorbance was immediately measured at 37°C ( $\lambda_{\text{Ex}} = 485 \text{ nm}$ ,  $\lambda_{\text{Em}} = 515 \text{ nm}$ ) using the Infinity®2000 Reader (Tecan).

Additionally a similar setup was performed in Collaboration with Dr. Thomas O. Eichmann (Graz, Austria). The incorporation of radiolabeled fatty acids was measured over a shorter time frame.

#### 7.7.4 Cholesterol Storage Assay

The storage of cholesterol was microscopically assayed using a NBD-Cholesterol derivative. Cells were plated and adapted for one day. Then 100  $\mu\text{L}$  of freshly prepared serum reduced medium (5% (v/v) FBS) containing the bioactive small molecule/ DMSO (5  $\mu\text{M}$ ) and NBD-Cholesterol (1  $\mu\text{g}/\text{mL}$ ) was added, either with or without oleic acid (400  $\mu\text{M}$ ). After 18 h treatment, the cells were fixed and stained for LD and nuclei (see 7.2.8).

#### 7.7.5 Lipid Extraction

Cells were cultured in 6-well plates to a confluency of 60-80%. Cells were washed trice in PBS and resuspended in 1 mL PBS. 100  $\mu\text{L}$  sample was removed for BCA protein determination (see 7.3.2, while the remaining solution was pelleted again (5.000 rpm, 5 min, 4°C). Cells were resuspended in 500  $\mu\text{L}$  PBS and was mixed in 2.5 mL chloroform/ methanol (2:1) in Pyrex® vials. Lipids were extracted for 1h at room temperature under constant agitation. Phase separation was accelerated by centrifugation (2.500 rpm, 5 min). The lower chloroform phase containing the lipids, was transferred into a fresh Pyrex® vial and was fully dried in a constant  $\text{N}_2$  flow. The samples were solved in chloroform adjusting the protein concentration. The lipid was then separated by TLC (see 7.7.6) or HPLC (see 7.7.7).

#### 7.7.6 Thin- layer Chromatography (TLC)

Samples from lipid extractions (see 7.7.5) normalized to the protein content, were separated on silica plates (Merck) using the required solvent mixture for the respective lipid species: triglycerides/ sterylesters were separated in hexan/ diethylether/ acetic acid [70:30:1], monoglycerols/ diglycerols/ cholesterol in a mixture containing chloroform/ acetone/ acetic acid [90:8:1], while phospholipids were separated in chlorofom/ methanol/ acetone/ acetic acid [50:10:20:12:6]. The chromatographic separation usually took 30 min in a well equilibrated TLC chamber. Lipids were visualized on fully dried plates (room temperature) by applying a cupric spray (10% (w/v)  $\text{CuSO}_4$ , 10% (v/v) phosphoric acid) and subsequent heating at 120°C (~30 min). Lipids appear as black bands at their respective  $R_F$ -values.



### 7.7.7 High Pressure Liquid Chromatography (HPLC)

HPLC measurement of the lipid extracts of small molecule treated cells were analyzed by Dr. Thomas O. Eichmann at the University of Graz.

## 7.8 METHODS FOR VALIDATION OF ENZYME AND PATHWAY ACTIVITY

### 7.8.1 Cell Viability Assay

*Principle:* Cell viability was quantified using the CellTiterGlo<sup>®</sup> Reaction Kit (Promega) based on quantitation of cellular ATP levels as an indicator of metabolically active cells. The quantification bases on an ATP dependent luciferase reaction which catalyzes the mono-oxygenation of beetle luciferin in the presence of ATP, Mg<sup>2+</sup> and molecular oxygen (see Supplemental Figure17, p.210). The resulting luminescence signal is proportional to the ATP concentration which correlates linearly with the cell number.

*Assay:* Cells were plated and treated according to the standard LD assay keeping all times and concentrations identical to the respective assay conditions. The CellTiterGlo<sup>®</sup> reagent was added (100 µL in 96-well plate; 35 µL in 384-well plate), incubated at 37°C and then measured for luminescence intensity using the Tecan Infinite M200 plate reader.

### 7.8.2 Deoxycytidine Kinase Assay (DCK)

#### 7.8.2.1 Enzyme based DCK Assay

*Principle:* DCK activity was measured in an enzymatic *in vitro* assay on the basis that DCK provides the phosphorylation of both purine and pyrimidine deoxynucleosides. In the first reaction deoxyinosine (dIR) is phosphorylated in the presence of ATP by the DCK reaction to Deoxyinosine monophosphate (dIMP). Latter, it is then oxidized in a second reaction to deoxyxanthosine monophosphate (dXMP) by IMPDH in the presence of NAD, leading to NADH<sub>2</sub> formation, which can be measured at 340 nm (see Supplemental Figure19, p.210).

*Assay:* The assay was performed in the screening facility of NovoCIB (Lyon) following the RECICE<sup>®</sup> dCK Assay Protocol. Gemcitabine was used as an internal control.

#### 7.8.2.2 Cell based DCK Assay

*Principle:* In a cellular environment inhibition of DCK prevents the incorporation of AraC into DNA. This rescues AraC cytotoxicity and can be quantified by viability readout such as the ATP level by the CellTiterGlo<sup>®</sup> reagent (Promega). The assay was described for HTS by (Yu et al, 2010) (see Supplemental Figure 20, p.212).

*Assay:* Cells were seeded in 96-well white culture plates (Nunc), in a total volume of 100  $\mu$ L of the respective medium supplemented with AraC (30 nM) and test substances (final DMSO concentration, 0.5% (v/v)). The cells were grown at 37°C in a CO<sub>2</sub> incubator for three days. To each well 100  $\mu$ L of CellTiter-Glo® Luminescent Cell Viability Assay reagent (Promega) were added. After incubation at room temperature for 60 min the luminescence was recorded using a Tecan Infinite M200 reader.

*Evaluation:* The luminescence represents total ATP concentration in the well, which is proportional to the number of viable cells.

### 7.8.3 Diacylglycerol-O-Acyltransferase Assay (DGAT)

*Principle:* DGAT catalyzes the final step in TAG synthesis by forming an ester bond between a fatty acyl CoA and the free hydroxyl group in the *sn*-3 position of a 1,2-diacylglycerol (DAG). The incorporation of radiolabeled fatty acids can be quantified as a measure for the DGAT activity in overexpressing COS7 cells.

*Assay:* The assay measurements were performed by Dr. Thomas O. Eichmann (University of Graz, Austria). Cell homogenate (50  $\mu$ g total protein) from COS7 cells, which either express murine isoforms of DGAT1 or DGAT2, were incubated with 0.2 mM emulsified DAG substrates (*sn*-1,2-, *sn*-1,3-DAG or racemic 1,2/2,3 diolein) in Tris Buffer (50 mM, Tris, 20 mM MgCl<sub>2</sub>, pH 7.4) and 0.8 mM phosphatidylcholine. The test substance was added (5  $\mu$ M). After sonification oleoyl-CoA and [<sup>14</sup>C] oleoyl-CoA (55  $\mu$ Ci/7 $\mu$ mol) were added to final concentrations of 20  $\mu$ M. The substrate and the sample were mixed in equal volumes to give a final volume of 200  $\mu$ L and were then incubated for 10 min at room temperature. The reaction was stopped by lipid extraction with chloroform/methanol (2:1, v/v) and the extracts were separated by TLC in a [hexane/ diethyl ether/ acetic acid (70/29/1, v/v/v)] mixture. TLC bands corresponding to the synthesized TAG were scraped off and their radioactivity was determined by liquid scintillation counting (Tri-Carb 2300 TR).

### 7.8.4 Soluble Ephoxide Hydrolase Assay (EPHX2)

#### 7.8.4.1 N-terminal Phosphatase Activity Assay

*Principle:* The N-terminal phosphatase activity (EC 3.1.3.76) of recombinant murine EPHX2 was measured by EPHX2 dependent production of the fluorescent dephosphorylation BBT Product of the AttoPhos® substrate (BBTP: 2'-[2-benzothiazoyl]-6'-hydroxybenzothiazole phosphate). The assay was performed in analogy to the method described by Morisseau (Morisseau et al, 2012). (see Supplemental Figure , p.211)

*Assay:* 150  $\mu\text{L}$  of a 2.8 nM solution of purified mouse EHPX2 (Cayman Chemicals) was added to 152  $\mu\text{L}$  of the test substance dilution (5  $\mu\text{M}$ ) in Reaction Buffer A (25 mM BisTris/HCl (pH 7.0), 1 mM  $\text{MgCl}_2$ , 0.1 mg/mL BSA) to reach a final enzyme concentration of 2.1 nM per well. After mixing and pre-incubation at room temperature for 5 minutes, the reaction was started by addition of 30  $\mu\text{L}$  of the AttoPhos<sup>®</sup> solution in Reaction Buffer A to reach a final substrate concentration of 2.5  $\mu\text{M}$ . After 10 min incubation at room temperature in the dark, 100  $\mu\text{L}$  NaOH (0.1 M) were added to each well. Following strong mixing, the amount of fluorescent alcohol produced was measured with a Tecan Infinite M200 reader (Tecan) at room temperature ( $\lambda_{\text{Ex}}$  435 nm,  $\lambda_{\text{EM}}$  555 nm,  $\lambda_{\text{cutoff}}$  515 nm).

*Evaluation:* The results were averaged  $\pm$  standard deviation from three separate data points. The background control was subtracted.

#### 7.8.4.2 C-terminal cell based Epoxide Hydrolase Assay

*Principle:* To monitor the C-terminal epoxide hydrolase activity in a cell based assay, an Epoxy Fluor 7 was provided as a substrate. The hydrolysis by endogenous EPHX2 in cell lysates yields the highly fluorescent product 6-methoxy-2-naphthaldehyde. This can be monitored at excitation and emission wavelengths of 330 nm and 465 nm.

*Assay:* The assay was measured according to the instructions of the Soluble Epoxide Hydrolase Kit (Cayman Chemicals). The treated cells were washed with assay buffer (200  $\mu\text{L}$ , 800 g, 5 min) and lysed in 100  $\mu\text{L}$  lysis buffer for 30 min on an orbital shaker at room temperature. Cell debris were removed by centrifugation (3000 g, 20 min, 4°C) and 90  $\mu\text{L}$  of the supernatant were transferred in a black 96-well assay plate (Cayman Chemicals). The inhibitor dilution (10  $\mu\text{L}$ ; 5 $\mu\text{M}$ ) or DMSO in assay buffer was added and the enzymatic reaction was started by addition of Epoxy Fluor7 substrate (100  $\mu\text{L}$ ). The positive control contained recombinant human EPHX2 (0.1  $\mu\text{g}$ 7 $\mu\text{L}$ ) instead of cell lysate. After 30 min incubation time at 37°C the fluorescence was measured ( $\lambda_{\text{Ex}}$  330 and  $\lambda_{\text{EM}}$  465 nm).

*Evaluation:* The results were averaged  $\pm$  standard deviation from three separate data points. The background control was subtracted.

#### 7.8.4.3 C-terminal enzyme based Epoxide Hydrolase Assay

*Principle:* The enzyme based EPHX2 assay was performed in analogy to the cell based assay described in 8.8.4.2. Instead of cell lysates recombinant human and mouse EPHX2 was used in a similar assay setup.

*Assay:* 90  $\mu$ L recombinant human EPHX2 (Abnova) or recombinant mouse (Cayman Chemicals) in Assay Buffer were transferred in a black 96-well assay plate (Cayman Chemicals). The inhibitor dilution (10  $\mu$ L; 5 $\mu$ M) or DMSO in Assay Buffer respectively was added and the enzymatic reaction was started by addition of Epoxy Fluor7 substrate (100  $\mu$ L). After 30 min incubation at 37°C the fluorescence was measured at  $\lambda_{\text{Ex}}$  330 and  $\lambda_{\text{Em}}$  465 nm.

*Evaluation:* The results were averaged  $\pm$  standard deviation from three separate data points. The background control was subtracted.

#### 7.8.5 HTS Hedgehog driven Osteogenesis Screen

*Principle:* In order to test for effects of the test substances in the process of a sonic hedgehog driven process in osteogenesis of mouse fibroblast cells, the activity of alkaline phosphatase activated by smoothed (Katsuura et al, 1999) was quantified via luminescence detection. The known smoothed agonist Purmorphamine (Wu et al, 2004) was used as a reference.

*Assay:* The mouse embryonic fibroblast cells (C3H/10T1/2) were plated in 384-well format (800 cells/well in 25  $\mu$ L DMEM high glucose medium, 10% (v/v) FBS, 1mM sodium pyruvate, 2 mM L-glutamate) directly after thawing the stock solution. After an initial adaption phase for  $\sim$ 24 h at 37°C and 5% CO<sub>2</sub> in a humidity controlled incubator (95%), the test substances/ DMSO were added (30  $\mu$ M to 0.01  $\mu$ M in a 1:3 dilution) and incubated for one additional hour at 37°C. Purmorphamine (1.5  $\mu$ M) was used as a positive control for osteoblast differentiation, while untreated (DMSO) and Vismodegib (Abidi, 2014) as well as Cycloheximidine (Chen et al, 2011) were used as negative controls. The cells were then treated for four days at 37°C at standard cell culture conditions. The cells were finally lysed (100 mM Tris (pH 9.5), 250 mM NaCl, 25 mM MgCl<sub>2</sub>, 1% (v/v) Triton X-100) and the luminescence was measured with the CDP-Star Kit (Roche) in the Tecan Infinite M200 Plate Reader (Tecan). The assay is routinely performed in the COMAS Screening Center, Dortmund.

### 7.8.6 11 $\beta$ -Hydroxysteroid Dehydrogenase Assay (HSD)

*Principle:* The cell based 11  $\beta$ -HSD assay measures the 11  $\beta$ -HSD1 dependent oxo-reduction from cortisol and the 11 $\beta$ -HSD2 dependent oxidation of cortisone from lysates of stably transfected HEK293-cells. Using  $^3\text{H}$ -labeled substrates allowed quantification of the steroid products by scintillation counting (see Supplemental Figure14, p.210).

*Assay:* The 11 $\beta$ -HSD assay was performed in collaboration with Dr. Odermatt (University of Basel). Stably transfected HEK-293 cells for 11 $\beta$ -HSD1 and 11 $\beta$ -HSD2 were cultured in steroid-free medium for 16 h, washed with PBS and isolated by centrifugation (3 min, 150g). The cell pellet was solved in TG1 Buffer (20 mM Tris-HCl (pH7.4), 1 mM EGTA, 1 mM  $\text{MgCl}_2$ , 100 mM NaCl, 20% (v/v) glycerol) and were subsequently disrupted by sonication. The 11 $\beta$ -HSD activity was immediately measured in 96-well format.

10  $\mu\text{L}$  cell lysate were mixed with 12  $\mu\text{L}$  Reaction Solution (400  $\mu\text{M}$   $\text{NADP}^+$  or  $\text{NADPH}$ , 30 nCi [ $^3\text{H}$ ]-labeled substrate (HSD1: [1,2,6,7- $^3\text{H}$ ]-cortisone (American Radiolabeled Chemicals); HSD2: [1,2,6,7- $^3\text{H}$ ]-cortisol (Amersham Biosciences), 25 nM unlabeled cortisol (HSD2) or 200  $\mu\text{M}$  unlabeled cortisone (HSD1) and 0-200  $\mu\text{M}$  inhibitor in TG1 buffer) and incubated for 10 min at 37°C. The reaction was stopped by addition of 10  $\mu\text{L}$  of unlabeled steroid (2 mM). The steroids were separated by TLC (SIL G-25 UV254 plates, Macherey-Nagel) using the following solvent mixture [ $\text{CHCl}_3$ /methanol (9:1) (v/v)]. The steroid containing bands identified under UV-light were cut out and quantified via scintillation counting.

*Evaluation:* The enzyme kinetic was analyzed by non-linear regression using the Data Analysis Toolbox (Elsevier MDL, San Leandro, USA) assuming a first order kinetic.

### 7.8.7 Isocitrate Dehydrogenase Activity Assay (IDH)

*Principle:* The enzymatic activity of both IDH isoforms ( $\text{NADP}^+$ /  $\text{NAD}^+$  dependent) was measured in cell lysates based on  $\text{NADP}^+$ /  $\text{NAD}^+$  conversion, which was measured at 450 nm.

*Assay:* The assay was performed according to the manufacturer's instructions using the Isocitrate Dehydrogenase Activity Assay Kit (BioVision). The fluorescence was measured at the Tecan Infinite M200 reader.

### 7.8.8 Invitrogen™ Kinase Profiling

*Principle:* Kinase Binding was screened at Invitrogen™ in the form of the LanthaScreen® Eu Kinase Binding Assay based on a High TR-FRET interaction, which is disrupted if the test substance binds to the binding pocket of the respective kinase and thus replacing the tracer FRET pair.

Additionally, kinase activity changes introduced by the test substance were assayed by the Z'LYTE® Screen (Invitrogen™). In the primary reaction, the kinase transfers the  $\gamma$ -phosphate of ATP to a single residues in a synthetic FRET-peptide. In the secondary reaction this peptide can only be cleaved by a site-specific protease when no phosphorylation occurs, thereby disrupting the FRET interaction between the donor and acceptor fluorophore on the synthetic-peptide. Uncleaved, phosphorylated FRET-peptides can be quantified and correlated with the underlying kinase activity.

*Assay:* Both assays were performed by the Invitrogen European Screening Center, Paisley, UK.

*Evaluation:* A ratiometric method, which calculates the ratio of donor emission to acceptor emission after excitation of the donor fluorophore at 400 nm, is used to quantitate the reaction progress.

### 7.8.9 Pyruvate Kinase Assay

*Principle:* The cell based assay relies on the pyruvate kinase dependent reaction of phosphoenolpyruvate (PEP) and ADP to pyruvate and ATP in the primary reaction. Pyruvate is oxidized to acetyl phosphate under stoichiometric production of  $H_2O_2$ , which then can be quantified in an Amplex Red™ reaction. Fluorescence is measured at  $\lambda_{Ex}$  535 nm and  $\lambda_{EM}$  587 nm.

*Assay:* The assay was performed according to the manufacturer's instructions using the Pyruvate Kinase Activity Assay Kit (BioVision). The fluorescence was measured at the Tecan Infinite M200 reader.

### 7.8.10 WNT reporter gene Assay

*Principle:* Wnt ligands bind to *frizzled* (Fz) to trigger a signaling cascade that leads to the stabilization of  $\beta$ -catenin. This can enter the nucleus to form a complex with T cell transcription factor (TCF/LEF) to activate *wnt* target gene expression. In the reporter gene assay increased  $\beta$ -catenin levels induce luciferase expression by  $\beta$ -catenin-mediated transcriptional activation of the TOPFlash plasmid to levels ~100x times higher than the endogenous level. The luminescent readout can be directly correlated with the *wnt*- receptor activity or potential inhibition or activation, respectively.

*Assay:* Wnt conditioned media (50% (v/v)) as a source for exogenous wnt, was prepared by culturing L-cells (wnt- negative) and Wnt-3a cells (wnt- positive) for four days in the required media (DMEM

high glucose medium (PAN) containing 10% (v/v) FBS, 1% (v/v) L- glutamine (200 mM), 1% (v/v) MEM NEAA (100x), 1% Sodium pyruvate (100 mM) and 0.2 mg/mL G418). The supernatants were mixed in equal contributions and filtered to guarantee sterility.

For assaying wnt activity Hek293-Fz TOPFlash cells (4000/ well) were plated per well in a low volume 384-well plate (Corning) in 12.5  $\mu$ L wnt- conditioned medium (50%) (Positive Control) or in 12.5  $\mu$ L wnt free L-cell medium (Negative Control). The test substances/ DMSO were incubated for 6 h at 37°C and 5% CO<sub>2</sub>. The reaction was cooled to room temperature (10 min) and 12.5  $\mu$ L OneGlo<sup>®</sup> reagent (Promega) was added per well. The luminescence signal was subsequently measured after 5 min using the Tecan Infinite M200 Reader. The assay is routinely performed in the COMAS Screening Center, Dortmund.

#### 7.8.11 Mitochondrial Depolarization Assay

*Principle:* TMRE (tetramethylrhodamine) is a cell permeant, positively-charged, red-orange dye that readily accumulates in active mitochondria due to their relative negative charge. Depolarized or inactive mitochondria have decreased membrane potential and fail to sequester TMRE. The protonophore CCCP (*m*-chlorophenylhydrazone) is used as a positive control for mitochondrial depolarization.

*Assay:* The assay follows a modified assay protocol of MitoPT<sup>®</sup> TMRE Assay Kit (Immunochemistry Technologies). Cells were treated with 1  $\mu$ M of the respective small molecules in presence of 200  $\mu$ M in 5% (v/v) FBS medium for 16 h. 25  $\mu$ M CCCP was incubated for 1 h prior staining. Life cells were stained with 200 nM TMRE and 1  $\mu$ g/mL Hoechst 33342 for 30 min. Surplus staining solution was washed out three times by TMRE Buffer. Life cells were imaged at 40x magnification at the Zeiss Axiovert Z.1 fluorescence microscope.

## 7.9 METHODS IN MICROSCOPY

**TABLE 11: FILTER SETTINGS** for the used fluorophores

Fluorophor	$\lambda_{EX}$ [nm]	$\lambda_{EM}$ [nm]	Filtersetting
BODIPY® 493/503	488	493-598	FITC
HCS LipidTox™	633	638-759	Texas Red
Hoechst33342	405	410-496	Hoechst

## 7.9.1 Manual fluorescence Microscopy

Non-confocal fluorescence imaging was performed using the Zeiss Observer Z.1 inverse fluorescence microscope equipped with a Zeiss PlanNEOFLUAR (20x/ 0.4 Korr., $\infty$  0-1.5), a Zeiss LD Plan-NEOFLUAR (40x/0.6 Korr., $\infty$  0-1.5) and a Zeiss Plan APOCHROMAT (63x/ 1.4 oil ok) objective. Images were recorded with an AxioCam MRM camera. Zenbio ZenPRO 2012 (blue edition, Version 1.1.1.0) was used for image acquisition and processing (Carl Zeiss Microscopy). Glass bottom imaging well plates (CellContact) and coverslips were used.

## 7.9.2 Automated fluorescence Microscopy

## 7.9.2.1 Small Scale automated fluorescence Microscopy

Automated fluorescence imaging was performed using a Zeiss microscope connected to an automated stage handling and acquisition setup by Visitron Systems. This system could handle 96- and 384- well imaging plates (Corning). The images were acquired with a CoolSNAP ES camera (Visitron) and were evaluated with MetaMorph Cell Analysis Software (Molecular Devices).

## 7.9.2.2 High Content Screening (HCS)

HCS based screens (see 7.7.1) were acquired in 384-well plate format (Corning) using a setup including the ImageXpress Micro XLS Widefield High Content Screening System (Molecular Devices) coupled to an Orbitor RS Microplate Mover (Thermo Scientific). Screening images were acquired using an Objective E (20X, S-Plan FluorELWD 0.45, NA cc 0-2mm). The images were analyzed using MetaXpress®.

## 7.9.3 Confocal Microscopy

Confocal images were acquired from cover slips using a Leica TCS SP5 confocal microscope equipped with a HCX PLAPO lambda blue 63x 1.40 oil objective. Images were processed in the Leica Application Suite Lite™.



## 7.10 METHODS USING DROSOPHILA AS A MODELL ORGANISM

### 7.10.1 Keeping Drosophila Stocks

Fly stocks were kept according to established standard methods (Ashburner et al, 2005) in plastic vials with an air permeable lid. Flies were fed with a complex medium (0.5% (w/v) agar-agar, 7.1% (w/v) corn grain, 0.95% (w/v) soy flour, 1.68% (w/v) dry yeast, 4% (w/v) treacle, 4.5% (w/v) malt extract, 1.5% (v/v) nipagin (10% in ethanol) and 4.5% (v/v) propionic acid) and were cultured at 18°C or 25°C respectively, at a humidity of 20-30% keeping a day-night rhythm of 12 h intervals.

### 7.10.2 Treating Drosophila Flies with Bioactive Small Molecules

Cohorts of eight virgin male flies (< 12h age) were collected and fed on complex medium containing 7.5 µM of the test substance or DMSO as control. Flies were cultured for three days at 25°C and were then analyzed for TAGs (see 7.7.2) and Proteins (7.3.2) originating from total fly homogenates.

## CHAPTER 8: REFERENCES

**Abidi A (2014)** Hedgehog signaling pathway: a novel target for cancer therapy: vismodegib, a promising therapeutic option in treatment of basal cell carcinomas. *Indian journal of pharmacology* **46**: 3–12

**Ables GP, Yang, Krystilla Jian Zhang, Vogel S, Hernandez-Ono A, Yu S, Yuen JJ, Birtles S, Buckett LK, Turnbull AV, Goldberg IJ, Blamer WS, Huang L, Ginsberg HN (2012)** Intestinal DGAT1 deficiency reduces postprandial triglyceride and retinyl ester excursions by inhibiting chylomicron secretion and delaying gastric emptying. *J Lipid Res* **53**: 2364–2379

**Affleck JG, Walker VK (2008)** A role for Drosophila in understanding drug-induced cytotoxicity and teratogenesis. *Cytotechnology* **57**: 1–9

**Anderson CM, Stahl A (2013)** SLC27 fatty acid transport proteins. *Mol Aspects Med* **34**: 516–528

**Andersson L, Bostrom P, Ericson J, Rutberg M, Magnusson B, Marchesan D, Ruiz M, Asp L, Huang P, Frohman MA, Boren J, Olofsson S (2006)** PLD1 and ERK2 regulate cytosolic lipid droplet formation. *J Cell Sci* **119**: 2246–2257

**Andrianov V, Borisjuk N, Pogrebnyak N, Brinker A, Dixon J, Spitsin S, Flynn J, Matyszczyk P, Andryszak K, Laurelli M, Golovkin M, Koprowski H (2010)** Tobacco as a production platform for biofuel: overexpression of Arabidopsis DGAT and LEC2 genes increases accumulation and shifts the composition of lipids in green biomass. *Plant Biotechnol. J.* **8**: 277–287

**Aon MA, Bhatt N, Cortassa SC (2014)** Mitochondrial and cellular mechanisms for managing lipid excess. *Frontiers in physiology* **5**: 282

**Araújo JR, Martel F (2012)** Sibutramine effects on central mechanisms regulating energy homeostasis. *Curr Neuropharmacol* **10**: 49–52

**Ashburner M, Golic KG, Hawley RS (2005)** *Drosophila: A laboratory handbook*. Cold Spring Harbor Laboratory Press, Cold Spring Harbor, N.Y.

**Astrup A, Carraro R, Finer N, Harper A, Kunesova M, Lean, M E J, Niskanen L, Rasmussen MF, Rissanen A, Rossner S, Savolainen MJ, van Gaal L (2012)** Safety, tolerability and sustained weight loss over 2 years with the once-daily human GLP-1 analog, liraglutide. *Int J Obes (Lond)* **36**: 843–854

**Ausubel FM (1995)** *Current protocols in molecular biology*. Wiley, New York [u.a.]

- Babu M, Butland G, Pogoutse O, Li J, Greenblatt JF, Emili A (2009)** Sequential peptide affinity purification system for the systematic isolation and identification of protein complexes from *Escherichia coli*. *Methods in molecular biology (Clifton, N.J.)* **564**: 373–400
- Barbas CF, Burton DR, Scott JK, Silverman GJ (2007)** Quantitation of DNA and RNA. *CSH Protoc* **2007**: pdb.ip47
- Barlind JG, Bauer UA, Birch AM, Birtles S, Buckett LK, Butlin RJ, Davies, Robert D M, Eriksson JW, Hammond CD, Hovland R, Johannesson P, Johansson MJ, Kemmitt PD, Lindmark BT, Morentin Gutierrez P, Noeske TA, Nordin A, O'Donnell CJ, Petersson AU, Redzic A et al (2012)** Design and optimization of pyrazinecarboxamide-based inhibitors of diacylglycerol acyltransferase 1 (DGAT1) leading to a clinical candidate dimethylpyrazinecarboxamide phenylcyclohexylacetic acid (AZD7687). *Journal of medicinal chemistry* **55**: 10610–10629
- Baumbach J, Hummel P, Bickmeyer I, Kowalczyk KM, Frank M, Knorr K, Hildebrandt A, Riedel D, Jäckle H, Kühnlein RP (2014)** A *Drosophila* in vivo screen identifies store-operated calcium entry as a key regulator of adiposity. *Cell Metab.* **19**: 331–343
- Beller M, Riedel D, Jansch L, Dieterich G, Wehland J, Jackle H, Kuhnlein RP (2006)** Characterization of the *Drosophila* lipid droplet subproteome. *Mol Cell Proteomics* **5**: 1082–1094
- Beller M, Sztalryd C, Southall N, Bell M, Jackle H, Auld DS, Oliver B (2008)** COPI complex is a regulator of lipid homeostasis. *PLoS Biol* **6**: e292
- Beller M, Thiel K, Thul PJ, Jäckle H (2010)** Lipid droplets: a dynamic organelle moves into focus. *FEBS Lett.* **584**: 2176–2182
- Beresford JN, Bennett JH, Devlin C, Leboy PS, Owen ME (1992)** Evidence for an inverse relationship between the differentiation of adipocytic and osteogenic cells in rat marrow stromal cell cultures. *J Cell Sci* **102 ( Pt 2)**: 341–351
- Berge K, Tronstad KJ, Bohov P, Madsen L, Berge RK (2003)** Impact of mitochondrial beta-oxidation in fatty acid-mediated inhibition of glioma cell proliferation. *J Lipid Res* **44**: 118–127
- Birch AM, Buckett LK, Turnbull AV (2010)** DGAT1 inhibitors as anti-obesity and anti-diabetic agents. *Curr Opin Drug Discov Devel* **13**: 489–496
- Blad CC, Tang C, Offermanns S (2012)** G protein-coupled receptors for energy metabolites as new therapeutic targets. *Nat Rev Drug Discov* **11**: 603–619
- Bonen A, Campbell SE, Benton CR, Chabowski A, Coort, Susan L M, Han X, Koonen, Debby P Y, Glatz, Jan F C, Luiken, Joost J F P (2004)** Regulation of fatty acid transport by fatty acid translocase/CD36. *Proc Nutr Soc* **63**: 245–249
- Boni LT, Rando RR (1985)** The nature of protein kinase C activation by physically defined phospholipid vesicles and diacylglycerols. *J Biol Chem* **260**: 10819–10825
- Bostrom P, Andersson L, Rutberg M, Perman J, Lidberg U, Johansson BR, Fernandez-Rodriguez J, Ericson J, Nilsson T, Boren J, Olofsson S (2007)** SNARE proteins mediate fusion between cytosolic lipid droplets and are implicated in insulin sensitivity. *Nat Cell Biol* **9**: 1286–1293
- Bradford MM (1976)** A rapid and sensitive method for the quantitation of microgram quantities of protein utilizing the principle of protein-dye binding. *Anal Biochem* **72**: 248–254
- Brasaemle DL (2011)** Disseminating Phospholipid Function in Lipid Droplet Dynamics. *Cell Metabolism* **14**: 437–438
- Breymaier S (2013)** *American Medical Association.*: <http://www.ama-assn.org/ama/pub/news/news/2013/2013-06-18-new-ama-policies-annual-meeting.page>
- Brown MS, Goldstein JL (2008)** Selective versus total insulin resistance: a pathogenic paradox. *Cell Metabolism* **7**: 95–96

- Buhman KK, Chen HC, Farese, R V Jr (2001)** The enzymes of neutral lipid synthesis. *J Biol Chem* **276**: 40369–40372
- Cabrerizo Garcia L, Ramos-Levi A, Moreno Lopera C, Rubio Herrera, Miguel A (2013)** Update on pharmacology of obesity: benefits and risks. *Nutr Hosp* **28 Suppl 5**: 121–127
- Cahill K, Ussher M (2007)** Cannabinoid type 1 receptor antagonists (rimonabant) for smoking cessation. *Cochrane Database Syst Rev*: CD005353
- Cao J, Zhou Y, Peng H, Huang X, Stahler S, Suri V, Qadri A, Gareski T, Jones J, Hahm S, Perreault M, McKew J, Shi M, Xu X, Tobin JF, Gimeno RE (2011)** Targeting Acyl-CoA:Diacylglycerol Acyltransferase 1 (DGAT1) with Small Molecule Inhibitors for the Treatment of Metabolic Diseases. *J Biol Chem* **286**: 41838–41851
- Carrillo B, Lekpor K, Yanofsky C, Bell AW, Boismenu D, Kearney RE (2005)** Increasing Peptide Identification in Tandem Mass Spectrometry Through Automatic Function Switching Optimization. *Journal of the American Society for Mass Spectrometry* **16**: 1818–1826
- Carvalho FA, Carneiro FA, Martins IC, Assuncao-Miranda I, Faustino AF, Pereira RM, Bozza PT, Castanho, Miguel A R B, Mohana-Borges R, Da Poian, Andrea T, Santos NC (2012)** Dengue virus capsid protein binding to hepatic lipid droplets (LD) is potassium ion dependent and is mediated by LD surface proteins. *J Virol* **86**: 2096–2108
- Cases S, Zhou P, Shillingford JM, Wiseman BS, Fish JD, Angle CS, Hennighausen L, Werb Z, Farese, Robert V Jr (2004)** Development of the mammary gland requires DGAT1 expression in stromal and epithelial tissues. *Development* **131**: 3047–3055
- Cassisa A (2013)** Pathophysiology of subcutaneous fat. *G Ital Dermatol Venereol* **148**: 315–323
- Cermelli S, Guo Y, Gross SP, Welte MA (2006)** The Lipid-Droplet Proteome Reveals that Droplets Are a Protein-Storage Depot. *Current Biology* **16**: 1783–1795
- Chang G (2003)** Multidrug resistance ABC transporters. *126th Nobel Symposium. Membrane Proteins: Structure, Function and Assembly* **555**: 102–105
- Chen HC, Smith SJ, Ladha Z, Jensen DR, Ferreira LD, Pulawa LK, McGuire JG, Pitas RE, Eckel RH, Farese, Robert V Jr (2002)** Increased insulin and leptin sensitivity in mice lacking acyl CoA:diacylglycerol acyltransferase 1. *J Clin Invest* **109**: 1049–1055
- Chen X, Tukachinsky H, Huang C, Jao C, Chu Y, Tang H, Mueller B, Schulman S, Rapoport TA, Salic A (2011)** Processing and turnover of the Hedgehog protein in the endoplasmic reticulum. *The Journal of cell biology* **192**: 825–838
- Cheng B, Wu X, Sun S, Wu Q, Mei C, Xu Q, Wu J, He P (2014)** MAPK-PPARalpha/gamma signal transduction pathways are involved in Chlamydia pneumoniae-induced macrophage-derived foam cell formation. *Microb Pathog* **69-70**: 1–8
- Cherbas L, Willingham A, Zhang D, Yang L, Zou Y, Eads BD, Carlson JW, Landolin JM, Kapranov P, Dumais J, Samsonova A, Choi J, Roberts J, Davis CA, Tang H, van Baren, Marijke J, Ghosh S, Dobin A, Bell K, Lin W et al (2011)** The transcriptional diversity of 25 Drosophila cell lines. *Genome research* **21**: 301–314
- Cheung W, Gill M, Esposito A, Kaminski CF, Courousse N, Chwetzoff S, Trugnan G, Keshavan N, Lever A, Desselberger U (2010)** Rotaviruses associate with cellular lipid droplet components to replicate in viroplasms, and compounds disrupting or blocking lipid droplets inhibit viroplasm formation and viral replication. *J. Virol.* **84**: 6782–6798
- Chien S (2002)** Homophila: human disease gene cognates in Drosophila. *Nucleic Acids Research* **30**: 149–151
- Choi CS, Savage DB, Abu-Elheiga L, Liu Z, Kim S, Kulkarni A, Distefano A, Hwang Y, Reznick RM, Codella R, Zhang D, Cline GW, Wakil SJ, Shulman GI (2007)** Continuous fat oxidation in acetyl-CoA

carboxylase 2 knockout mice increases total energy expenditure, reduces fat mass, and improves insulin sensitivity. *Proc Natl Acad Sci U S A* **104**: 16480–16485

**Chou K, Perry CM (2013)** Metreleptin: first global approval. *Drugs* **73**: 989–997

**Colman E (2007)** Dinitrophenol and obesity: an early twentieth-century regulatory dilemma. *Regul Toxicol Pharmacol* **48**: 115–117

**Colon-Gonzalez F, Kim GW, Lin JE, Valentino MA, Waldman SA (2013)** Obesity pharmacotherapy: What is next? *Mol Aspects Med* **34**: 71–83

**Coughlan KA, Valentine RJ, Ruderman NB, Saha AK (2014)** AMPK activation: a therapeutic target for type 2 diabetes? *Diabetes Metab Syndr Obes* **7**: 241–253

**Cox J, Mann M (2008)** MaxQuant enables high peptide identification rates, individualized p.p.b.-range mass accuracies and proteome-wide protein quantification. *Nat. Biotechnol.* **26**: 1367–1372

**Czabany T, Wagner A, Zweytick D, Lohner K, Leitner E, Ingolic E, Daum G (2008)** Structural and biochemical properties of lipid particles from the yeast *Saccharomyces cerevisiae*. *The Journal of biological chemistry* **283**: 17065–17074

**Daniel J, Maamar H, Deb C, Sirakova TD, Kolattukudy PE (2011)** Mycobacterium tuberculosis uses host triacylglycerol to accumulate lipid droplets and acquires a dormancy-like phenotype in lipid-loaded macrophages. *PLoS Pathog* **7**: e1002093

**Davidson MH, Hauptman J, DiGirolamo M, Foreyt JP, Halsted CH, Heber D, Heimbürger DC, Lucas CP, Robbins DC, Chung J, Heymsfield SB (1999)** Weight control and risk factor reduction in obese subjects treated for 2 years with orlistat: a randomized controlled trial. *JAMA* **281**: 235–242

**D'Avila H, Melo, Rossana C N, Parreira GG, Werneck-Barroso E, Castro-Faria-Neto HC, Bozza PT (2006)** Mycobacterium bovis bacillus Calmette-Guerin induces TLR2-mediated formation of lipid bodies: intracellular domains for eicosanoid synthesis in vivo. *J Immunol* **176**: 3087–3097

**DeGraw AJ, Keiser MJ, Ochocki JD, Shoichet BK, Distefano MD (2010)** Prediction and evaluation of protein farnesyltransferase inhibition by commercial drugs. *J Med Chem* **53**: 2464–2471

**Dellomonaco C, Clomburg JM, Miller EN, Gonzalez R (2011)** Engineered reversal of the  $\beta$ -oxidation cycle for the synthesis of fuels and chemicals. *Nature* **476**: 355–359

**DeVita RJ, Pinto S (2013)** Current status of the research and development of diacylglycerol O-acyltransferase 1 (DGAT1) inhibitors. *J. Med. Chem.* **56**: 9820–9825

**Diaz MB, Herzig S, Vegiopoulos A (2014)** Thermogenic adipocytes: from cells to physiology and medicine. *Metabolism: clinical and experimental* **63**: 1238–1249

**Djouder N, Tuerk RD, Suter M, Salvioni P, Thali RF, Scholz R, Vaahtomeri K, Auchli Y, Rechsteiner H, Brunisholz RA, Viollet B, Mäkelä TP, Wallimann T, Neumann D, Krek W (2010)** PKA phosphorylates and inactivates AMPK $\alpha$  to promote efficient lipolysis. *The EMBO journal* **29**: 469–481

**do Carmo, J M, da Silva, A A, Morgan J, Jim Wang Y, Munusamy S, Hall JE (2012)** Inhibition of soluble epoxide hydrolase reduces food intake and increases metabolic rate in obese mice. *Nutr Metab Cardiovasc Dis* **22**: 598–604

**Dow RL, Li J, Pence MP, Gibbs EM, LaPerle JL, Litchfield J, Piotrowski DW, Munchhof MJ, Manion TB, Zavadski WJ, Walker GS, McPherson RK, Tapley S, Sugarman E, Guzman-Perez A, DaSilva-Jardine P (2011)** Discovery of PF-04620110, a Potent, Selective, and Orally Bioavailable Inhibitor of DGAT-1. *ACS Med Chem Lett* **2**: 407–412

**Draczkowski P, Matosiuk D, Jozwiak K (2012)** Affinity Chromatography as a Tool for Quantification of Interactions Between Drug Molecules and Their Protein Targets. In *Affinity Chromatography*, Magdeldin S (ed): InTech

- Drosatos K, Schulze PC (2013)** Cardiac lipotoxicity: molecular pathways and therapeutic implications. *Current heart failure reports* **10**: 109–121
- Dunican KC, Adams NM, Desilets AR (2010)** The role of pramlintide for weight loss. *Ann Pharmacother* **44**: 538–545
- Egan AG, Blind E, Dunder K, de Graeff, Pieter A, Hummer BT, Bourcier T, Rosebraugh C (2014)** Pancreatic safety of incretin-based drugs--FDA and EMA assessment. *N. Engl. J. Med.* **370**: 794–797
- Eichmann TO, Kumari M, Haas JT, Farese, Robert V Jr, Zimmermann R, Lass A, Zechner R (2012)** Studies on the substrate and stereo/regioselectivity of adipose triglyceride lipase, hormone-sensitive lipase, and diacylglycerol-O-acyltransferases. *J Biol Chem* **287**: 41446–41457
- Eidhammer I, Barsnes H, Eide GE, Martens L (2013)** *Computational and statistical methods for protein quantification by mass spectrometry*
- EMA (2013)** *Withdrawal of the marketing authorisation application for Belviq (lorcaserin)*, London
- Falconer RJ, Collins BM (2011)** Survey of the year 2009: applications of isothermal titration calorimetry. *J Mol Recognit* **24**: 1–16
- Farese RV, Walther TC (2009)** Lipid droplets finally get a little R-E-S-P-E-C-T. *Cell* **139**: 855–860
- FDA (2007)** *Questions and Answers about Withdrawal of Fenfluramine (Pondimin) and Dexfenfluramine (Redux)*
- FDA Release (1997)** *FDA Announces Withdrawal Fenfluramine and Dexfenfluramine (Fen-Phen)*. <http://www.fda.gov/Drugs/DrugSafety/PostmarketDrugSafetyInformationforPatientsandProviders/ucm179871.htm>. July 2014
- FDA Release (2007)** *Rimonabant Briefing Document: NDA 21-888*. Clinical Review of Safety and Efficacy:
- Fedorenko A, Lishko PV, Kirichok Y (2012)** Mechanism of Fatty-Acid-Dependent UCP1 Uncoupling in Brown Fat Mitochondria. *Cell* **151**: 400–413
- Fernandez-Patron C, Castellanos-Serra L, Hardy E, Guerra M, Estevez E, Mehl E, Frank RW (1998)** Understanding the mechanism of the zinc-ion stains of biomacromolecules in electrophoresis gels: generalization of the reverse-staining technique. *Electrophoresis* **19**: 2398–2406
- Fidler MC, Sanchez M, Raether B, Weissman NJ, Smith SR, Shanahan WR, Anderson CM (2011)** A one-year randomized trial of lorcaserin for weight loss in obese and overweight adults: the BLOSSOM trial. *J. Clin. Endocrinol. Metab.* **96**: 3067–3077
- Finkelstein EA, Trogdon JG, Cohen JW, Dietz W (2009)** Annual medical spending attributable to obesity: payer-and service-specific estimates. *Health Aff (Millwood)* **28**: w822-31
- Fong TM, Heymsfield SB (2009)** Cannabinoid-1 receptor inverse agonists: current understanding of mechanism of action and unanswered questions. *Int J Obes (Lond)* **33**: 947–955
- Foster DW (2012)** Malonyl-CoA: the regulator of fatty acid synthesis and oxidation. *J. Clin. Invest.* **122**: 1958–1959
- Fox B, Furukawa N, Hao X, Iio K, Inaba T, Jackson S, Kayser F, Labelle M, Li K, Matsui T, McMinn D, Ogawa N, Rubenstein S, Sagawa S, Sugimoto K, Suzuki M, Tanaka M, Ye G, Yoshida A, Zhang J (2003)** *Fused bicyclic nitrogen-containing heterocycles*
- Freitas P, Carvalho D (2013)** Lipodystrophy: beyond generalization? *Panminerva Med* **55**: 253–268
- Fujimoto T, Ohsaki Y (2006)** Cytoplasmic lipid droplets: rediscovery of an old structure as a unique platform. *Ann N Y Acad Sci* **1086**: 104–115
- Galmarini CM, Mackey JR, Dumontet C (2001)** Nucleoside analogues: mechanisms of drug resistance and reversal strategies. *Leukemia* **15**: 875–890

- Ganguly J (1960)** Studies on the mechanism of fatty acid synthesis: VII. Biosynthesis of fatty acids from malonyl CoA. *Biochimica et Biophysica Acta* **40**: 110–118
- Goh VJ, Silver DL (2013)** The lipid droplet as a potential therapeutic target in NAFLD. *Seminars in liver disease* **33**: 312–320
- Gonnet M, Lethuaut L, Boury F (2010)** New trends in encapsulation of liposoluble vitamins. *J Control Release* **146**: 276–290
- Grahn TH, Kaur R, Yin J, Schweiger M, Sharma V, Lee M, Ido Y, Zechner R, Lass A, Puri V (2014)** Fat-specific protein 27 (FSP27) interacts with adipose triglyceride lipase (ATGL) to regulate lipolysis and insulin sensitivity in human adipocytes. *J Biol Chem* **289**: 12029–12039
- Granchi C, Fancelli D, Minutolo F (2014)** An update on therapeutic opportunities offered by cancer glycolytic metabolism. *Bioorg Med Chem Lett*
- Greenberg AS, Coleman RA, Kraemer FB, McManaman JL, Obin MS, Puri V, Yan Q, Miyoshi H, Mashek DG (2011)** The role of lipid droplets in metabolic disease in rodents and humans. *J. Clin. Invest.* **121**: 2102–2110
- Gregoire FM, Smas CM, Sul HS (1998)** Understanding adipocyte differentiation. *Physiol Rev* **78**: 783–809
- Griffin JP, Posner J, Barker GR (2013)** *The textbook of pharmaceutical medicine*. Wiley-Blackwell; BMJ Books, Chichester, West Sussex [U.K.]
- Grimard V, Massier J, Richter D, Schwudke D, Kalaidzidis Y, Fava E, Hermetter A, Thiele C (2008)** siRNA screening reveals JNK2 as an evolutionary conserved regulator of triglyceride homeostasis. *J Lipid Res* **49**: 2427–2440
- Gronke S, Beller M, Fellert S, Ramakrishnan H, Jackle H, Kuhnlein RP (2003)** Control of fat storage by a Drosophila PAT domain protein. *Curr Biol* **13**: 603–606
- Gross SP, Guo Y, Martinez JE, Welte MA (2003)** A determinant for directionality of organelle transport in Drosophila embryos. *Curr Biol* **13**: 1660–1668
- Guebre-Egziabher F, Alix PM, Koppe L, Pelletier CC, Kalbacher E, Fouque D, Soulage CO (2013)** Ectopic lipid accumulation: A potential cause for metabolic disturbances and a contributor to the alteration of kidney function. *Biochimie* **95**: 1971–1979
- Guengerich FP (2006)** Cytochrome P450s and other enzymes in drug metabolism and toxicity. *AAPS J* **8**: E101-11
- Guo Y, Walther TC, Rao M, Stuurman N, Goshima G, Terayama K, Wong JS, Vale RD, Walter P, Farese RV (2008)** Functional genomic screen reveals genes involved in lipid-droplet formation and utilization. *Nature* **453**: 657–661
- Gupta V, Wellen KE, Mazurek S, Bamezai, Rameshwar N K (2014)** Pyruvate kinase M2: regulatory circuits and potential for therapeutic intervention. *Curr Pharm Des* **20**: 2595–2606
- Hamilton JA (1998)** Fatty acid transport: difficult or easy? *J Lipid Res* **39**: 467–481
- Hanahan D (1983)** Studies on transformation of Escherichia coli with plasmids. *J Mol Biol* **166**: 557–580
- Hanke S, Besir H, Oesterhelt D, Mann M (2008)** Absolute SILAC for accurate quantitation of proteins in complex mixtures down to the attomole level. *Journal of proteome research* **7**: 1118–1130
- Harper JA, Dickinson K, Brand MD (2001)** Mitochondrial uncoupling as a target for drug development for the treatment of obesity. *Obesity Reviews* **2**: 255–265

- He S, McPhaul C, Li JZ, Garuti R, Kinch L, Grishin NV, Cohen JC, Hobbs HH (2010)** A sequence variation (I148M) in PNPLA3 associated with nonalcoholic fatty liver disease disrupts triglyceride hydrolysis. *The Journal of biological chemistry* **285**: 6706–6715
- Heckmann BL, Zhang X, Xie X, Liu J (2013)** The G0/G1 switch gene 2 (GOS2): regulating metabolism and beyond. *Biochim. Biophys. Acta* **1831**: 276–281
- Herker E, Harris C, Hernandez C, Carpentier A, Kaehlcke K, Rosenberg AR, Farese RV, Ott M (2010)** Efficient hepatitis C virus particle formation requires diacylglycerol acyltransferase-1. *Nat. Med.* **16**: 1295–1298
- Herker E, Ott M (2011)** Unique ties between hepatitis C virus replication and intracellular lipids. *Trends Endocrinol. Metab.* **22**: 241–248
- Hermes A, Bosch M, Ariotti N, Reddy, Babu J N, Fajardo A, Fernández-Vidal A, Alvarez-Guaita A, Fernández-Rojo MA, Rentero C, Tebar F, Enrich C, Geli M, Parton RG, Gross SP, Pol A (2013)** Cell-to-cell heterogeneity in lipid droplets suggests a mechanism to reduce lipotoxicity. *Curr. Biol.* **23**: 1489–1496
- Heslegrave AJ, Hussain K (2013)** Novel insights into fatty acid oxidation, amino acid metabolism, and insulin secretion from studying patients with loss of function mutations in 3-hydroxyacyl-CoA dehydrogenase. *J Clin Endocrinol Metab* **98**: 496–501
- Hildebrandt A, Bickmeyer I, Kühnlein RP (2011)** Reliable Drosophila body fat quantification by a coupled colorimetric assay. *PLoS one* **6**: e23796
- Hill-Baskin AE, Markiewski MM, Buchner DA, Shao H, DeSantis D, Hsiao G, Subramaniam S, Berger NA, Croniger C, Lambris JD, Nadeau JH (2009)** Diet-induced hepatocellular carcinoma in genetically predisposed mice. *Human molecular genetics* **18**: 2975–2988
- Hiramane Y, Tanabe T (2011)** Characterization of acyl-coenzyme A:diacylglycerol acyltransferase (DGAT) enzyme of human small intestine. *J Physiol Biochem* **67**: 259–264
- Hirosumi J, Tuncman G, Chang L, Gorgun CZ, Uysal KT, Maeda K, Karin M, Hotamisligil GS (2002)** A central role for JNK in obesity and insulin resistance. *Nature* **420**: 333–336
- Imig JD, Hammock BD (2009)** Soluble epoxide hydrolase as a therapeutic target for cardiovascular diseases. *Nat Rev Drug Discov* **8**: 794–805
- Ivashov VA, Grillitsch K, Koefeler H, Leitner E, Baeumlisberger D, Karas M, Daum G (2013)** Lipidome and proteome of lipid droplets from the methylotrophic yeast *Pichia pastoris*. *Biochim. Biophys. Acta* **1831**: 282–290
- Jacquier N, Choudhary V, Mari M, Toulmay A, Reggiori F, Schneiter R (2011)** Lipid droplets are functionally connected to the endoplasmic reticulum in *Saccharomyces cerevisiae*. *J. Cell. Sci.* **124**: 2424–2437
- James AW, Leucht P, Levi B, Carre AL, Xu Y, Helms JA, Longaker MT (2010)** Sonic Hedgehog influences the balance of osteogenesis and adipogenesis in mouse adipose-derived stromal cells. *Tissue Eng Part A* **16**: 2605–2616
- Jerabek-Willemsen M, Wienken CJ, Braun D, Baaske P, Duhr S (2011)** Molecular Interaction Studies Using Microscale Thermophoresis. *Assay Drug Dev Technol* **9**: 342–353
- Kaplan LM (2010)** Pharmacologic therapies for obesity. *Gastroenterol Clin North Am* **39**: 69–79
- Katsuura M, Hosono-Sakuma Y, Wagatsuma M, Yanagisawa S, Okazaki M, Kimura M (1999)** The NH<sub>2</sub>-terminal region of the active domain of sonic hedgehog is necessary for its signal transduction. *FEBS Letters* **447**: 325–328
- Keiser MJ, Roth BL, Armbruster BN, Ernsberger P, Irwin JJ, Shoichet BK (2007)** Relating protein pharmacology by ligand chemistry. *Nat Biotechnol* **25**: 197–206



**Keiser MJ, Setola V, Irwin JJ, Laggner C, Abbas A, Hufeisen SJ, Jensen NH, Kuijter MB, Matos RC, Tran TB, Whaley R, Glennon RA, Hert J, Thomas KL, Edwards DD, Shoichet BK, Roth BL (2009)** Predicting new molecular targets for known drugs. *Nature* **462**: 175–181

**KENNEDY EP (1957)** Metabolism of lipides. *Annu Rev Biochem* **26**: 119–148

**Kim GW, Lin JE, Blomain ES, Waldman SA (2014)** Anti-Obesity Pharmacotherapy: New Drugs and Emerging Targets. *Clin Pharmacol Ther* **95**: 53–66

**Koenig T, Menze BH, Kirchner M, Monigatti F, Parker KC, Patterson T, Steen JJ, Hamprecht FA, Steen H (2008)** Robust prediction of the MASCOT score for an improved quality assessment in mass spectrometric proteomics. *J Proteome Res* **7**: 3708–3717

**Konieczny SF, Emerson, C P Jr (1984)** 5-Azacytidine induction of stable mesodermal stem cell lineages from 10T1/2 cells: evidence for regulatory genes controlling determination. *Cell* **38**: 791–800

**Krahmer N, Guo Y, Wilfling F, Hilger M, Lingrell S, Heger K, Newman HW, Schmidt-Supprian M, Vance DE, Mann M, Farese RV, Walther TC (2011)** Phosphatidylcholine synthesis for lipid droplet expansion is mediated by localized activation of CTP:phosphocholine cytidyltransferase. *Cell Metab.* **14**: 504–515

**Kuerschner L, Moessinger C, Thiele C (2008)** Imaging of lipid biosynthesis: how a neutral lipid enters lipid droplets. *Traffic* **9**: 338–352

**Kulkarni SS, Karlsson, Hakan K R, Szekeres F, Chibalin AV, Krook A, Zierath JR (2011)** Suppression of 5'-nucleotidase enzymes promotes AMP-activated protein kinase (AMPK) phosphorylation and metabolism in human and mouse skeletal muscle. *J Biol Chem* **286**: 34567–34574

**Laemmli UK (1970)** Cleavage of structural proteins during the assembly of the head of bacteriophage T4. *Nature* **227**: 680–685

**Lakshman R, Elks CE, Ong KK (2012)** CHILDHOOD OBESITY. *Circulation* **126**: 1770–1779

**Lass A, Zimmermann R, Oberer M, Zechner R (2011)** Lipolysis - a highly regulated multi-enzyme complex mediates the catabolism of cellular fat stores. *Prog. Lipid Res.* **50**: 14–27

**Lawrence Bachorik (1997)** FDA Announces Withdrawal Fenfluramine and Dexfenfluramine (Fen-Phen). P97-32. FDA

**Lee C, Woo Y, Wang Y, Yeung C, Xu A, Lam K (2014)** Obesity, adipokines and cancer: An update. *Clin Endocrinol (Oxf)*

**Lee JJ, Kong M, Ayers GD, Lotan R (2007)** Interaction index and different methods for determining drug interaction in combination therapy. *J Biopharm Stat* **17**: 461–480

**Li AC, Glass CK (2002)** The macrophage foam cell as a target for therapeutic intervention. *Nature medicine* **8**: 1235–1242

**Li K, Brownley A (2010)** Primer design for RT-PCR. *Methods Mol. Biol.* **630**: 271–299

**Lisi S, Mazzon I, White K (2000)** Diverse domains of THREAD/DIAP1 are required to inhibit apoptosis induced by REAPER and HID in *Drosophila*. *Genetics* **154**: 669–678

**Liu Q, Siloto, Rodrigo M. P., Lehner R, Stone SJ, Weselake RJ (2012a)** Acyl-CoA:diacylglycerol acyltransferase: Molecular biology, biochemistry and biotechnology. *Progress in Lipid Research* **51**: 350–377

**Liu Y, Dang H, Li D, Pang W, Hammock BD, Zhu Y (2012b)** Inhibition of soluble epoxide hydrolase attenuates high-fat-diet-induced hepatic steatosis by reduced systemic inflammatory status in mice. *PLoS One* **7**: e39165

- Lopes, José L. S., Nobre TM, Cilli EM, Beltramini LM, Araújo, Ana P. U., Wallace BA (2014)** Deconstructing the DGAT1 enzyme: Binding sites and substrate interactions. *Biochimica et Biophysica Acta (BBA) - Biomembranes* **1838**: 3145–3152
- Lopez-Jaramillo P, Gomez-Arbelaez D, Lopez-Lopez J, Lopez-Lopez C, Martinez-Ortega J, Gomez-Rodriguez A, Triana-Cubillos S (2014)** The role of leptin/adiponectin ratio in metabolic syndrome and diabetes. *Horm Mol Biol Clin Investig* **18**: 37–45
- Lopez-Jimenez F (2009)** Speakable and unspeakable facts about BMI and mortality. *The Lancet* **373**: 1055–1056
- Luria A, Morisseau C, Tsai H, Yang J, Inceoglu B, Taeye B de, Watkins SM, Wiest MM, German JB, Hammock BD (2009)** Alteration in plasma testosterone levels in male mice lacking soluble epoxide hydrolase. *Am J Physiol Endocrinol Metab* **297**: E375-83
- Mahgerefteh B, Vigue M, Freestone Z, Silver S, Nguyen Q (2013)** New Drug Therapies for the Treatment of Overweight and Obese Patients. *Am Health Drug Benefits* **6**: 423–430
- Manhattan Pharmaceuticals (2007)** *Phase 2a Obesity Study of Oral Doses of Oleoyl-Estrone (MP-101)*: NCT00449202, New York
- Mann M (2014)** Fifteen Years of Stable Isotope Labeling by Amino Acids in Cell Culture (SILAC). *Methods Mol. Biol.* **1188**: 1–7
- Manning S, Pucci A, Finer N (2014)** Pharmacotherapy for obesity: novel agents and paradigms. *Ther Adv Chronic Dis* **5**: 135–148
- Marshall AJ (1961)** *Biology and comparative physiology of birds: Band II*
- Martin S, Parton RG (2006)** Lipid droplets: a unified view of a dynamic organelle. *Nature reviews. Molecular cell biology* **7**: 373–378
- Mathias Beller (2005)** *Identification and characterization of Drosophila lipid droplet-associated proteins*. Dissertation, Braunschweig
- Matsuda D, Tomoda H (2010)** Triazolo compounds useful as diacylglycerol acyltransferase1 inhibitor - WO2009126624. *Expert Opin Ther Pat* **20**: 1097–1102
- Mattos KA, D'Avila H, Rodrigues LS, Oliveira, Viviane G C, Sarno EN, Atella GC, Pereira GM, Bozza PT, Pessolani, Maria Cristina V (2010)** Lipid droplet formation in leprosy: Toll-like receptor-regulated organelles involved in eicosanoid formation and Mycobacterium leprae pathogenesis. *J Leukoc Biol* **87**: 371–384
- Mayer N, Schweiger M, Romauch M, Grabner GF, Eichmann TO, Fuchs E, Ivkovic J, Heier C, Mrak I, Lass A, Hofler G, Fledelius C, Zechner R, Zimmermann R, Breinbauer R (2013)** Development of small-molecule inhibitors targeting adipose triglyceride lipase. *Nat Chem Biol* **9**: 785–787
- McDonough PM, Agustin RM, Ingermanson RS, Loy PA, Buehrer BM, Nicoll JB, Prigozhina NL, Mikic I, Price JH (2009)** Quantification of Lipid Droplets and Associated Proteins in Cellular Models of Obesity via High-Content/High-Throughput Microscopy and Automated Image Analysis. *Assay Drug Dev Technol* **7**: 440–460
- McGee SL, van Denderen, Bryce J W, Howlett KF, Mollica J, Schertzer JD, Kemp BE, Hargreaves M (2008)** AMP-activated protein kinase regulates GLUT4 transcription by phosphorylating histone deacetylase 5. *Diabetes* **57**: 860–867
- McManaman JL, Bales ES, Orlicky DJ, Jackman M, MacLean PS, Cain S, Crunk AE, Mansur A, Graham CE, Bowman TA, Greenberg AS (2013)** Perilipin-2-null mice are protected against diet-induced obesity, adipose inflammation, and fatty liver disease. *Journal of lipid research* **54**: 1346–1359

- Morak M, Schmidinger H, Riesenhuber G, Rechberger GN, Kollroser M, Haemmerle G, Zechner R, Kronenberg F, Hermetter A (2012)** Adipose triglyceride lipase (ATGL) and hormone-sensitive lipase (HSL) deficiencies affect expression of lipolytic activities in mouse adipose tissues. *Molecular & cellular proteomics : MCP* **11**: 1777–1789
- Morisseau C (2013)** Role of epoxide hydrolases in lipid metabolism. *Biochimie* **95**: 91–95
- Morisseau C, Schebb NH, Dong H, Ulu A, Aronov PA, Hammock BD (2012)** Role of soluble epoxide hydrolase phosphatase activity in the metabolism of lysophosphatidic acids. *Biochem Biophys Res Commun* **419**: 796–800
- Murphy DJ (2001)** The biogenesis and functions of lipid bodies in animals, plants and microorganisms. *Progress in Lipid Research* **40**: 325–438
- Nagelin MH, Srinivasan S, Nadler JL, Hedrick CC (2009)** Murine 12/15-lipoxygenase regulates ATP-binding cassette transporter G1 protein degradation through p38- and JNK2-dependent pathways. *J. Biol. Chem.* **284**: 31303–31314
- Nathan PJ, O'Neill BV, Napolitano A, Bullmore ET (2011)** Neuropsychiatric adverse effects of centrally acting antiobesity drugs. *CNS Neurosci Ther* **17**: 490–505
- Nestle M (2007)** *Food politics: How the food industry influences nutrition and health*. University of California Press, Berkeley
- Novo Nordisk-Company Announcement (2013)** *Novo Nordisk reports 8% weight loss in phase 3a obesity trial with liraglutide 3 mg*, Bagsværd
- Ogawa K, Hishiki T, Shimizu Y, Funami K, Sugiyama K, Miyanari Y, Shimotohno K (2009)** Hepatitis C virus utilizes lipid droplet for production of infectious virus. *Proc Jpn Acad Ser B Phys Biol Sci* **85**: 217–228
- Ohsaki Y, Suzuki M, Fujimoto T (2014)** Open questions in lipid droplet biology. *Chem Biol* **21**: 86–96
- Okumura T (2011)** Role of lipid droplet proteins in liver steatosis. *Journal of physiology and biochemistry* **67**: 629–636
- Oral EA, Simha V, Ruiz E, Andewelt A, Premkumar A, Snell P, Wagner AJ, DePaoli AM, Reitman ML, Taylor SI, Gorden P, Garg A (2002)** Leptin-replacement therapy for lipodystrophy. *N. Engl. J. Med.* **346**: 570–578
- Osto E, Matter CM, Kouroedov A, Malinski T, Bachschmid M, Camici GG, Kilic U, Stallmach T, Boren J, Iliceto S, Luscher TF, Cosentino F (2008)** c-Jun N-terminal kinase 2 deficiency protects against hypercholesterolemia-induced endothelial dysfunction and oxidative stress. *Circulation* **118**: 2073–2080
- Ouimet M, Franklin V, Mak E, Liao X, Tabas I, Marcel YL (2011)** Autophagy regulates cholesterol efflux from macrophage foam cells via lysosomal acid lipase. *Cell Metabolism* **13**: 655–667
- Padmanabha D, Baker KD (2014)** Drosophila gains traction as a repurposed tool to investigate metabolism. *Trends Endocrinol. Metab.*
- Pi-Sunyer FX, Aronne LJ, Heshmati HM, Devin J, Rosenstock J (2006)** Effect of rimonabant, a cannabinoid-1 receptor blocker, on weight and cardiometabolic risk factors in overweight or obese patients: RIO-North America: a randomized controlled trial. *JAMA* **295**: 761–775
- Ploss A, Dubuisson J (2012)** New advances in the molecular biology of hepatitis C virus infection: towards the identification of new treatment targets. *Gut* **61 Suppl 1**: i25-35
- Pospisilik J, Schramek D, Schnidar H, Cronin, Shane J. F., Nehme NT, Zhang X, Knauf C, Cani PD, Aumayr K, Todoric J, Bayer M, Haschemi A, Puvion-Vandier V, Tar K, Orthofer M, Neely, G. Gregory,**

- Dietzl G, Manoukian A, Funovics M, Prager G et al (2010)** Drosophila Genome-wide Obesity Screen Reveals Hedgehog as a Determinant of Brown versus White Adipose Cell Fate. *Cell* **140**: 148–160
- Poulos SP, Dodson MV, Hausman GJ (2010)** Cell line models for differentiation: preadipocytes and adipocytes. *Exp Biol Med (Maywood)* **235**: 1185–1193
- Prasad, G V Ramesh (2014)** Metabolic syndrome and chronic kidney disease: Current status and future directions. *World J Nephrol* **3**: 210–219
- Qi J, Lang W, Geisler JG, Wang P, Petrounia I, Mai S, Smith C, Askari H, Struble GT, Williams R, Bhanot S, Monia BP, Bayoumy S, Grant E, Caldwell GW, Todd MJ, Liang Y, Gaul MD, Demarest KT, Connelly MA (2012)** The use of stable isotope-labeled glycerol and oleic acid to differentiate the hepatic functions of DGAT1 and -2. *J Lipid Res* **53**: 1106–1116
- Rappsilber J, Mann M, Ishihama Y (2007)** Protocol for micro-purification, enrichment, pre-fractionation and storage of peptides for proteomics using StageTips. *Nat Protoc* **2**: 1896–1906
- Rasouli N, Molavi B, Elbein SC, Kern PA (2007)** Ectopic fat accumulation and metabolic syndrome. *Diabetes, obesity & metabolism* **9**: 1–10
- Regensteiner JG, Reusch J, Stewart KJ, Veves A (2009)** *Diabetes and Exercise*. Humana Press
- Remesar X, Fernandez-Lopez JA, Alemany M (2012)** Oleoyl-estrone. *Med Res Rev* **32**: 1263–1291
- Ricci R, Sumara G, Sumara I, Rozenberg I, Kurrer M, Akhmedov A, Hersberger M, Eriksson U, Eberli FR, Becher B, Borén J, Chen M, Cybulsky MI, Moore KJ, Freeman MW, Wagner EF, Matter CM, Lüscher TF (2004)** Requirement of JNK2 for scavenger receptor A-mediated foam cell formation in atherogenesis. *Science* **306**: 1558–1561
- Robenek H, Hofnagel O, Buers I, Robenek MJ, Troyer D, Severs NJ (2006)** Adipophilin-enriched domains in the ER membrane are sites of lipid droplet biogenesis. *J Cell Sci* **119**: 4215–4224
- Rodgers RJ, Tschöp MH, Wilding, John P H (2012)** Anti-obesity drugs: past, present and future. *Dis Model Mech* **5**: 621–626
- Rogers MA, Liu J, Song B, Li B, Chang, Catherine C Y, Chang T (2014a)** Acyl-CoA:cholesterol acyltransferases (ACATs/SOATs): Enzymes with multiple sterols as substrates and as activators. *The Journal of steroid biochemistry and molecular biology*
- Rogers SL, Hughes BA, Jones CA, Freedman L, Smart K, Taylor N, Stewart PM, Shackleton, Cedric H L, Krone NP, Blissett J, Tomlinson JW (2014b)** Diminished 11 $\beta$ -hydroxysteroid dehydrogenase type 2 activity is associated with decreased weight and weight gain across the first year of life. *The Journal of clinical endocrinology and metabolism* **99**: E821-31
- Rohla M, Weiss TW (2013)** Metabolic syndrome, inflammation and atherothrombosis. *Hamostaseologie* **33**: 283–294
- Rosso N, Chavez-Tapia NC, Tiribelli C, Bellentani S (2014)** Translational approaches: From fatty liver to non-alcoholic steatohepatitis. *World J Gastroenterol* **20**: 9038–9049
- Sabini E, Hazra S, Konrad M, Burley SK, Lavie A (2007)** Structural basis for activation of the therapeutic L-nucleoside analogs 3TC and troxacitabine by human deoxycytidine kinase. *Nucleic Acids Res* **35**: 186–192
- Sabini E, Ort S, Monnerjahn C, Konrad M, Lavie A (2003)** Structure of human dCK suggests strategies to improve anticancer and antiviral therapy. *Nat Struct Biol* **10**: 513–519
- Sanchis D, Balada F, del Mar Grasa, M, Virgili J, Peinado J, Monserrat C, Fernandez-Lopez JA, Remesar X, Alemany M (1996)** Oleoyl-estrone induces the loss of body fat in rats. *Int J Obes Relat Metab Disord* **20**: 588–594
- Schlemper T (2014)** *Drosophila als Modellorganismus zur Charakterisierung von neuen pharmakologisch aktiven Inhibitoren der Lipidspeicherung: Masterarbeit angefertigt an der HHU*

- Schmidt C, Ploier B, Koch B, Daum G (2013)** Analysis of yeast lipid droplet proteome and lipidome. *Methods Cell Biol.* **116**: 15–37
- Schulz N, Himmelbauer H, Rath M, van Weeghel M, Houten S, Kulik W, Suhre K, Scherneck S, Vogel H, Kluge R, Wiedmer P, Joost H, Schurmann A (2011)** Role of medium- and short-chain L-3-hydroxyacyl-CoA dehydrogenase in the regulation of body weight and thermogenesis. *Endocrinology* **152**: 4641–4651
- Scully T (2014)** Public health: Society at large. *Nature* **508**: S50-1
- Seckl JR, Dow RC, Low SC, Edwards CR, Fink G (1993)** The 11 beta-hydroxysteroid dehydrogenase inhibitor glycyrrhetic acid affects corticosteroid feedback regulation of hypothalamic corticotrophin-releasing peptides in rats. *J Endocrinol* **136**: 471–477
- Shafqat N, Marschall H, Filling C, Nordling E, Wu X, Bjork L, Thyberg J, Martensson E, Salim S, Jornvall H, Oppermann U (2003)** Expanded substrate screenings of human and Drosophila type 10/17beta-hydroxysteroid dehydrogenases (HSDs) reveal multiple specificities in bile acid and steroid hormone metabolism: characterization of multifunctional 3alpha/7alpha/7beta/17beta/20beta/21-HSD. *Biochem J* **376**: 49–60
- Shahrezaei V, Swain PS (2008)** The stochastic nature of biochemical networks. *Curr. Opin. Biotechnol.* **19**: 369–374
- Shin SM, Cho IJ, Kim SG (2009)** Resveratrol protects mitochondria against oxidative stress through AMP-activated protein kinase-mediated glycogen synthase kinase-3beta inhibition downstream of poly(ADP-ribose)polymerase-LKB1 pathway. *Molecular pharmacology* **76**: 884–895
- Shockey JM, Gidda SK, Chapital DC, Kuan J, Dhanoa PK, Bland JM, Rothstein SJ, Mullen RT, Dyer JM (2006)** Tung tree DGAT1 and DGAT2 have nonredundant functions in triacylglycerol biosynthesis and are localized to different subdomains of the endoplasmic reticulum. *Plant Cell* **18**: 2294–2313
- Siegel-Axel D, Daub K, Seizer P, Lindemann S, Gawaz M (2008)** Platelet lipoprotein interplay: trigger of foam cell formation and driver of atherosclerosis. *Cardiovasc. Res.* **78**: 8–17
- Sjostrom L, Rissanen A, Andersen T, Boldrin M, Golay A, Koppeschaar HP, Krempf M (1998)** Randomised placebo-controlled trial of orlistat for weight loss and prevention of weight regain in obese patients. European Multicentre Orlistat Study Group. *Lancet* **352**: 167–172
- Sliwoski G, Kothiwale S, Meiler J, Lowe, Edward W Jr (2014)** Computational methods in drug discovery. *Pharmacol Rev* **66**: 334–395
- Smirnova E, Goldberg EB, Makarova KS, Lin L, Brown WJ, Jackson CL (2006)** ATGL has a key role in lipid droplet/adiposome degradation in mammalian cells. *EMBO Rep* **7**: 106–113
- Speakman JR (2013)** Evolutionary perspectives on the obesity epidemic: adaptive, maladaptive, and neutral viewpoints. *Annu. Rev. Nutr.* **33**: 289–317
- Stevens GA, Singh GM, Lu Y, Danaei G, Lin JK, Finucane MM, Bahalim AN, McIntire RK, Gutierrez HR, Cowan M, Paciorek CJ, Farzadfar F, Riley L, Ezzati M (2012)** National, regional, and global trends in adult overweight and obesity prevalences. *Popul Health Metr* **10**: 22
- Stone SJ, Levin MC, Zhou P, Han J, Walther TC, Farese RV (2009)** The endoplasmic reticulum enzyme DGAT2 is found in mitochondria-associated membranes and has a mitochondrial targeting signal that promotes its association with mitochondria. *The Journal of biological chemistry* **284**: 5352–5361
- Stone SJ, Myers HM, Watkins SM, Brown BE, Feingold KR, Elias PM, Farese, Robert V Jr (2004)** Lipopenia and skin barrier abnormalities in DGAT2-deficient mice. *J Biol Chem* **279**: 11767–11776
- Suzuki M, Ohsaki Y, Tatematsu T, Shinohara Y, Maeda T, Cheng J, Fujimoto T (2012)** Translation inhibitors induce formation of cholesterol ester-rich lipid droplets. *PLoS one* **7**: e42379

- Suzuki M, Shinohara Y, Ohsaki Y, Fujimoto T (2011)** Lipid droplets: size matters. *J Electron Microsc (Tokyo)* **60 Suppl 1**: S101-16
- Teixeira L, Rabouille C, Rorth P, Ephrussi A, Vanzo NF (2003)** Drosophila Perilipin/ADRP homologue Lsd2 regulates lipid metabolism. *Mech Dev* **120**: 1071–1081
- Thaller G, Kramer W, Winter A, Kaupe B, Erhardt G, Fries R (2003)** Effects of DGAT1 variants on milk production traits in German cattle breeds. *J Anim Sci* **81**: 1911–1918
- Thiam AR, Farese RV, Walther TC (2013)** The biophysics and cell biology of lipid droplets. *Nat. Rev. Mol. Cell Biol.* **14**: 775–786
- Thupari JN, Pinn ML, Kuhajda FP (2001)** Fatty Acid Synthase Inhibition in Human Breast Cancer Cells Leads to Malonyl-CoA-Induced Inhibition of Fatty Acid Oxidation and Cytotoxicity. *Biochemical and Biophysical Research Communications* **285**: 217–223
- Tomoda H, Omura S (2007)** Potential therapeutics for obesity and atherosclerosis: inhibitors of neutral lipid metabolism from microorganisms. *Pharmacol. Ther.* **115**: 375–389
- Towbin H, Staehelin T, Gordon J (1979)** Electrophoretic transfer of proteins from polyacrylamide gels to nitrocellulose sheets: procedure and some applications. *Proc Natl Acad Sci U S A* **76**: 4350–4354
- Tronstad KJ, Gjertsen BT, Krakstad C, Berge K, Brustugun OT, Døskeland SO, Berge RK (2003)** Mitochondrial-Targeted Fatty Acid Analog Induces Apoptosis with Selective Loss of Mitochondrial Glutathione in Promyelocytic Leukemia Cells. *Chemistry & Biology* **10**: 609–618
- Tsuchiya S, Kobayashi Y, Goto Y, Okumura H, Nakae S, Konno T, Tada K (1982)** Induction of maturation in cultured human monocytic leukemia cells by a phorbol diester. *Cancer Res* **42**: 1530–1536
- Tuncman G, Hirosumi J, Solinas G, Chang L, Karin M, Hotamisligil GS (2006)** Functional in vivo interactions between JNK1 and JNK2 isoforms in obesity and insulin resistance. *Proc Natl Acad Sci U S A* **103**: 10741–10746
- Turchetto-Zolet AC, Maraschin FS, de Morais, Guilherme L, Cagliari A, Andrade, Cláudia M B, Margis-Pinheiro M, Margis R (2011)** Evolutionary view of acyl-CoA diacylglycerol acyltransferase (DGAT), a key enzyme in neutral lipid biosynthesis. *BMC evolutionary biology* **11**: 263
- Ui K, Nishihara S, Sakuma M, Togashi S, Ueda R, Miyata Y, Miyake T (1994)** Newly established cell lines from Drosophila larval CNS express neural specific characteristics. *In Vitro Cell Dev Biol Anim* **30A**: 209–216
- Vander Heiden, Matthew G., Cantley LC, Thompson CB (2009)** Understanding the Warburg Effect: The Metabolic Requirements of Cell Proliferation. *Science* **324**: 1029–1033
- Vickers MH (2014)** Developmental programming and transgenerational transmission of obesity. *Ann. Nutr. Metab.* **64 Suppl 1**: 26–34
- Vigouroux C, Caron-Debarle M, Le Dour C, Magré J, Capeau J (2011)** Molecular mechanisms of human lipodystrophies: from adipocyte lipid droplet to oxidative stress and lipotoxicity. *The international journal of biochemistry & cell biology* **43**: 862–876
- Vingtdeux V, Chandakkar P, Zhao H, Davies P, Marambaud P (2011)** Small-molecule activators of AMP-activated protein kinase (AMPK), RSVA314 and RSVA405, inhibit adipogenesis. *Mol Med* **17**: 1022–1030
- Viollet B, Horman S, Leclerc J, Lantier L, Foretz M, Billaud M, Giri S, Andreelli F (2010)** AMPK inhibition in health and disease. *Crit Rev Biochem Mol Biol* **45**: 276–295
- Walther TC, Farese RV (2012)** Lipid droplets and cellular lipid metabolism. *Annu. Rev. Biochem.* **81**: 687–714

- Wang H, Sreenivasan U, Hu H, Saladino A, Polster BM, Lund LM, Gong D, Stanley WC, Sztalryd C (2011)** Perilipin 5, a lipid droplet-associated protein, provides physical and metabolic linkage to mitochondria. *J Lipid Res* **52**: 2159–2168
- Wang S, Soni KG, Semache M, Casavant S, Fortier M, Pan L, Mitchell GA (2008)** Lipolysis and the integrated physiology of lipid energy metabolism. *Mol. Genet. Metab.* **95**: 117–126
- Wendel AA, Cooper DE, Ilkayeva OR, Muoio DM, Coleman RA (2013)** Glycerol-3-phosphate acyltransferase (GPAT)-1, but not GPAT4, incorporates newly synthesized fatty acids into triacylglycerol and diminishes fatty acid oxidation. *The Journal of biological chemistry* **288**: 27299–27306
- Wendy AL, Simeonov A (2011)** Fluorescence Polarization Assays in Small Molecule Screening. *Expert Opin Drug Discov* **6**: 17–32
- Wessel D, Flugge UI (1984)** A method for the quantitative recovery of protein in dilute solution in the presence of detergents and lipids. *Anal Biochem* **138**: 141–143
- Wetzel S, Klein K, Renner S, Rauh D, Oprea TI, Mutzel P, Waldmann H (2009)** Interactive exploration of chemical space with Scaffold Hunter. *Nat. Chem. Biol.* **5**: 581–583
- Wilfling F, Thiam AR, Olarte M, Wang J, Beck R, Gould TJ, Allgeyer ES, Pincet F, Bewersdorf J, Farese RV, Walther TC (2014)** Arf1/COPI machinery acts directly on lipid droplets and enables their connection to the ER for protein targeting. *Elife (Cambridge)* **3**: e01607
- Wilfling F, Wang H, Haas JT, Krahmer N, Gould TJ, Uchida A, Cheng J, Graham M, Christiano R, Fröhlich F, Liu X, Buhman KK, Coleman RA, Bewersdorf J, Farese RV, Walther TC (2013)** Triacylglycerol synthesis enzymes mediate lipid droplet growth by relocalizing from the ER to lipid droplets. *Dev. Cell* **24**: 384–399
- Wu JW, Wang SP, Alvarez F, Casavant S, Gauthier N, Abed L, Soni KG, Yang G, Mitchell GA (2011)** Deficiency of liver adipose triglyceride lipase in mice causes progressive hepatic steatosis. *Hepatology (Baltimore, Md.)* **54**: 122–132
- Wu X, Walker J, Zhang J, Ding S, Schultz PG (2004)** Purmorphamine Induces Osteogenesis by Activation of the Hedgehog Signaling Pathway. *Chemistry & Biology* **11**: 1229–1238
- Wurie HR, Buckett L, Zammit VA (2012)** Diacylglycerol acyltransferase 2 acts upstream of diacylglycerol acyltransferase 1 and utilizes nascent diglycerides and de novo synthesized fatty acids in HepG2 cells. *FEBS J* **279**: 3033–3047
- Xia T, Mostafa N, Bhat BG, Florant GL, Coleman RA (1993)** Selective retention of essential fatty acids: the role of hepatic monoacylglycerol acyltransferase. *Am J Physiol* **265**: R414–9
- Xu N, Zhang SO, Cole RA, McKinney SA, Guo F, Haas JT, Bobba S, Farese, Robert V Jr, Mak HY (2012)** The FATP1-DGAT2 complex facilitates lipid droplet expansion at the ER-lipid droplet interface. *J Cell Biol* **198**: 895–911
- Xu X, Park J, So J, Lee A (2014)** Transcriptional activation of Fsp27 by the liver-enriched transcription factor CREBH promotes lipid droplet growth and hepatic steatosis. *Hepatology (Baltimore, Md.)*
- Yamaguchi T (2010)** Crucial Role of CGI-58/ $\alpha/\beta$  Hydrolase Domain-Containing Protein 5 in Lipid Metabolism. *Biol. Pharm. Bull.* **33**: 342–345
- Yang C, Kazanietz MG (2003)** Divergence and complexities in DAG signaling: looking beyond PKC. *Trends in pharmacological sciences* **24**: 602–608
- Yen CE, Stone SJ, Koliwad S, Harris C, Farese RV (2008)** Thematic review series: glycerolipids. DGAT enzymes and triacylglycerol biosynthesis. *J. Lipid Res.* **49**: 2283–2301

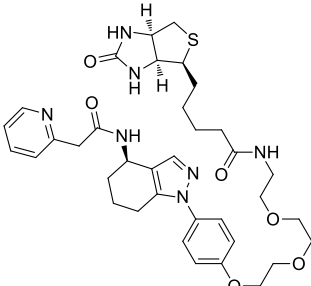
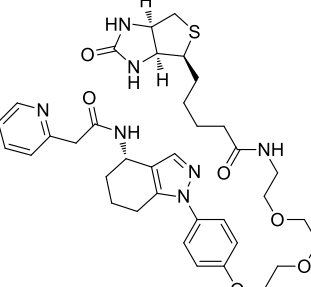
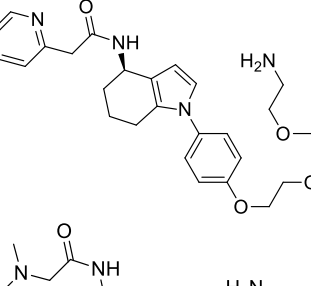
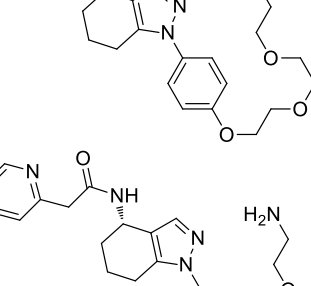
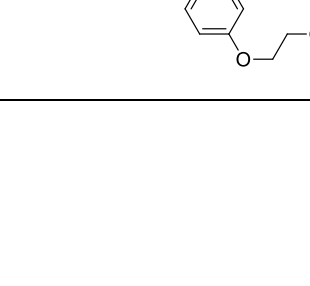
- Yoo HJ, Choi KM (2014)** Adipokines as a novel link between obesity and atherosclerosis. *World J Diabetes* **5**: 357–363
- Yu X, Miranda M, Liu Z, Patel S, Nguyen N, Carson K, Liu Q, Swaffield JC (2010)** Novel potent inhibitors of deoxycytidine kinase identified and compared by multiple assays. *J Biomol Screen* **15**: 72–79
- Yuan Y, Li P, Ye J (2012)** Lipid homeostasis and the formation of macrophage-derived foam cells in atherosclerosis. *Protein Cell* **3**: 173–181
- Zechner R, Madeo F (2009)** Cell biology: Another way to get rid of fat. *Nature* **458**: 1118–1119
- Zehmer JK, Huang Y, Peng G, Pu J, Anderson, Richard G W, Liu P (2009)** A role for lipid droplets in inter-membrane lipid traffic. *Proteomics* **9**: 914–921
- Zeldin DC, Wei S, Falck JR, Hammock BD, Snapper JR, Capdevila JH (1995)** Metabolism of epoxyeicosatrienoic acids by cytosolic epoxide hydrolase: substrate structural determinants of asymmetric catalysis. *Arch Biochem Biophys* **316**: 443–451
- Zhang B, Porto AF (2013)** Cholesteryl ester storage disease: protean presentations of lysosomal acid lipase deficiency. *Journal of pediatric gastroenterology and nutrition* **56**: 682–685
- Zhang F, Du G (2012)** Dysregulated lipid metabolism in cancer. *World J Biol Chem* **3**: 167–174
- Zhao G, Souers AJ, Voorbach M, Falls HD, Droz B, Brodjian S, Lau YY, Iyengar RR, Gao J, Judd AS, Wagaw SH, Ravn MM, Engstrom KM, Lynch JK, Mulhern MM, Freeman J, Dayton BD, Wang X, Grihalde N, Fry D et al (2008)** Validation of diacyl glycerolacyltransferase I as a novel target for the treatment of obesity and dyslipidemia using a potent and selective small molecule inhibitor. *J Med Chem* **51**: 380–383
- Zhukova MV, Kiseleva EV (2011)** Effects of starvation on the lifespan and apoptosis in the ovarian cells of *Drosophila melanogaster*. *Russ J Genet Appl Res* **1**: 315–320

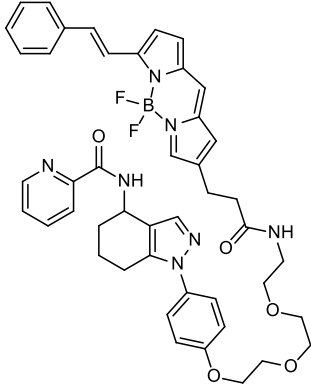
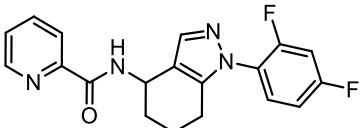
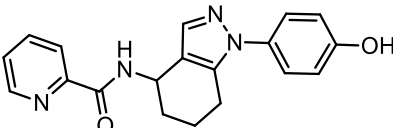
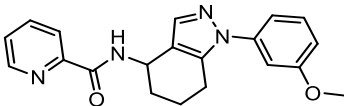
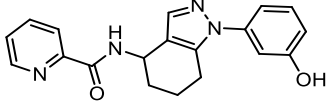
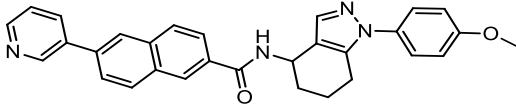
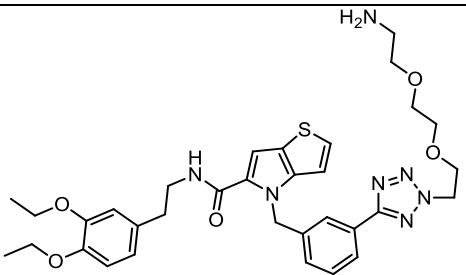


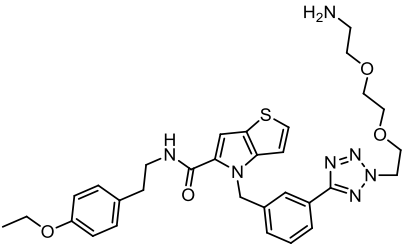
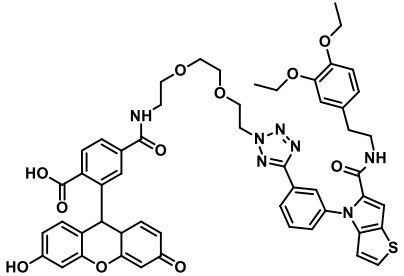
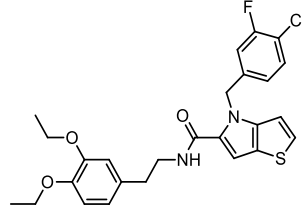
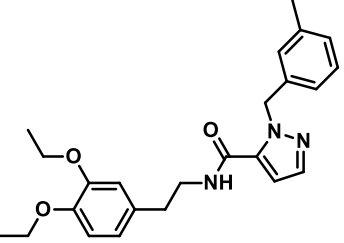
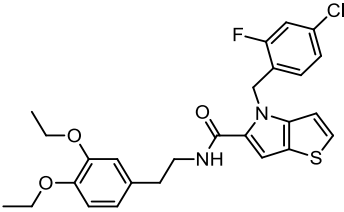
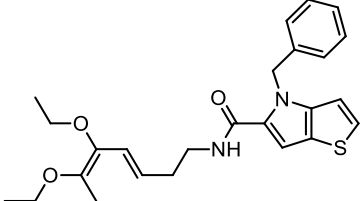
## CHAPTER 9: SUPPLEMENTAL DATA

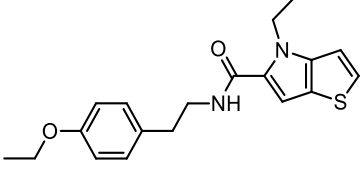
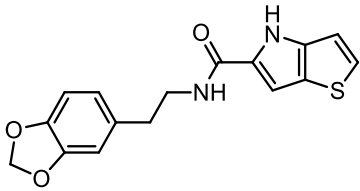
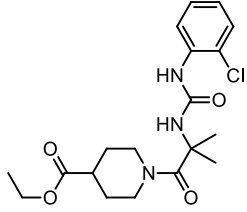
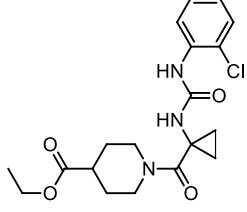
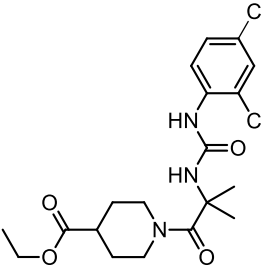
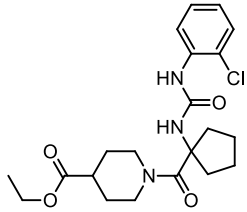
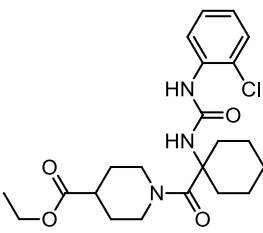
## 9.1 SMALL MOLECULES

**SUPPLEMENTAL TABLE 1: Selected small molecules of all three Chemotypes which were preferentially used in biological studies. The synthesis was performed by Dr. Mathew Boxer, NIH (Bethesda, USA).**

Chemotype 1	NCGC ID	Structure
1	T01	<p>Positive enantiomer (Biotin Pull- down Probe; Active)</p> 
1	T02	<p>Negative enantiomer (Biotin Pull- down Probe; Inactive)</p> 
1	T03	<p>NCGC00263797-01 (Free Amine Pull- down Probe; Active)</p> 
1	T04	<p>NCGC00274282-01 (Free Amine Pull- down Probe; Inactive)</p> 
1	T05	<p>NCGC00273960-01 (Free Amine Pull- down Probe; Less active)</p> 

1	T06	NCGC00247874-01 (BODIPY Label; Active)	
1	T07	NCGC00189555-01	
1	T08	NCGC00242549-01	
1	T09	NCGC00242573-01	
1	T10	NCGC00242574-01	
1	T11	NCGC00250255-01	
<b>Chemotype 2</b>			<b>Structure</b>
2	P01	NCGC00344516-01 (Free Amine Pull-down Probe; Active)	

2	P02	NcGC00344517-01 (Free Amine Pull-down Probe; Inactive)	
2	P03	NCGC (Fluorescein Label; Active)	
2	P04	NCGC00241429-01	
2	P05	NCGC00345354-01	
2	P06	NCGC00241427-01	
2	P07	NCGC00238551-01	

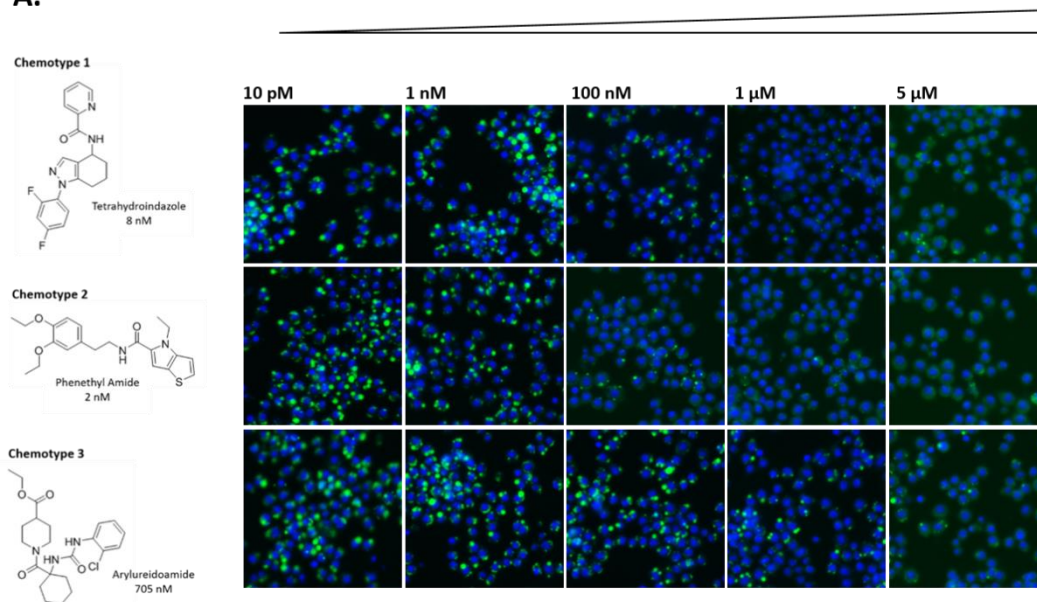
2	P08	NCGC00238540-02	
2	P09	NCGC00241444-01	
Chemotype 3			Structure
3	A01	NCGC00241450-01	
3	A02	NCGC00241446-01	
3	A03	NCGC00242560-01	
3	A04	NCGC00241448-01	
3	A05	NCGC00034917-03	

**SUPPLEMENTAL TABLE 2: Selected SAR derivatives of all three Chemotypes.** The three small molecule classes were named according to the respective chemical scaffold (Tetrahydroindazol [T01-T45], Phenylethylamies [P01-P44] and Arylureidoamides [A01-A26]. The synthesis was performed in the group of Dr. Matthew Boxer, NIH (Bethesda, USA). The respective NCGC identifiers are included in this table.

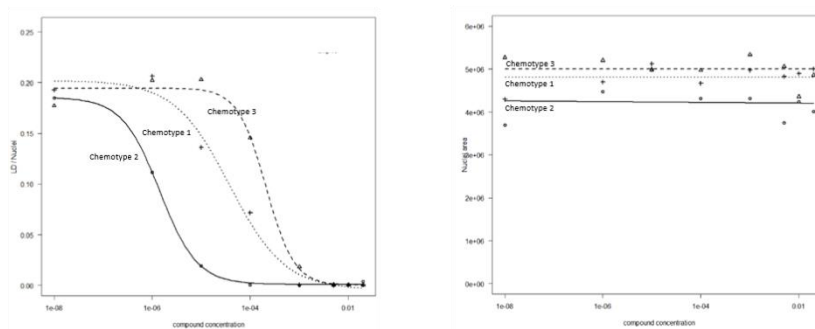
Tetrahydroindazol Series Chemotype 1		Phenylethylamide Series Chemotype 2		Arylureidoamide Series Chemotype 3	
ID	NCGC-ID	ID	NCGC-ID	ID	NCGC-ID
T01	NCGC00244462-01	P01	NCGC00344516-01	A01	NCGC00241450-01
T02	NCGC00244462-01	P02	NCGC00344517-01	A02	NCGC00241446-01
T03	NCGC00263797-01	P03	NCGC00356820-01	A03	NCGC00242560-01
T04	NCGC00274282-01	P04	NCGC00241429-01	A04	NCGC00241448-01
T05	NCGC00273960-01	P05	NCGC00345354-01	A05	NCGC00034917-03
T06	NCGC00247874-01	P06	NCGC00241427-01	A06	NCGC00241449-01
T07	NCGC00189555-01	P07	NCGC00238551-01	A07	NCGC00241447-01
T08	NCGC00242549-01	P08	NCGC00238540-02	A08	NCGC00242550-01
T09	NCGC00242573-01	P09	NCGC00241444-01	A09	NCGC00242553-01
T10	NCGC00244462-01	P10	NCGC00241414-01	A10	NCGC00242554-01
T11	NCGC00250255-01	P11	NCGC00241418-01	A11	NCGC00242555-01
T12	NCGC00241451-01	P12	NCGC00241426-01	A12	NCGC00242556-01
T13	NCGC00242548-01	P13	NCGC00241442-01	A13	NCGC00242557-01
T14	NCGC00242551-01	P14	NCGC00241415-01	A14	NCGC00242558-01
T15	NCGC00242572-01	P15	NCGC00241419-01	A15	NCGC00242559-01
T16	NCGC00242574-01	P16	NCGC00241443-01	A16	NCGC00242563-01
T17	NCGC00238536-01	P17	NCGC00241416-01	A17	NCGC00242564-01
T18	NCGC00238537-01	P18	NCGC00241428-01	A18	NCGC00242565-01
T19	NCGC00238555-01	P19	NCGC00241433-01	A19	NCGC00242566-01
T20	NCGC00238557-01	P20	NCGC00241440-01	A20	NCGC00242567-01
T21	NCGC00238558-01	P21	NCGC00241420-01	A21	NCGC00242568-01
T22	NCGC00238559-01	P22	NCGC00241437-01	A22	NCGC00238542-01
T23	NCGC00238560-01	P23	NCGC00241441-01	A23	NCGC00250258-01
T24	NCGC00238547-01	P24	NCGC00241421-01	A24	NCGC00250259-01
T25	NCGC00238548-01	P25	NCGC00241430-01	A25	NCGC00250262-01
T26	NCGC00238544-01	P26	NCGC00241439-01	A26	NCGC00250263-01
T27	NCGC00238553-01	P27	NCGC00241452-01		
T28	NCGC00238539-01	P28	NCGC00241422-01		
T29	NCGC00238541-01	P29	NCGC00241431-01		
T30	NCGC00238561-01	P30	NCGC00241434-01		
T31	NCGC00189332-02	P31	NCGC00241445-01		
T32	NCGC00189556-01	P32	NCGC00241453-01		
T33	NCGC00250265-01	P33	NCGC00241423-01		
T34	NCGC00250256-01	P34	NCGC00241424-01		
T35	NCGC00250257-01	P35	NCGC00241435-01		
T36	NCGC00250264-01	P36	NCGC00241438-01		
T37	NCGC00250253-01	P37	NCGC00241417-01		
T38	NCGC00250260-01	P38	NCGC00241425-01		
T39	NCGC00250254-01	P39	NCGC00241436-01		
T40	NCGC00272464-01	P40	NCGC00241432-01		
T41	NCGC00274028-01	P41	NCGC00238550-01		
T42	NCGC00273407-01	P42	NCGC00092589-02		
T43	NCGC00273418-01	P43	NCGC00238546-02		
T44	NCGC00273466-01	P44	NCGC00241007-01		
P45	NCGC00241429-01				

## 9.2 MECHANISM OF ACTION

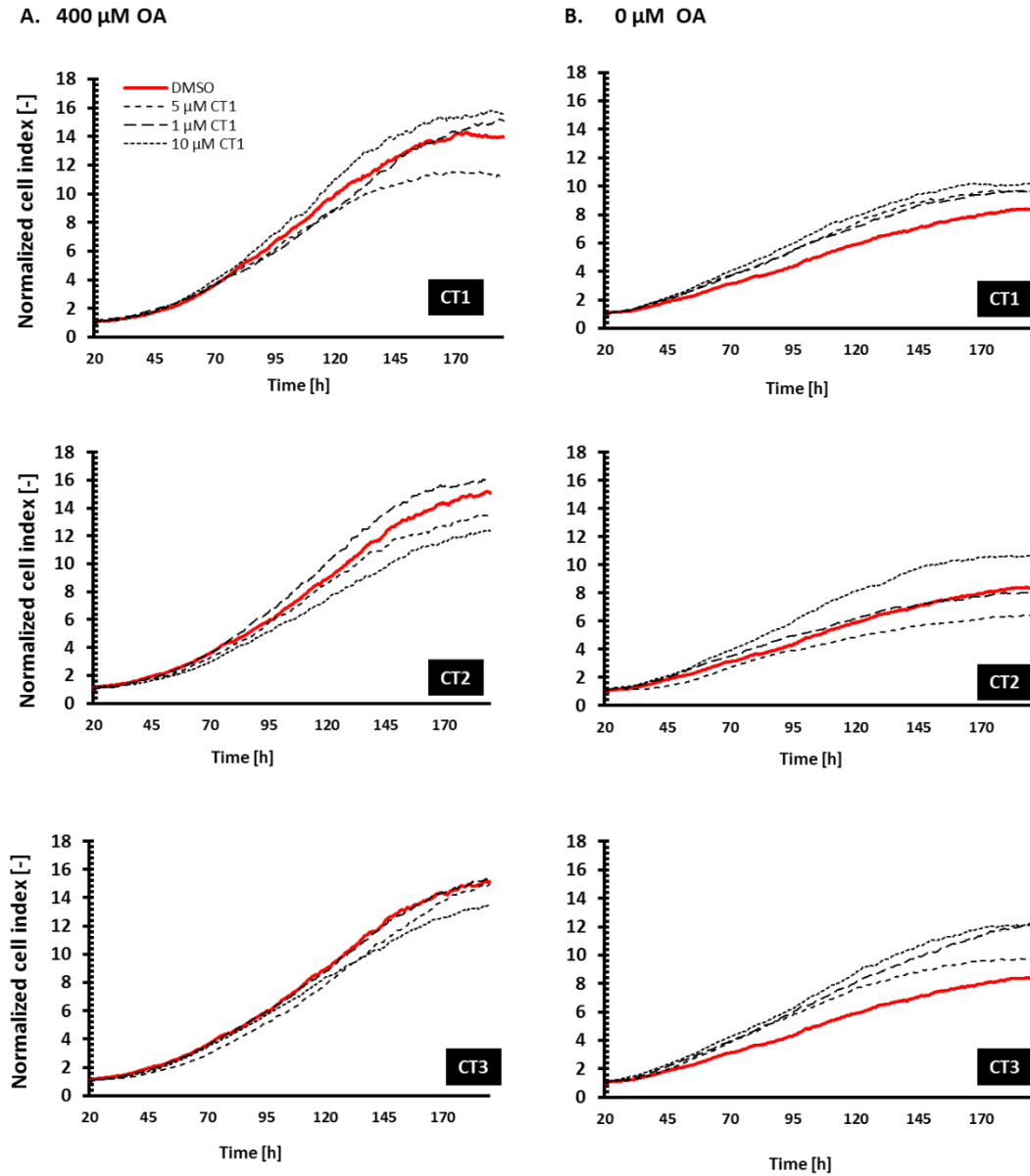
A.



B.



**SUPPLEMENTAL FIGURE 1: The small molecule effect follows a concentration dependent manner, which allows the determination of  $EC_{50}$  values in order to quantify the affinity. **AI** Microscopic images of *Drosophila* S3 cells show a visually obvious concentration dependency with a high number of LDs in cells below the respective  $EC_{50}$  values (10 nM), while at high concentration the LD are nearly vanished (5  $\mu$ M). The cell number as a measure for cytotoxicity was not affected. *Drosophila* S3 cells ( $1.5 \times 10^5$  cells/well) were incubated in Schneider's Medium containing 5% (v/v) FBS, penicillin/streptomycin, 400  $\mu$ M OA and the respective small molecule concentration (10 pM-5  $\mu$ M in DMSO, at a constant DMSO level of 0.2% (v/v)). The treatment took place for 1h at 25°C. Fixed and permeabilized cells were stained for lipid droplets (BODIPY® 493/503, 1:2000 dilution) and nuclei (Hoechst 33342, 1:500 dilution). Acquisition of three images per well at a 17x magnification. **BI** The images of small molecule treated S3 cells were segmented by CellProfiler. The ratio of the LD/ Nuclei area was plotted against the small molecule concentration for  $EC_{50}$  determination. (Chemotype 1 [T08], Chemotype 2 [P04], Chemotype 3 [A03]; Controls: Chemotype 1 [T11], Chemotype 2 [P08], Chemotype 3 [A02])**

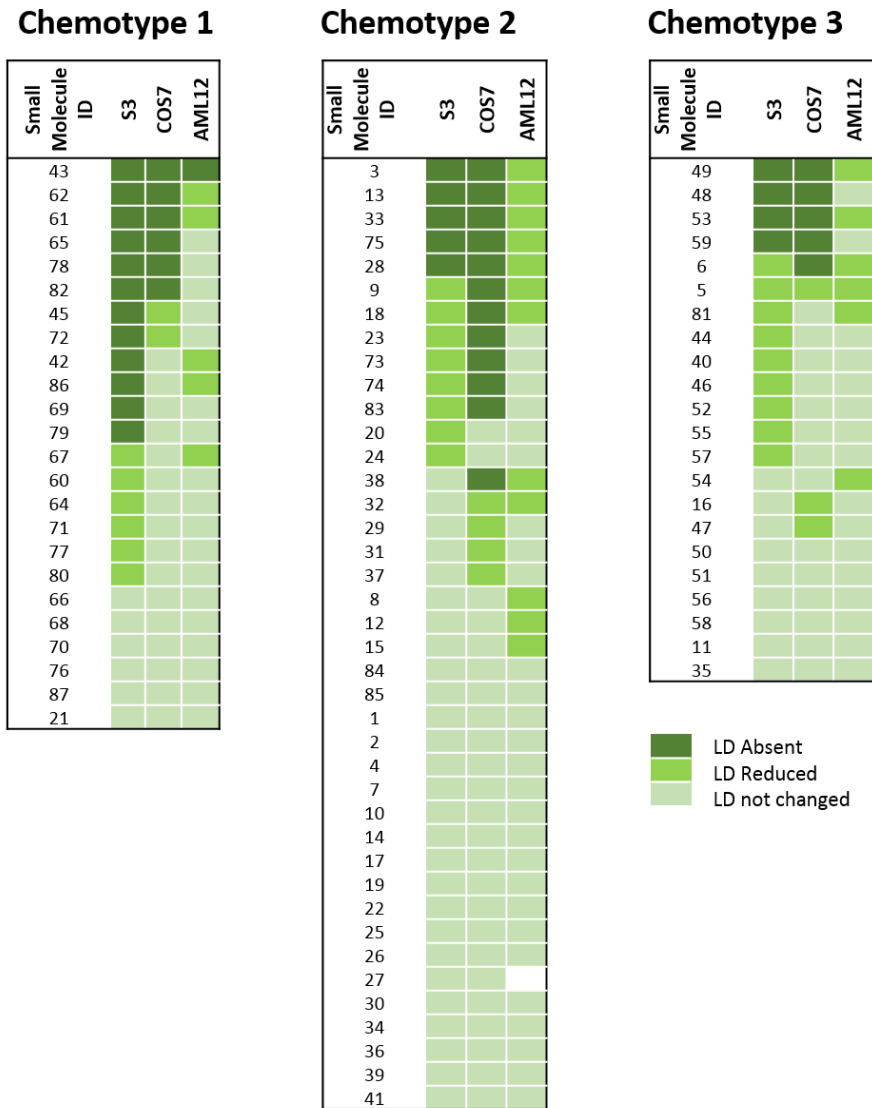


**SUPPLEMENTAL FIGURE 2: Long term real time cell analysis (RTCA) did not indicate significantly altered cell growth when AML12 cells were treated with small molecules.** Adapted AML12 cells were treated with 5  $\mu\text{M}$  of the respective active derivatives of each chemotype. The impedance of the cell solution was measured for 7 days. The resultant curve shows all characteristic stages of a mammalian cell growth curve.

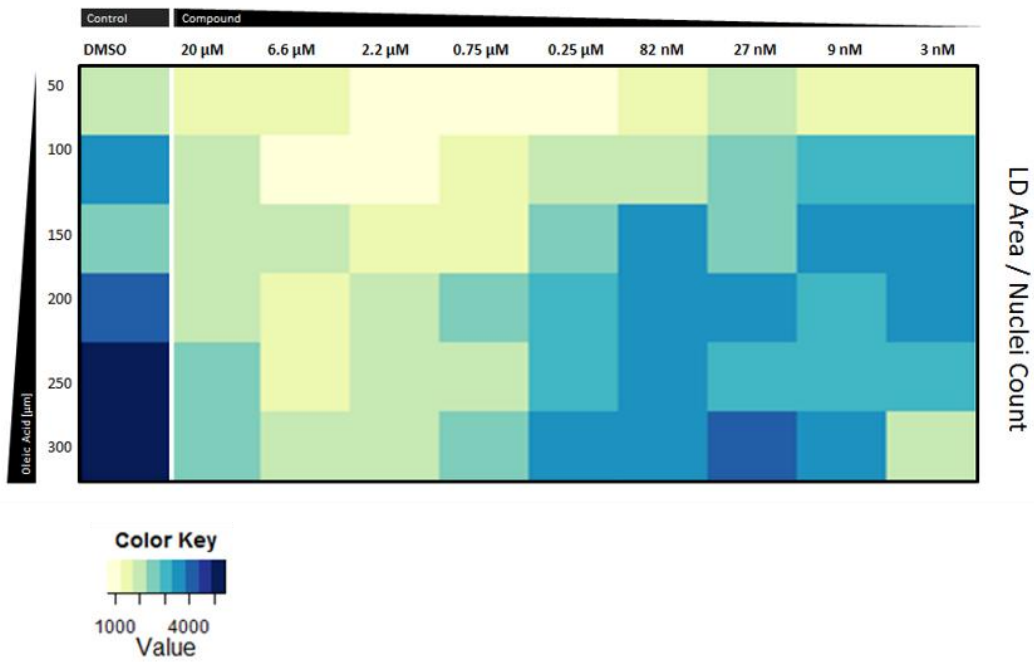
**SUPPLEMENTAL TABLE 3: The neutral lipid level in cells and flies was checked by different assays.** The quantification of identically treated *Drosophila* Kc167 cells, revealed differences between the microscopic LD assay based on visual examination of stained cells and the exact quantification by the colorimetric cell based assay with the given thresholds. The colorimetric assay reached high sensitivities. (A= LD absent, R = LD count reduced, N = LD level not changed. Microscopic assay: visual scoring of stained *Drosophila* Kc167 cells in comparison to DMSO treated cells (negative control) and unfed cells (0  $\mu$ M OA, positive control). Colorimetric assay: evaluation based on rel. TAG/protein level: A < 0.25 (Absent), R < 0.6 (reduced), N > 0.65 (no change). *In vivo* assay in w- *Drosophila* flies: evaluation based on rel. TAG/protein level with the thresholds described for the colorimetric assay.)

	<b>Molecule</b>	<b>Chemotype</b>	<b>Microscopic cell based Assay</b>	<b>Colorimetric cell based Assay</b>	<b>Colorimetric <i>in vivo</i> fly Assay</b>
[P12]	NCGC00241426-01	2	A	A	N
[P18]	NCGC00241428-01	2	A	A	N
[P11]	NCGC00241431-01	2	A	A	N
[P06]	NCGC00241427-01	2	R	A	N
[P08]	NCGC00241429-01	2	R	A	R
[P25]	NCGC00241430-01	2	R	A	N
[P23]	NCGC00241441-01	2	R	R	N
[P30]	NCGC00241434-01	2	N	R	N
[P36]	NCGC00241438-01	2	N	R	N
[P10]	NCGC00241414-01	2	N	N	N
[P37]	NCGC00241417-01	2	N	N	N
[A04]	NCGC00241448-01	3	R	A	R
[A06]	NCGC00034917-03	3	R	A	N
[A01]	NCGC00241450-01	3	N	A	N
[A02]	NCGC00241446-01	3	N	R	N





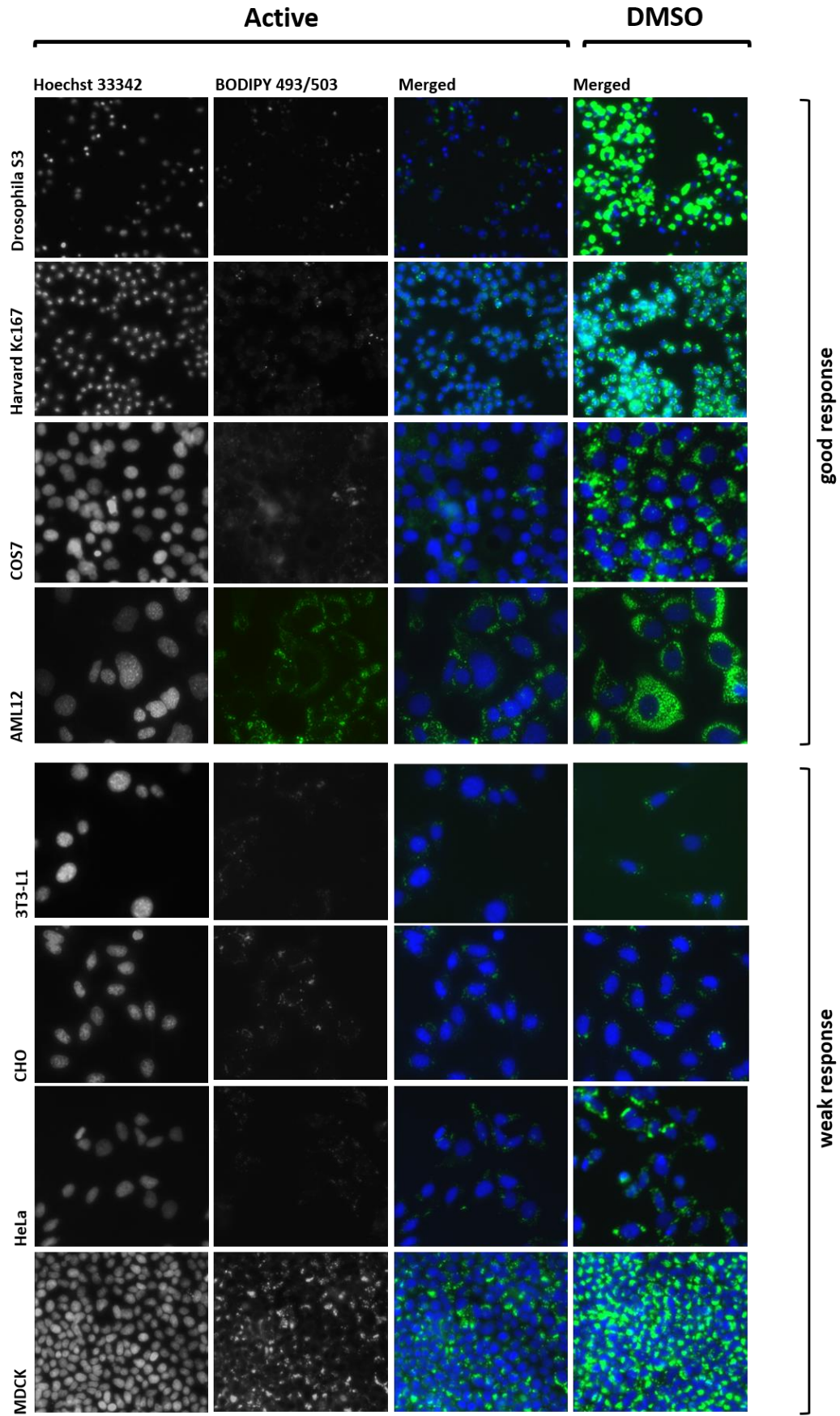
**SUPPLEMENTAL FIGURE 3: Small molecule activity is conserved in cells deriving from different species and organs as systematically analyzed for *Drosophila* S3 (embryo), monkey COS7 (kidney) and murine AML12 (liver) cells. The cells were cultured in their respective media supplemented with 400  $\mu$ M OA during small molecule treatment (5  $\mu$ M) for 18h. Cells were fixed and stained for LD and nuclei. The BODIPY<sup>®</sup>-493/503 LD stain was considered for visual classification of the phenotype.**

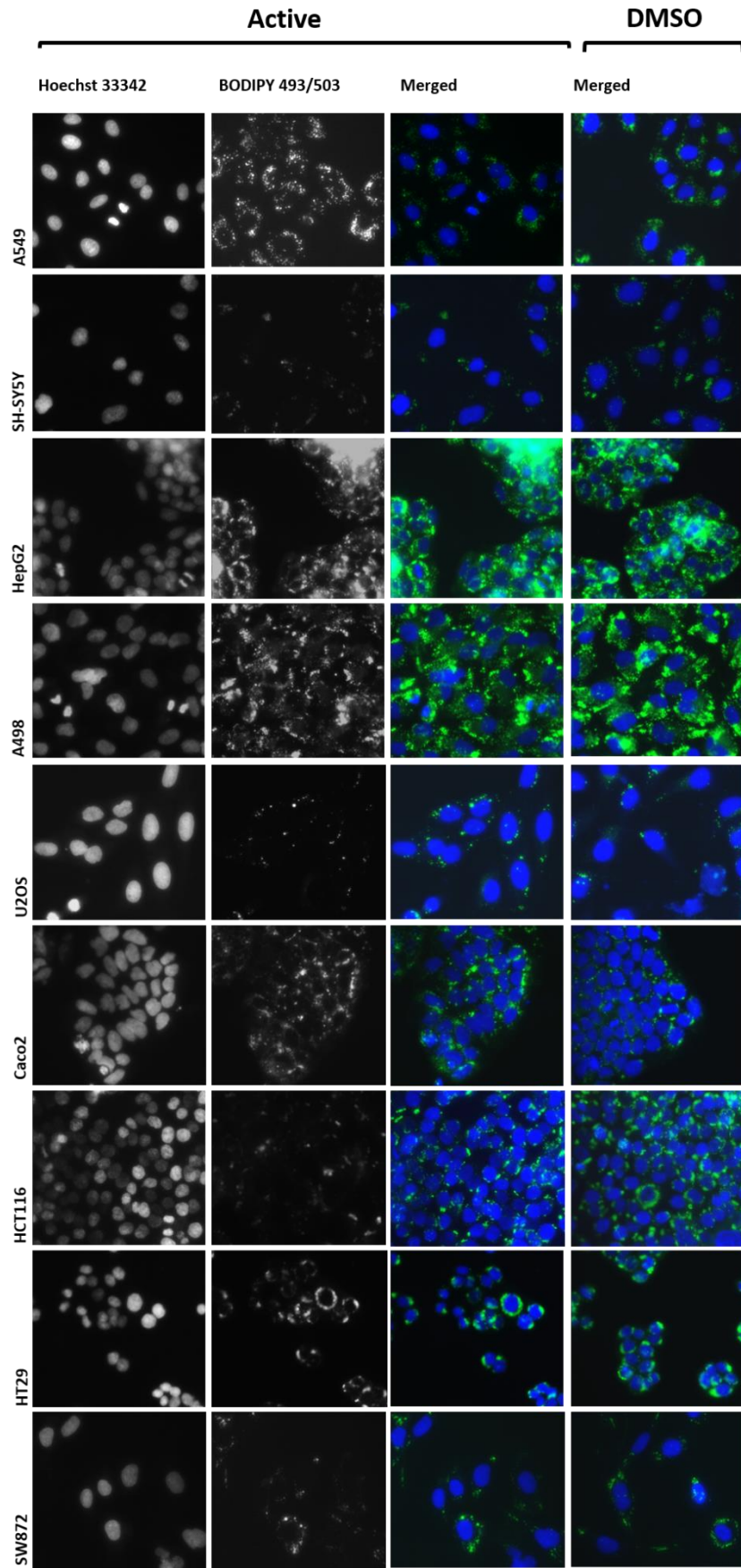


**SUPPLEMENTAL FIGURE 4: Investigation of the LD assay response towards alterations in small molecule concentration and OA concentration in AML12 cells.** AML12 cells were treated with different OA concentrations at different small molecule concentrations for an 18h. The cells were fixed and stained for LDs (BODIPY<sup>®</sup>493/503) and nuclei (Hoechst 33342). Nine images per well were segmented for LDs and nuclei and the LD area was normalized to the respective nuclei counts. The CellProfiler analysis was performed by Dr. Mathias Beller, HHU Düsseldorf.

**SUPPLEMENTAL TABLE 4: Swiss Target Prediction analysis for the three novel discovered Chemotypes (www.swisstargetprediction.ch/).** The online tools uses a combination of 2D and 3D similarity search of the examined small molecules with 280.000 known small molecules against 2000 known targets. This might support the target prediction and gains information about likely off targets. The predicted targets were compared with the respective 4<sup>th</sup> generation pull-down results. However, most of the predicted target proteins, were not identified (X) in the practical experiments. For Chemotype 3 no pull-downs were performed (n.D., not determined).

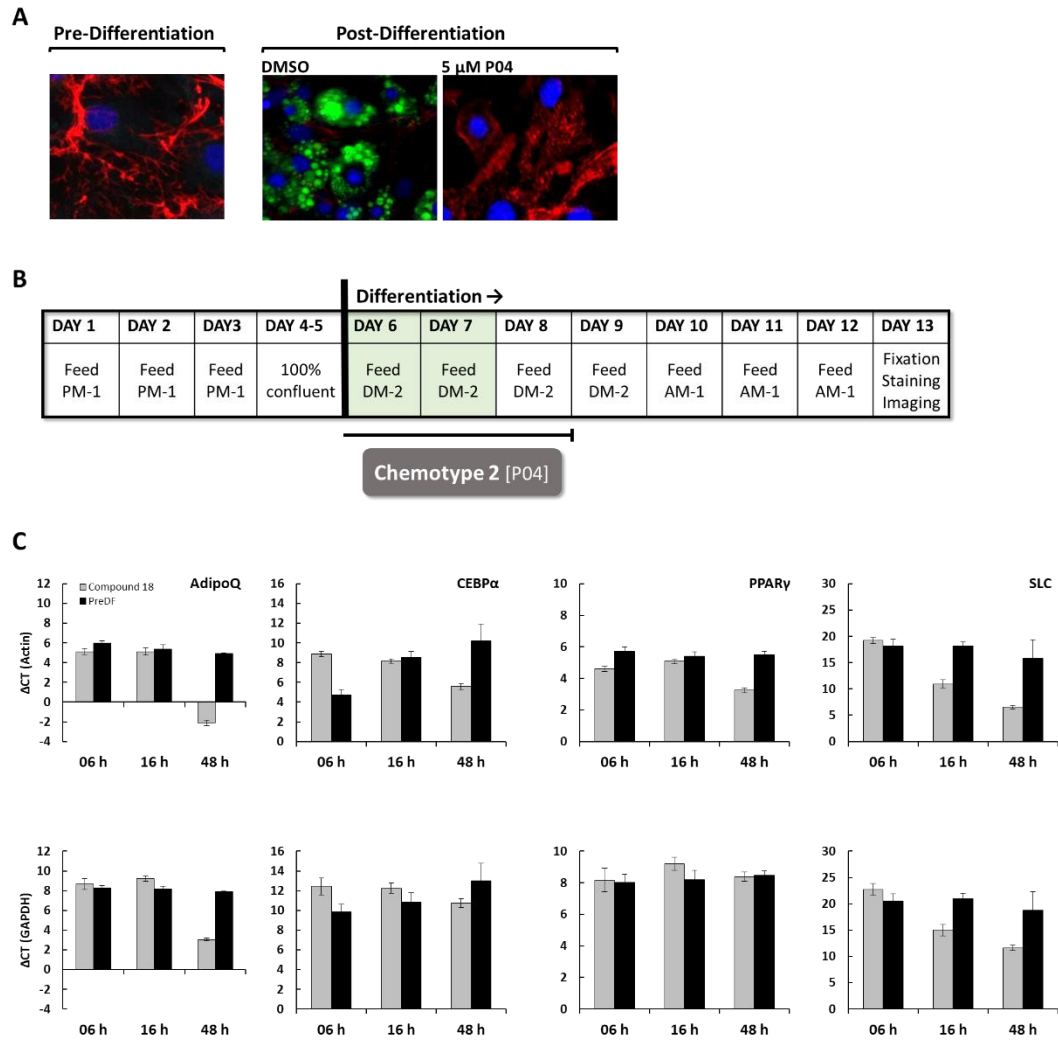
	Target	Name	Uniprot ID	Target Class	Pull-down
Chemotype 1	FAD-linked sulfhydryl oxidase ALR**	Gfer	<a href="#">P56213</a>	Enzyme	X
	Microtubule-associated protein tau**	Mapt	<a href="#">P10637</a>	Unclassified	X
	Corticosteroid 11-beta-dehydrogenase isozyme 1**	Hsd11b1	<a href="#">P50172</a>	Enzyme	X
	Tyrosyl-DNA phosphodiesterase **	Tdp1	<a href="#">B8JJC1</a>	Enzyme	X
	Dipeptidyl peptidase 4 membrane form **	Dpp4	<a href="#">P28843</a>	Serine Protease	X
	Seprase**	Fap	<a href="#">P97321</a>	Serine Protease	X
	Mitogen-activated protein kinase 14**	Mapk14	<a href="#">P47811</a>	Ser- Thr Kinase	X
	Mitogen-activated protein kinase 11 **	Mapk11	<a href="#">Q9WU11</a>	Ser- Thr Kinase	X
	C-C chemokine receptor type 1 **	Ccr1	<a href="#">P51675</a>	Membrane receptor	X
	C-C chemokine receptor 1-like protein 1**	Ccr1l1	<a href="#">P51676</a>	Membrane receptor	X
	Probable C-C chemokine receptor type 3 **	Ccr3	<a href="#">P51678</a>	Membrane receptor	X
	D(2) dopamine receptor**	Drd2	<a href="#">P61168</a>	Membrane receptor	X
	5-hydroxytryptamine receptor 1A **	Htr1a	<a href="#">Q64264</a>	Membrane receptor	X
5-hydroxytryptamine receptor 2A **	Htr2a	<a href="#">P35363</a>	Membrane receptor	1.0	
5-hydroxytryptamine receptor 7 **	Htr7	<a href="#">P32304</a>	Membrane receptor	X	
Chemotype 2	Microtubule-associated protein tau **	Mapt	<a href="#">P10637</a>	Unclassified	X
	Tyrosyl-DNA phosphodiesterase 1 **	Tdp1	<a href="#">B8JJC1</a>	Enzyme	X
	Muscleblind-like protein **	Mbnl1	<a href="#">G3X9Q0</a>	Unclassified	0.8
	Glycogen phosphorylase, liver form **	Pygl	<a href="#">Q9ET01</a>	Enzyme	X
	Glycogen phosphorylase, brain form **	Pygb	<a href="#">Q8CI94</a>	Enzyme	1.0
	Glycogen phosphorylase, muscle form **	Pygm	<a href="#">Q9WUB3</a>	Enzyme	X
	Factor X heavy chain **	F10	<a href="#">Q88947</a>	Serine Protease	X
	Coagulation factor IXa heavy chain**	F9	<a href="#">P16294</a>	Serine Protease	X
	Histamine H4 receptor **	Hrh4	<a href="#">Q91ZY2</a>	Membrane receptor	X
	Melatonin receptor type 1A **	Mtnr1a	<a href="#">Q61184</a>	Membrane receptor	X
	Histamine H3 receptor **	Hrh3	<a href="#">P58406</a>	Membrane receptor	X
	Carbonic anhydrase 13 **	Ca13	<a href="#">Q9D6N1</a>	Enzyme	X
	Carbonic anhydrase 2 **	Ca2	<a href="#">P00920</a>	Enzyme	X
	Carbonic anhydrase 1 **	Ca1	<a href="#">P13634</a>	Enzyme	X
	Carbonic anhydrase 3 **	Ca3	<a href="#">P16015</a>	Enzyme	X
Chemotype 3	Cholecystokinin receptor type A	Cckar	<a href="#">P32238</a>	Membrane receptor	n.D.
	Gastrin/cholecystokinin type B receptor	Cckbr	<a href="#">P32239</a>	Membrane receptor	n.D.
	Muscleblind-like protein 1	Mbnl1	<a href="#">Q9NR56</a>	Unclassified	n.D.
	Muscleblind-like protein 2 **	Mbnl2	<a href="#">Q5VZF2</a>	Unclassified	n.D.
	Muscleblind-like protein 3 **	Mbnl3	<a href="#">Q9NUK0</a>	Unclassified	n.D.
	Substance-K receptor **	Tacr2	<a href="#">P21452</a>	Membrane receptor	n.D.
	Substance-P receptor	Tacr1	<a href="#">P25103</a>	Membrane receptor	n.D.
	Neuromedin-K receptor	Tacr3	<a href="#">P29371</a>	Membrane receptor	n.D.
	C-C chemokine receptor type 1	Ccr1	<a href="#">P32246</a>	Membrane receptor	n.D.
	C-C chemokine receptor type 2 **	Ccr2	<a href="#">P41597</a>	Membrane receptor	n.D.
	C-C chemokine receptor type 3	Ccr3	<a href="#">P51677</a>	Membrane receptor	n.D.
	C-C chemokine receptor type 5 **	Ccr5	<a href="#">P51681</a>	Membrane receptor	n.D.
	C-C chemokine receptor-like 2 **	Ccr12	<a href="#">C9JP23</a>	Membrane receptor	n.D.
	Lipid-phosphate phosphatase	Ephx2	<a href="#">P34913</a>	Serine Protease	n.D.
	Tyrosyl-DNA phosphodiesterase 1	Tdp1	<a href="#">Q9NUW8</a>	Enzyme	n.D.



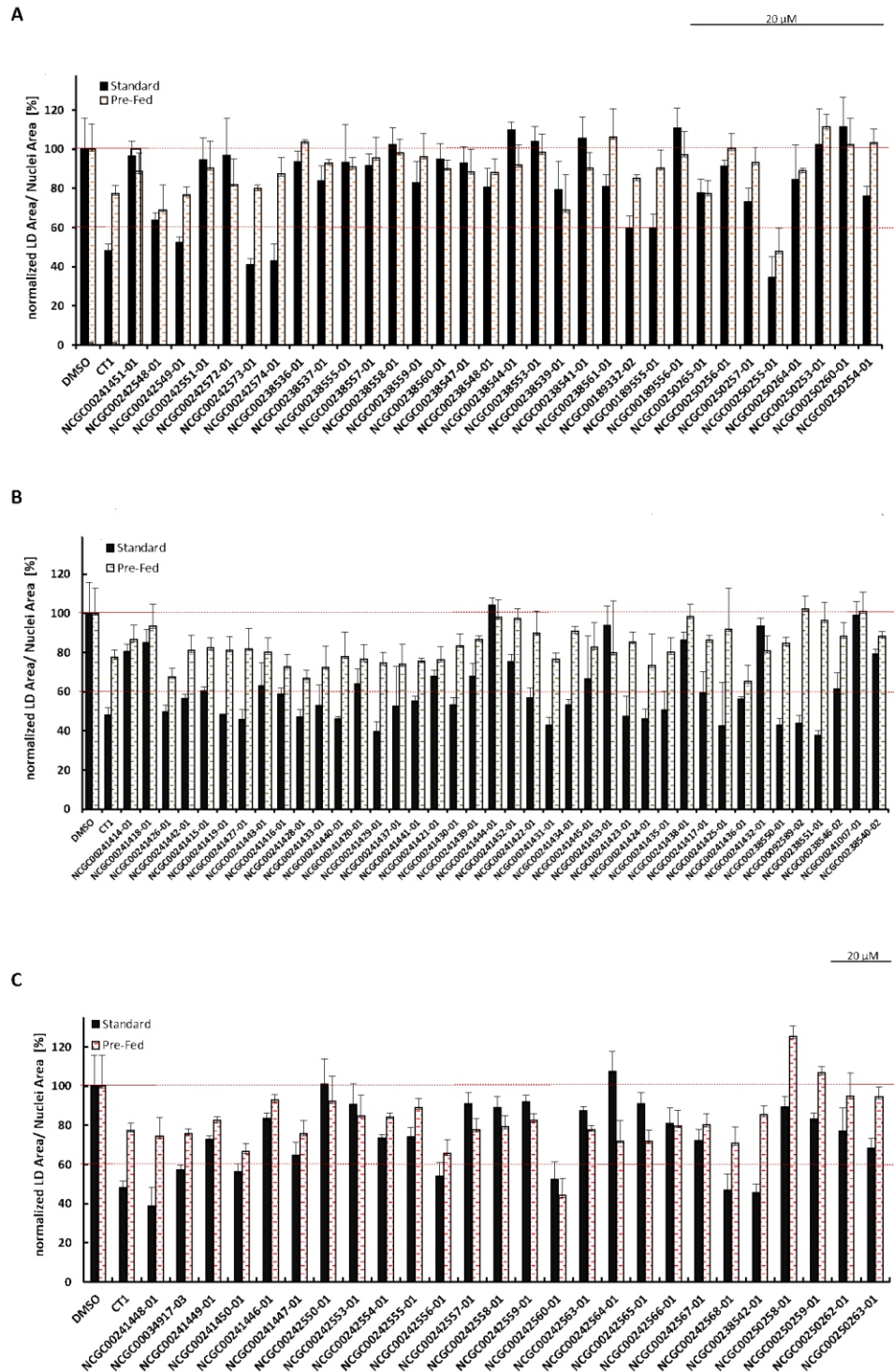


weak response

**SUPPLEMENTAL FIGURE 5: Summary of Chemotype 2 treated cells in different cell lines.** The different cell lines showed variances in the capability to store LDs in the control state already, presumably depending on their endogenous energy demand. The basal level has a severe impact on the LD assay readout. The cells were all treated with 5  $\mu\text{M}$  small molecule in presence of 400 OA for 18 h. LDs were stained in fixed cells with BODIPY® 493/503 (green) and nuclei with Hoechst 33342 (blue).



**SUPPLEMENTAL FIGURE 6: Relative expression of differentiation markers involved in adipogenesis in murine 3T3 cells. A1** 3T3- cells treated with 1  $\mu\text{M}$  P04 according to the standard differentiation protocol without any addition of external FFAs. were stained at day 13 for nuclei (blue), LDs (green) and fibronectin (red). The differentiation was performed by Yaqin Zhang (NIH, USA) **B1** 3T3 cells were differentiated according to standard procedure. Total RNA was isolated at different time points throughout the experiment and the relative gene expression was measured by quantitative real-time PCR. The  $\Delta\text{CT}$  method was used for evaluation in regard for **C1** actin or GAPDH normalization. (day 5 (undifferentiated state), day 8 (stop of small molecule treatment) and day 12 (prolonged cultivation in differentiated state)).



**SUPPLEMENTAL FIGURE 7: Altered LD assay in regard of the initial LD load of the cell.** Murine AML12 cells were treated with 1 μM small molecule of the respective chemotypes in oleic acid enriched media (200 μM) for 16 h. The cells were either “lean” at the timepoint of small molecule application (standard protocol, bold bares) or were LD loaded due to pre-incubation in 200 μM OA for 16 h (dashed bares). The cells were stained for LDs (BODIPY® 493/503) and nuclei (Hoechst 33342) and automatically images (Olympus Axiovert Microscope, 20x). Images were quantified by CellProfiler and separated by chemical structure: Chemotype **AI** Chemotype 1 **BI** Chemotype 2 **CI** Chemoytype 3.

## 9.3 CHEMICAL PROTEOMICS

**SUPPLEMENTAL TABLE 5: Hit candidates from 1<sup>st</sup> generation pull- down based on the enantiomers of Chemotype 1 [T01] bound to Neutravidin non-magnetic agarose beads (Thermo Scientific) via a biotin interaction.** Bulk protein lysate from *Drosophila* Kc167 was used for target protein enrichment. Most proteins showed similar qualitative ratios in the active derivative [T01] and the control [T02] and were thus excluded from evaluation. The enrichment in the active probe was the only criteria for target definition in the chosen qualitative setup. The proteins presented in this table were present at least 3 out of 5 times in the active probe and showed an enrichment in the active probe by a difference of >2 count. (n=5, biological independent replicates, p= 0.001).

Protein name	Protein ID	[T01]	[T02]
T-complex protein 1 subunit gamma	TCPG	5	2
60S ribosomal protein L11	RL11	5	3
60S ribosomal protein L7	RL7	5	3
40S ribosomal protein S3a	RS3A	5	3
40S ribosomal protein S4	RS4	5	3
Elongation factor 1-gamma	EF1G	4	1
Eukaryotic initiation factor 44	IF4A	4	2
40S ribosomal protein S11	RS11	4	2
T-complex protein 1 subunit alpha	TCPA	4	2
Pyruvate kinase ***	KPYK	4	3
Importin subunit alpha	IMA	3	0
Actin, indirect flight muscle	ACT6	3	1
Nascent polypeptide-associated complex subunit alpha	NACA	3	1
60S ribosomal protein L10	RL10	3	1
60S ribosomal protein L18a	RL18A	3	1
60S ribosomal protein L24	RL24	3	1

\*\*\* disregarding the low ratio PKY was temporarily considered as a likely protein target based enzyme functionality

**SUPPLEMENTAL TABLE 6: Hit candidates from a modified 1<sup>st</sup> generation pull- down based on total *w-Drosophila* fly lysates.** Male and female flies were raised on standard fly cultivation media and were allowed to develop for 6 days. Total flies were homogenized in standard lysis buffer. Bulk protein lysate from *Drosophila* was used in pull- down experiments of the first generation. Target protein enrichment towards the active biotin labeled derivative of Chemotype 1 [T01]. Most proteins showed similar qualitative ratios in the active [T01] and the control [T02] probe (n=1, p= 0.001).

Protein Name	[T01]	[T02]
Serine/threonine-protein phosphatase PP2A 65 kDa regulatory subunit	2AAA	
Acetyl-coenzyme A synthetase	ACSA	
Alcohol dehydrogenase	ADH	
Apolipoporphins	APLP	
C-1-tetrahydrofolate synthase, cytoplasmic	C1TC	
60 kDa heat shock protein, mitochondrial	CH60	
Calcium-binding mitochondrial carrier protein Aralar1	CMC	
Cytochrome P450 4g1	CP4G1	
Elongation factor 1-alpha 1	EF1A1	
Glucose-6-phosphate isomerase	G6PI	
Heat shock 70 kDa protein cognate 3	HSP7C	
Heat shock 70 kDa protein cognate 5	HSP7E	
Putative mitochondrial inner membrane protein	IMMT	
Larval serum protein 1 gamma chain	LSP1G	
Probable maltase H	MAL2	
Probable methylcrotonoyl-CoA carboxylase beta chain, mitochondrial	MCCB	
NADH-ubiquinone oxidoreductase 75 kDa subunit, mitochondrial	NDUS1	
Neither inactivation nor afterpotential protein C	NINAC	
Proline oxidase, mitochondrial	PROD	
Glycogen phosphorylase	PYG	
Tubulin alpha-2 chain	TBA2	
T-complex protein 1 subunit alpha	TCPA	
Troponin T, skeletal muscle	TNNT	
Tropomyosin-1, isoforms 9A/A/B	TPM1	
Tropomyosin-1, isoforms 33/34	TPM4	
Probable medium-chain specific acyl-CoA dehydrogenase, mitochondrial	ACADM	ACADM
Actin-5C	ACT1	ACT1

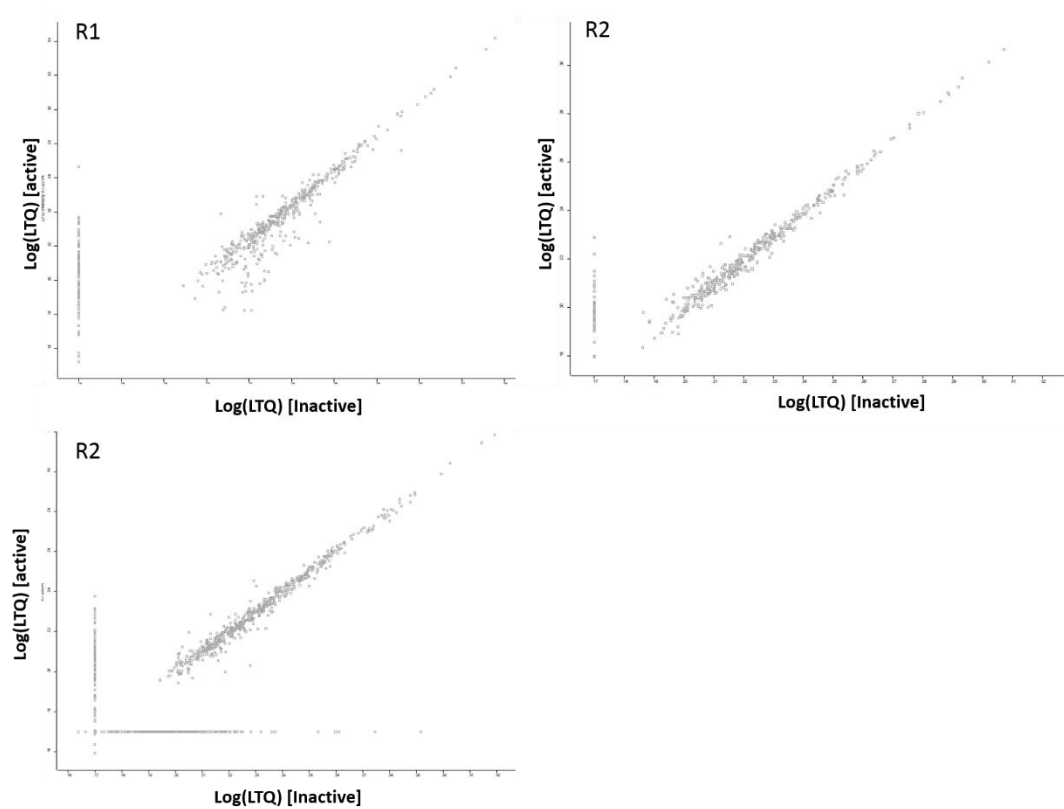


Actin-42A	ACT2	ACT2
Actin-57B	ACT3	ACT3
Actin, larval muscle	ACT4	ACT4
Actin-87E	ACT5	ACT5
Actin, indirect flight muscle	ACT6	ACT6
ADP,ATP carrier protein	ADT	ADT
Calcium-transporting ATPase sarcoplasmic/endoplasmic reticulum type	ATC1	ATC1
Sodium/potassium-transporting ATPase subunit alpha	ATNA	ATNA
ATP synthase subunit alpha, mitochondrial	ATPA	ATPA
ATP synthase subunit beta, mitochondrial	ATPB	ATPB
ATP synthase subunit gamma, mitochondrial	ATPG	ATPG
Catalase	CATA	CATA
Cytochrome c-2	CYC2	CYC2
Succinate dehydrogenase [ubiquinone] flavoprotein subunit, mitochondrial	DHSA	DHSA
Dynamin	DYN	DYN
Glyceraldehyde-3-phosphate dehydrogenase 1	G3P1	G3P1
Glyceraldehyde-3-phosphate dehydrogenase 2	G3P2	G3P2
Probable UDP-glucose 4-epimerase	GALE	GALE
Glutathione S-transferase S1	GST1	GST1
Putative glycogen [starch] synthase	GYS	GYS
3-hydroxyacyl-CoA dehydrogenase type-2	HCD2	HCD2
Heat shock 70 kDa protein cognate 4	HSP7D	HSP7D
Heat shock protein 83	HSP83	HSP83
Probable isocitrate dehydrogenase [NAD] subunit alpha, mitochondrial	IDH3A	IDH3A
6-phosphofructokinase	K6PF	K6PF
Pyruvate kinase	KPYK	KPYK
Probable methylmalonate-semialdehyde dehydrogenase [acylating], mitochondrial	MMSA	MMSA
Myosin heavy chain, muscle	MYSA	MYSA
Myosin heavy chain, non-muscle	MYSN	MYSN
Opsin Rh1	OPS1	OPS1
Succinyl-CoA ligase [GDP-forming] subunit alpha, mitochondrial	SUCA	SUCA
Tubulin alpha-1 chain	TBA1	TBA1
Tubulin alpha-3 chain	TBA3	TBA3
Tubulin beta-1 chain	TBB1	TBB1
Tubulin beta-2 chain	TBB2	TBB2
Tropomyosin-2	TPM2	TPM2
V-type proton ATPase catalytic subunit A isoform 1	VATA1	VATA1
V-type proton ATPase catalytic subunit A isoform 2	VATA2	VATA2

\*\*\* PYK, HCD2 were temporarily considered as a likely protein target based enzyme functionality

**SUPPLEMENTAL TABLE 7: Hit candidates from the 2<sup>nd</sup> generation pull-down based on a new sample set of Chemotype 1 derivatives [T03] (securely inactive control probe).** The small molecules were covalently immobilized to NHS-magnetic sepharose beads (GE Healthcare). Bulk protein lysate from murine hepatocyte cell culture cells (AML12) was used for target protein enrichment. The bound proteins were processed by IGD. Most proteins showed similar qualitative ratios in the active [T03] and the control [T04] and were thus excluded from evaluation, since an enrichment in the active probe was the only criteria for target definition in the chosen qualitative setup. The proteins presented in this table were present at least 2 out of 3 times in the active probe and showed an enrichment in the active probe by a difference of >2 counts. (n=3, biological and technically independent replicates,  $p=0.001$ ).

protein name	Protein	[T03]	[T04]
Annexin A2	ANXA2	3	0
Alpha-enolase	ENOA	3	0
Protein FRG1	FRG1	3	0
Pyruvate kinase isozymes M1/M2	KPYM	3	1
Prohibitin-2	PHB2	3	1
Tubulin alpha-1B chain	TBA1B	3	1
Tubulin beta-4B chain	TBB4B	3	1
Tubulin beta-5 chain	TBB5	3	1
Voltage-dependent anion-selective channel protein 1	VDAC1	3	1
Zinc finger CCCH domain-containing protein 15	ZC3HF	3	1
Aspartate aminotransferase, mitochondrial	AATM	2	0
Annexin A4	ANXA4	2	0
ATP synthase subunit gamma, mitochondrial	ATPG	2	0
60 kDa heat shock protein, mitochondrial	CH60	2	0
Desmoplakin	DESP	2	0
Glutamate dehydrogenase 1, mitochondrial	DHE3	2	0
Elongation factor 1-gamma	EF1G	2	0
L-lactate dehydrogenase A chain	LDHA	2	0
Ribosylidihydronicotinamide dehydrogenase [quinone]	NQO2	2	0
Dolichyl-diphosphooligosaccharide--protein glycosyltransferase 48 kDa	OST48	2	0
Pyridoxal kinase	PDXK	2	0
Dolichyl-diphosphooligosaccharide--protein glycosyltransferase subunit 1	RPN1	2	0
Septin-11	SEP11	2	0
D-3-phosphoglycerate dehydrogenase	SERA	2	0
Tubulin beta-3 chain	TBB3	2	0



**SUPPLEMENTAL FIGURE 8: Label free quantification in the 3<sup>rd</sup> generation pull- down with Chemotype 1 [T03].** Three biological independent replicates (R) consisting of three technical replicates each were compared. Logarithmic median LTQ values between the active and inactive sample were correlated. Proteins without preference have similar values and are found within the resulting correlation line. Proteins solely identified in the active probe [T03] are artificially introduced in this figure in the straight line left (total 45 proteins). Significant enriched proteins for the active probe (t-test, p 0.001) were considered for further evaluation (see Supplemental Table 8).

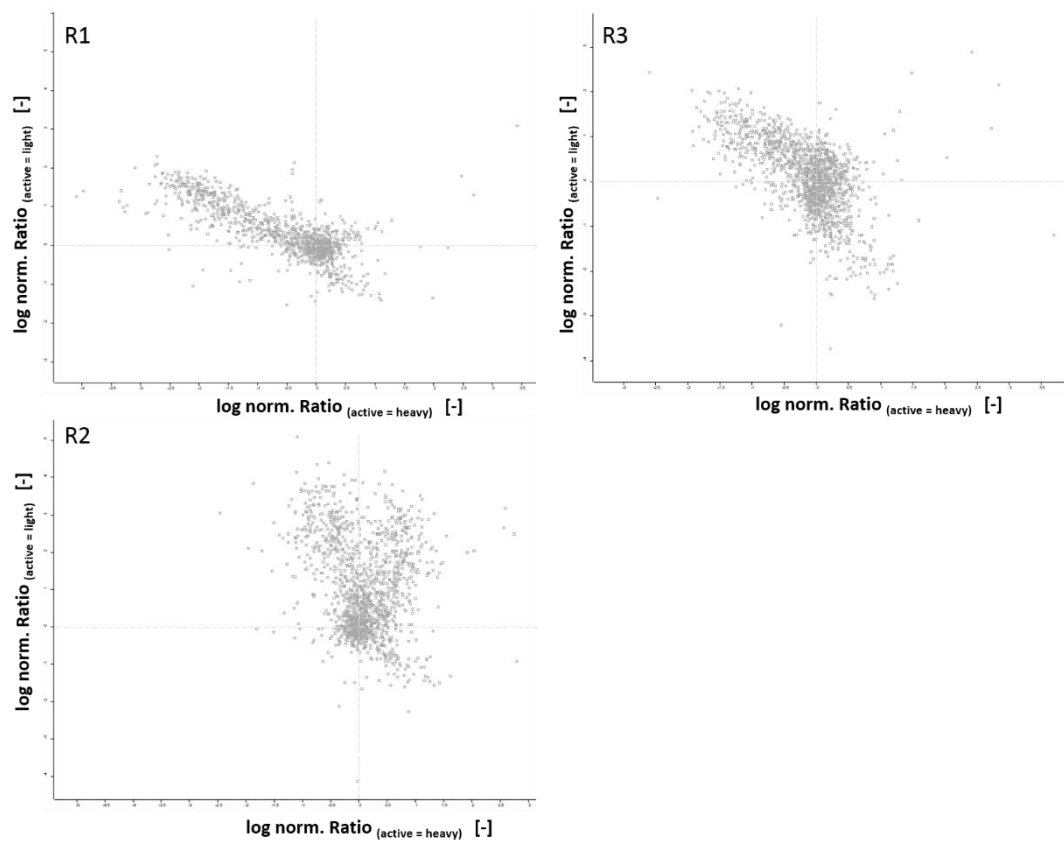
**SUPPLEMENTAL TABLE 8: Hit candidates from the 3<sup>rd</sup> generation pull-down based on label free quantitative evaluation of enriched proteins for Chemotype 1 [T03].** Chemotype 1 derivatives were covalently immobilized to NHS-magnetic sepharose beads (GE Healthcare). Bulk protein lysate from murine hepatocyte cell culture cells (AML12) was used for target protein enrichment. Significantly enriched proteins in the active probe [T03] compared to the control [T04] based on the difference of the median QLT levels. The log-transformed LTQ values between the active and inactive probe were compared (n.D. protein not present). Additionally, uncoupled beads and the negative enantiomer [T05] of Chemotype 1 (decreased activity to T03) and uncoupled NHS-magnetic beads were tested as controls. This allowed a definition of five clusters. (A) Proteins specific for the active probe, (B) proteins specific for both the highly active and the low active probe, (C-E) Likely bead contaminants. The experiment was performed in 3 biological replicates of three technical replicates each. (N= number of biological replicates where the respective protein was identified significant). Significant enriched proteins in the active probe in all replicates are highlighted red. (n=9, 3x biological replicates in 3 technical replicates each, p= 0.001).

	Protein names	Gene names	T03	T05	Bead	T04	N	
A	Histone H3	<i>Gm10257</i>	22.88	n.D.	n.D.	n.D.	2	
	<b>Sepiapterin reductase</b>	<i>Spr</i>	21.50	n.D.	n.D.	n.D.	<b>3</b>	
	<b>5-nucleotidase domain-containing protein 1</b>	<i>Nt5dc1</i>	21.29	n.D.	n.D.	n.D.	<b>3</b>	
	Peptidyl-prolyl cis-trans isomerase FKBP5	<i>Fkbp5</i>	20.69	n.D.	n.D.	n.D.	2	
	Lysophospholipase-like protein 1	<i>Lyplal1</i>	19.90	n.D.	n.D.	n.D.	2	
	<b>Epoxide hydrolase 2</b>	<i>Ephx2</i>	19.65	n.D.	n.D.	n.D.	<b>3</b>	
	Protein transport protein Sec31A	<i>Sec31a</i>	19.60	n.D.	n.D.	n.D.	1	
	Delta-1-pyrroline-5-carboxylate synthase	<i>Aldh18a1</i>	19.57	n.D.	n.D.	n.D.	1	
	Aspartate aminotransferase, mitochondrial	<i>Got2</i>	19.49	n.D.	n.D.	n.D.	2	
	Far upstream element-binding protein 1	<i>Fubp1</i>	19.29	n.D.	n.D.	n.D.	2	
	ATP-binding cassette sub-family F member 2	<i>Abcf2</i>	19.25	n.D.	n.D.	n.D.	2	
	26S proteasome non-ATPase regulatory subunit 3	<i>Psmc3</i>	19.04	n.D.	n.D.	n.D.	2	
	Importin-5	<i>Ipo5</i>	19.03	n.D.	n.D.	n.D.	1	
	Ras-related protein Rab-5C	<i>Rab5c</i>	18.56	n.D.	n.D.	n.D.	1	
Apoptosis-inducing factor 2	<i>Aifm2</i>	20.95	21.91	n.D.	n.D.	2		
B	Retinal dehydrogenase 1	<i>Aldh1a1</i>	20.21	20.68	n.D.	n.D.	1	
	Voltage-dependent anion-selective channel protein 1	<i>Vdac1</i>	20.04	20.49	n.D.	n.D.	2	
	Proliferating cell nuclear antigen	<i>Pcna</i>	20.15	20.40	n.D.	n.D.	1	
	14-3-3 protein gamma	<i>Ywhag</i>	19.99	20.29	n.D.	n.D.	2	
	Hsc70-interacting protein	<i>St13</i>	20.18	20.17	n.D.	n.D.	1	
	Aspartyl aminopeptidase	<i>Dnpep</i>	19.81	19.55	n.D.	n.D.	2	
	Protein transport protein Sec24A	<i>Sec24c</i>	19.15	19.47	n.D.	n.D.	1	
	Protein dpy-30 homolog	<i>Dpy30</i>	18.57	18.76	n.D.	n.D.	2	
C	Thymosin beta-10	<i>Tmsb10</i>	20.82	n.D.	21.52	n.D.	1	
	60S ribosomal protein L32	<i>Rpl32</i>	21.08	n.D.	21.22	n.D.	1	
	Cadherin-1;E-Cad/CTF1	<i>Cdh1</i>	19.45	n.D.	19.98	n.D.	1	
	DnaJ homolog subfamily A m3, mitochondrial	<i>Dnaja3</i>	19.94	n.D.	19.82	n.D.	1	
	EH domain-containing protein 1	<i>Ehd1</i>	19.96	n.D.	19.79	n.D.	1	
	ATP-binding cassette sub-family E member 1	<i>Abce1</i>	19.17	n.D.	19.46	n.D.	1	
	Ribosome-binding protein 1	<i>Rrbp1</i>	19.01	n.D.	19.00	n.D.	1	
	40S ribosomal protein S27-like	<i>Rps27l</i>	22.20	22.52	22.37	n.D.	2	
D	Citrate synthase, mitochondrial	<i>Csl</i>	20.42	20.37	20.36	n.D.	2	
	Synaptosomal-associated protein 23	<i>Snap23</i>	20.24	20.19	20.15	n.D.	1	
	Eukaryotic translation initiation factor 3 subunit D	<i>Eif3d</i>	19.70	20.17	19.77	n.D.	2	
	Leucine--tRNA ligase, cytoplasmic	<i>Lars</i>	19.79	20.11	19.95	n.D.	1	
	Hypoxanthine-guanine phosphoribosyltransferase	<i>Hprt1</i>	19.85	20.07	20.04	n.D.	1	
	Chloride intracellular channel protein 1	<i>Clc1</i>	19.79	20.04	19.90	n.D.	1	
	3-ketoacyl-CoA thiolase	<i>Hadhb</i>	19.45	19.36	19.33	n.D.	1	
	Eukaryotic translation initiation factor 1A	<i>Eif1ay</i>	22.63	23.04	20.95	21.23	1	
	E	Long-chain specific acyl-CoA dehydrogenase, mitochondrial	<i>Acadl</i>	22.91	22.95	21.67	21.55	2

**SUPPLEMENTAL TABLE 9: Hit candidates from the 3<sup>rd</sup> generation pull- down for Chemotype 2 [P01] based on an improved sample handling (ISD) which allowed quantitative evaluation by label free quantification.** Chemotype 2 derivatives were covalently immobilized to NHS-magnetic sepharose beads (GE Healthcare). Bulk protein lysate from murine hepatocyte cell culture cells (AML12) was used for target protein enrichment. The bound proteins were processed by ISD. Most proteins showed similar qualitative ratios in the active [P01] and the control [P02] and were thus excluded from evaluation, since an enrichment in the active probe was the only criteria for target definition in the chosen qualitative setup. The proteins presented in this table were present at least 2 out of 3 times in the active probe with a label free quantification ratio >1.5. (n=9, 3x biological replicates in 3 technical replicates each, p= 0.001).

Protein names	Gene	+++	---	A/I
Nucleoplasmin-3	Npm3	3	0	only A
Sec1 family domain-containing protein 1	Scfd1	3	0	only A
ATP synthase subunit delta, mitochondrial	Atp5d	2	0	only A
Protein NipSnap homolog 1	Nipsnap1	2	0	only A
Heterogeneous nuclear ribonucleoprotein A0	Hnrnpa0	2	0	only A
Protein MEMO1	Memo1	2	0	only A
Heterogeneous nuclear ribonucleoproteins C1/C2	Hnrnpc	2	0	only A
26S proteasome non-ATPase regulatory subunit 6	Psm6	2	0	only A
Protein MEMO1	Memo1	2	0	only A
39S ribosomal protein L40, mitochondrial	Mrpl40	2	0	only A
Histone H2A.x	H2afx	2	0	only A
Vesicular integral-membrane protein VIP36	Lman2	2	0	only A
Transmembrane 9 superfamily member 2	Tm9sf2	2	0	only A
Heterogeneous nuclear ribonucleoprotein D0	Hnrnpd	2	0	only A
SEC23-interacting protein	Sec23ip	2	0	only A
Ubiquitin-associated protein 2	Ubap2	2	0	only A
AMP deaminase 3	Ampd3	2	0	only A
Filamin-binding LIM protein 1	Fblim1	2	0	only A
SEC23-interacting protein	Sec23ip	2	0	only A
Aladin	Aaas	2	0	only A
RNA-binding protein 26	Rbm26	2	0	only A
Methylated-DNA--protein-cysteine methyltransferase	Mgmt	2	0	only A
AP-1 complex subunit mu-1	Ap1m1	2	0	only A
E3 ubiquitin-protein ligase BRE1A	Rnf20	2	0	only A
Threonine--tRNA ligase, cytoplasmic	Tars	2	2	5.77
Proliferation-associated protein 2G4	Pa2g4	3	2	5.40
Histidine--tRNA ligase, cytoplasmic	Hars	2	1	4.68
Peptidyl-prolyl cis-trans isomerase FKBP3	Fkbp3	3	3	4.54
Radixin	Rdx	3	3	4.23
Histone H2A type 1	Hist1h2ab	2	2	3.49
Ubiquitin-conjugating enzyme E2 variant 1	Ube2v	2	2	3.13
26S proteasome non-ATPase regulatory subunit 4	Psm4	2	2	2.96
Actin-related protein 2/3 complex subunit 1B	Arpc1b	2	2	2.72
Cysteine--tRNA ligase, cytoplasmic	Cars	3	3	2.63
DnaJ homolog subfamily A member 1	Dnaja1	2	1	2.50
Asparagine--tRNA ligase, cytoplasmic	Nars	3	3	2.42
Transcription elongation factor A protein 1	Tcea1	3	3	2.34
Serine--tRNA ligase, cytoplasmic	Sars	3	3	2.21
DNA-(apurinic or apyrimidinic site) lyase, mitochondrial	Apex1	3	3	2.21
Eukaryotic translation initiation factor 2A	Eif2a	3	3	2.19
Moesin	Msn	3	3	2.08
Protein kinase C and casein kinase substrate in neurons protein 2	Pacsin2	3	3	1.97
Up-regulated during skeletal muscle growth protein 5	Usmg5	2	3	1.94
Estradiol 17-beta-dehydrogenase 8	Hsd17b8	3	2	1.92
Isochorismatase domain-containing protein 2A, mitochondrial	Isoc2a	3	3	1.87
ATP synthase subunit e, mitochondrial	Atp5i	3	2	1.85
Vesicle-trafficking protein SEC22b	Sec22b	2	1	1.72
Eukaryotic translation initiation factor 2 subunit 3	Eif2s3x	3	3	1.71
Actin-related protein 2/3 complex subunit 2	Arpc2	2	3	1.71

Mitochondrial dicarboxylate carrier	Slc25a10	3	2	1.71
ATP-binding cassette sub-family E member 1	Abce1	3	3	1.69
Phosphatidylinositol phosphatase SAC1	Sacm1l	3	3	1.68
Atlastin-3	Atl3	3	3	1.66
Glycerol-3-phosphate dehydrogenase, mitochondrial	Gpd2	2	3	1.65
High mobility group protein B1	Hmgb1	3	3	1.63
Zinc transporter SLC39A7	Slc39a7	3	2	1.63
Eukaryotic translation initiation factor 3 subunit M	Eif3m	2	2	1.62
Ezrin	Ezr	3	3	1.60
ATP-binding cassette sub-family F member 2	Abcf2	3	3	1.60
Peptidyl-prolyl cis-trans isomerase FKBP5	Fkbp5	3	3	1.58
Sideroflexin-1	Sfxn1	3	3	1.58
Rho-related GTP-binding protein RhoG	Rhog	3	2	1.57
Glutamate dehydrogenase 1, mitochondrial	Glud1	3	3	1.57
Dehydrogenase/reductase SDR family member 1	Dhrs1	3	2	1.57
Estradiol 17-beta-dehydrogenase 12	Hsd17b12	3	2	1.56
Long-chain-fatty-acid--CoA ligase 4	Acsl4	3	3	1.55
Glyceraldehyde-3-phosphate dehydrogenase	Gapdh	3	3	1.54
Mitochondrial import inner membrane translocase subunit TIM44	Timm44	3	2	1.54
Ras-related protein Rab-7a	Rab7a	3	3	1.54
3-ketoacyl-CoA thiolase	Hadhb	3	3	1.54
Nascent polypeptide-associated complex subunit alpha	Naca	3	3	1.53
cAMP-regulated phosphoprotein 19	Arpp19	2	3	1.53
General transcription factor IIF subunit 2	Gtf2f2	2	1	1.52
Myoferlin	Myof	3	3	1.52
MOSC domain-containing protein 2, mitochondrial	Mosc	3	3	1.52
Glycylpeptide N-tetradecanoyltransferase 1	Nmt1	3	3	1.52
Long-chain-fatty-acid--CoA ligase 3	Acsl3	3	2	1.51
Syntaxin-12	Stx12	1	1	1.51
ATPase family AAA domain-containing protein 1	Atad1	2	2	1.50



**SUPPLEMENTAL FIGURE 9: SILAC quantification in the 4<sup>th</sup> generation pull-down for Chemotype 1 [T03].** Three technical independent replicates (R) were compared. Each dataset based on metabolically labeled lysate incubated with the respective active and inactive derivatives of Chemotype 1 including a label switch. Unspecific proteins are found at SILAC ratios around zero. Proteins with preferences towards the active probe have positive values and were considered for further investigation. The three replicates show different distributions, which attenuates statistical deviations in regard to broad standard deviations.

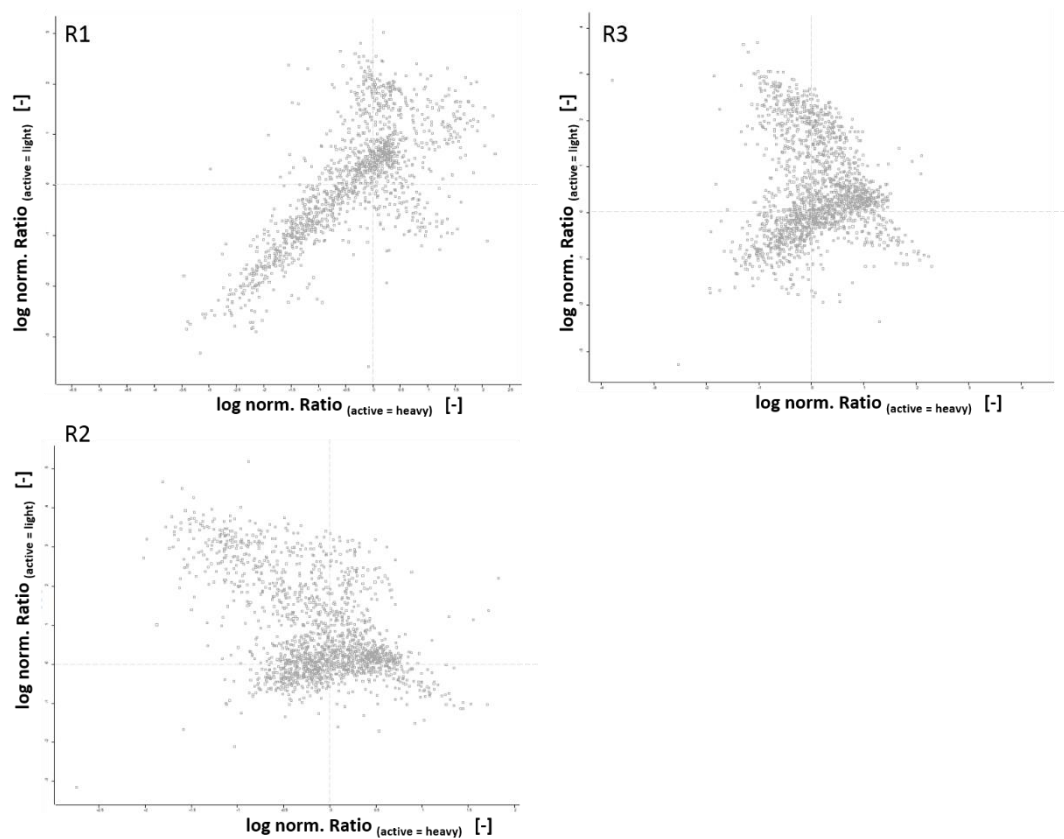
**SUPPLEMENTAL TABLE 10: Hit candidates from the 4<sup>th</sup> generation pull-down based on a SILAC.** Chemotype 1 derivatives [T03] and the control [T04] were covalently immobilized to NHS-magnetic sepharose beads (GE Healthcare). Bulk protein lysate from metabolically labeled murine hepatocyte cell culture cells (AML12) was used for target protein enrichment. Each replicate consisted of a label switch (active treated with heavy lysate/ control with light and vice versa). Based on the obtained LTQ values, the SILAC ratio (Heavy/Light) was built. Significantly enriched proteins have log SILAC ratios >0. Proteins which showed respective significance values (SigA or SigB, FDR 0.05, s0=2) were considered for further target validations. Proteins which were previously identified with high significance in the 3<sup>rd</sup> generation, are highlighted. (n=3, independent technical replicates each, p= 0.001, Pep: Sum of identified peptides).

Protein names	Gene	Mean	STD	Median	variation	Sig A	Sig B	Pep
Deoxycytidine kinase	<i>Dck</i>	2.8	0.3	2.7	0.1	2	3	19
<b>5-nucleotidase domain-containing protein 1</b>	<b><i>Nt5dc1</i></b>	<b>2.4</b>	<b>0.4</b>	<b>2.5</b>	<b>0.2</b>	<b>3</b>	<b>3</b>	<b>51</b>
Pyridoxal kinase	<i>Pdxk</i>	2.3	1	2.7	0.4	2	2	14
Mitogen-activated protein kinase 9	<i>Mapk9</i>	2.3	0.5	2.5	0.2	2	2	18
<b>Epoxide hydrolase 2</b>	<b><i>Ephx2</i></b>	<b>2.1</b>	<b>1</b>	<b>2</b>	<b>0.5</b>	<b>2</b>	<b>2</b>	<b>40</b>
<b>Sepiapterin reductase</b>	<b><i>Spr</i></b>	<b>1.7</b>	<b>0.7</b>	<b>2</b>	<b>0.4</b>	<b>2</b>	<b>2</b>	<b>89</b>
2.5-phosphodiesterase 12	<i>Pde12</i>	1.6	3.4	-0.2	2.1	1	1	10
Stomatin-like protein 2	<i>Stoml2</i>	1.5	0.3	1.4	0.2	1	2	26
Surfeit locus protein 4	<i>Surf4</i>	1.2	0.5	1.3	0.4	1	1	11
GDP-mannose 4.6 dehydratase	<i>Gmds</i>	1.1	1.9	1.1	1.7	1	1	6
Heterogeneous nuclear ribonucleoprotein U-like protein 1	<i>Hnrnpul1</i>	0.9	0.5	1.2	0.5	1	1	66
UPF0688 protein C1orf174 homolog	<i>L14Rik</i>	0.9	0.5	1.1	0.6	1	1	6
Protein MEMO1	<i>Memo1</i>	0.8	0.3	0.8	0.4	1	0	48
Translocator protein	<i>Tspo</i>	0.7	0.9	0.7	1.4	1	1	7
Multivesicular body subunit 12A	<i>Fam125a</i>	0.7	1	0.3	1.5	1	1	8
Presequence protease, mitochondrial	<i>Pitrm1</i>	0.6	1.3	-0.1	2.1	1	0	13
Transcriptional repressor p66-beta	<i>Gatad2b</i>	0.4	1.2	0.6	2.9	2	2	19
Protein S100-A6	<i>S100a6</i>	0.3	0.8	0.3	2.3	1	1	28
Enhancer of mRNA-decapping protein 4	<i>Edc4</i>	0.3	1.7	-0.3	4.9	1	1	13
C-terminal-binding protein 2	<i>Ctbp2</i>	0.3	1.1	-0.2	3.6	1	1	24
Leydig cell tumor 10 kDa protein homolog	<i>D8Erttd738e</i>	0.1	2.4	0.2	21.9	1	2	31
Uncharacterized protein C8orf59 homolog	<i>Gm4540</i>	0.1	3.1	0	30.9	2	2	11

\*\*\* Significance A gives no weight to signal intensity

\*\*\* Significance B weighted signal intensity (important as the width of the bulk distribution of logarithmic ratios depends on the protein intensity. High abundant proteins show more focused spreadings, than low abundant proteins).





**SUPPLEMENTAL FIGURE 10: SILAC quantification in the 4<sup>th</sup> generation pull-down for Chemotype 2 [P01].** Three technical independent replicates (R) were compared. Each dataset based on metabolically labeled lysate incubated with the respective active and inactive derivatives of Chemotype 1 including a label switch. The A/I ratio based on the LTQ values and was considered for evaluation. Unspecific proteins are around 0. Proteins with preferences towards the active probe have positive values and were considered for further investigation. The three replicates show different distributions, which attenuates statistical deviations in regard to broad standard deviations.

**SUPPLEMENTAL TABLE 11: Hit candidates from the 4<sup>th</sup> generation pull-down based on a SILAC for Chemotype 2.** Chemotype 2 derivative [P01] and the control [P02] were covalently immobilized to NHS-magnetic sepharose beads (GE Healthcare). Bulk protein lysate from metabolically labeled murine hepatocyte cell culture cells (AML12) was used for target protein enrichment. Each replicate consisted of a label switch (active treated with heavy lysate/ control with light and vice versa). Based on the obtained LTQ values, the SILAC ratio (Heavy/Light) was built. Significantly enriched proteins have log SILAC ratios >0. Proteins which showed respective significance values (SigA or SigB; FDR 0.05, s0= 2) were considered for further target validations. Proteins which were previously identified with high significance in the 3<sup>rd</sup> generation, are highlighted. (n=3, independent technical replicates each, p= 0.001, Pep: Sum of identified peptides).

Protein names	Gene	Mean	STD	Median	Sig A	SigB	Pep
A-kinase anchor protein 12	Akap12	2.0	2.1	1.0			13
Ras GTPase-activating protein-binding protein	G3bp1	1.3	1.5	0.7			107
Nucleolin	Ncl	1.5	1.5	1.0			172
PR domain zinc finger protein 16	Prdm16	12.9	11.2	12.9			7
Isochorismatase domain-containing protein 2A,	Isoc2a	1.7	1.5	1.1			44
Glutathione S-transferase Mu 1	Gstm1	1.6	1.3	1.2			60
Rho-associated protein kinase 2	Rock2	1.6	0.6	1.9			9
Nucleolin	Ncl	1.5	1.5	1.0			172
DNA-binding protein SMUBP-2	Ighmbp2	1.4	0.6	1.4			9
Eukaryotic translation initiation factor 3	Eif3e	1.4	0.6	1.5			13
Protein SET	Set	1.4	0.8	1.2			13
Nucleolar MIF4G domain-containing protein 1	Nom1	1.4	1.5	0.3			14
Ubiquitin-associated protein 2	Ubp2	1.3	1.0	1.1			58
Apoptosis inhibitor 5	Api5	1.3	0.9	1.4			51
Nucleolar protein of 40 kDa	Zcchc17	1.3	0.5	1.4			9
Obg-like ATPase 1	Ola1	1.3	0.6	1.1			14
Heterogeneous nuclear ribonucleoprotein K	Hnrnpk	1.3	0.8	1.1			119
WW domain-binding protein 11	Wbp11	1.2	1.0	1.0			62
Elongation factor 1-delta	Eef1d	1.2	0.7	1.1			58
Rho GDP-dissociation inhibitor 1	Arhgdia	1.2	0.7	0.7			28
Pre-mRNA-processing factor 19	Prpf19	1.2	1.0	1.0			53
Histone H1.4	Hist1h1e	1.2	1.1	1.0			86
Histone H1.3	Hist1h1d	1.2	1.0	0.9			79
Poly(U)-binding-splicing factor PUF60	Puf60	1.2	0.5	1.4			48
Hepatoma-derived growth factor-related	Hdgfrp2	1.1	0.6	1.0			8
Serine/arginine repetitive matrix protein 1	Srrm1	1.1	0.9	1.0			44
Coiled-coil domain-containing protein 124	Ccdc124	1.1	0.6	1.1			13
U6 snRNA-associated Sm-like protein LSM2	Lsm2	1.1	0.8	1.0			10
Protein LSM12 homolog	Lsm12	1.1	0.7	1.0			17
U2 small nuclear ribonucleoprotein B	Snrpb2	1.1	0.6	1.4			16
Protein Srsf11	Srsf11	1.0	0.5	1.0			38
Ubiquitin-conjugating enzyme E2 L3	Ube2l3	1.0	0.5	0.7			10
26S proteasome non-ATPase regulatory S7	Psmc7	1.0	0.4	0.7			8
Calreticulin	Calr	1.0	0.6	0.7			7
NFX1-type zinc finger-containing protein 1	Znfx1	1.0	0.9	0.4			11
Protein PAT1 homolog 1	Pat1	1.0	0.7	1.0			19
Interleukin enhancer-binding factor 2	Ilf2	0.9	0.6	0.9			11
Dynein light chain roadblock-type 1	Dynlrb1	0.9	0.4	0.7			7
Splicing factor 1	Sf1	0.9	0.6	0.8			73
Cyclin-K	Ccnk	0.9	0.5	0.9			10
DNA-3-methyladenine glycosylase	Mpg	0.8	0.7	0.4			10
PHD finger-like domain-containing protein 5A	Phf5a	0.8	0.5	0.6			9
CLIP-associating protein 1	Clasp1	0.7	0.5	0.5			21
Regulator of nonsense transcripts 1	Upf1	0.7	0.5	0.3			15
Apoptotic chromatin condensation inducer	Acin1	0.5	0.5	0.3			16
Filamin-C	Flnc	0.4	0.0	0.4			40
Pre-mRNA-splicing regulator WTAP	Wtap	0.3	0.1	0.3			6

\*\*\* Significance A gives no weight to signal intensity

\*\*\* Significance B weighted signal intensity

**SUPPLEMENTAL TABLE 12: 3<sup>rd</sup> generation of pull-downs with Chemotype 1 [T03] with an altered protocol applying lysate from cells grown at 400  $\mu$ M OA for target protein identification (see Chapter 4.2.5.2).** This experimental setup bases on the theory that the potential target might not be expressed at standard conditions, but require OA for induction of transcription, as also set in the standard LD assay. (n=3, p= 0.001, biological replicates, murine AML12 cell lysate). In grey highlighted proteins, were previously defined as high priority target candidates for Chemotype 1.

Protein names	Gene names	+++	---	A/I
5-nucleotidase domain-containing protein 1	<i>Nt5dc1</i>	3	0	only A
Deoxycytidine kinase	<i>Dck</i>	3	0	only A
Protein DEK	<i>Dek</i>	3	0	only A
Epoxide hydrolase 2	<i>Ephx2</i>	2	0	only A
Mitotic spindle assembly checkpoint protein MAD2A	<i>Mad2l1</i>	2	0	only A
Protein MEMO1	<i>Memo1</i>	2	0	only A
Pyridoxal kinase	<i>Pdxk</i>	2	0	only A
Peptidyl-prolyl cis-trans isomerase-like 3	<i>Ppil3</i>	2	0	only A
H/ACA ribonucleoprotein complex subunit 4	<i>Dkc1</i>	2	0	only A
Alpha-crystallin B chain	<i>Cryab</i>	2	0	only A
Cytohesin-2	<i>Cyth2</i>	2	0	only A
Histone-arginine methyltransferase CARM1	<i>Carm1</i>	2	0	only A
Protein SON	<i>Son</i>	2	0	only A
RNA-binding protein 47	<i>Rbm47</i>	2	0	only A
Cyclin-dependent kinase 18	<i>Cdk18</i>	2	0	only A
60S acidic ribosomal protein P1	<i>Rplp1</i>	3	3	3.9
Cyclin-G-associated kinase	<i>Gak</i>	3	3	3.4
Cytochrome c oxidase subunit 6B1	<i>Cox6b1</i>	2	2	2.4
Isochorismatase domain-containing protein 2A	<i>Isoc2a</i>	2	1	2.1
Peptidyl-prolyl cis-trans isomerase-like 4	<i>Ppil4</i>	3	3	2.1
ATP synthase subunit b, mitochondrial	<i>Atp5f1</i>	2	1	2.1
Voltage-dependent anion-selective channel protein 2	<i>Vdac2</i>	3	3	2.0
Electron transfer flavoprotein subunit alpha, mitochondrial	<i>Etfa</i>	3	3	2.0
Voltage-dependent anion-selective channel protein 1	<i>Vdac1</i>	3	2	2.0
Leucine-rich repeat protein SHOC-2	<i>Shoc2</i>	2	1	2.0
Complement component 1 Q subcomponent protein	<i>C1qbp</i>	3	3	2.0
Alpha-mannosidase 2C1	<i>Man2c1</i>	2	1	2.0
Tubulin alpha-1A chain;Tubulin alpha-3 chain	<i>Tuba1a</i>	3	3	2.0
39S ribosomal protein L33, mitochondrial	<i>Mrp133</i>	2	2	1.9
RNA-binding protein with multiple splicing	<i>Rbpms</i>	2	2	1.9
Putative RNA-binding protein 3	<i>Rbm3</i>	3	3	1.8
Isocytate dehydrogenase 3	<i>Idh3b</i>	2	2	1.7
Protein disulfide-isomerase A6	<i>Pdia6</i>	3	2	1.7
Actin-binding protein anillin	<i>Anln</i>	3	3	1.7
Histone H2A type 1	<i>Hist1h2ab</i>	3	3	1.6
Survival of motor neuron-related-splicing factor 30	<i>Smndc1</i>	2	1	1.6
ATP synthase subunit d, mitochondrial	<i>Atp5h</i>	2	2	1.6
Serine/arginine-rich splicing factor 3	<i>Srsf3</i>	3	3	1.6
ATP-binding cassette sub-family F member 1	<i>Abcf1</i>	3	2	1.6
Actin-related protein 10	<i>Actr10</i>	2	2	1.6
Epiplakin	<i>Eppk1</i>	2	2	1.6
Far upstream element-binding protein 2	<i>Khgrp</i>	2	2	1.6
Beta-centractin	<i>Actr1b</i>	2	2	1.5
Tubulin beta-5 chain	<i>Tubb5</i>	3	3	1.5
Aspartyl aminopeptidase	<i>Dnpep</i>	3	3	1.5
A-kinase anchor protein 8	<i>Akap8</i>	3	3	1.5
Epidermal growth factor receptor kinase substrate 8-lie P2	<i>Eps8l2</i>	2	1	1.5
Replication protein A 32 kDa subunit	<i>Rpa2</i>	2	2	1.5
S-phase kinase-associated protein 1	<i>Skp1</i>	2	1	1.5
Alpha-parvin	<i>Parva</i>	2	1	1.5
Cysteine-rich protein 2	<i>Crip2</i>	2	2	1.5
Peptidyl-prolyl cis-trans isomerase A	<i>Ppia</i>	3	3	1.5

**SUPPLEMENTAL TABLE 13: Modified 4<sup>th</sup> generation (SILAC), here named the two-tiered pull-down, which allows the identification of chemotype specific binding proteins.** The MS hit were analyzed as described before. Only few proteins were statistical significant (Significance A, Significance B). For that reason A/I ratios were additionally considered. Previously identified proteins with significant enrichment in the active probe are highlighted in red (4<sup>th</sup> generation) and green (2<sup>nd</sup> generation). (n=3, independent technical replicates each, p= 0.001).

Protein	Gene	CT	Mean	STDV	MEDIAN	a	b	pep
<b>Deoxycytidine kinase</b>	<b><i>Dck</i></b>	<b>CT1</b>	<b>6.8</b>	<b>7.3</b>	<b>4.8</b>	<b>2</b>	<b>2</b>	<b>19</b>
<b>Sepiapterin reductase</b>	<b><i>Spr</i></b>	<b>CT1</b>	<b>5.1</b>	<b>5.3</b>	<b>3.5</b>	<b>2</b>	<b>1</b>	<b>86</b>
<b>Epoxide hydrolase 2</b>	<b><i>Ephx2</i></b>	<b>CT1</b>	<b>4.9</b>	<b>6.2</b>	<b>2.8</b>	<b>2</b>	<b>2</b>	<b>28</b>
<b>5-nucleotidase domain-containing protein 1</b>	<b><i>Nt5dc1</i></b>	<b>CT1</b>	<b>5.4</b>	<b>5.6</b>	<b>4.0</b>	<b>1</b>	<b>1</b>	<b>45</b>
Prothymosin alpha;Thymosin alpha	<i>Ptma</i>	CT1	2.5	2.7	1.7			18
Mitogen-activated protein kinase 9	<i>Mapk9</i>	CT1	2.1	1.3	2.6			14
Eukaryotic translation initiation factor 2A	<i>Eif2a</i>	CT1	1.6	0.8	1.7			16
Transcription elongation factor SPT5	<i>Supt5h</i>	CT1	1.5	0.1	1.6			10
Protein MEMO1	<i>Memo1</i>	CT1	1.5	0.9	1.2			45
Endophilin-A2	<i>Sh3gl1</i>	CT1	1.3	0.5	1.4			10
DNA-3-methyladenine glycosylase	<i>Mpg</i>	CT1	1.3	0.5	1.4			8
U6 snRNA-associated Sm-like protein LSM2	<i>Lsm2</i>	CT1	1.2	0.5	1.5			9
General transcription factor IIF subunit 1	<i>Gtf2f1</i>	CT1	1.2	0.3	1.3			11
U2 small nuclear ribonucleoprotein B	<i>Snrpb2</i>	CT1	1.2	0.7	1.2			17
40S ribosomal protein S21	<i>Rps21</i>	CT1	1.2	0.5	1.4			12
Small nuclear ribonucleoprotein F	<i>Snrpf</i>	CT1	1.1	0.6	1.1			12
Heterogeneous nuclear ribonucleoprotein U-like	<i>Hnrnpul1</i>	CT1	1.0	0.5	0.9			55
Filamin-B	<i>Flnb</i>	CT1	1.0	0.4	1.0			228
Annexin A5	<i>Anxa5</i>	CT1	1.0	0.4	1.0			19
U2 small nuclear ribonucleoprotein A	<i>Snrpa1</i>	CT1	1.0	0.6	1.3			19
DnaJ homolog subfamily C member 9	<i>Dnajc9</i>	CT1	1.0	0.4	1.1			11
Splicing regulatory glutamine/lysine-rich protein	<i>Srek1</i>	CT1	1.0	0.4	1.0			26
Eukaryotic translation initiation factor 2 subunit	<i>Eif2s3x</i>	CT1	1.0	0.4	1.0			24
Protein unc-45 homolog A	<i>Unc45a</i>	CT1	1.0	0.7	0.6			12
U4/U6.U5 tri-snRNP-associated protein 2	<i>Usp39</i>	CT1	1.0	0.4	1.0			22
Pre-mRNA-splicing factor SPF27	<i>Bcas2</i>	CT1	0.9	0.6	0.9			20
Splicing factor 3B subunit 4	<i>Sf3b4</i>	CT1	0.9	0.6	0.8			20
PHD finger-like domain-containing protein 5A	<i>Phf5a</i>	CT1	0.7	0.5	0.5			8
Protein FAM76B	<i>Fam76b</i>	CT1	0.7	0.5	0.4			8
Ribosome biogenesis regulatory protein	<i>Rrs1</i>	CT1	0.4	0.2	0.2			10
Taperin	<i>Tprn</i>	CT1	0.3	0.0	0.3			11

Protein	Gene	CT	Mean	STDV	MEDIAN	a	b	Pep
V(D)J recombinant activating protein	<i>Rag1</i>	CT2	0.3	0.4	0.1	2	2	7
Nesprin-1	<i>Syne1</i>	CT2	0.2	0.2	0.2	1	1	6
Microsomal glutathione S-transferase 1	<i>Mgst1</i>	CT2	35.6	56.4	3.4			13
ATP synthase subunit delta. mitochondrial	<i>Atp5d</i>	CT2	29.1	31.4	20.0			10
Prohibitin-2	<i>Phb2</i>	CT2	28.7	50.0	1.9			137
Cytochrome c oxidase subunit 7A2. mitochondrial	<i>Cox7a2</i>	CT2	12.7	12.7	10.4			11
Amine oxidase [flavin-containing] A	<i>Maoa</i>	CT2	10.6	12.8	2.9			90
ATP synthase subunit epsilon. mitochondrial	<i>Atp5e</i>	CT2	10.4	13.9	1.1			18
Voltage-dependent anion-selective channel P2	<i>Vdac2</i>	CT2	9.5	12.2	2.4			88
DP-diacylglycerol-inositol phosphatidyltransferase	<i>Cdipt</i>	CT2	8.3	6.7	7.7			8
ATP synthase subunit O. mitochondrial	<i>Atp5o</i>	CT2	7.0	9.8	1.0			75
Elongation of very long chain fatty acids protein 1	<i>Elov1</i>	CT2	6.2	8.7	1.7			10
Phosphate carrier protein. mitochondrial	<i>Slc25a3</i>	CT2	6.0	6.4	3.2			89
Surfeit locus protein 4	<i>Surf4</i>	CT2	6.0	8.5	1.8			21
ATP synthase-coupling factor 6. mitochondrial	<i>Atp5j</i>	CT2	5.9	6.1	2.9			29
Dolichyl-diphosphooligosaccharide--protein glycosyltransferase subunit STT3A	<i>Stt3a</i>	CT2	5.8	5.5	5.7			30
Elongation of very long chain fatty acids protein 5	<i>Elov5</i>	CT2	5.3	8.5	0.5			9

ATP synthase subunit f. mitochondrial	<i>Atp5j2</i>	CT2	5.2	7.7	1.7	31
ATP synthase subunit b. mitochondrial	<i>Atp5f1</i>	CT2	5.0	6.1	1.6	58
Protein Tex264	<i>Tex264</i>	CT2	4.9	5.7	0.5	15
Glyceraldehyde-3-phosphate dehydrogenase	<i>Gm5069</i>	CT2	4.8	4.6	4.6	77
Isochorismatase domain-containing protein 2A	<i>Isoc2a</i>	CT2	4.8	4.5	3.9	35
Inactive hydroxysteroid dehydrogenase-like P1	<i>Hsd1l</i>	CT2	4.8	4.4	4.8	15
Glyceraldehyde-3-phosphate dehydrogenase	<i>Gapdh</i>	CT2	4.7	4.4	3.7	185
ATP synthase subunit g. mitochondrial	<i>Atp5l</i>	CT2	4.6	5.1	2.0	24
Protein MON2 homolog	<i>Mon2</i>	CT2	4.3	3.6	4.5	66
Sterol O-acyltransferase 1	<i>Soat1</i>	CT2	4.2	6.1	1.2	20
Voltage-dependent anion-selective channel P3	<i>Vdac3</i>	CT2	4.2	5.1	2.1	70
Ceramide synthase 2	<i>Cers2</i>	CT2	4.1	4.6	2.2	17
Vacuole membrane protein 1	<i>Vmp1</i>	CT2	4.0	4.3	1.9	10
NAD(P) transhydrogenase. mitochondrial	<i>Nnt</i>	CT2	3.9	3.6	4.1	77
Dolichyl-diphosphooligosaccharide--protein glycosyltransferase subunit 1	<i>Rpn1</i>	CT2	3.8	4.0	2.3	124
Exportin-1	<i>Xpo1</i>	CT2	3.7	4.2	2.2	111
Exportin-7	<i>Xpo7</i>	CT2	3.7	3.7	2.8	43
Aladin	<i>Aaas</i>	CT2	3.7	3.6	3.0	17
Atlastin-2	<i>Atl2</i>	CT2	3.6	3.6	3.1	15
Ras-related protein Rab-2A	<i>Rab2a</i>	CT2	3.6	3.8	2.0	50
3-beta-hydroxysteroid-Delta(8).Delta(7)-isomerase	<i>Ebp</i>	CT2	3.5	3.1	2.9	10
Ceramide synthase 5	<i>Cers5</i>	CT2	3.5	3.4	3.0	21
Signal peptidase complex subunit 2	<i>Spcs2</i>	CT2	3.5	3.5	2.4	23
Receptor expression enhancing protein	<i>Reep5</i>	CT2	3.4	3.8	2.1	14
Transmembrane 9 superfamily member 3	<i>Tm9sf3</i>	CT2	3.4	3.9	1.3	44
Transportin-1	<i>Tnpo1</i>	CT2	3.4	3.7	2.1	81
Atlastin-3	<i>Atl3</i>	CT2	3.3	3.5	1.5	58
Lipase maturation factor 2	<i>Lmf2</i>	CT2	3.3	3.4	1.8	27
Apoptosis regulator BAX	<i>Bax</i>	CT2	3.3	2.4	4.7	13
CAAX prenyl protease 1 homolog	<i>Zmpste24</i>	CT2	3.3	3.1	3.2	19
Vesicle-trafficking protein SEC22b	<i>Sec22b</i>	CT2	3.3	3.3	2.0	34
Mitochondrial carrier homolog 2	<i>Mtch2</i>	CT2	3.3	3.2	2.6	46
Protein transport protein Sec61 subunit alpha	<i>Sec61a1</i>	CT2	3.3	2.9	2.9	34
Ras-related protein Rab-14	<i>Rab14</i>	CT2	3.2	3.3	1.8	60
Transmembrane protein 120A	<i>Tmem120a</i>	CT2	3.2	2.8	3.4	20
ATP synthase subunit e. mitochondrial	<i>Atp5i</i>	CT2	3.2	3.7	1.6	44
NADH-cytochrome b5 reductase 3	<i>Cyb5r3</i>	CT2	3.1	3.4	1.6	39
Solute carrier organic anion transporter family	<i>Slco2a1</i>	CT2	3.1	0.8	2.9	9
Amine oxidase [flavin-containing] B	<i>Maob</i>	CT2	3.1	3.1	2.0	22
Sarcoplasmic reticulum calcium ATPase 2	<i>Atp2a2</i>	CT2	3.0	3.0	1.9	131
Ras-related protein Rab-5C	<i>Rab5c</i>	CT2	3.0	3.0	2.1	50
Sterol-4-alpha-carboxylate 3-dehydrogenase	<i>Nsdhl</i>	CT2	3.0	2.9	2.7	24
Major facilitator superfamily domain-containing P1	<i>Mfsd1</i>	CT2	2.9	3.9	0.2	7
Exportin-2	<i>Cse1l</i>	CT2	2.9	2.9	2.2	107
Dehydrogenase/reductase SDR family member 1	<i>Dhrs1</i>	CT2	2.9	2.9	2.0	47
Ras-related protein Rab-7a	<i>Rab7a</i>	CT2	2.9	3.0	1.5	68
Ras-related protein Rab-38	<i>Rab38</i>	CT2	2.9	2.7	2.7	25
Transmembrane emp24 domain-containing P10	<i>Tmed10</i>	CT2	2.9	2.8	1.5	33
85 kDa calcium-independent phospholipase A2	<i>Pla2g6</i>	CT2	2.8	2.6	2.3	40
Signal peptidase complex catalytic subunit SEC11A	<i>Sec11a</i>	CT2	2.8	3.7	0.2	11
Serine palmitoyltransferase 2	<i>Sptlc2</i>	CT2	2.8	2.8	2.0	22
Ras-related protein Rab-9A	<i>Rab9</i>	CT2	2.7	2.6	2.1	14
Thyroid adenoma-associated protein homolog	<i>Thada</i>	CT2	2.7	3.4	0.3	23
Lysophospholipid acyltransferase 5	<i>Lpcat3</i>	CT2	2.6	3.0	1.3	14
Perilipin-2	<i>Plin2</i>	CT2	2.6	2.3	2.3	43
Tripeptidyl-peptidase 1	<i>Tpp1</i>	CT2	2.6	2.2	1.9	25

Dolichyl-diphosphooligosaccharide--protein glycosyltransferase	<i>Ddost</i>	CT2	2.6	2.4	1.9	54
Zinc transporter SLC39A7	<i>Slc39a7</i>	CT2	2.5	2.3	2.4	16
Fatty acid desaturase 3	<i>Fads3</i>	CT2	2.5	2.1	2.1	39
Mitochondrial inner membrane organizing system	<i>Minos1</i>	CT2	2.5	1.6	2.4	9
Ras-related protein Rab-5B	<i>Rab5b</i>	CT2	2.5	2.0	2.4	29
Dolichyl-diphosphooligosaccharide--protein glycosyltransferase subunit 2	<i>Rpn2</i>		2.5	2.2	2.1	67
Phosphatidylinositide phosphatase SAC1	<i>Sacm1l</i>	CT2	2.4	2.2	2.2	64
Cytochrome c oxidase subunit 4 isoform 1	<i>Cox4i1</i>	CT2	2.4	1.7	2.7	30
Ras-related protein Rab-21	<i>Rab21</i>	CT2	2.4	2.0	2.1	31
Serine/threonine-protein kinase mTOR	<i>Mtor</i>	CT2	2.4	2.2	2.0	120
Very long-chain specific acyl-CoA dehydrogenase	<i>Acadvl</i>	CT2	2.4	2.1	1.8	88
Ras-related protein Rab-5A	<i>Rab5a</i>	CT2	2.3	2.1	2.0	42
Transmembrane emp24 domain-containing P9	<i>Tmed9</i>	CT2	2.3	2.0	2.2	16
GTP-binding protein SAR1a	<i>Sar1a</i>	CT2	2.3	2.1	2.3	24
Probable cation-transporting ATPase 13A1	<i>Atp13a1</i>	CT2	2.3	2.1	2.1	73
Transportin-3	<i>Tnpo3</i>	CT2	2.3	2.1	2.3	42
CUGBP Elav-like family member 1	<i>Celf1</i>	CT2	2.3	1.8	3.1	17
Protein Gcn11l	<i>Gcn11l</i>	CT2	2.3	2.1	1.9	335
Cleft lip and palate transmembrane protein 1	<i>Clptm1</i>	CT2	2.3	1.8	2.8	22
GTP-binding protein SAR1b	<i>Sar1b</i>	CT2	2.3	2.8	0.4	20
Protein YIPF5	<i>Yipf5</i>	CT2	2.3	2.0	2.2	10
Synaptojanin-2-binding protein	<i>Cox16</i>	CT2	2.3	2.2	1.7	12
Importin-5	<i>Ipo5</i>	CT2	2.3	2.3	1.4	125
Protein Tmed7	<i>Tmed7</i>	CT2	2.3	2.0	2.1	17
Long-chain-fatty-acid--CoA ligase 4	<i>Acsl4</i>	CT2	2.3	2.0	2.2	113
Dolichyl-phosphate beta-glucosyltransferase	<i>Alg5</i>	CT2	2.3	2.0	2.0	21
Ras-related protein Rab-34	<i>Rab34</i>	CT2	2.2	2.3	0.6	23
Tyrosine--tRNA ligase, mitochondrial	<i>Yars2</i>	CT2	2.2	1.7	3.1	15
Transmembrane emp24 domain-containing P2	<i>Tmed2</i>	CT2	2.2	2.0	2.0	14
Proteasome-associated protein ECM29 homolog	<i>Ecm29</i>	CT2	2.2	2.1	1.7	70
Sodium/potassium-transporting ATPase Sß	<i>Atp1b3</i>	CT2	2.2	2.0	1.8	11
Prenylcysteine oxidase	<i>Pcyox1</i>	CT2	2.2	1.9	1.9	11
Sodium- /chloride-dependent taurine transporter	<i>Slc6a6</i>	CT2	2.2	2.1	1.8	13
Sodium/potassium-transporting ATPase subunit a	<i>Atp1a1</i>	CT2	2.2	1.8	1.8	124
Acid ceramidase;Acid ceramidase subunit alpha	<i>Asah1</i>	CT2	2.2	1.9	1.9	18
Sphingosine-1-phosphate lyase 1	<i>Sgpl1</i>	CT2	2.1	1.8	1.9	53
Tetratricopeptide repeat protein 35	<i>Ttc35</i>	CT2	2.1	1.7	2.0	15
Protein YIF1B	<i>Yif1b</i>	CT2	2.1	2.4	0.5	8
Fatty acid desaturase 2	<i>Fads2</i>	CT2	2.1	1.8	1.9	37
Acetolactate synthase-like protein	<i>Ilvbl</i>	CT2	2.1	1.8	1.8	15
CD151 antigen	<i>Cd151</i>	CT2	2.1	2.6	0.3	6
Protein lunapark	<i>Lnp</i>	CT2	2.1	2.6	0.3	19
Ras-related protein Rab-10	<i>Rab10</i>	CT2	2.1	1.5	1.8	29
TAR DNA-binding protein 43	<i>Tardbp</i>	CT2	2.0	1.7	2.0	61
Uncharacterized protein KIAA0090	<i>Kiaa0090</i>	CT2	2.0	1.6	1.9	29
Brefeldin A-inhibited nucleotide exchange protein	<i>Arfgef2</i>	CT2	2.0	1.5	2.0	17
Prostaglandin E synthase 2	<i>Ptges2</i>	CT2	2.0	1.8	1.6	28
Dolichyl-diphosphooligosaccharide--protein glycosyltransferase subunit STT3B	<i>Stt3b</i>	CT2	2.0	1.7	1.5	25
Peroxisomal 2.4-dienoyl-CoA reductase	<i>Decr2</i>	CT2	2.0	1.7	1.8	26
Carnitine O-palmitoyltransferase 2, mitochondrial	<i>Cpt2</i>	CT2	2.0	1.8	1.3	14
Endoplasmic-Golgi intermediate compartmentP1	<i>Ergic1</i>	CT2	1.9	1.6	1.9	40
Importin-11	<i>Ipo11</i>	CT2	1.9	1.8	1.7	13
Major facilitator superfamily domain-containing P	<i>Mfsd10</i>	CT2	1.9	1.7	1.8	17
Golgi SNAP receptor complex member 2	<i>Gosr2</i>	CT2	1.9	1.7	1.5	20
Fatty acid desaturase 1	<i>Fads1</i>	CT2	1.9	1.7	1.7	48
Far upstream element-binding protein 1	<i>Fubp1</i>	CT2	1.9	1.4	1.5	113

Rho-related GTP-binding protein RhoG	<i>Rhog</i>	CT2	1.9	1.6	1.7	31
Membrane magnesium transporter 1	<i>Mmgt1</i>	CT2	1.9	1.1	2.1	8
Golgi resident protein GCP60	<i>Acbd3</i>	CT2	1.9	1.5	1.7	22
Serine palmitoyltransferase 1	<i>Sptlc1</i>	CT2	1.9	2.3	0.5	14
Stomatin-like protein 2	<i>Stoml2</i>	CT2	1.9	1.8	1.0	56
Membrane-associated progesterone receptor C2	<i>Pgrmc2</i>	CT2	1.9	2.3	0.3	9
Exportin-5	<i>Xpo5</i>	CT2	1.8	1.7	1.3	62
Importin-7	<i>Ipo7</i>	CT2	1.8	1.5	1.5	74
Ras-related protein Rab-18	<i>Rab18</i>	CT2	1.8	1.8	0.6	34
Peroxisomal trans-2-enoyl-CoA reductase	<i>Pecr</i>	CT2	1.8	1.2	1.6	24
3-ketoacyl-CoA thiolase	<i>Hadhb</i>	CT2	1.8	1.3	1.6	103
Mitochondrial import inner membrane translocase	<i>Timm50</i>	CT2	1.8	1.4	1.8	50
Bcl-2-like protein 1	<i>Bcl2l1</i>	CT2	1.8	1.6	1.5	8
Syntaxin-5	<i>Stx5</i>	CT2	1.8	1.1	1.7	8
Mitochondrial import receptor subunit TOM40	<i>Tomm40</i>	CT2	1.8	1.6	1.4	14
Transmembrane 9 superfamily member 4	<i>Tm9sf4</i>	CT2	1.8	1.4	1.5	11
ADP-ribosylation factor-like protein 1	<i>Arl1</i>	CT2	1.8	1.4	1.7	20
Dephospho-CoA kinase domain-containing protein	<i>Dcackd</i>	CT2	1.8	1.4	1.5	24
Protein FAM173A	<i>Fam173a</i>	CT2	1.8	1.2	1.9	10
Acyl-CoA desaturase 2;Acyl-CoA desaturase 1	<i>Scd3</i>	CT2	1.8	1.6	1.4	6
Ras-related protein Rab-8A	<i>Rab8a</i>	CT2	1.8	1.5	1.5	39
Estradiol 17-beta-dehydrogenase 8	<i>Hsd17b8</i>	CT2	1.8	1.3	1.6	36
B-cell receptor-associated protein 31	<i>Bcap31</i>	CT2	1.8	1.8	0.7	37
Heme oxygenase 2	<i>Hmox2</i>	CT2	1.7	1.6	1.3	17
NADH dehydrogenase [ubiquinone] 1 alpha sub	<i>Ndufa8</i>	CT2	1.7	1.4	1.4	15
Estradiol 17-beta-dehydrogenase 11	<i>Hsd17b11</i>	CT2	1.7	1.7	0.4	27
Transmembrane protein 11. mitochondrial	<i>Tmem11</i>	CT2	1.7	0.8	2.2	8
ATP-dependent dihydroxyacetone kinase	<i>Dak</i>	CT2	1.7	1.2	1.7	46
Short-chain dehydrogenase/reductase 3	<i>Dhrs3</i>	CT2	1.7	1.5	1.6	22
Malectin	<i>Mlec</i>	CT2	1.7	1.7	1.1	19
ATP-binding cassette sub-family D member 3	<i>Abcd3</i>	CT2	1.7	1.3	1.7	21
Peptidyl-tRNA hydrolase 2. mitochondrial	<i>Ptrh2</i>	CT2	1.7	1.6	1.3	13
Probable palmitoyltransferase ZDHHC6	<i>Zdhhc6</i>	CT2	1.7	1.4	1.5	15
Cytochrome c oxidase subunit 5B. mitochondrial	<i>Cox5b</i>	CT2	1.7	1.3	1.3	26
Importin-9	<i>Ipo9</i>	CT2	1.7	1.3	1.5	49
Transmembrane 9 superfamily member 2	<i>Tm9sf2</i>	CT2	1.7	2.0	0.3	27
NADH dehydrogenase [ubiquinone]	<i>Ndufa12</i>	CT2	1.7	1.3	1.5	17
Protoporphyrinogen oxidase	<i>Ppox</i>	CT2	1.7	1.6	0.8	8
ATPase family AAA domain-containing protein 1	<i>Atad1</i>	CT2	1.6	1.3	1.5	22
Long-chain-fatty-acid--CoA ligase 5	<i>Acs15</i>	CT2	1.6	1.3	1.5	58
Redox-regulatory protein FAM213A	<i>5730469M10Rik</i>	CT2	1.6	2.0	0.3	11
Acyl-CoA:lysophosphatidylglycerolacyltransferase1	<i>Lpgat1</i>	CT2	1.6	1.5	1.2	19
Signal recognition particle receptor subunit beta	<i>Gm20425</i>	CT2	1.6	0.9	2.1	11
Lamin-B receptor	<i>Lbr</i>	CT2	1.6	1.3	1.3	28
Acetyl-coenzyme A transporter 1	<i>Slc33a1</i>	CT2	1.6	1.8	0.5	10
Protein RER1	<i>Rer1</i>	CT2	1.6	1.1	1.5	13
Far upstream binding protein 3	<i>Fubp3</i>	CT2	1.6	1.0	1.5	94
UPF0480 protein C15orf24 homolog	<i>ORF3</i>	CT2	1.6	1.5	0.5	10
NADH dehydrogenase [ubiquinone]	<i>Ndufs8</i>	CT2	1.6	1.2	1.3	26
ATP-binding cassette sub-family B	<i>Abcb7</i>	CT2	1.6	1.3	1.4	59
NADH dehydrogenase [ubiquinone]	<i>Ndufs3</i>	CT2	1.6	1.2	1.5	23
Hexokinase-1	<i>Hk1</i>	CT2	1.5	1.0	1.4	16
Cytochrome c oxidase subunit 6C	<i>Cox6c</i>	CT2	1.5	1.0	1.6	20
Fatty aldehyde dehydrogenase	<i>Aldh3a2</i>	CT2	1.5	1.2	1.2	51
Protein ERGIC-53	<i>Lman1</i>	CT2	1.5	1.3	0.6	15
FAD synthase	<i>Flad1</i>	CT2	1.5	1.0	1.5	23
ADP-ribosylation factor-like protein 2	<i>Arl2</i>	CT2	1.5	1.1	1.4	15
4F2 cell-surface antigen heavy chain	<i>Slc3a2</i>	CT2	1.5	1.3	1.2	25

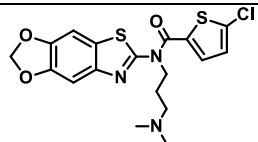
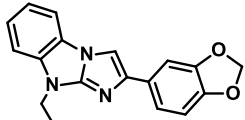
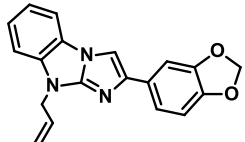
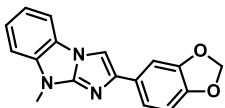
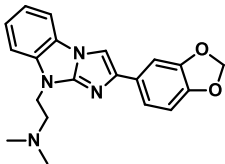
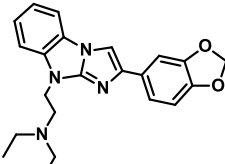
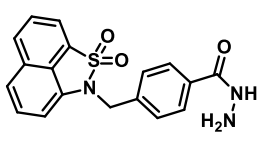
NADH dehydrogenase [ubiquinone] flavoprotein 1	<i>Ndufv1</i>	CT2	1.5	1.0	1.4	40
PRA1 family protein 3	<i>Arl6ip5</i>	CT2	1.5	1.2	1.2	27
Small glutamine-rich tetratricopeptide protein	<i>Sgta</i>	CT2	1.5	1.0	1.3	20
3-hydroxyacyl-CoA dehydratase 3	<i>ptplad1</i>	CT2	1.5	1.3	1.0	16
Ubiquitin-conjugating enzyme E2 G2	<i>Ube2g2</i>	CT2	1.5	1.1	1.3	11
Neighbor of COX4	<i>Cox4nb</i>	CT2	1.5	0.9	1.3	15
V-type proton ATPase subunit H	<i>Atp6v1h</i>	CT2	1.5	1.1	1.4	47
NADH dehydrogenase [ubiquinone]	<i>Ndufs6</i>	CT2	1.4	1.1	1.4	15
NADH dehydrogenase [ubiquinone] 1	<i>Ndufa10</i>	CT2	1.4	1.0	1.6	22
Orotate phosphoribosyltransferase	<i>Umps</i>	CT2	1.4	1.0	1.5	15
Long-chain-fatty-acid--CoA ligase 3	<i>Acs13</i>	CT2	1.4	1.1	1.1	35
Alcohol dehydrogenase class-3	<i>Adh5</i>	CT2	1.4	0.8	1.3	19
ADP-ribosylation factor-like protein 8B	<i>Arl8b</i>	CT2	1.4	1.4	0.4	24
Nucleolysin TIAR	<i>Tial1</i>	CT2	1.4	1.3	0.5	14
Tyrosine-protein phosphatase non-receptor type 1	<i>Ptpn1</i>	CT2	1.4	1.3	0.7	11
NADH dehydrogenase [ubiquinone] 1 alpha	<i>Ndufa9</i>	CT2	1.4	0.9	1.4	50
Trans-2,3-enoyl-CoA reductase	<i>Tecr</i>	CT2	1.4	1.0	1.2	45
Peroxisomal acyl-coenzyme A oxidase 2	<i>Acox2</i>	CT2	1.4	0.9	1.3	26
NADH dehydrogenase [ubiquinone] 1 alpha	<i>Ndufa13</i>	CT2	1.4	1.1	0.6	15
Cullin-2	<i>Cul2</i>	CT2	1.4	1.0	1.4	33
Ancient ubiquitous protein 1	<i>Aup1</i>	CT2	1.4	1.0	1.0	29
CDGSH iron-sulfur domain-containing protein 1	<i>Cisd1</i>	CT2	1.4	1.0	1.3	15
Calcium uniporter protein. mitochondrial	<i>Mcu</i>	CT2	1.4	1.1	1.3	15
24-hydroxycholesterol 7-alpha-hydroxylase	<i>Cyp39a1</i>	CT2	1.4	1.0	1.3	28
Polypeptide N-acetylgalactosaminyltransferase 2	<i>Galnt2</i>	CT2	1.3	0.9	1.2	18
Anoctamin-6	<i>Ano6</i>	CT2	1.3	1.4	0.5	8
Sorting and assembly machinery component	<i>Samm50</i>	CT2	1.3	1.0	1.1	42
Nicalin	<i>Ncln</i>	CT2	1.3	0.9	1.2	16
cAMP-dependent protein kinase type II-beta	<i>Prkar2b</i>	CT2	1.3	1.0	1.0	11
Pyruvate dehydrogenase E1 component	<i>Pdha1</i>	CT2	1.3	0.8	1.2	22
Ubiquitin-protein ligase E3C	<i>Ube3c</i>	CT2	1.3	1.0	0.9	19
Alkylidihydroxyacetonephosphate synthase. peroxisomal	<i>Agps</i>	CT2	1.3	1.3	0.5	32
Transferrin receptor protein 1	<i>Tfrc</i>	CT2	1.3	0.9	1.2	33
Dehydrogenase/reductase SDR family member 7B	<i>Dhrs7b</i>	CT2	1.3	1.1	1.0	24
MMS19 nucleotide excision repair protein	<i>Mms19</i>	CT2	1.3	1.5	0.3	29
All-trans-retinol 13,14-reductase	<i>Retsat</i>	CT2	1.3	1.1	0.6	23
Cytochrome P450 3A13	<i>Cyp3a13</i>	CT2	1.3	1.2	0.4	25
Sideroflexin-1	<i>Sfxn1</i>	CT2	1.3	0.7	1.2	57
Alpha-1,3/1,6-mannosyltransferase ALG2	<i>Alg2</i>	CT2	1.3	0.9	1.2	33
Basic leucine zipper	<i>Bzw1</i>	CT2	1.3	0.8	1.1	36
Poly [ADP-ribose] polymerase 16	<i>Parp16</i>	CT2	1.3	1.3	0.4	6
StAR-related lipid transfer protein 3	<i>Stard3</i>	CT2	1.3	0.9	1.1	11
Transmembrane protein 33	<i>Tmem33</i>	CT2	1.3	0.8	1.2	20
Phosphatidylinositol 4-kinase type 2-alpha	<i>Pi4k2a</i>	CT2	1.3	1.4	0.3	12
NADH dehydrogenase [ubiquinone]	<i>Ndufa6</i>	CT2	1.3	0.6	1.4	22
Catechol O-methyltransferase domain-containing	<i>Comtd1</i>	CT2	1.2	0.6	1.2	22
Transmembrane emp24 domain-containing	<i>Tmed5</i>	CT2	1.2	1.2	0.4	9
Glycerol-3-phosphate dehydrogenase.	<i>Gpd2</i>	CT2	1.2	0.7	1.2	54
Derlin-1	<i>Der11</i>	CT2	1.2	1.2	0.5	7
Glycerol-3-phosphate dehydrogenase [NAD(+)]	<i>Gpd1</i>	CT2	1.2	0.5	1.5	31
Acyl-CoA dehydrogenase family member 9	<i>Acad9</i>	CT2	1.2	0.7	1.2	22
Retinoid-inducible serine carboxypeptidase	<i>Scpep1</i>	CT2	1.2	0.9	0.7	13
MOSC domain-containing protein 2. mitochondrial	<i>Marc2</i>	CT2	1.2	0.8	1.0	56
Carnitine O-palmitoyltransferase 1. liver isoform	<i>Cpt1a</i>	CT2	1.2	0.7	1.2	67
Magnesium transporter protein 1	<i>Magt1</i>	CT2	1.2	1.1	0.5	13
Immunity-related GTPase family M protein 1	<i>Irgm1</i>	CT2	1.2	0.7	1.3	39
ATP-dependent zinc metalloprotease YME1L1	<i>Yme1l1</i>	CT2	1.2	0.7	1.0	18



Cytochrome c1. heme protein. mitochondrial	<i>Cyc1</i>	CT2	1.2	0.8	0.6	16
Mitochondrial Rho GTPase 1	<i>Rhot1</i>	CT2	1.2	1.3	0.3	6
Ferrochelatase;Ferrochelatase. mitochondrial	<i>Fech</i>	CT2	1.2	0.5	1.2	19
ABC transporter family protein member 4	<i>Abcc4</i>	CT2	1.2	0.7	1.2	43
Dual specificity mitogen-activated protein kinase	<i>Map2k3</i>	CT2	1.2	0.5	1.1	7
UDP-glucuronosyltransferase 1-7C	<i>Ugt1a6</i>	CT2	1.1	0.8	1.0	41
Peflin	<i>Pef1</i>	CT2	1.1	0.5	1.1	14
RNA 3-terminal phosphate cyclase	<i>Rtcd1</i>	CT2	1.1	0.5	1.5	15
Up-regulated during skeletal muscle protein	<i>Usmg5</i>	CT2	1.1	0.5	1.1	12
Erythrocyte band 7 integral membrane protein	<i>Stom</i>	CT2	1.1	0.5	1.1	16
NADH dehydrogenase [ubiquinone] 1 subunit C2	<i>Ndufc2</i>	CT2	1.1	0.8	1.1	10
Translocon-associated protein subunit delta	<i>Ssr4</i>	CT2	1.1	0.6	1.1	17
Monoacylglycerol lipase ABHD12	<i>Abhd12</i>	CT2	1.1	0.8	1.0	34
FAS-associated factor 2	<i>Faf2</i>	CT2	1.1	0.8	1.1	24
Retinol dehydrogenase 10	<i>Rdh10</i>	CT2	1.1	1.0	0.8	15
Patatin-like phospholipase domain-containing P2	<i>Pnpla2</i>	CT2	1.1	0.8	1.1	12
Thymidylate kinase	<i>Dtymk</i>	CT2	1.1	0.5	1.0	20
Glycerol-3-phosphate acyltransferase 4	<i>Agpat6</i>	CT2	1.1	1.1	0.4	14
Isobutyryl-CoA dehydrogenase. mitochondrial	<i>Acad8</i>	CT2	1.1	0.5	0.7	27
MCG201409	<i>Mettl7a1</i>	CT2	1.1	0.9	0.5	16
Reticulon-4	<i>Rtn4</i>	CT2	1.1	0.6	0.7	10
Erlin-2	<i>Erlin2</i>	CT2	1.1	0.7	1.1	14
Syntaxin-12	<i>Stx12</i>	CT2	1.1	0.9	0.5	14
NADH dehydrogenase flavoprotein, mitochondrial	<i>Ndufv3</i>	CT2	1.1	1.0	0.5	6
Alpha-soluble NSF attachment protein	<i>Napa</i>	CT2	1.1	0.6	0.7	14
GTP-binding protein	<i>Irfi47</i>	CT2	1.1	0.8	1.0	16
Estradiol 17-beta-dehydrogenase 12	<i>Hsd17b12</i>	CT2	1.1	0.5	1.1	79
Ras-related protein R-Ras	<i>Rras</i>	CT2	1.1	0.8	0.4	31
Emerin	<i>Emd</i>	CT2	1.0	0.6	1.4	17
Apolipoprotein O	<i>Apoo</i>	CT2	1.0	0.7	0.6	9
Ataxin-10	<i>Atxn10</i>	CT2	1.0	0.8	0.9	13
Fatty acyl-CoA reductase 1	<i>Far1</i>	CT2	1.0	0.7	0.9	28
Prolectin regulatory element-binding protein	<i>Preb</i>	CT2	1.0	0.6	1.0	17
Sideroflexin-3	<i>Sfxn3</i>	CT2	1.0	0.5	1.0	46
Importin-4	<i>Ipo4</i>	CT2	1.0	0.6	1.0	22
G-protein coupled receptor family C group 5	<i>Gprc5c</i>	CT2	1.0	0.5	1.0	14
Glutathione S-transferase kappa 1	<i>Gstk1</i>	CT2	1.0	0.5	1.0	17
Oxidoreductase HTATIP2	<i>Htatip2</i>	CT2	1.0	0.8	0.5	10
NADH dehydrogenase [ubiquinone] iron-sulfurP7	<i>Ndufs7</i>	CT2	1.0	0.8	0.4	11
Calcium-binding mitochondrial carrier Aralar1	<i>Slc25a12</i>	CT2	0.9	0.6	0.9	22
Basic leucine zipper and W2 domain-containing P2	<i>Bzw2</i>	CT2	0.9	0.5	0.7	14
CDGSH iron-sulfur domain-containing protein 2	<i>Cisd2</i>	CT2	0.9	0.9	0.3	9
2-oxoisovalerate dehydrogenase subunit beta	<i>Bckdhb</i>	CT2	0.9	0.6	0.7	9
Ubiquitin carboxyl-terminal hydrolase 3	<i>Usp3</i>	CT2	0.9	0.4	0.6	7
Sec1 family domain-containing protein 1	<i>Scfd1</i>	CT2	0.9	0.8	0.4	15
Cytochrome c oxidase subunit 7A-related protein	<i>Cox7a2l</i>	CT2	0.8	0.8	0.3	7
F-box only protein 22	<i>Fbxo22</i>	CT2	0.8	0.5	0.6	8
Peroxisomal membrane protein 11B	<i>Pex11b</i>	CT2	0.8	0.5	0.6	8
H-2 class I histocompatibility antigen	<i>H2-D1</i>	CT2	0.7	0.4	0.4	9
26S proteasome non-ATPase regulatory subunit 1	<i>Psmc1</i>	CT2	0.7	0.5	0.5	17
FUN14 domain-containing protein 2	<i>Fundc2</i>	CT2	0.7	0.5	0.4	9
CCAAT/enhancer-binding protein zeta	<i>Cebpz</i>	CT2	0.6	0.0	0.6	10
NADH dehydrogenase [ubiquinone] 1	<i>Ndufb4</i>	CT2	0.6	0.1	0.5	12
Cytochrome c-type heme lyase	<i>Hccs</i>	CT2	0.3	0.1	0.3	11
Nucleoporin NDC1	<i>Tmem48</i>	CT2	0.3	0.1	0.3	10

## 9.4 TARGET IDENTIFICATION FOR CHEMOTYPE 1

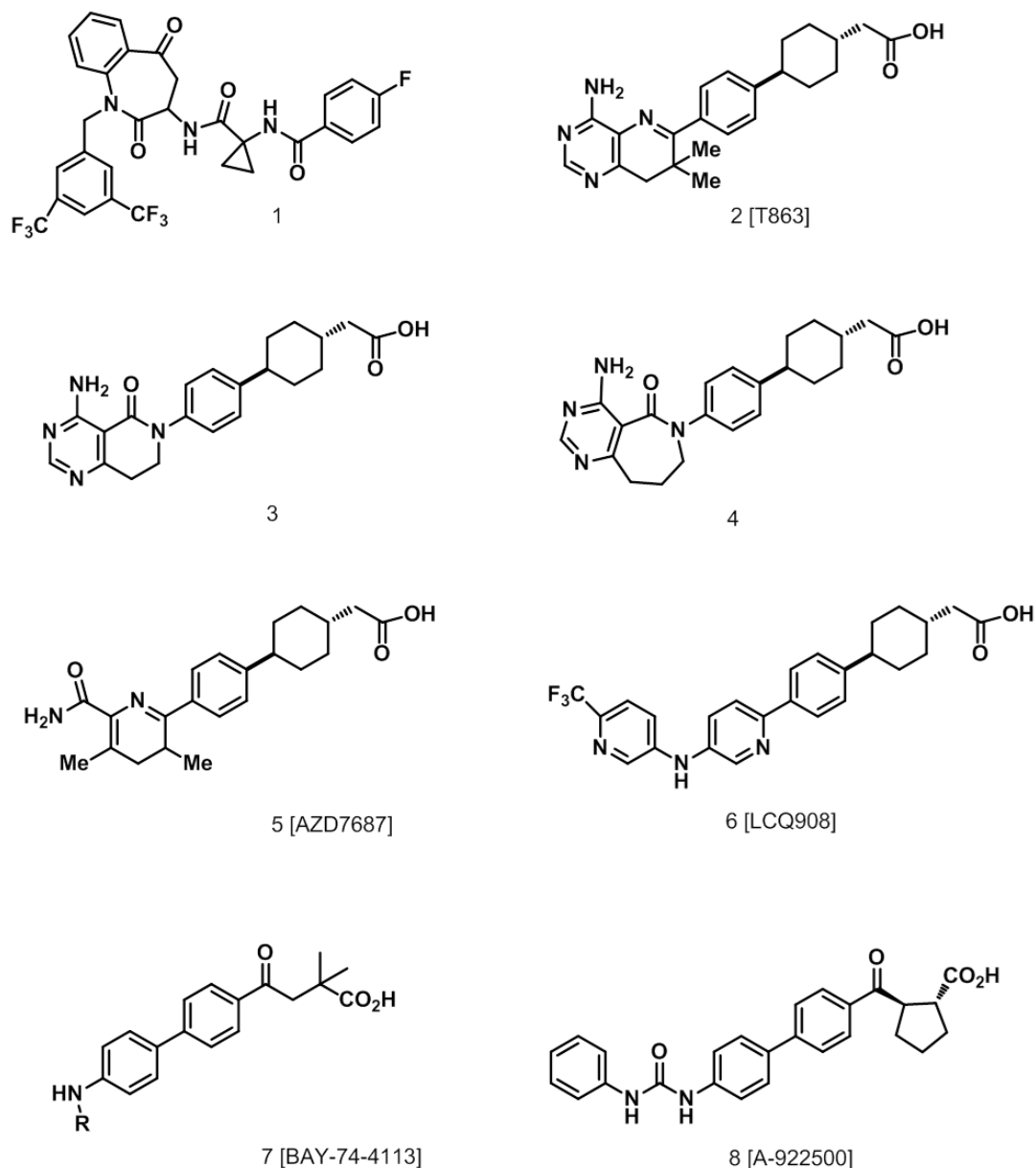
**SUPPLEMENTAL TABLE 14: Hits from a literature described pyruvate kinase screen** originating from virtual scaffold libraries (Wetzel et al, 2009). The PKYK inhibitors were tested in the LD assay for a phenocopy which would indicate an involvement of the glycolytic enzyme in the generation of the LD reduced phenotype.

ID	Structure	Activity Type	AC <sub>50</sub> [μM]
<b>W1</b> PKL-39		Inhibitor	8.9 ± 1.1
<b>W2</b> PKL-66		Inhibitor	2.0 ± 0.3
<b>W3</b> PKL-68		Inhibitor	10.5 ± 1.6
<b>W4</b> PKL-65		Inhibitor	1.0 ± 0.1
<b>W5</b> PKL-69		Inhibitor	1.7 ± 0.3
<b>W6</b> PKL-70		Inhibitor	2.2 ± 0.3
<b>W7</b> PKL-1		Activator	4.9 ± 0.6

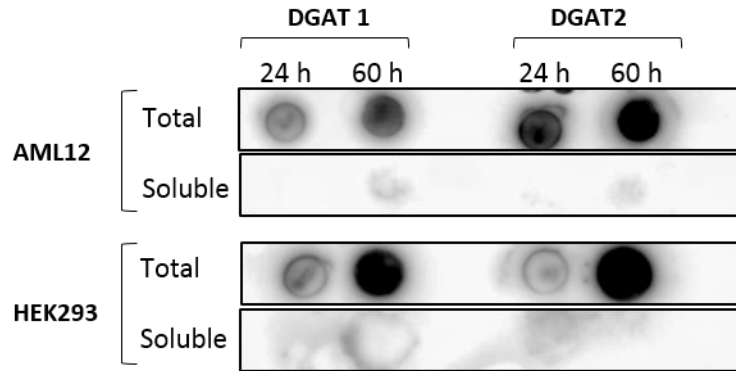
## 9.5 TARGET IDENTIFICATION FOR CHEMOTYPE 2

**SUPPLEMENTAL TABLE 15: Selected Hits from SEA analysis for Chemotype 2 (Similarity Ensemble Approach; [sea.bkslab.org/](http://sea.bkslab.org/)).** The respective hits represent human proteins (if not noted differently). Similarity was considered based on the estimation value (E- value) and routinely is considered if lower than  $10^{-10}$ . However, the cut off for prediction is not clear and cases where increased values led to the target are known (DeGraw et al, 2010; Keiser et al, 2009).

Hit	CODE	# Ligands	Reference Name	E-value	Max TC
1	DGAT1	129	Diacylglycerol O-acyltransferase 1 [1000 nM]	5.93e-49	0.36
2	DGAT1	145	Diacylglycerol O-acyltransferase 1 [10000 nM]	5.85e-46	0.36
3	PRKDC	560	DNA-dependen protein kinase [10000 nM]	9.42e-34	0.38
4	DGAT1	65	Diacylglycerol O-acyltransferase 1 [100 nM]	9.29e-30	0.35
5	B2CL11	10	Apoptosis regulator Bcl-X [1nM]	2.67e-26	0.31
8	LT4R2 (GPCR)	22	Leukotriene B4 eceptor 2 [1 nM]	2.35e-17	0.30
11	DCMC (mouse)	9	Malonyl-CoA decarboxylase, mitochondrial [10000 nM]	1.98e-15	0.32



**SUPPLEMENTAL FIGURE 11: Know DGAT1 inhibitors.** **1I** Merck (Benzazepinedone); causes weight loss in diet induced obesity mice by prolonged GLP-1 and PYY release. **2I** Japan Tobacco (Tularik/ T863: phenylcyclohexane acetic acid), initiate weight reduction in mice by lowering the cholesterol and TAG levels by competition at the DGAT oleoyl-CoA binding site. The small molecule was the tool small molecule for probe optimization of small molecules (3-6). Clinical studies were stopped 2007. **3I** Pfizer (Carbon linked lactam) with unsuitable metabolic properties. **4I** Pfizer (pyrimidin oxazepinone core) results in high activities ( $IC_{50} = 19$  nM (biochemically); 8 nM (cell based). Clinical study in 2009. **5I** AstraZeneca (AZD7687) inhibits selectively ACAT1, ACAT2, DGAT2 with high activities (80 nM). Clinical studies were stopped in 2011 due to nausea, diarrhea, vomiting. **6I** Novartis (LCQ908), improved metabolic stability compared to (3), however, clinical studies were stopped 2011, due to a lack of efficacy and gastrointestinal side effects. **7I** Bayer AG (BAY-74113). The biaryl amides were optimized from a ketoacid lead from a HTS screen. This small molecule was then licensed to Pfizer 8PF-04415060). **8I** Abbott Laboratories (A-922500), was developed from (7) and showed first positive clinical results. (Reviewed by DeVita & Pinto, 2013).

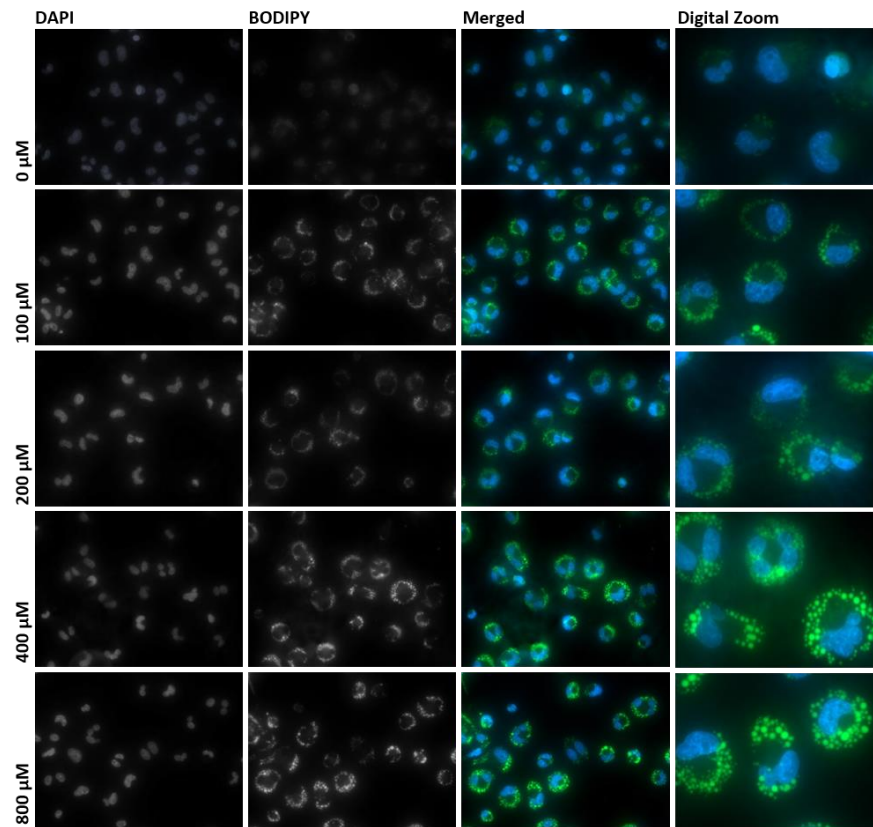


**SUPPLEMENTAL FIGURE 12** Dotblot of DGAT1-His and DGAT2-His overexpression in AML12 and Hek293 cells. The cells were transfected and cultured for 24h and 60h respectively. Total cell lysates base on the direct lysis in detergent rich SDS-Sample loading buffer without any centrifugation steps. Soluble lysates only contain mild detergent concentrations and the insoluble membrane fraction is removed by centrifugation. Recombinant DGAT enzymes were detected by immunoblotting targeting the His-Tag. Both DGAT isoforms were enriched in the detergent rich total lysate (includes membrane fraction), while both enzymes remained absent in the soluble lysate.

**SUPPLEMENTAL TABLE 16: Manually identified DGAT1 peptides in the affinity based chemical proteomic approach for TARGET ID.** AI Active probe (Heavy; > 1 A/I ratios expected), BI inactive probe (Heavy; <1 A/I ratios expected). Due to the low number of peptides the validity was diminished.

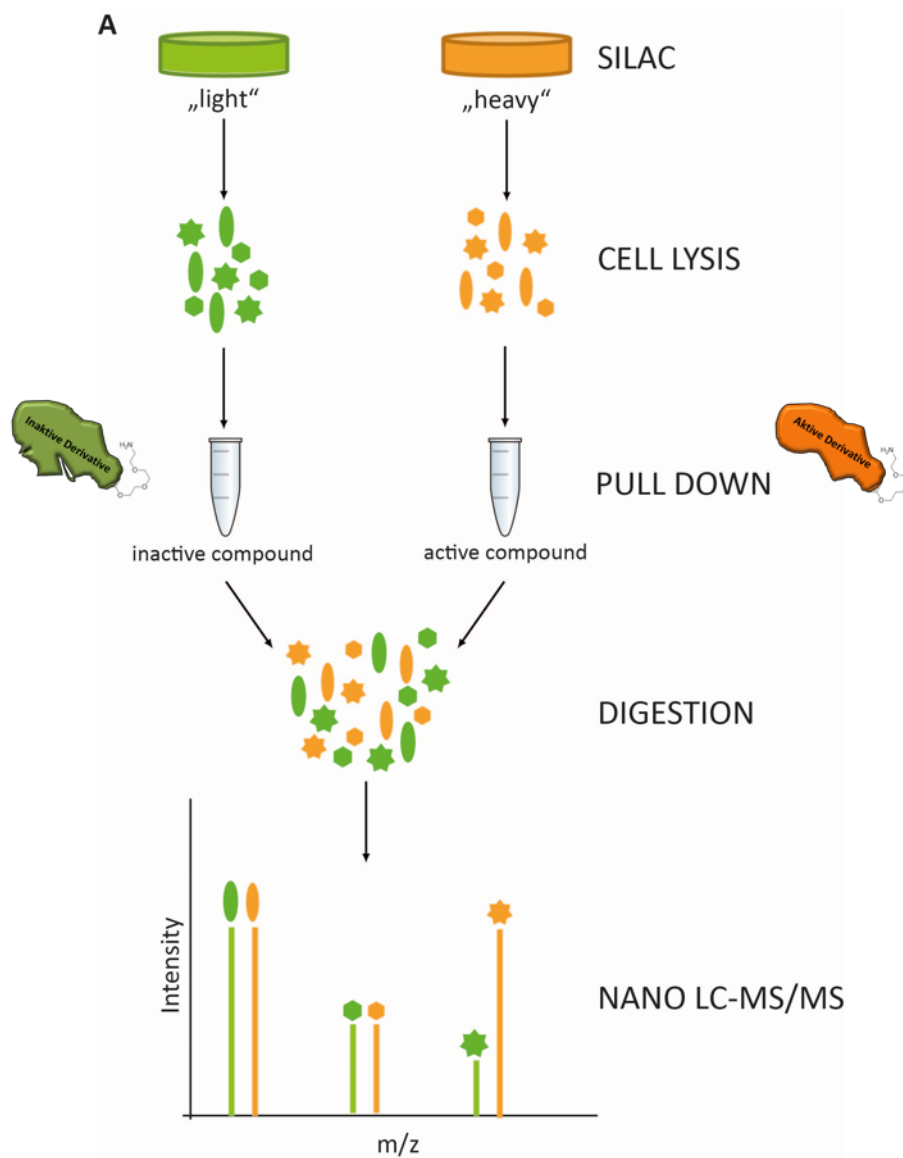
A	Sequence	Gene	MS/MS m/z	Charge	m/z	Mass	MS/MS Count	Ratio H/L		Max intensity m/z 0	Max intensity m/z 1	Retention time	MS/MS Scan Number	Kommentar
								Ratio H/L	normalize d					
	DAAVSPDLGAGGDAPAPAPAHTR	Dgat1	761.71	3	761.3769	2281.109	1	0.31823	0.51178	761.7112	765.0475	43.617	20723	ok
	TSVGDGYWDLR	Dgat1	640.87	2	634.7989	1267.583	1	0.35149	0.57101	634.7988	639.8026	58.242	29219	ok
	DAAVSPDLGAGGDAPAPAPAHTR	Dgat1	761.72	3	761.3769	2281.109	1	0.48411	0.75326	761.7114	765.0476	43.813	20844	ok
	DAAVSPDLGAGGDAPAPAPAHTR	Dgat1	761.71	3	761.3769	2281.109	1	0.31823	0.51178	761.7112	765.0475	43.617	20723	ok
	TSVGDGYWDLR	Dgat1	640.87	2	634.7989	1267.583	1	0.35149	0.57101	634.7988	639.8026	58.242	29219	Ok
	VSVQGGSGPKVEEDEV	Dgat1	591.63	3	591.2989	1770.875	1	2.1056	2.9041	NaN	NaN	32.597	12660	Noise
	DAAVSPDLGAGGDAPAPAPAHTR	Dgat1	762.05	3	761.3769	2281.109	1	0.13952	0.25999	761.7111	764.7133	44.537	16903	Ok
	VSVQGGSGPKVEEDEV	Dgat1	591.63	3	591.2989	1770.875	1	4.9574	7.1064	NaN	NaN	33.089	11710	Signal overlay
	VSVQGGSGPKVEEDEV	Dgat1	591.63	3	591.2989	1770.875	1	3.024	5.5372	NaN	NaN	32.682	11427	Signal overlay
	DAAVSPDLGAGGDAPAPAPAHTR	Dgat1	761.72	3	761.3769	2281.109	1	0.48411	0.75326	761.7115	765.0476	43.813	20844	ok
<b>B</b>	DAAVSPDLGAGGDAPAPAPAHTR	Dgat1	765.87	3	761.3769	2281.109	1	1.3415	1.6632	761.7117	765.0477	43.367	20610	ok
	DAAVSPDLGAGGDAPAPAPAHTR	Dgat1	765.37	3	761.3769	2281.109	1	0.88837	1.0284	761.7109	765.0475	43.656	20916	ok
	VSVQGGSGPKVEEDEV	Dgat1	592.67	3	591.2989	1770.875	1	1.213	1.4017	591.2989	596.6416	32.137	14272	Signal overlay
	DAAVSPDLGAGGDAPAPAPAHTR	Dgat1	761.71	3	761.3769	2281.109	1	1.1053	3.6425	NaN	NaN	44.022	20347	Noisy signal
	DAAVSPDLGAGGDAPAPAPAHTR	Dgat1	765.87	3	761.3769	2281.109	1	1.3415	1.6632	761.7117	765.0478	43.367	20610	Ok
	DAAVSPDLGAGGDAPAPAPAHTR	Dgat1	765.37	3	761.3769	2281.109	1	4.0652	2.4105	761.7112	764.7136	44.449	17060	Ok
	TSVGDGYWDLR	Dgat1	639.8	2	634.7989	1267.583	1	4.8272	3.1248	NaN	NaN	59.538	24021	Noisy signal
	DAAVSPDLGAGGDAPAPAPAHTR	Dgat1	765.37	3	761.3769	2281.109	1	3.0227	1.9608	761.3745	765.0477	44.411	16846	ok
	DAAVSPDLGAGGDAPAPAPAHTR	Dgat1	765.37	3	761.3769	2281.109	1	0.88837	1.0284	761.7109	765.0475	43.656	20916	ok
	DAAVSPDLGAGGDAPAPAPAHTR	Dgat1	765.37	3	761.3769	2281.109	1	0.97788	1.2928	761.3737	764.713	44.523	17591	ok

## 9.7 COMAS SCREEN

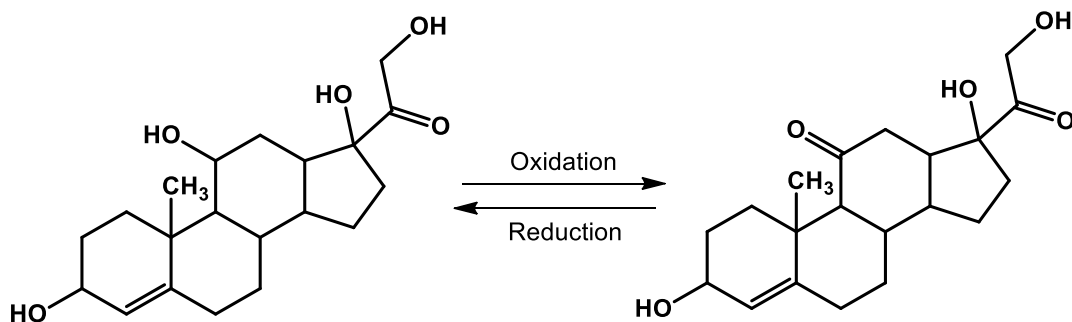


**SUPPLEMENTAL FIGURE 13: Oleic Acid Titration in THP-1 cells** in order to identify a suitable OA screening concentration in differentiated THP-1 cells. Fluorescent images were acquired at 40x magnification at a Zeiss Observer Microscope (blue: nuclei, green: lipid droplets).

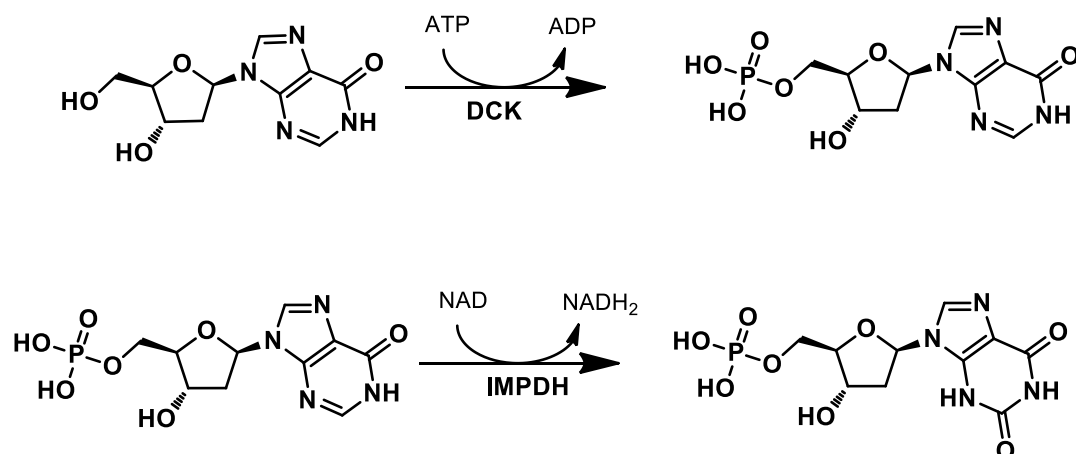
## 9.8 BACKGROUND INFORMATION ON ASSAYS AND METHODS



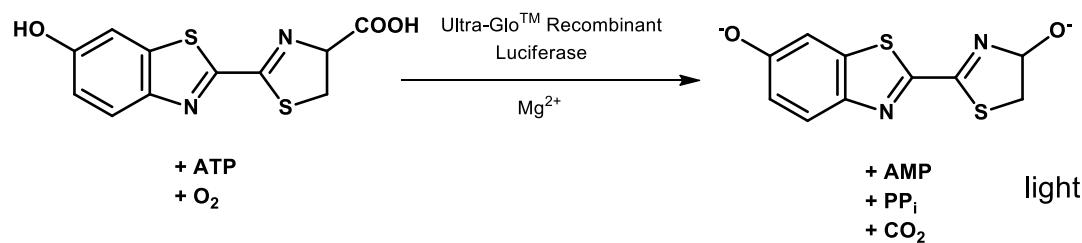
**SUPPLEMENTAL FIGURE 14: Schematic summary of stable isotope labeling by amino acids in cell culture (SILAC).** Cells are metabolically labeled by presence or absence of heavy amino acids  $^{13}\text{C}_6$ -L-lysine and  $^{13}\text{C}_6^{15}\text{N}_4$ -L-arginine in the respective culture medium. The heavy and light lysates were then individually used in chemical proteomic affinity purification depending on active and inactive derivatives of the investigated chemotype. The protein decorated beads were mixed and digested as one sample. The peptides were then mass spectrometrically analyzed using a Q-Exactive™ Hybrid Quadrupol (Thermo Scientific). The mass difference ( $\Delta 6$  Da) of labeled peptides were considered for protein quantification. (Image: Adapted from Dr. Verena Pries, MPI Dortmund).



**SUPPLEMENTAL FIGURE 15:** The cell based 11 $\beta$ -HSD assay measures the 11 $\beta$ -HSD1 dependent oxo-reduction from cortisol and the 11 $\beta$ -HSD2 dependent oxidation of cortisone from lysates of stably transfected HEK293-cells. Using 3H-labeled substrates allowed quantification of the steroid products by scintillation counting.

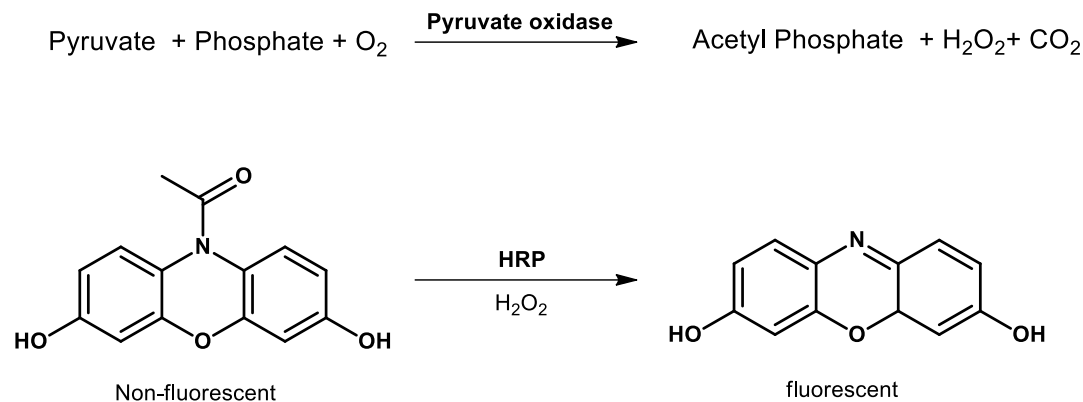


**SUPPLEMENTAL FIGURE 16: PRECICE® DCK SCREENING ASSAY.** DCK activity was measured in an enzymatic in vitro assay on basis that DCK provides the phosphorylation of both purine and pyrimidine deoxynucleosides. In the first reaction deoxyinosine (DIR) is phosphorylated in presence of ATP by the DCK reaction to Deoxyinosine monophosphate (dIMP). Latter is then oxidized in a second reaction to deoxyxanthosine monophosphate (dXMP) by IMPDH in the presence of NAD, leading to NADH<sub>2</sub> formation, which can be measured at 340 nm.

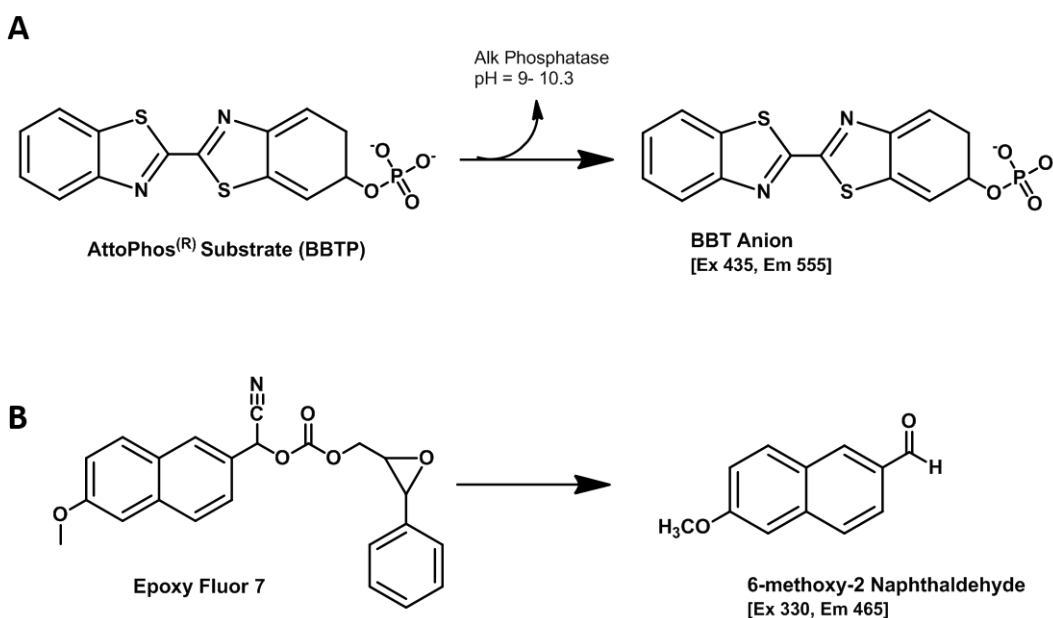


**SUPPLEMENTAL FIGURE 17:** Cell viability was quantified using the CellTiterGlo® Reaction Kit (Promega) based on quantitation of cellular ATP levels as an indicator of metabolically active cells. The quantification bases on an ATP dependent luciferase reaction which catalyzes the mono-oxygenation of beetle luciferin in presence of ATP, Mg<sup>2+</sup> and molecular oxygen. The resulting luminescence signal is proportional to the ATP concentration which correlates linearly with the cell number.

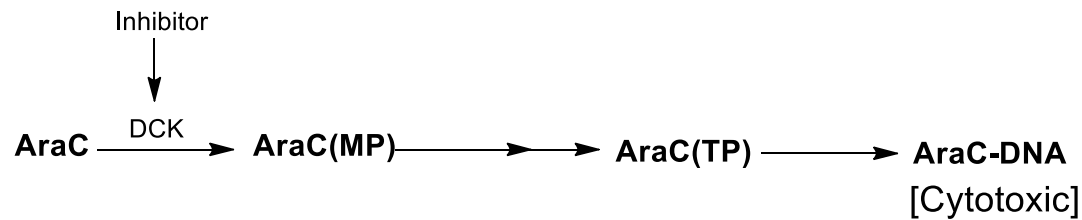




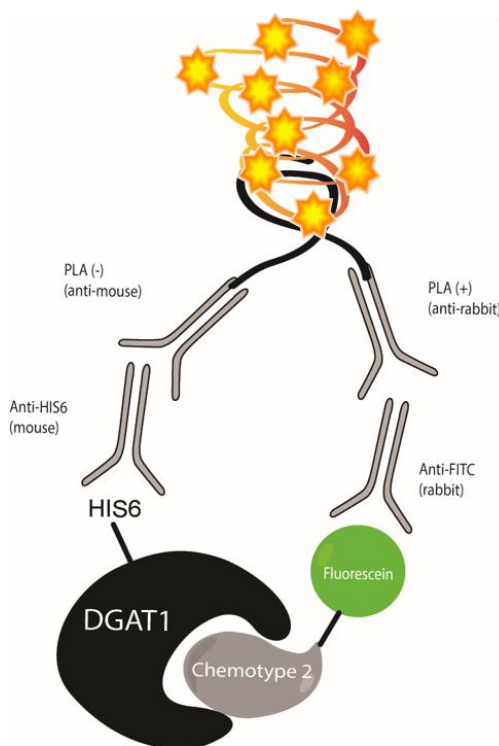
**SUPPLEMENTAL FIGURE 18:** The cell based assay bases on the KPYK dependent reaction from phosphoenolpyruvate (PEP) and ADP to pyruvate and ATP in the primary reaction. Pyruvate is by pyruvate oxidized to acetyl phosphate under a stoichiometric production of H<sub>2</sub>O<sub>2</sub>, which then can be quantified in an Amplex Red™ reaction. Fluorescence is measured at λEx 535 nm and λEm 587 nm.



**SUPPLEMENTAL FIGURE 19:** The N-terminal phosphatase activity (EC 3.1.3.76) of recombinant murine EPHX2 was measured by EPHX2 dependent production of the fluorescent dephosphorylation BBT Product of the AttoPhos<sup>®</sup> Substrate (BBTP: 2'-[2-benzothiazoyl]-6'-hydroxybenzothiazole phosphate). The assay was performed in analogy to the method described by Morisseau (Morisseau et al. 2012). To monitor the c-terminal epoxide hydrolase activity in a cell based assay, an Epoxy Fluor 7 was provided as a substrate. The hydrolysis by endogenous EPHX2 in cell lysates yields the highly fluorescent product 6-methoxy-2-Naphthaldehyde. This can be monitored at excitation and emission wavelengths of 330 and 465 nm, respectively.



**SUPPLEMENTAL FIGURE 20: Schematic summary of the AraC cell based assay.** Inhibition of DCK prevents in a cellular environment the incorporation of AraC into DNA. This rescues AraC cytotoxicity and can be quantified by viability readout such as the ATP level by the CellTiterGlo<sup>®</sup> reagent (Promega). The assay was described for HTS by (Yu et al, 2010).



- 5) rolling circle amplification results in a concatemeric product containing fluorescently labeled nucleotides
- 4) ligation of the two PLA probes or a closed circle if a close proximity is guaranteed.
- 3) secondary antibody detection using PLA antibodies with conjugated complementary oligonucleotides (Plus/ Minus strand)
- 2) Primary antibody detection of small molecule label and target protein label
- 1) small molecule target interaction

**SUPPLEMENTAL FIGURE 21: Schematic summary of the applied in situ Duolink<sup>®</sup> using PLA<sup>®</sup> Technology (Sigma Aldrich) in order to investigate the potential interaction of DGAT1 and Chemotype 2.** If the fluorescein labeled derivative of Chemotype 2 is in close proximity to overexpressed DGAT1-His, both species can be detected via antibody recognition. The PLA<sup>®</sup> specific antibodies contain complementary oligonucleotide sequences, which allow rolling cycle amplification if both primers are in close proximity. The signal dependent on fluorescent nucleotides can be detected during fluorescence microscopy as orange dots.

## ACKNOWLEDGEMENTS

Wie ich schon direkt zu Beginn der Arbeit mit dem Zitat von Graham Greene hervorgehoben habe „*Keiner kommt von einer Reise so zurück wie er weggefahren ist*“, war die Doktorarbeit für mich eine Reise die mich wissenschaftlich, aber auch menschlich geprägt hat. Ich möchte hiermit den Personen danken, die mich auf dem Weg begleitet haben und mir mit Rat und Tat zur Seite standen. Besonders hervorheben möchte die folgenden Personen:

**DR. MATHIAS BELLER** (HHU) – der mich als Doktorvater auf dem Weg der Doktorarbeit immer mit vollem Einsatz begleitet hat. Ohne ihn wäre diese Arbeit nicht möglich gewesen.

**PROF. DR. HERBERT WALDMANN** (MPI DORTMUND) – der mir die Möglichkeit gegeben hat Teil seiner interdisziplinären Arbeitsgruppe der Chemischen Biologie in Dortmund zu werden, in der ich die Chance hatte *state of the art* Methoden zu Erlernen und von langjähriger wissenschaftlicher Erfahrung profitieren konnte.

**PROF. DR. HERBERT JÄCKLE** (MPI GÖTTINGEN) – der meine Doktorarbeit finanziell und wissenschaftlich Unterstützt hat und zudem die Teilnahme an der internationalen Lipid Droplet Konferenz in Vermont unterstützt hat.

**DR. SLAVA ZIEGLER** (MPI DORTMUND) – die mir als Doktormutter am MPI in Dortmund immer mit gutem Rat zur Seite stand.

**DR. PETRA JANNING** (MPI DORTMUND) – die gefühlt Tausende meiner MS-Proben, die ich im Laufe meiner Doktorarbeit produziert habe, analysiert hat und sich immer die Zeit genommen hat, jeden einzelnen gewünschten Datenpunkt im Detail zu diskutieren.

**DR. SONJA SIEVERS** (COMAS) – die es mir ermöglicht hat das *high end* Equipment des COMAS Screening Centers auch für Routineanwendungen zu verwenden und mit Rat und Tat bei der Adaption der *Lipid Droplet* Assays zur Seite standen.

**DR. MATTHEW BOXER** (NIH) – for constantly synthesizing new derivatives and modified probes, which allowed the constant flow of experiments with tailor-made compounds.

**DR. KSENIYA GOLOVNINA & DR. BRIAN OLIVER** (NIDDK) - for the opportunity to generate the huge next generation sequencing dataset. Thank you for all the work you spent in data analysis.

**THOMAS SCHLEMPER, PETRA KOLKHOFF, PETER THUL** (HHU) – die Fliegenseite des Projektes. Die mich trotz der räumlichen Distanz zwischen Dortmund und Düsseldorf immer als aktiven Teil der Gruppe behalten haben.

Und zu guter Letzt, geht besonderer Dank an meine **FAMILIE UND FREUNDE**, die mich immer unterstützt haben.

**DANKE!**

## 10.2 Index of Figures

<b>Figure 1:</b> Worldwide prevalence of obesity has nearly doubled from 6.4% in 1980 to 12.0% in 2008. (Figure modified from Scully, 2014; original study by Stevens et al, 2012).....	3
**Copy right Licence Key: 3515900054439	
<b>Figure 2:</b> Summary of selected anti-obesity drugs approved or withdrawn from the market. ....	7
<b>Figure 3:</b> Lipid Droplets in closer detail (adapted from Al Mathias Beller, 2005; Images B& CI Wang et al, 2008). ....	9
**Copy right Licence Key: 3515851119916	
<b>Figure 4:</b> TAG Synthesis leading to the Generation of LDs (Images modified from to Al Yen et al, 2008; BI Wilfling et al, 2013 modified according to information from Thiam et al, 2013).....	11
**Copy right Licence Key: 3515851045688	
<b>Figure 5:</b> Identification of small molecules that Induce the LD reduced Phenotype. ....	16
<b>Figure 6:</b> Summary of the different levels of investigation in the Target Identification Process.....	18
<b>Figure 7:</b> Potentially targeted pathways affected by the newly discovered small molecule classes (Chemotype 1-3). ....	20
<b>Figure 8:</b> The colorimetric TAG Assay (ZenBio, Triglyceride Quantification Kit) confirmed the reduced neutral lipid storage amounts in small molecule treated cells.....	22
<b>Figure 9:</b> Small molecule activity in selected mammalian cell lines. ....	23
<b>Figure 10:</b> Small molecule activity in whole flies. ....	26
<b>Figure 11:</b> Small molecule activity in whole flies after small molecule administration during larval development for Chemotype 2 derivative P04. ....	26
<b>Figure 12:</b> LD formation with increasing treatment times in AML12 cells fed with 400 $\mu$ M OA and 5 $\mu$ M Chemotype 1 [T08]. ....	27
<b>Figure 13:</b> Small molecule wash out experiments in <i>Drosophila</i> S3 cells indicate reversible non-covalent binding of Chemotype 1. ....	28
<b>Figure 14:</b> Replacement experiments in <i>Drosophila</i> S3 cells confirm non-covalent interactions. ....	29
<b>Figure 15:</b> Cellular localization studies of fluorescently labeled derivatives. ....	30
<b>Figure 16:</b> Chemoinformatics based target prediction using the online prediction tool "Swiss Target Prediction" ( <a href="http://www.swisstargetprediction.ch/">www.swisstargetprediction.ch/</a> ) ....	31
<b>Figure 17:</b> Expression profiles of differentially expressed genes between treated and control samples in <i>Drosophila</i> S3 cells after 4 h treatment. ....	33
<b>Figure 18:</b> Chromatographic analysis of lipid extracts from small molecule treated cells. AI Separation of triglycerides and sterylesters of small molecule treated AML12 cells in thin layer chromatography did only show a decrease in TAG. ....	35
<b>Figure 19:</b> Cholesterylester droplet formation is not altered upon Chemotype 2 [P04] treatment.....	36
<b>Figure 20:</b> Chemotype 2 [P04] treatment provokes a temporarily increase in sn-1,3 DAG levels.....	37
<b>Figure 21:</b> Quantitative real time PCR analysis of differentiation markers involved in adipogenesis of 3T3-L1 cells showed no significant changes between DMSO treated or Chemotype 2 [P04] treated cells throughout the differentiation process ....	38
<b>Figure 22:</b> FFA uptake assays confirmed that a blocked FFA is not the underlying cause for the observed LD reduced phenotype. ....	40
<b>Figure 23:</b> LD remobilization assay in cells with already existing lipid droplets prior to Chemotype 2 [P04] treatment in order to test lipolytic activation. ....	41
<b>Figure 24:</b> Mitochondrial staining of small molecule treated AML12 .....	42
<b>Figure 25:</b> Tetradecylthioacetic acid (TTA) was used to study oxidative lipid degradation.....	43
<b>Figure 26:</b> Analysis for $\beta$ -oxidation activation by Chemotypes 1+2 as a cause for the LD reduced Phenotype. ....	44
<b>Figure 27:</b> Expression levels of undifferentiated 3T3-L1 pre-adipocytes in presence of oleic acid and Chemotype 2 in order to test for induction of adipogenesis by P04.....	45

<b>Figure 28:</b> THP-1 cell based assay to study small molecule modulation in PMA dependent monocyte differentiation and foam cell generation..	47
<b>Figure 29:</b> Current hypothesis of potential Target and/or concerned Pathways.	48
<b>Figure 30:</b> Schematic summary of the process optimization workflow for the chemical proteomic target ID ( <i>pull- down</i> ). ...	49
<b>Figure 31:</b> The 1 <sup>st</sup> generation affinity probes for the chemical proteomic target identification approach for Chemotype 1 were based on a biotin linker attached to the terminal phenol moiety without affecting bioactivity.	51
<b>Figure 32:</b> New 2 <sup>nd</sup> generation pull- down probes for Chemotype 1..	53
<b>Figure 33:</b> in-gel digestion (IGD) and in-solution digestion (ISD) upon pull- down for Chemotype 1	54
<b>Figure 34:</b> Schematic summary of the “two-tiered” pull- down approach	57
<b>Figure 35:</b> Experiments to test if NT5DC1 is a potential target of Chemotype 1.	63
<b>Figure 36:</b> Experiments to test if DCK is a potential target of Chemotype 1.)	65
<b>Figure 37:</b> Experiments to test if EPHX2 is a potential target candidate of Chemotype 1.	68
<b>Figure 38:</b> Indirect test for EPHX2 as a potential target of Chemotype 1	69
<b>Figure 39:</b> Experiments to test if SPR is a potential target of Chemotype 1	70
<b>Figure 40:</b> Experiments to test if SPR is a potential target of Chemotype 1	73
<b>Figure 41:</b> Experiments to test if the pyruvate kinase as a potential target of Chemotype 1.	75
<b>Figure 42:</b> Experimental test if MAPK9 is a potential target of Chemotype 1	77
<b>Figure 43:</b> Target hypothesis for Chemotype 2.	80
<b>FIGURE 44:</b> DGAT1 is a potential direct target of Chemotype 2 [P04].	81
<b>FIGURE 45:</b> <i>In vivo</i> validation of DGAT1 inhibition by Chemotype 2 [P04] as a cause for the observed LD reduced phenotype..	82
<b>Figure 46:</b> Binding studies with recombinant murine DGAT1-His (55 kDa) and murine DGAT2-His (44 kDa) in an affinity purification approach to Chemotype 2 [P01].	84
<b>Figure 47:</b> The fluorescein labeled Chemotype 2 derivative is enriched in the ER.	85
<b>Figure 48:</b> <i>In vitro</i> binding of a fluorescein labeled derivative to DGAT1 in a proximity ligation assay (PLA).	87
<b>Figure 49:</b> DGAT1 and DGAT2 expression profiles in cell lines with known activity for Chemotype 2.	89
<b>Figure 50:</b> Summary of the COMAS Screening off LD-reducing compounds.	104
<b>Supplemental Figure 1:</b> The small molecule effect follows a concentration dependent manner, which allows the determination of EC <sub>50</sub> values in order to quantify the affinity.	176
<b>Supplemental Figure 2:</b> Long term real time cell analysis (RTCA) did not indicated significantly altered cell growth introduced by small molecule application.	1777
<b>Supplemental Figure 3:</b> Small molecule activity is conserved in cells deriving from different species and organs as systematically analyzed for <i>Drosophila</i> S3 (embryo), monkey COS7 (kidney) and murine AML12 (liver) cells.	179
<b>Supplemental Figure 4:</b> Investigation of the LD assay response towards alterations in small molecule concentration and OA concentration in AML12 cells.	180
<b>Supplemental Figure 5:</b> Summary of Chemotype 2 treated cells in different cell lines.	184
<b>Supplemental Figure 6:</b> Relative expression of differentiation markers involved in adipogenesis in murine 3T3 cells.	184
<b>Supplemental Figure 7:</b> Altered LD assay in regard of the initial LD load of the cell.	185
<b>Supplemental Figure 8:</b> Label free quantification in the 3 <sup>rd</sup> generation pull- down with Chemotype 1 [T03].	189
<b>Supplemental Figure 9:</b> SILAC quantification in the 4 <sup>th</sup> generation pull- down for Chemotype 1 [T03]. s.	193
<b>Supplemental Figure 10:</b> SILAC quantification in the 4 <sup>th</sup> generation pull- down for Chemotype 2 [P01].	195
<b>Supplemental Figure 11:</b> Know DGAT1 inhibitors.	206
<b>Supplemental Figure 12:</b> Dotblot of DGAT1-His and DGAT2-His overexpression in AML12 and Hek293 cells.	207

---

<b>Supplemental Figure 13:</b> Oleic Acid Titration in THP-1 cells in order to identify a suitable OA screening concentration in differentiated THP-1 cells.....	20808
<b>Supplemental Figure 14:</b> Schematic summary of stable isotope labeling by amino acids in cell culture (SILAC).....	209
<b>Supplemental Figure 15:</b> The cell based 11 $\beta$ -HSD assay measures the 11 $\beta$ -HSD1 dependent oxo-reduction from cortisol and the 11 $\beta$ -HSD2 dependent oxidation of cortisone .....	210
<b>Supplemental Figure 16:</b> PRECICE <sup>®</sup> dCK Screening Assay.....	210
<b>Supplemental Figure 17:</b> Cell viability was quantified using the CellTiterGlo <sup>®</sup> Reaction Kit (Promega) .....	210
<b>Supplemental Figure 18:</b> The cell based assay bases on the KPYK dependent reaction from phosphoenolpyruvate (PEP) and ADP to pyruvate and ATP.....	211
<b>Supplemental Figure 19:</b> The N-terminal phosphatase activity.....	211
<b>Supplemental Figure 20:</b> Schematic summary of the AraC cell based assay.....	212
<b>Supplemental Figure 21:</b> Schematic summary of the applied in situ Duolink <sup>®</sup> using PLA <sup>®</sup> Technology (Sigma Aldrich) in order to investigate the potential interaction of DGAT1 and Chemotype 2.....	212

### 10.3 Collaboration Partners

- [1] Prof. Waldmann, Dr. Slava Ziegler  
Max Planck Institute for Physiology, Department for Chemical Biology, Otto-Hahn Straße 11, 44227 Dortmund, Germany
- [2] Dr. Petra Janning  
Max Planck Institute for Physiology, Department for Chemical Biology, Otto-Hahn Straße 11, 44227 Dortmund, Germany
- [3] Dr. Sonja Sievers  
Compound Management and Screening Center (COMAS), Biomedizinisches Zentrum, Otto-Hahn Straße 15, 44227 Dortmund, Germany.
- [4] Dr. Matthew Boxer, Li Zhuyin  
National Center for Advancing Translational Sciences, National Institutes of Health, 9800 Medical Center Drive, 20850 Bethesda, USA
- [5] Dr. Biran Oliver, Dr. Kseniya Golovkina  
Laboratory of Cell and Developmental Biology, National Institutes of Diabetes, Digestive and Kidney Diseases, National Institutes of Health, MD 20892-2560, Bethesda, USA
- [6] Dr. Thomas O. Eichmann  
University of Graz, Institute of Molecular Biosciences, Heinrichstr. 31, 8010 Graz, Austria
- [7] Dr. Carole Sztalryd· University of Maryland, School of Medicine, 655 W. Baltimore Street, 21201 Baltimore, USA



## 10.4 Curriculum Vitae

### PERSÖNLICHE INFORMATIONEN



Name: Kirsten Tschapalda  
Geburtsdatum: 29.Juni.1986  
Geburtsort: Oelde, NRW  
Nationalität: German

### UNIVERSITÄRE AUSBILDUNG

- 2011- 2015     **Dissertation an der Heinrich- Heine Universität Düsseldorf**  
                  Institut für Mathematische Modellierung biologischer  
                  Systeme
- 2008-2011     ***Master of Science (M.Sc.) in Molekularer Biotechnologie***  
                  Universität Bielefeld
- 2005-2008     ***Bachelor of Science (B.Sc.) in Molekularer Biotechnologie***  
                  Universität Bielefeld

## 10.6 Eidesstattliche Erklärung

Ich versichere an Eides Statt, dass die Dissertation von mir selbständig und ohne unzulässige fremde Hilfe unter Beachtung der „Grundsätze zur Sicherung guter wissenschaftlicher Praxis an der Heinrich-Heine-Universität Düsseldorf“ erstellt worden ist.

.....  
(Place, Date)

.....  
(Kirsten Tschapalda)